MORPHOLOGY AND GENETIC CHARACTERIZATION OF AMNESIC SHELLFISH TOXIN PRODUCING DIATOM SPECIES, *Pseudo-nitzschia* AND *Nitzschia* (Bacillariophyceae) IN MALAYSIAN WATERS

TAN SUH NIH

INSTITUTE OF GRADUATE STUDIES
UNIVERSITY OF MALAYA
KUALA LUMPUR

2018

MORPHOLOGY AND GENETIC CHARACTERIZATION OF AMNESIC SHELLFISH TOXIN PRODUCING DIATOM SPECIES, *Pseudo-nitzschia* AND *Nitzschia* (Bacillariophyceae) IN MALAYSIAN WATERS

TAN SUH NIH

THESIS SUBMITTED IN FULFILMENT OF THE REQUIREMENTS FOR THE DEGREE OF DOCTOR OF PHILOSOPHY

INSTITUTE OF GRADUATE STUDIES
UNIVERSITY OF MALAYA
KUALA LUMPUR

2018

UNIVERSITY OF MALAYA

ORIGINAL LITERARY WORK DECLARATION

Name of Candidate: Tan Suh Nih

Matric No: HHQ150008

Name of Degree: Doctoral degree

Title of Project Paper/Research Report/Dissertation/Thesis ("this Work"):

Morphology and Genetic Characterization of Amnesic Shellfish Toxin Producing Diatom Species, *Pseudo-nitzschia* and *Nitzschia* (Bacillariophyceae) in Malaysian Waters

Field of Study: Environmental Science (Marine Biotechnology)

I do solemnly and sincerely declare that:

I am the sole author/writer of this Work;
This Work is original;
Any use of any work in which copyright exists was done by way of fair dealing and for permitted purposes and any excerpt or extract from, or reference to or reproduction of any copyright work has been disclosed expressly and sufficiently and the title of the Work and its authorship have been acknowledged in this Work;
I do not have any actual knowledge nor do I ought reasonably to know that the making of this work constitutes an infringement of any copyright work;
I hereby assign all and every rights in the copyright to this Work to the University of Malaya ("UM"), who henceforth shall be owner of the copyright in this Work and that any reproduction or use in any form or by any means whatsoever is prohibited without the written consent of UM having been first had and obtained;
I am fully aware that if in the course of making this Work I have infringed any copyright whether intentionally or otherwise, I may be subject to legal action or any other action as may be determined by UM.

Candidate's Signature Date:

Subscribed and solemnly declared before,

Witness's Signature Date:

Name:

Designation:

MORPHOLOGY AND GENETIC CHARACTERIZATION OF AMNESIC SHELLFISH TOXIN PRODUCING DIATOM SPECIES, *Pseudo-nitzschia* AND *Nitzschia* (Bacillariophyceae) IN MALAYSIAN WATERS

ABSTRACT

Diatom *Pseudo-nitzschia* and *Nitzschia* are widely distributed in brackish and marine environments. Some species are known to produce the neurotoxin domoic acid (DA) that responsible for Amnesic Shellfish Poisoning (ASP) in humans and marine organism. While several species have been reported to be toxic in Malaysian waters, there was no confirmed ASP case reported thus far. In this study, samplings were conducted throughout the coastal and mangrove waters of Malaysia to determine the occurrence, distribution and toxicity of *Pseudo-nitzschia* and *Nitzschia* species. A total of 548 strains of *Pseudo-nitzschia* and *Nitzschia* were established and identified by light and electron microscopy; they are *P. batesiana*, *P. bipertita*, *P. brasiliana*, *P. circumpora*, *P. cuspidata*, *P. fukuyoi*, *P. pungens*, and *N. navis-varingica*.

Species identification in *Pseudo-nitzschia* based sorely on morphological characters is challenging owing to the minute morphological differences. Thus, molecular characterization has become an essential supporting criterion in species delineation. In this study, the phylogenetic relationships of *Pseudo-nitzschia* species were inferred based on three genetic markers. A pair of genus-specific primer targeting *cox*1 gene were developed *in silico*. The results revealed three distinct clades in the *P. pseudodelicatissima* complex, while the *P. delicatissima* complex formed a distinct clade (Group IV) in both the LSU and ITS2 phylogeny. ITS2 dataset resulted in the most resolved trees, followed by *cox1* and LSU.

For the benthic diatom *Nitzschia navis-varingica*, it was found widely distributed in the brackish mangrove areas of Malaysia. To examine the potential

contamination of DA in the local shellfish industry, both the *N. navis-varingica* strains and shellfish collected were analyzed by FMOC-LC-FLD and LC-MS/MS. DA and its geometrical isomers, isodomoic A and B, were detected in 48 strains of *N. navis-varingica*. Their cellular DA content ranged from 0.37–11.06 pg/cell. For the 25 shellfish samples analyzed, only two cockle samples from Asajaya, Sarawak were detected with 283.72 and 465.04 µg/kg, respectively.

To understand the population dynamics of *N. navis-varingica* in the Western Pacific, the genetic diversity was investigated using LSU rDNA and ITS2 markers. The LSU dataset revealed high sequence homogeneity among all strains examined (0–0.9%). The ITS2 inferences identified eight distinct clades, with high sequence heterogeneity (0.5–19.7%); analysis of haplotype diversity recovered 44 haplotypes. Our results showed strong gene flow among *N. navis-varingica* populations in the Western Pacific region (Φ_{ST}=0.48095). However, isolates from Vietnam and Japan formed a distinct haplotype H3 (F_{ST}, 0.41–1.00), suggesting possible genetic structuring between the water bodies of northwestern Pacific and the South China Sea (SCS). It is speculated that ocean current circulations (SCS and Kuroshiro currents) may play a role in this allopatric differentiation of *N. navis-varingica*.

This study has demonstrated the occurrence and wide distribution of the toxigenic *Pseudo-nitzschia* species and *N. navis-varingica* in Malaysian waters. The potential ASP risk of in Malaysia should be assessed continuously by monitoring the toxic plankton and level of DA in shellfish mollusks to safeguard public health and ensure seafood safety.

Keywords: *Pseudo-nitzschia*; *Nitzschia*; domoic acid (DA); *cox*1; LSU rDNA; and ITS2.

PENCIRIAN MORFOLOGI DAN GENETIK SPESIES DIATOM PENHASIL TOKSIN KERANG AMNESIK, *Pseudo-nitzschia* DAN *Nitzschia* (Bacillariophyceae) DI PERAIRAN MALAYSIA

ABSTRAK

Diatom *Pseudo-nitzschia* dan *Nitzschia* tertabur secara meluas di persekitaran air payau dan marin. Beberapa spesies telah diketahui menghasilkan asid domoik neurotoksin (DA) yang boleh menyebabkan keracunan kerang-kerangan amnesik (ASP) pada manusia dan organisma marin. Walaupun beberapa spesies telah dikenalpasti sebagai toksik di perairan Malaysia, tiada kes keracunan ASP dilaporkan setakat ini. Dalam kajian ini, kajian lapangan telah dijalankan di seluruh perairan persiaran pantai dan bakau untuk menentukan kehadiran, taburan dan ketoksikan spesies *Pseudo-nitzschia* dan *Nitzschia*. Sebanyak 548 strain *Pseudo-nitzschia* dan *Nitzschia* telah berjaya didirikan dan dikenalpasti dengan menggunakan mikroskop cahaya dan mikroskop elektron lanjutan; iaitu *P. batesiana*, *P. bipertita*, *P. brasiliana*, *P. circumpora*, *P. cuspidata*, *P. fukuyoi*, *P. pungens*, dan *N. navis-varingica*.

Pengenalpastian spesies dalam *Pseudo-nitzschia* hanya berdasarkan ciri-ciri morfologi adalah mencabar memandangkan perbezaan morfologi yang kecil. Oleh itu, pencirian molekul telah menjadi satu kriteria sokongan yang penting bagi penentuan spesies. Dalam kajian ini, hubungan filogenetik spesies *Pseudo-nitzschia* yang disimpulkan berdasarkan tiga jenis gen. Sepasang penjujuk mensasarkan gen *cox*1 telah direkabentuk secara in silico. Semua pokok filogenetik daripada *Pseudo-nitzschia* mendedahkan bahawa kompleks *P. pseudodelicatissima* dibahagikan kepada tiga klad yang berbeza manakala kompleks P. delicatissima membentuk klad yang berbeza (Kumpulan IV) di kedua-dua pokok filogenetik LSU dan ITS2. Data set ITS2 menghasilkan pokok yang paling terasing dengan baik, diikuti dengan *cox*1 dan LSU.

Bagi bentik *N. navis-varingica*, spesies ini didapati tertabur secara meluas di seluruh kawasan bakau Malaysia. Untuk mengkaji potensi pencemaran DA dalam kerang-kerangan tempatan, kedua-dua strain *N. navis-varingica* dan kerang telah dikumpul untuk analisis DA dengan menggunakan FMOC-LC-FLD dan LC-MS / MS. DA dan isomer geometrinya, isodomoik A dan B telah dikesan dalam 48 strain *N. navis-varingica*. Kandungan DA selular adalah di antara 0.37 dan 11.06 pg / sel. Bagi 25 sampel kerang yang dianalisis, hanya dua sampel kerang dari Asajaya, Sarawak dikesan dengan 283.72 dan 465.04 μg/kg, masing-masing.

Untuk memahami dinamika populasi *N. navis-varingica* di rantau Pasifik Barat, kepelbagaian genetic *N. navis-varingica* telah disiasat dengan menggunakan penanda LSU dan ITS2. Set data LSU rDNA mendedahkan kehomogenan urutan yang tinggi di antara semua strain yang diperiksa (0–0.9%). Filogenetik ITS2 rDNA menunjukkan lapan klad yang berbeza dengan pencapahan jujukan yang tinggi (0.5–19.7%); sebanyak 44 haplotip telah dikenalpasti dalam analisis kepelbagaian haplotip. Kajian ini menunjukkan aliran gen yang kuat di kalangan populasi *N. navis-varingica* di Pasifik Barat laut (Φ_{ST}=0.48095). Walau bagaimanapun, pengasingan populasi Vietnam dan Jepun membentuk haplotop H3 yang berbeza (F_{ST}, 0.41–1.00), adalah kemungkinan berlakunya penstrukturan genetik antara perairan di barat laut Pasifik dan laut China Selatan (SCS). Peredaran arus laut (misalnya arus SCS dan arus Kuroshiro) mungkin memainkan peranan dalam pembezaan allopatrik populasi *N. navis-varingica* di rantau ini.

Kajian ini telah menunjukkan kehadiran dan pengedaran luas bagi spesies *Pseudo-nitzschia* dan *N. navis-varingica* yang di kawasan perairan Malaysia. Risiko ASP yang berpotensi di Malaysia perlu dinilai secara berterusan dengan memantau plankton toksik dan paras DA dalam kerang-kerangan untuk melindungi kesihatan awam dan keselamatan makanan laut.

Kata kunci: *Pseudo-nitzschia*; *Nitzschia*; asid domoik (DA); *cox*1; LSU rDNA; dan ITS2.

ACKNOWLEDGMENTS

I would like to extend my sincere gratitude and appreciation to all those who had contributed to the completion of my study. Their supports in various ways had made this thesis possible.

Firstly, I would like to thank my supervisors, Assoc. Prof. Dr. Lim Po Teen and Assoc. Prof. Dr. Leaw Chui Pin for their guidance, encouragement and valuable advices and suggestions throughout the past four years. My great appreciation to the *Ministry of Education for Mybrain15 scholarship for the sponsorship.* This research project was financially supported by MOHE IOES-HICOE (IOES-2014C) to Assoc. Prof. Dr. Lim Po Teen.

My special thanks to Prof Dr. Kotaki Yuichi, Kitasato University, Japan and Prof Gao Chunlei, First Institute of Oceanography, China, who assisted in analysis of toxin in cultures and bivalves samples; Prof. Dr Gu Haifeng (Third Institute of Oceanography, China) for the SEM analysis; and Dr. Chen Chanping (Xiamen University, China) for his advice on the taxonomy of *Nitzschia* species. I would like to thank my seniors and lab members for the assistance in data collection and analyses.

To my Mum, Dad, sisters Maggie and Nichole, and brothers Keat and Wei, I owe my greatest thanks for your encouragement and support throughout my study.

TABLE OF CONTENTS

LIST OF FIGURES

LIST OF TABLES

LIST OF SYMBOLS AND ABBREVIATIONS

AIC	:	Akaike information criterion
AMOVA	:	Analysis of molecular variance
ASP	:	Amnesic shellfish poisoning
BEAST	:	Bayesian evolutionary analysis sampling trees
BEAUti	:	Bayesian evolutionary analysis utility
BI	:	Bayesian inference
BLAST	:	Basic local alignment search tool
CBCs	:	Compensatory base changes
*cox*1	:	Mitochondrial cytochrome *c* oxidase 1
CTAB	:	Cetyl-trimethyl-ammonium-bromide
DA	:	Domoic acid
DNA	:	Deoxyribonucleic acid
FMOC-LC-FLD	:	9-fluorenylmethylchloroformate
F_{ST}	:	Fixation index
HABs	:	Harmful algal blooms
HPLC	:	High-performance liquid chromatography
IA	:	Isodomoic acid A
IB	:	Isodomoic acid B
ITS	:	Internal transcribed spacer
ITS2	:	Second internal transcribed spacer
LC-MS/MS	:	Liquid chromatography-mass spectrometry
LM	:	Light microscope
LSU	:	Large subunit
ML	:	Maximum likelihood

MP	:	Maximum parsimony
MRM	:	Multiple reaction monitoring
MUSCLE	:	Multiple Sequence Comparison by Log-Expectation
NCBI	:	National center of biotechnology information
NJ	:	Neighbour-joining
NNI	:	Nearest neighbour interchange
PAUP*	:	Phylogenetic analysis using parsimony*
PCR	:	Polymerase chain reaction
rDNA	:	Ribosomal deoxyribonucleic acid
rRNA	:	Ribosomal ribonucleic acid
SA	:	Stepwise addition
SEM	:	Scanning electron microscope
TBR	:	Tree bisection-reconnection
TEM	:	Transmission electron microscope

LIST OF APPENDICES

CHAPTER 1: GENERAL INTRODUCTION

Phytoplankton serves as the basal of the trophic level and acts as an energy provider in the marine ecosystem. However, the proliferation of selected algal species that reach high concentration of cells in the coastal water have caused the formation of harmful algal blooms (HABs), also known as 'red tides'. Several types of shellfish poisonings are associated with algal-origin toxins that derived from HABs, including Paralytic Shellfish Poisoning (PSP), Diarrhetic Shellfish Poisoning (DSP), Neurotoxin Shellfish Poisoning (NSP), Amnesic Shellfish Poisoning (ASP), and Ciguatera Fish Poisoning (CFP) (Zingone & Enevoldsen, 2000). ASP is a human illness occurs after consuming the shellfish mollusk that contaminated by the biotoxin, domoic acid (DA). DA is a neuro-excitatory amino acid that bind irreversible to the glutamate receptor. Contamination of bivalve shellfish by the biotoxins especially DA has responsible for severe damage to public health as well as seafood industry globally.

Distribution of DA producers has been reported worldwide. The toxic and potentially toxic *Pseudo-nitzschia* species have been reported in different countries and regions after the first incident of ASP in Canada, in 1987; three deaths and 105 cases of acute human intoxication were documented after consuming the contaminated blue mussels (*Mytilus edulis* Linnaeus) (Martin et al., 1990; Perl et al., 1990; Buck et al., 1992; Fritz et al., 1992; Garrison et al., 1992; Lundholm et al., 1994; Scholin et al., 2000; Pan et al., 2001; Cusack et al., 2002, 2004; Fehling et al., 2004, 2006; Marić et al., 2011; Dao et al., 2014, 2015; Teng et al., 2014). The neurotoxin, domoic acid (DA), $C_{15}H_{21}NO_6$, was confirmed subsequently in the diatom, *Pseudo-nitzschia multiseries* (Hasle) Hasle (formerly known as *Nitzschia pungens* f. *multiseries*) (Bates et al. 1989).

Species identification in *Pseudo-nitzschia* and *Nitzschia* species based sorely on morphological characters are often challenging owing to the minute morphological difference. Thus, molecular approaches have been widely applied in species

identification to support the morphological identification. Sequence analyses of the nuclear-encoded large-subunit (LSU) ribosomal RNA gene (rDNA) and the internal transcribed spacer (ITS) region were commonly used for the *Pseudo-nitzschia* identification (Lundholm et al., 2002a, 2003; Amato & Montresor, 2008; Quijano-Scheggia et al., 2009; Moschandreou et al., 2010; Lelong et al., 2012; Lim et al. 2010, 2012a, 2012b, 2013, 2014, 2018; Teng et al., 2013, 2014, 2015).

Various approaches have been taken to gain better understanding of the taxonomy, genetics and toxin production of *Pseudo-nitzschia*. However, species delineation by using mitochondrial genetic marker, cytochrome oxidase I (*cox*1) gene is scarce. Thus, the first objective was to examine the molecular characteristics of *Pseudo-nitzschia* from Malaysian waters by using the mitochondrial genetic marker cytochrome oxidase I (*cox*1) gene, which is a common marker in solving phylogenetic relationships of organisms. In Chapter III, the information of the unambiguous sequence alignment of *cox*1 was used to reconstruct a reliable phylogenetic framework to infer the phylogenetic lineage of *Pseudo-nitzschia* species.

Most toxigenic *Pseudo-nitzschia* species are planktonic while *Nitzschia navis-varingica* is frequently found in the benthic brackish ecosystem (Kotaki et al., 2004, 2005; Romero et al., 2012). *Nitzschia navis-varingica* was found in estuarine areas or brackish waters of Western Pacific regions such as Japan, Philippines, Thailand, Vietnam, and Indonesia (Kotaki et al., 2000, 2004, 2005, 2006, 2008; Bajarias et al., 2006; Romero et al., 2008, 2011, 2012; Takata et al., 2009; Thoha et al., 2012). The species was also found in Australia (Higgins et al., 2003; Ayaz et al., 2018).

Although DA is a water-soluble toxin, the toxin is able to cause fatality at higher trophic levels in the marine ecosystem. Mass mortality of marine mammals (sea lion and whales) and other marine life was clearly an evidence of DA transfer to higher trophic levels (Sierra Beltran et al., 1997; Lefebvre et al., 1999, 2002; Scholin et al.,

2000; Bargu et al., 2002; Gulland et al., 2002; Silvagni et al., 2005; Goldstein et al., 2008; Fire et al., 2010).

In the tropical-subtropical brackish ecosystem, the mangrove forest plays an important role as shelters to many marine life. They often host many commercially valuable molluscan shellfish (e.g., benthic clams: *Polymesoda*; rock oyster: *Crassostrea*; razor clams: *Solen*) and crustacean (mud crabs: *Scylla serrate*) (Rönnbäck, 1999; Honculada-Primavera, 2000), which may serve as vectors of DA (Noordin and Lim, per. comm.). In the Western Pacific region, DA contamination in bivalves have been reported in Japan (Takata et al., 2009), Vietnam (Huyen et al., 2006, Dao et al., 2006, 2009, 2014; Takata et al., 2009) and Philippines (Takata et al., 2009). However, very little studies had shown the contaminated bivalves were associated to toxigenic *Pseudo-nitzschia* species (Dao et al., 2014, 2015). In the mangrove ecosystem, shellfish are likely to play a role in the transfer of DA through the marine food chain if toxigenic diatom such as *N. navis-varingica* occurred in the waters. Therefore, it is important to investigate the occurrence, distribution and abundance of these DA producers and examined the potential vectors of DA in our waters that might be a threat to public health. Thus, the second objective in this study was to investigate the occurrence and distribution of *N. navis-varingica* from Malaysian mangrove waters with detailed examination of the morphology, genetics and toxicity. DA toxicity in bivalves shellfish from our waters was also investigated (Chapter IV).

In recent years, studies of population genetics have been undertaken using various genetic approaches for *Pseudo-nitzschia*, i.e. microsatellites markers (Evans et al., 2005; Adams et al., 2009; Casteleyn et al., 2009; 2010) and inference based on the ITS region (Casteleyn et al., 2008), but no study was undertaken for the toxigenic *N. navis-varingica*. Therefore, the intraspecific genetic variation and geographical

distribution patterns of Malaysian *N. navis-varingica* were studied and the findings compiled in Chapter V.

Specific objectives of this study were listed as below:

i. To determine the distribution of the harmful diatoms *Pseudo-nitzschia* and *Nitzschia* species along the coasts of Malaysia;
ii. To characterize the species of *Pseudo-nitzschia* and *Nitzschia* morphologically by advanced microscopy and molecularly by inferring their phylogenies;
iii. To identify the level of domoic acid in toxic *Pseudo-nitzschia* and *Nitzschia* species from Malaysian waters;
iv. To investigate the accumulation of DA in commercially important mollusks and other marine organisms;
v. To investigate the genetic structure and gene flow of the toxigenic *N. navis-varingica* natural populations.

Hypotheses were as follow:

i. H_0: The cox1 gene is a better genetic marker compare to LSU and ITS2 rDNA in the phylogenetic analysis of *Pseudo-nitzschia*
ii. H_1: ITS2 rDNA and LSU rDNA are better genetic marker than the cox1 in the phylogenetic analysis of *Pseudo-nitzschia*;
iii. H_0: *N. navis-varingica* is widely distributed in Malaysian waters
H_1: the distrubution of *N. navis-varingica* is restricted in Malaysian water;
iv. H_0: No DA contamination in shellfish samples from Malaysian waters
H_1: DA contamination is common in shellfish samples from Malaysian waters;
v. H_0: No population structuring in *N. navis-varingica* from the Western Pacific region

H_1: Populations of *N. navis-varingica* from Western Pacific region is genetically structured.

This dissertation is prepared in an 'Article Style Format' (as in Guidelines for the Preparation of Research Reports Dissertations and Theses, 2017), and consists of a total of six chapters. **CHAPTER I** provide an overview of the general background of this study, explaining the occurrence of DA contamination in the Western Pacific region and several research problems and questions to be answered. **CHAPTER II** includes a literature review that provided scientific information for this study. In **CHAPTER III**, genetic markers of *cox*1, LSU and ITS2 rDNAs were used to the phylogeny and species delineation in the marine diatom *Pseudo-nitzschia* species. In **CHAPTER IV**, the distribution of the toxigenic *N. navis-varingica* in Malaysian mangrove waters was documented. Detailed morphology was observed under light microscopy and electron microscopy. Toxicity of the *N. navis-varingica* isolates was detected and confirmed by FMOC-LC-FLD and LC-MS/MS. While in shellfish samples, only two cockle samples out of the 25 samples were detected with DA. In **CHAPTER V**, the population genetic structure of *N. navis-varingica* in the Western Pacific region was examined. The genetic diversity and geographical distribution pattern were evaluated using the ITS2 rDNA marker with the inference of secondary structure information. In **CHAPTER VI**, a summary was drawn to conclude the findings of this study.

CHAPTER 2: LITERATURE REVIEW

2.1 Amnesic Shellfish Poisoning (ASP)

Amnesic Shellfish Poisoning (ASP) is a human illness caused by consumption of wild or cultured shellfish contaminated with a type of algal origin neurotoxin, domoic acid (DA). ASP was first reported in Canada during the year of 1987; three deaths and more than 100 cases of acute human intoxication were documented after consuming the DA contaminated blue mussels (*Mytilus edulis* Linnaeus) (Perl et al., 1990). People who consumed the contaminated shellfish showed gastrointestinal and neurological effect. Gastrointestinal symptoms included abdominal cramps, confusion, decrease the level of consciousness, diarrhea, disorientation, headache, nausea, seizures, and vomiting (Teitelbaum et al., 1990; Todd, 1993). In several events, victims experienced symptoms similar to Alzheimer's disease, which resulted in the loss of short-term memory (Perl et al., 1990). DA could be fatal to people if consumed highly contaminated shellfish and. This toxin is produced naturally by marine diatoms, some *Pseudo-nitzschia* species (e.g Bates et al, in press) and the species *Nitzschia navis-varingica* and *N. bizertensis* (xxx).

The neurotoxin, DA, $C_{15}H_{21}NO_6$, binds irreversible to glutamate receptor, is known to be produced by red alga *Chondria armata* (Kützing) Okamura (Zaman et al., 1997). DA was later found to be produced by the diatom, *Pseudo-nitzschia multiseries* (Hasle) Hasle (formerly known as *Nitzschia pungens* f. *multiseries*) (Bates et al., 1989). DA was detected in several species of *Pseudo-nitzschia* and *Nitzschia* species (Subba Rao et al., 1988; Bates et al., 1989; Martin et al., 1990; Buck et al., 1992; Fritz et al., 1992; Garrison et al., 1992; Villac et al., 1993b; Lundholm et al., 1994; Rhodes, 1998; Kotaki et al., 1999, 2000, 2004, 2005, 2006, 2008; Trainer et al., 2000; Pan et al., 2001; Bargu et al., 2002; Cussack et al., 2002; Orsini et al., 2002; Fehling et al., 2004; Cerino et al., 2005; Anderson et al., 2006; Bajarias et al., 2006; Orlova et al., 2008; Romero et

al., 2008, 2011, 2012; Sahraoui et al., 2011; Takata et al., 2009; Thoha et al., 2012; Bouchouicha Smida et al., 2014; Dao et al., 2014, 2015; Teng et al., 2014).

DA was also reported to cause disruption to marine food web during *Pseudo-nitzschia* bloom resulted in mass mortality of marine mammals that stay at higher trophic level of the food chain, i.e. sea lions (Lefebvre et al., 1999; Scholin et al., 2000; Trainer et al., 2000; Gulland et al., 2002; Silvagni et al., 2005; Goldstein et al., 2008); whales (Lefebvre et al., 2002; Fire et al., 2009, 2010); seabirds (Fritz et al., 1992; Work et al., 1993; Sierra Beltran et al., 1997; Bargu et al., 2012); and dolphins (Schwacke et al., 2010; Fire et al., 2011). Apart from DA, other derivatives such as isodomoic acid A (IA) and isodomoic acid B (IB) were also detected in *N. navis-varingica* (Kotaki et al., 2005).

2.2 The genus *Pseudo-nitzschia*

The genus *Pseudo-nitzschia* Peragallo (Peragallo & Peragallo, 1990) has been found distributed globally. After the incident of ASP occurred in Canada, studies of toxicity, morphology, genetics and physiology ecology of the pennate *Pseudo-nitzschia* have increased and documented. Many species of *Pseudo-nitzschia* are widespread in the coastal and oceanic waters (reviewed in Lelong et al., 2012; Trainer et al., 2012), and some have been proven cosmopolitan (Hasle, 2002; Casteleyn et al., 2008; Lim et al., 2012b, 2014).

For the past decade, there is an increase on the research studies of *Pseudo-nitzschia* in this region, especially in Malaysian waters (Lim et al., 2012a, 2012b, 2013; Teng et al., 2013, 2014, 2015, 2016), with many new species reported. Other new records were also reported from other parts of the South China Sea (Dao et al., 2014, 2015; Li et al., 2017). However, the taxonomy of *Pseudo-nitzschia* is still remained

unresolved due to the presence of species complexes (Lundholm et al., 2002b, 2003, 2006, 2012). Therefore, molecular tools were used to support the distinctions among species and used as supporting evidences for new species description (Lundholm et al., 2003, 2006, 2012; Amato & Monstresor, 2008; Quijano-Scheggia et al., 2009; Lim et al., 2012a, 2012b, Orive et al., 2013, Percopo et al., 2016).

2.2.1 Taxonomy of *Pseudo-nitzschia*

Diatom *Pseudo-nitzschia* H. Peragallo was first identified as *Nitzschia* (Peragallo & Peragallo, 1990) and separated from the section of *Nitzschia* Hassall after the comparison of morphological characteristics between both genera (Hasle, 1993, 1994). Before the year of 1994, classification of *Pseudo-nitzschia* species was based on the transapical axis; the group level (*seriata*- and *delicatissima*- group) is able to differentiate under light microscope: *seriata*- (width > 3 μm) group and *delicatissima*- (width < 3 μm) groups (Table 2.1; Hasle & Syvertsen, 1997).

Table 2.1: Classification of *Pseudo-nitzschia* species based on width of cell valves.

Group	Width	Species
seriata	width > 3 μm	*P. antarctica*, *P. australis*, *P. dolorosa*, *P. fraudulenta*, *P. heimii*, *P. multiseries*, *P. pungens*, *P. roundii*, *P. seriata*
delicatissima	width < 3 μm	*P. arenysensis*, *P. brasiliana*, *P. caciantha*, *P. cuspidata*, *P. decipiens*, *P. delicatissima*, *P. fryxelliana*, *P. galaxiae*, *P. granii*, *P. hasleana*, *P. inflatula*, *P. linea*, *P. lineola*, *P. mannii*, *P. micropora*, *P. pseudodelicatissima*

Taxonomy studies of *Pseudo-nitzschia* species were further refined with the improvement of electron microscopes. By using the scanning electron microscope (SEM) and transmission electron microscope (TEM), the fine details of frustule ultrastructure in valve view (by looking down at the valve face from the top), girdle

view (by looking the valve from the side) and transverse section view play roles in taxonomic characters (Figure 2.1). The siliceous cell wall (frustule) of diatom composed of silica and organic material. The frustule is comprised of two components: the epitheca (larger upper-theca; a combination of epivalve and epicingulum) and the hypotheca (smaller lower-theca; a combination of hypovalve and hypocingulum). Each theca is composed of a valve and a cingulum band. Apical axis and transapical axis also used for species description, where apical axis forms the longest axis that is parallel to the valve face; transapical axis is perpendicular to the apical axis (again parallel to the valve face). A schematic overview of the siliceous components of frustules is shown in Figure 2.1.

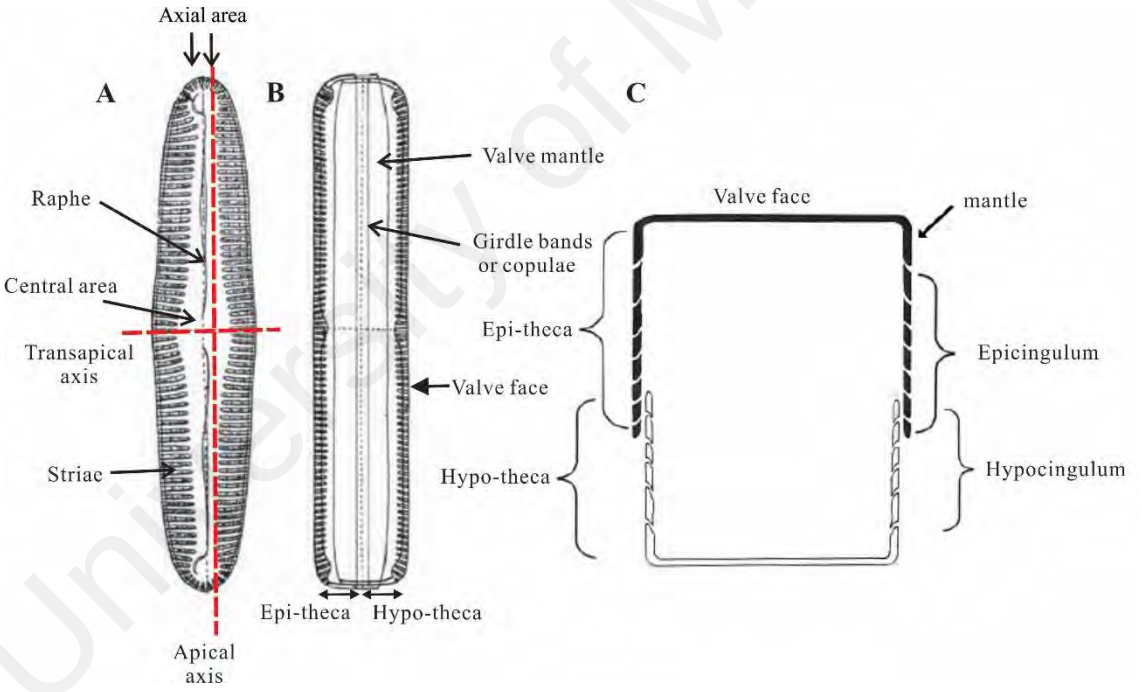

Figure 2.1: Schematic overview of the siliceous components of diatom frustules. (A) Valve view, (B) Girdle view. (C) Transverse section. (Source: modified from Taylor et al., 2006).

When the novel of *Pseudo-nitzschia* species increasing for the past decade, morphology characteristics (i.e. valve shape, structure of apex, cell overlapping, absent or present of central interspace, number of fibulae and striae, number of poroids and poroid hymen, and valvopula) in *Pseudo-nitzschia* species were used in species delineation (Figure 2.2; Lundholm et al., 2002b, 2003, 2006, 2012, Quijano-Scheggia et al., 2009; Lim et al., 2012a). In 2003, *Pseudodelicatissima* complex was first discovered due to the unclear on the delineation of the *P. pseudodelicatissima* and *P. cuspidata*. Based on the valve outline of species, *P. pseudodelicatissima* had linear valve shape, which is different compared to *P. cuspidata*, lanceolate valve shape. This study had proved that valve shapes are useful taxonomic characters in species identification (Lundholm et al., 2003). In 2009, *P. arenysensis* was described as a cryptic species from *P. delicatissima*. Although no different in morphometric data for the two species, *P. arenysensis* was sexually incompatible with the *P. delicatissima*. In molecular approach, internal transcribed spacers (ITS) (region ITS2) phylogeny shows difference among *P. arenysensis* and *P. delicatissima* (Quijano-Scheggia et al., 2009).

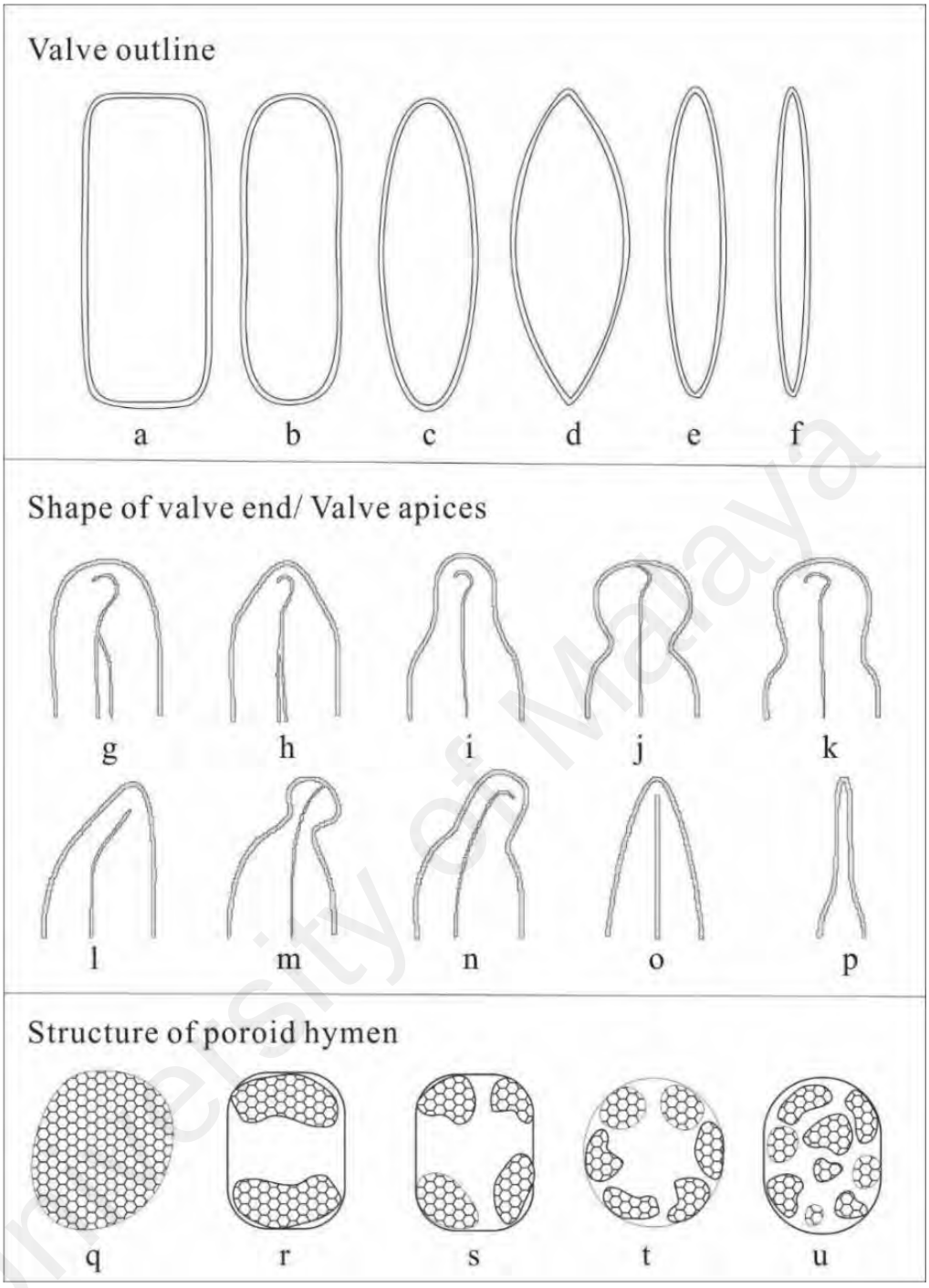

Figure 2.2: Schematic drawings of morphological characteristics of pennate diatom. Valve outline (a–f): (a) rectangular, (b) linear, (c) narrow elliptical, (d) broadly lanceolate, (e) lanceolate, (f) narrowly lanceolate; Shape of valve end (g–p): (g) obtusely or broadly rounded, (h) cuneate, (i) rostrate, (j) capitate, (k) subcapitate, (l) sigmoidly cuneate, (m) capitate, (n) rostrate, (o) acutely or sharply rounded, (p) elongate; Structure of the poroid hymen (q–u): (q) no hymen sector, (r) 2 hymen sector, (s) 4 hymen sector, (t) 6 hymen sector, (u) > 6 hymen sector.

2.2.2 Genetics of *Pseudo-nitzschia*

Molecular approach has been proven as supporting tools in identification of *Pseudo-nitzschia* species especially for crytic and pseudo-crytic species in the *P. pseudodelicatissima* complex (Lundholm et al., 2006; Amato & Monstresor, 2008; Lundholm et al., 2012; Lim et al., 2013) and the *P. delicatissima* complex (Lundholm et al., 2006; Quijano-Scheggia et al., 2009), i.e. the nuclear-encoded large subunit (LSU) ribosomal rRNA gene (Lundholm et al., 2002), internal transcribed spacer (ITS) (Lundholm et al., 2006, 2012 ; Lim et al., 2012a, 2012b, 2013; Orive et al., 2013; Teng et al., 2014, 2015), mitochondrial-encoded cytochrome c oxidase 1 (*cox*1) (Kaczmarska et al., 2008; Lundholm et al., 2012), chloroplast-encoded large subunit of ribulose-1, 5-biophosphate carboxylase/oxygenase (RUBISCO/ *rbcL*) (Amato et al., 2007; Casteleyn et al., 2009), and 18S ribosomal RNA (18S rRNA) (Lim et al., 2016).

2.2.3 Toxicology of *Pseudo-nitzschia*

Diatom *Pseudo-nitzschia* was classified as a harmful diatom after the bloom *P. multiseries* (Hasle) Hasle and the first incident of ASP in year 1987 at Prince Edward Island (Bates et al., 1989). The number of *Pseudo-nitzschia* species is increasing abruptly in the past two decades (Figure 2.3); currently this genus comprises 49 species of which one third of the species were known to be DA producer, i.e. *P. australis* (0.0002–37.0 pg DA/cell) (Garrison et al., 1992; Rhodes et al., 1996; Cusack et al., 2002; Álvarez et al., 2009; Gunnel et al., 2011), *P. brasiliana* (0.0095 pg DA/cell) (Sahraoui et al., 2011), *P. calliantha* (0.0057–0.221 pg DA/cell) (Martin et al., 1990; Lundholm et al., 1997; Álvarez et al., 2009; Thessen et al., 2009), *P. cuspidata* (0.0029–0.0312 pg DA/cell) (Lundholm et al., 2012), *P. delicatissima* (0.0002–0.12 pg DA/cell) (Rhodes et al., 1998; Baugh et al., 2006), *P. fraudulenta* (0.0008–0.03 pg DA/cell) (Rhodes et al., 1998; Thessen et al., 2009), *P. fukuyoi* (3.85–4.54 pg DA/cell) (Dao et

al., 2015), *P. galaxiae* (0.00036 pg DA/cell) (Cerino et al., 2005), *P. granii* (0.000004 pg DA/cell) (Trick et al., 2010), *P. kodamae* (1.2–42.5 pg DA/cell) (Teng et al., 2014), *P. multiseries* (0.261–144.0 pg DA/cell) (Bates et al., 1989, 1991, 1999; Vrieling et al., 1996; Rhodes et al., 1998; Baugh et al., 2006; Orlova et al., 2008; Trimborn et al., 2008; Thessen et al., 2009), *P. multistriata* (0.28–0.697 pg DA/cell) (Sarno & Dahlmann, 2000; Orsini et al., 2002; Amato et al., 2010), *P. plurisecta* (0.0086–0.13 pg DA/cell) (Fernandes et al., 2014), *P. pseudodelicatissima* (0.007–0.221 pg DA/cell) (Martin et al., 1990; Rhodes et al., 1996; Lundholm et al., 1997), *P. pungens* (0.0018–0.47 pg DA/cell) (Rhodes et al., 1996; Baugh et al., 2006), *P. seriata* (1.93–33.6 pg DA/cell) (Lundholm et al., 1994; Fehling et al., 2004; Hansen et al., 2011), *P. simmulans* (0.00105–0.00154 pg DA/cell) (Li et al., 2017), *P. subpacifica* (0.06–1.1 ng DA/mL) (Fernandes et al., 2014) and *P. turgidula* (0.0000052–0.033 pg DA/cell) (Rhodes et al., 1996; Trick et al., 2010). Although *P. brasiliana* and *P. pungens* were reported as DA producer (Rhodes et al., 1996; Baugh et al., 2006; Sahraoui et al., 2011), but strains from Malaysian waters shown undetectable of DA (Lim et al., 2010).

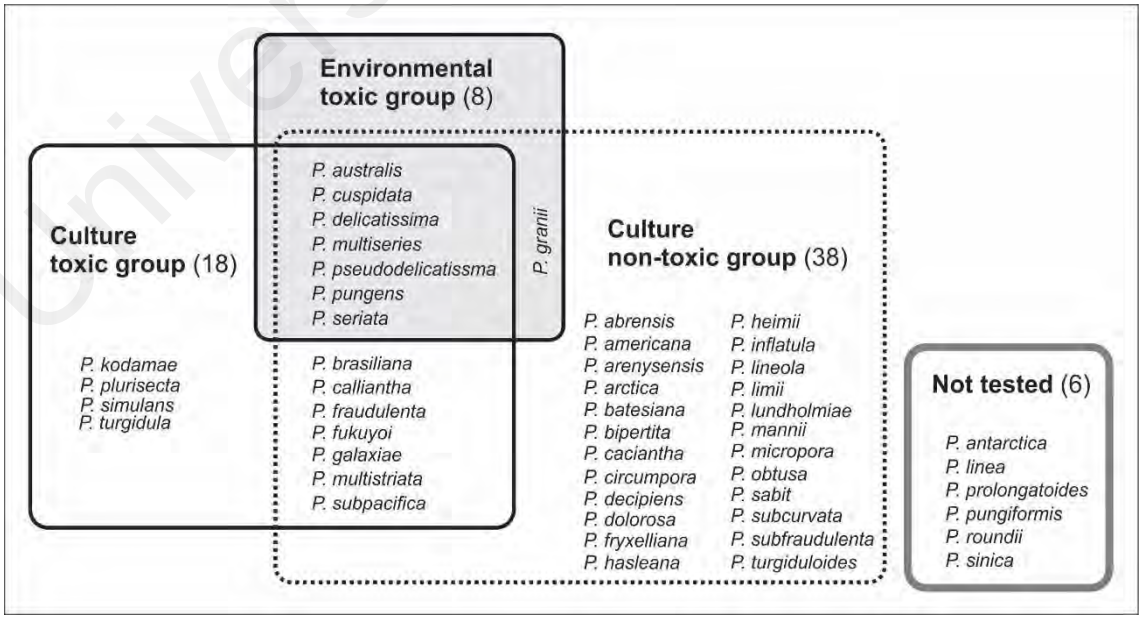

Figure 2.3: Venn diagram of all known Pseudo-nitzschia species, showing their ability to produce domoic acid in culture and/ or from environmental samples

(Teng et al., 2014, 2015, 2016; Percopo et al., 2016; Li et al., 2017), bringing the total to 49 species (Source: updated from Teng et al., 2014).

2.2.4 *Pseudo-nitzschia* in the Western Pacific region

There is no reported case of human illness associated with DA reported in Western Pacific region. A total of 38 species of *Pseudo-nitzschia* have been reported in Western Pacific countries; Malaysia (29 species), China (17 species), South Korea (15 species), Vietnam (14 species), Japan (12 species), Thailand (8 species), Philippine (5 species), Singapore (2 species) and Indonesia (1 species) (Table 2.2). Low number of species reported in some countries in South China sea was probably due to limited study effort on this group of diatom.

In Malaysia, high species diversity of *Pseudo-nitzschia* species in Malaysian coastal waters were reported, with a total of 29 species documented. Among the 29 species, eight species have been identified from the waters as new morphotypes and described as *P. batesiana* H. C. Lim, Teng, Leaw *et* P.T. Lim reported from Teluk Batik, Perak, Malacca strait (Lim et al., 2013), *P. bipertita* S.T. Teng, Lim, *et* C. P. Leaw from Miri, Sarawak (Teng et al., 2016), *P. circumpora* H. C. Lim, Teng, Leaw *et* P. T. Lim from Kuching coastal of Borneo (Lim et al., 2012), *P. fukuyoi* H. C. Lim, Teng, Leaw *et* P. T. Lim from Teluk Batik, Perak, Malacca Strait (Lim et al., 2013), *P. kodamae* S. T. Teng, Lim, Leaw *et* P. T. Lim from Port Dickson, Negeri Sembilan, Malacca strait (Teng et al., 2014), *P. limii* S.T. Teng, Lim, *et* C. P. Leaw from Miri, Sarawak (Teng et al., 2016), *P. lundholmiae* H. C. Lim, Teng, Leaw *et* P.T. Lim from Teluk Batik, Perak, Malacca Strait (Lim et al., 2013) and *P. sabit* S.T.Teng, H.C.Lim, C.P.Leaw & P.T.Lim reported from Port Dickson, Malacca strait (Teng et al., 2015); *P. kodamae* was first highly toxic species reported in South East Asia (1.2–42.5 pg DA cell^{-1}) (Teng et al., 2014); while others are non-toxic (Lim et al., 2012a, 2013; Teng et al., 2015, 2016).

Several studies reported the DA contamination of bivalve shellfish especially in Vietnam (Dao et al. 2006, 2009). However, no evidence showed that *Pseudo-nitzschia* was the DA producer in shellfish contamination. The two species reported, *P.* cf. *caciantha* and *P. fukuyoi* were proven to be toxic only in laboratory culture experiments (Dao et al. 2014, 2015).

Table 2.2: *Pseudo-nitzschia* species reported in the Western Pacific region.

Country	Species	Total number of species found	References
China	*P. americana*, *P. brasiliana*, *P. caciantha*, *P. calliantha*, *P. cuspidata*, *P. delicatissima*, *P.* cf. *lineola*, *P. mannii*, *P. multiseries*, *P. multistriata*, *P. pseudodelicatissima*, *P. pungens*, *P. seriata*, *P. simulans*, *P. sinica*, *P. subfraudulenta*, *P. subpacifica*	17	Villac & Fryxell, 1998; Liu et al., 2008; Lu et al., 2012; Wang et al., 2012; Kim et al., 2015; Li et al., 2017
Japan	*P. americana*, *P. brasiliana*, *P. caciantha*, *P. calliantha*, *P. delicatissima*, *P. galaxiae*, *P. fraudulenta*, *P. hasleana*, *P. multiseries*, *P. multistriata*, *P. pseudodelicatissima*, *P. pungens*	12	Villac & Fryxell, 1998; Kotaki et al., 1999; Lundholm et al., 2002b, 2006, 2012; Hasle & Lundholm, 2005; Casteleyn et al., 2008; Quijano-Scheggia et al., 2009; Yap-Dejeto et al., 2010; Sugie & Yoshimura, 2013
Indonesia	*P. brasiliana*	1	Lundholm et al., 2002b
Malaysia	*P. abrensis*, *P. americana*, *P. brasiliana*, *P. arenysensis*, *P. batesiana*, *P. bipertita*, *P. caciantha*, *P. calliantha*, *P. circumpora*, *P. cuspidata*, *P. decipiens*, *P. delicatissima*, *P. dolorosa*, *P. fukuyoi*, *P. hasleana*, *P. inflatula*, *P. kodamae*, *P. limii*, *P. linea*, *P. lineola*, *P. lundholmiae*, *P. mannii*, *P. micropora*, *P. multistriata*, *P. pseudodelicatissima*, *P. pungens*, *P. sabit*, *P. subfraudulenta*, *P. turgidula*	29	Lundholm et al., 2002b; Lim et al., 2012, 2013; Teng et al., 2013, 2015, 2016
Philippines	*P. brasiliana*, *P. caciantha*, *P. micropora*, *P. pseudodelicatissima*, *P. pungens*	5	Bajarias et al., 2006; Yap-Dejeto et al., 2013; Kim et al., 2015

Table 2.2, continued.

Country	Species	Total number of species found	References
South Korea	*P. americana*, *P. brasiliana*, *P. caciantha*, *P. calliantha*, *P. cuspidata*, *P. delicatissima*, *P. granii*, *P. micropora*, *P. multiseries*, *P. multistriata*, *P. pseudodelicatissima*, *P. pungens*, *P. seriata*, *P. subfraudulenta*, *P. subpacifica*.	15	Cho et al., 2001; Lundholm et al., 2002b, 2006; Hasle & Lundholm, 2005; Park et al., 2009; Kim et al., 2015; Jeong et al., 2017
Singapore	*P. pungens*, *P. seriata*	2	Pham et al., 2011
Thailand	*P. brasiliana*, *P. caciantha*, *P. cuspidata*, *P. delicatissima*, *P. heimii*, *P. inflatula*, *P. micropora*, *P. pseudodelicatissima*	8	Lundholm et al., 2002b, 2003, 2006; Priisholm et al., 2002; Quijano-Scheggia et al., 2009
Vietnam	*P. americana*, *P. brasiliana*, *P.* cf. *caciantha*, *P. calliantha*, *P. cuspidata*, *P. delicatissima*, *P. fukuyoi*, *P.* cf. *granii*, *P. inflatula*, *P. micropora*, *P. multistriata*, *P. pungens*, *P.* cf. *sinica*, *P. subfraudulenta*	14	Lundholm et al., 2002b, 2003, 2006; Larsen & Nguyen, 2004; Hasle & Lundholm, 2005; Quijano-Scheggia et al., 2009; Dao et al., 2014, 2015

2.3 The genus *Nitzschia*

The genus *Nitzschia* Hassall, 1845 is large and complex with 1091 valid species nomenclaturally, and 792 species have been flagged as currently accepted taxonomically (Guiry & Guiry, 2018). The genus *Nitzschia* is commonly found in a variety of environments: brackish, freshwater, mangrove areas or muddy areas and marine waters. It comprises both planktonic and benthic species. The genus *Nitzschia* was divided into six groups (Smith, 1853) but Grunow (1862) further subdivided the genus into twenty-four groups (in Cleve & Grunow, 1880). Grunow's system is still in use with some modifications (e.g. Lange-Bertalot & Simonsen, 1978; Mann, 1986; Round et al., 1990).

Nitzschia taxonomy is rather more complicated and confusing due to a large number of species. This genus is typically based on frustule morphology (Figure 2.1) and raphe, which only can be observed under electron microscope. Molecular tools are important to better understand the phylogenetic relationships among taxa of this genus, as the genus of *Pseudo-nitzschia* has been well studied among the taxa by using molecular tools (Lundholm et al., 2002a, 2003, 2006, 2012; Amato & Monstresor, 2008; Lim et al., 2013). However, there are less studies on *Nitzschia* phylogeny, i.e. LSU rDNA (Lundholm et al., 2002; Trobajo et al., 2006, 2010; Bouchouicha-Smida et al., 2014; Carballeira et al., 2017), nuclear small-subunit (SSU) (Bouchouicha-Smida et al., 2014), 18S rDNA (Rimet et al., 2011), rbcL (Trobajo et al., 2010; Carballeira et al., 2017), and *cox*1 (Trobajo et al., 2010). The phylogenetic studied showing the genus is polyphyletic (Lundholm et al., 2002; Trobajo et al., 2009; Rimet et al., 2011). Due to the uncertainties of taxonomic in *Nitzschia*, details morphological characteristics (Figure 2.1–2.2, 2.4) together with phylogenetics analyses are important when exploring the species identification.

2.3.1 Toxicology of *Nitzschia*

There are only two *Nitzschia* were found to be toxic, *N. navis-varingica* (0.04–15.3 pg DA/cell) (Kotaki et al., 2000, 2004, 2005, 2006, 2008 Bajarias et al., 2006; Romero et al., 2008, 2011) and *N. bitzertensis* (0.0002–0.036 pg DA/cell) (Bouchouicha Smida et al., 2014). DA and its isomers, isodomoic acid A (IA) and isodomoic acid B (IB) were detected in *N. navis-varingica* (Kotaki et al., 2005).

2.3.2 Taxonomy of DA producers, *Nitzschia navis-varingica* Lundholm et Moestrup and *Nitzschia bitzertensis* Smida, Lundholmm, Sakka, Hadj Mabrouk

The cells of *Nitzschia navis-varingica* and *N. bitzertensis* are yellow-brown and with two chloroplasts when observed under light microscope (LM). Both *Nitzschia* species are rectangular in girdle view. However, the valve of cells are lanceolate in *N. navis-varingica* but linear to lanceolate and valve appearing sigmoid in *N. bitzertensis*. The raphe of *N. navis-varingica* raised on a distinct keel, with the margins of the raphe slit extended as lips that flap outward distally but the canal raphe of *N. bitzertensis* is extremely eccentric, situated on the edge of the valve. For *N. navis-varingica*, the wall of raphe canal perforated by areolae and bearing longitudinal silica ridges (Figure 2.4a). In *N. bitzertensis*, the wall of raphe canal also perforated by areolae and the raphe consists of two parallel raphe slits under TEM (Figure 2.4b). The raphe for both species are divided by a central nodule; subtended by more or less equidistant and distinct fibulae in *N. navis-varingica* but irregularly spaced in *N. bitzertensis*. Morphological characteristics of these two cells are shown in Table 2.3.

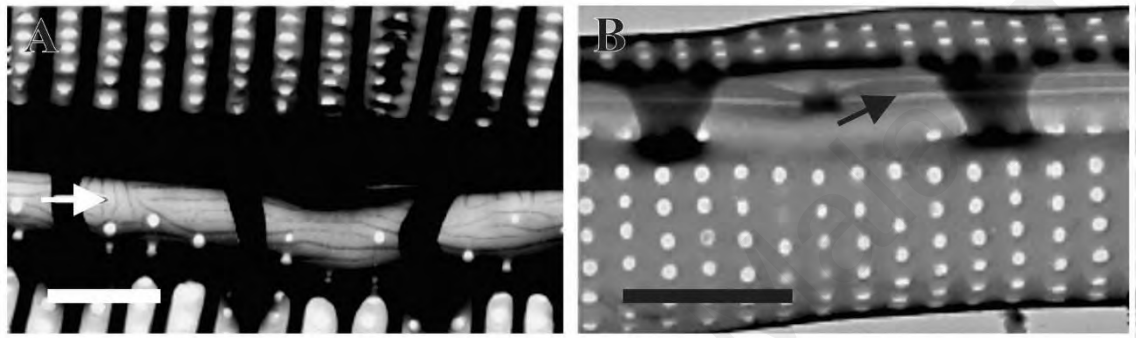

Figure 2.4: TEM. (A) *N. navis-varingica*. Central part of the valve with central raphe endings. Arrow indicates pattern of silica ridges on the wall of the raphe canal. (B) *N. bitzertensis*. Central part of the valve showing central nodule and central interspace. Arrow indicates two parallel raphe slits. (Source: Adapted from Lundholm & Moestrup, 2000; Bouchouicha Smida et al., 2014).

Table 2.3: Morphological characteristics of *N. navis-varingica* and *N. bitzertensis* (Lundholm & Moestrup, 2000; Bouchouicha Smida et al., 2014).

Species	Transapical axis (µm)	Apical axis (µm)	Central interspace	Fibulae/ 10 µm	Striae/ 10 µm	Poroids/ 1 µm	Rows of poroids	Cingular bands	Reference
N. navis-varingica	45–55	9–11	+	10–12	26–30	3–4	1	2−3	Lundholm & Moestrup, 2000)
N. bitzertensis	32.5–81.7	1.4–2.9	+	7.6–18.6	44.1–53.2	3.9–7.7	1	5.3–9.5	Bouchouicha Smida et al., 2014

2.3.4 *Nitzschia navis-varingica* in the Western Pacific region

In the Western Pacific region, ASP has never been reported. Studies on DA-producing diatoms are focused mainly on the species of *Pseudo-nitzschia*, very few studies have been conducted on *N. navis-varingica*. The toxigenic species was first found in shrimp-culture ponds in Vietnam (Kotaki et al., 2000), and later from brackish waters and estuaries of the Southeast Asian waters (Kotaki et al., 2004, 2005, 2006, 2008; Bajarias et al., 2006; Romero et al., 2008, 2011, 2012; Takata et al., 2009; Thoha et al., 2012) (Figure 2.5). In earlier studies on *N. navis-varingica*, toxin analysis was limited only for DA (Kotaki et al., 2000, 2004), but not the isomers of DA. Subsequent studies, however, isomers had been included in the analyses (Kotaki et al., 2005, 2006, 2008; Romero et al., 2008, 2011; Thoha et al., 2012). In 2008, *Nitzschia*-like diatom species was reported in Kota Kinabalu, Sabah with did not show DA production (Thoha et al., 2012).

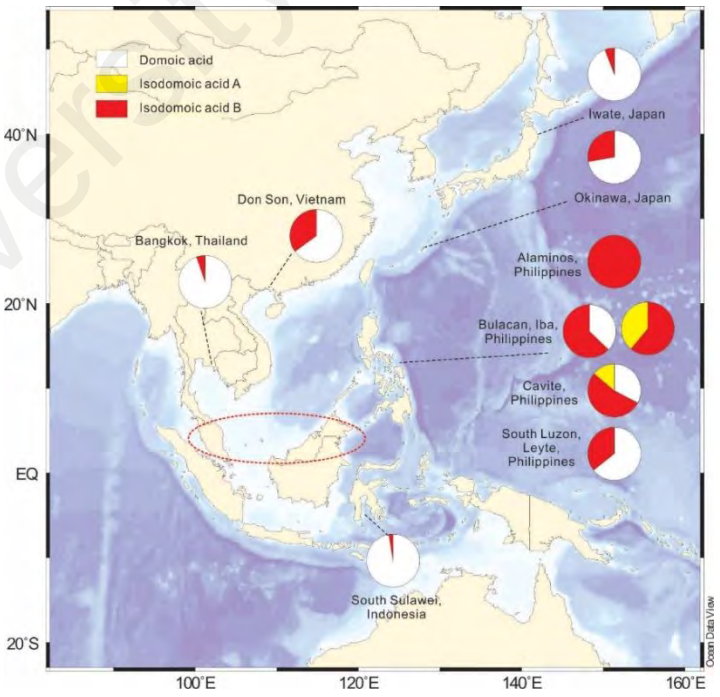

Figure 2.5: Distribution of *N. navis-varingica* in the Western Pacific region, with their toxin compositions as shown in the pie charts. The oval with dashed line indicate no toxin data from Malaysian waters (Kotaki et al., 2005, 2008; Bajarias et al., 2006; Romero et al., 2008, 2011).

CHAPTER 3: PHYLOGENY AND SPECIES DELINEATION IN THE MARINE DIATOM *PSEUDO-NITZSCHIA* (BACILLARIOPHYCEAE): A PERSPECTIVE IN CHARACTER EVOLUTION

3.1 Introduction

The taxonomic status of *Pseudo-nitzschia* (Peragallo, 1900) was revisited in the 1990s by Hasle (1994), who raised it to a new genus distinct from *Nitzschia* Hassall 1845, with *P. seriata* as the type species (Fryxell et al., 1991). The traditional identification of *Pseudo-nitzschia* species was based solely on the use of morphological characters. With the discovery of several new species, it became necessary to describe and compare additional detailed ultrastructural characters, e.g., types of poroids and details of cingular bands (Lundholm et al., 2003, 2006, 2012; Quijano-Scheggia et al., 2009; Lim et al., 2012a, 2013; Orive et al., 2013; Teng et al., 2014, 2015, 2016; Li et al., 2017).

At the same time, cryptic and pseudo-cryptic species were discovered, especially in the *P. pseudodelicatissima* complex sensu (one row of complex poroids) Lundholm et al. (2003) and in the *P. delicatissima* complex sensu (two rows of simple poroids) Lundholm et al. (2006). This made species identifications based only on morphological characters problematic, especially when identifying species in environmental samples, as well as cryptic species, which is not possible using morphology. For example, information on the ultrastructure of cingular bands is especially important when identifying species to the sub-species level, e.g., differentiating *P. pungens* var. *pungens*, *P. pungens* var. *cingulata* and *P. pungens* var. *aveirensis* (Villac & Fryxell 1998; Churro et al., 2009).

Advances in molecular characterization helped to alleviate these drawbacks, but selecting the appropriate genetic markers is crucial. In the early 2000s, molecular data was first incorporated to infer *Pseudo-nitzschia* phylogeny, in particular the nuclear-encoded large subunit ribosomal DNA (LSU; Lundholm et al., 2002a). Later, the ITS1-5.8S-ITS2 region was sequenced (Lundholm et al., 2003). Information on compensatory base changes (CBCs) from the ITS2 secondary-structure was then further explored (Amato et al., 2007; Orive et al., 2010). Owing to the molecular approaches, more cryptic and pseudo-cryptic diversity was discovered, which called for more detailed morphometric analyses (Amato & Montresor, 2008; Quijano-Scheggia et al., 2009; Lim et al., 2012, 2013; Lundholm et al., 2013; Orive et al., 2013; Teng et al., 2014, 2016; Li et al., 2017). The resolution of using LSU for *Pseudo-nitzschia* phylogeny is limited and alignment of the diverse ITS1-5.8S-ITS2 sequences is rather difficult (Lim et al., 2013). In an effort to improve the *Pseudo-nitzschia* phylogenetic relationship, ITS2 with sequence-structure information was used to infer the phylogeny (Lim et al., 2012a, 2013; Teng et al., 2014, 2015, 2016). Meanwhile, the cytochrome *c* oxidase subunit 1 gene (*cox1*) and SSU have only been used in a few studies (Lundholm et al., 2012; Lim et al., 2016). Little is known, however, about the evolution of the morphological characters of *Pseudo-nitzschia*, although evaluation of taxonomic-informative characters has previously been attempted (Orsini et al., 2002; Lim et al., 2013; Teng et al., 2013).

In this study, a pair of primers targeting *cox*1 of *Pseudo-nitzschia* was developed in silico, in-lab tested and used in phylogenetic reconstructions. This is because the primer sets that used previously in *Pseudo-nitzschia* studies (Lundholm et al., 2012) did not yield positive results in our attempt for tropical *Pseudo-nitzschia* strains. In this study, we incorporate nearly all of the currently available *Pseudo-nitzschia* sequences after a comprehensive sampling of the different species. Phylogenies were constructed

based on *cox1*, LSU and ITS2 datasets. We mapped the morphological data of each strain onto the ITS2 phylogenetic tree to elucidate the morphological character evolution. Here we use *cox1*, LSU and ITS2 to re-examine phylogenetic relationships in *Pseudo-nitzschia* in order to determine if the morphologically based species complexes in *Pseudo-nitzschia* show congruency in a phylogenetic context.

3.2 Literature Review

Identification of *Pseudo-nitzschia* species was based mainly on morphological evidence before year 2000; but rapidly evolved with the introduction of molecular technique (Lundholm et al., 2003, 2006, 2012; Quijano-Scheggia et al., 2009; Lim et al., 2012a, 2013; Orive et al., 2013; Teng et al., 2014, 2015; Li et al., 2017). Several laboratory mating experiments of *Pseudo-nitzschia* also supported the biological species concept and bridged the gap of understanding between morphological and molecular approaches (e.g., Amato et al., 2007; Quijano-Scheggia et al., 2009).

The phylogeny of *Pseudo-nitzschia* has been studied for the last two decades using the LSU, the whole region of ITS1-5.8S-ITS2 and the ITS2 sequences (with or without sequence-structure information for phylogenetic inferences). Molecular species characterization using nucleotide sequences of the nuclear-encoded large-subunit (LSU) ribosomal DNA (rDNA) and the internal transcribed spacer region (ITS1-5.8S-ITS2) has become an essential supporting criteria in species delineation (Lundholm et al., 2002a, 2006; Orsini et al., 2002; Amato & Montresor, 2008; Lim et al., 2012; Orive et al., 2013; Teng et al., 2014, 2015). The *rbcL*, *cox1,* and 18S rRNA genes have also been explored in recent *Pseudo-nitzschia* studies (Amato et al., 2007; Casteleyn et al., 2009; Lundholm et al., 2012; Lim et al., 2016).

Other molecular techniques used in *Pseudo-nitzschia* studies included the automated ribosomal intergenic spacer analysis (ARISA) (Hubbard et al., 2008, 2014; Quijano-Scheggia et al., 2009); rapid whole-cell detection using fluorescence *in-situ* hybridization (FISH) (Miller & Scholin, 1996, 1998; Parsons et al., 1999; Scholin et al., 1999; Lundholm et al., 2006); and the development of species-specific microsatellite markers for population genetics (Cerino et al., 2005; Evans et al., 2007).

3.3 Materials and Methods

3.3.1 Culture collection

A total of 15 strains of *Pseudo-nitzschia* (belonging to *P. batesiana*, *P. bipertita*, *P. brasiliana*, *P. circumpora*, *P. cuspidate*, *P. fukuyoi* and *P. pungens*) were newly isolated and established from Miri and Bintulu coasts of Sarawak (Malaysian Borneo), Port Dickson coast of Negeri Sembilan (Peninsular Malaysia) and St. John's Island (Singapore). Some cultured material used in this study was obtained from that previously established by Lim et al. (2012a, 2012b, 2013), Lundholm et al. (2012), Orive et al. (2013), and Teng et al. (2014, 2015, 2016). Detailed information on the strains used is listed in Appendix A. In general, plankton samples were collected with 10 μm mesh size plankton net. Live samples were kept in 500 mL bottles and brought back to the laboratory for single-cell isolation. Samples were observed under an Olympus IX51inverted light microscope (Olympus, Japan) for genus confirmation. Single-cell isolation was performed with a micropipette and cultures were established and maintain in f/2 medium (Guillard & Ryther 1962), with a salinity of 30. The cultures were maintained in a temperature-controlled incubator (SHEL LAB, Cornelius, OR, USA) at 25°C, with a 12:12 h light:dark (L:D) photoperiod, and a photon flux density of 100 μmol photons m^{-2} s^{-1}.

3.3.2 Morphological observation

Morphology of *Pseudo-nitzschia* species was observed under a transmission electron microscope (TEM). Prior to TEM observation, samples were undergone acid wash as described in Teng et al. (2013). One drop of acid wash-cleaned cells was then transferred onto a Formvar®-coated copper grid, air dried and observed under a JEOL JEM-1230 TEM (JEOL, Tokyo, Japan). Detailed morphometric information such as cell length, width, densities of striae, fibulae, and poroids, and perforation were obtained via TEM.

3.3.3 *In silico* oligonucleotide primer design targeting *cox*1

Taxon sampling was performed to retrieve the *cox*1 sequences of *Pseudo-nitzschia* species from NCBI GenBank nucleotide database (Table 3.1). The sequences were then multiple-aligned using the program Clustal X ver. 2.0 (Thompson et al., 1997), and manually checked for possible signature regions that can be used for primer design (Appendix B).

Table 3.1: *Pseudo-nitzschia* nucleotide sequences of COI gene used for primer design. The sequences were retrieved from Genbank with the species, strain, accession, and references.

Species	Strain	Accession	References
Pseudo-nitzschia cuspidata	NWFSC 194	JN050306	Lundholm *et al.,* 2012
Pseudo-nitzschia cuspidata	Sydney1	JN050307	Lundholm *et al.,* 2012
Pseudo-nitzschia fryxelliana	NWFSC 241	JN050308	Lundholm *et al.,* 2012
Pseudo-nitzschia fryxelliana	NWFSC 242	JN050309	Lundholm *et al.,* 2012
Pseudo-nitzschia hasleana	NWFSC 186	JN050310	Lundholm *et al.,* 2012
Pseudo-nitzschia hasleana	NWFSC 252	JN050311	Lundholm *et al.,* 2012
Pseudo-nitzschia lineola	NWFSC 188	JN050312	Lundholm *et al.,* 2012
Pseudo-nitzschia subcurvata	CCMP:1431	HQ317087	Hamsher *et al.,* 2011
Pseudo-nitzschia subcurvata	CCMP:1437	HQ317088	Hamsher *et al.,* 2011

The primer pairs were designed using OligoAnalyzer 3.1 (Owczarzy et al., 2008; http://eu.idtdna.com/analyzer/Applications/OligoAnalyzer/). Parameters used in the *in silico* primer design including the length of primers (18–30 bp), primer melting temperature (52–72°C), G/C concentration (40–60%), contiguous bases, hairpin structure (more than -9 kcal/mole) and G/C repeats at the 3′ end. A confirmatory test was performed using nucleotide BLAST (nblast) search in NCBI database. The primer was then tested using genomic DNAs extracted from *Pseudo-nitzschia* cultured strains. The designated primer pair targeted the *cox*1 region partially.

3.3.4 DNA extraction, PCR amplification, and sequencing

Newly established strains of *Pseudo-nitzschia* were harvested during the exponential phase, using centrifugation (9300*g* for 10 min). The DNA was extracted as in Lim et al. (2012b). Approximately 80 μg · μL^{-1} of the DNA extract was added to each of the 25 μL PCR reactions. Three molecular markers were sequenced: mitochondrial cytochrome *c* oxidase subunit 1 (*cox1*), the internal transcribed spacer (ITS1-5.8S-ITS2) and the nuclear-encoded large subunit (D1-D3 of LSU region). Gene amplification was performed using an Eppendorf Gradient thermocycler (Eppendorf, Germany). The PCR running conditions for *cox1* were pre-denaturation at 94°C for 5 min, followed by 35 cycles of 94°C for 45 s, 61°C for 30 s, and 72°C for 45 s, and a final extension at 72°C for 10 min. The ITS and LSU rRNA genes amplifications were performed using the primer pairs ITS1 and ITS4 (White et al., 1990), and D1R and D3Ca (Scholin et al., 1994), respectively. The amplicons were purified using the Wizard® PCR Preps DNA Purification kit according to the manufacturer's instructions (Promega, Madison, WI, USA). The purified PCR amplicons were directly sequenced for both strands by First Base Laboratories (Selangor, Malaysia). The obtained sequences were deposited in GenBank (Appendix A).

3.3.5 Mitochondrial *cox*1 and LSU rRNA region datasets

The *cox1* dataset consisted of 60 sequences with *Eunotia* sp. (EF164960) as outgroup. For the LSU dataset, 142 sequences were compiled, with four outgroup sequences from *N. frustulum*, *N. navis-varingica*, *N. pellucida,* and *Bacillaria paxillifer*. The selection of outgroup sequences was based on Lundholm et al. (2002a), Lim et al. (2012a) and Ashworth et al. (2013). The criteria for selecting available sequences include: 1) sequences obtained from the type strain, 2) sequences must have enough nucleotides after alignment (*cox1* >500 bp, LSU >700 bp and ITS2 >350 bp), and 3) absence of ambiguous nucleotides (other than A, G, C, T) in the sequence. Sequences that did not meet the criteria were excluded from the analyses. Sequence data for *cox1* and LSU obtained in this study and sequences retrieved from the NCBI GenBank nucleotide database were aligned using MUSCLE (Multiple Sequence Comparison by Log-Expectation; Edgar, 2004a, b).

Three independent analyses were used to construct the *cox1* and LSU phylogenies: maximum parsimony (MP), maximum likelihood (ML) and Bayesian inference (BI). MP and ML analyses were carried out using PAUP* V4.0b10 (Swofford, 2001). MP trees were obtained using the stepwise-addition (SA), tree bisection-reconnection (TBR) branch-swapping algorithms and heuristic searches with random addition of sequences (1,000 replications). The robustness of the clades recovered was evaluated by 1,000 bootstrap replicates (10 random addition sequence replicates per bootstrap replicate). The Akaike information criterion (AIC) implemented in jModelTest 2 (Posada, 2008; Darriba et al., 2012) was used to obtain the optimal substitution and rate heterogeneity model for the ML and BI analyses. ML was carried out with the selected model using PAUP, starting with 100 random-addition replicates and heuristic searches with stepwise-addition, plus TBR branch-swapping and 500

bootstrap replicates (with 1 random addition of sequence run per bootstrap replicate). Bayesian analyses were carried out using MrBayes v3.2.5 (Ronquist & Huelsenbeck, 2003) with 10,000,000 and 3,000,000 Markov chain Monte Carlo (MCMC) generations for the *cox1* and LSU datasets, respectively. The convergence of the runs, i.e., the effective sample size (ESS), was checked using Bayesian Evolutionary Analysis Sampling Trees (BEAST) (Drummond et al., 2012) and Tracer (http://beast.bio.ed.ac.uk/tracer). The 50% majority rule consensus tree was constructed using a burn-in of 25% and posterior probabilities were calculated to measure tree strength.

3.3.6 ITS2 dataset

Only ITS2 of the ITS region was used in this study as the conserved secondary structure of ITS2 can be used to guide the sequence alignment (Coleman, 2003, 2007, 2009; Keller et al., 2010). The ITS2 transcripts from previous studies were used as a template in the ITS2 database (Wolf et al., 2005; Schultz et al., 2006; Selig et al., 2008; Koetschan et al., 2010; Ankenbrand et al., 2015) for homology modeling folding of newly obtained *Pseudo-nitzschia* ITS2 sequences, as well as for outgroup sequences (obtained from GenBank). The sub-optimal helices were manually refolded using RNAStructure ver. 5.6 (Mathews, 2014) and the structures were checked with VARNA (Darty et al., 2009). The ITS2 dataset comprised 172 sequences, including *Nitzschia longissima* as outgroup. The ITS2 sequence-structure dataset was synchronously aligned using 4SALE 1.7 (Seibel et al., 2006, 2008). These sequences, guided by dot-bracket notation corresponding to the secondary structure information, were aligned and saved in two formats: a) one letter encoded/pseudo-protein (12 × 12 scoring matrix) as described in Wolf et al. (2014), and b) sequences only. Similarly, the ITS2 dataset was analyzed using MP, ML and BI phylogenetic analyses. In this context, the aligned data

file guided by secondary structure information of ITS2 was saved in one letter encoded format for MP/ML and sequences only for BI analyses. The MP and BI analyses of ITS2 were performed as described for the *cox1* and LSU dataset analyses. An ML tree based on the aligned dataset in one letter encoded format was calculated using R (R Core Team, 2014); the R script is available at http://4sale.bioapps.biozentrum.uniwuerzburg.de/mlseqstr.html. Phangorn (Schliep, 2011) was used to estimate the model parameters directly from the dataset. Bootstrap supports were obtained based on 100 replicates.

3.3.7 Genetic distance and character evolution

The pairwise genetic distances, based on *p*-distance, were estimated using MEGA5 (Tamura et al., 2011). The estimated *p*-distances for the three genetic markers were further illustrated using pheatmap (Kolde, 2015) as implemented in the statistical framework R. For analysis of character evolution, the character matrix was constructed using NEXUS Data Editor ver. 0.5.0 (Roderic, 2001). Seven morphological characters (central nodule, number of rows of poroids, number of sectors in poroids, number of fibulae vs. striae in 10 μm, the shape of valve, the shape of apices, and density of band striae in 10 μm) were given equal weight and treated as unordered. The character matrix was then used to map the evolution of character state onto the ITS2 BI tree using Mesquite ver. 3.2 (Maddison & Maddison, 2017).

3.4 Results

3.4.1 Morphological observation

15 *Pseudo-nitzschia* clonal cultures were established in this study. Here, we present the morphological data of *P. batesiana*, *P. bipertita*, *P. brasiliana*, *P. circumpora*, *P. cuspidate*, *P. fukuyoi* and *P. pungens* (Table 3.2, Figure 3.1–3.7).

Table 3.2: Morphometric data of *Pseudo-nitzschia* species obtained in this study.

Species	Strains	Transapical axis (µm)	Apical axis (µm)	Central interspace	Fibulae/ 10 µm	Striae/ 10 µm	Poroids/1 µm	Rows of poroids	Band striae/1 µm
P. batesiana	PnMi32	94.37–96.67	1.56–2.24						
	PnMi44	95.52±1.15 (*n*=15)	1.90±0.34 (*n*=15)	+	17–19	29–32	5–6	1	3–4
P. bipertita	PnMi108	96.30–98.64 97.47±1.17 (*n*=15)	2.56–2.94 2.75±0.19 (*n*=15)	+	16–18	28–29	5–7	2	3
P. brasiliana	PnPd34	40.01–41.53	2.14–2.36						
	PnPd35	40.77±0.76 (*n*=15)	2.25±0.11 (*n*=15)	–	21–23	23–24	7–8	2	5
P. circumpora	PnPd27	42.35–47.03 44.69±2.34 (*n*=30)	2.26–2.54 2.40±0.14 (*n*=30)	+	18–19	33–36	1–5	1	4
	PnPd29								

+, central interspace present, –, absent.

Table 3.2, continued.

Species	Strains	Transapical axis (µm)	Apical axis (µm)	Central interspace	Fibulae/ 10 µm	Striae/ 10 µm	Poroids/1 µm	Rows of poroids	Band striae/1 µm
P. cuspidata	PnSg10	32.51–45.95	1.33–1.51						
	PnPd29	39.23±6.72 (*n*=15)	1.42±0.09 (*n*=15)	+	17–19	34–37	5–6	1	5
P. fukuyoi	PnBi12	90.46–93.58	1.66–2.04						
	PnBi14	92.02±1.56 (*n*=15)	1.85±0.19 (*n*=15)	+	17–18	32–34	5–6	1	4
P. pungens	PnKL10	69.36–81.06	3.04–3.30						
	PnKL11	75.21±5.85 (*n*=78)	3.17±0.13 (*n*=78)						
	PnKL16								
	PnKL17								
	PnKL19			–	10–13	10–14	3–4	2	2–3
	PnKL22								
	PnKL29								
	PnKL36								

+, central interspace present, –, absent.

3.4.1.1 *Pseudo-nitzschia batesiana*

Morphology

Cells are lanceolate and symmetrical in valve view and linear-lanceolate in girdle view (Figure 3.1A). Transapical axis length is 94.37–96.67 µm and apical axis is 1.56–2.24 µm (Table 3.2). Valve apices are rounded (Figure 3.1B). A large central interspace with a central nodule is present (Figure 3.1C). The fibulae are irregularly spaced. The densities of fibulae and interstriae are 17–19 and 29–32 in 10 µm, respectively. Each stria contains one row of poroid with a density of 5–6 in 1 µm (Figure 3.1C). Each poroid contains two to three sectors and lacks a central sector. The density of band striae in the valvocopula is 3–4 in 1 µm (Figure 3.1D).

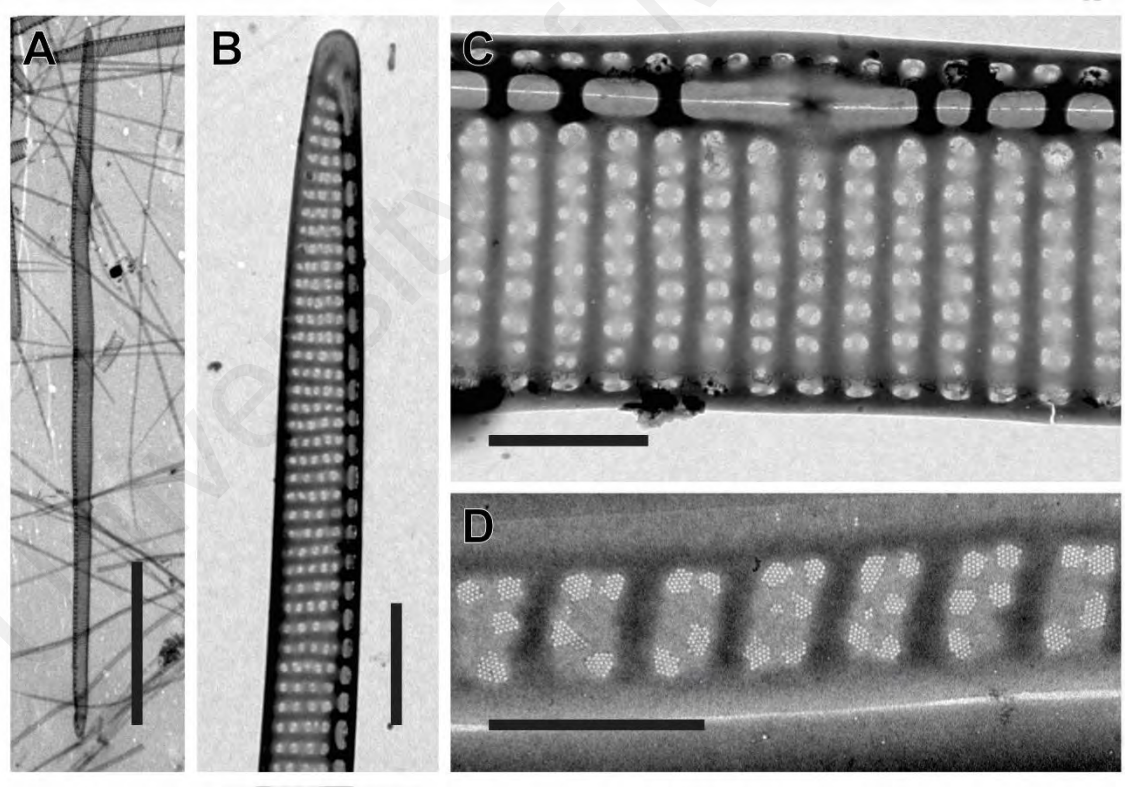

Figure 3.1: *Pseudo-nitzschia batesiana*. TEM. (A) Cell valve view, scale bar = 20 µm. (B) Valve ends, scale bar = 2 µm. (C) The central region of the valve showing the central interspace, valve mantle, striae, and poroid structure, scale bar = 1 µm. (D) Valvocopula band, scale bar = 0.5 µm.

3.4.1.2 *Pseudo-nitzschia bipertita*

Morphology

Cells are linear to lanceolate in valve view and lanceolate in girdle view (Figure 3.2A). Transapical axis length is 96.30–98.64 µm and apical axis is 2.56–2.94 µm (Table 3.2). Valve apices are pointed (Figure 3.2B). A central interspace with a central nodule is present (Figure 3.2C). The densities of fibulae and interstriae in 10 µm are 17–19 and 29–32, respectively. Each stria consist of two rows of poroids, with 5–7 poroids in 1 µm (Figure 3.2B–3.2D). Each poroid hymen is divided into 1–3 irregularly shaped sectors (Figure 3.2D). Two cingular bands (Valvocopula and second band) were observed and the band striae in the valvocopula is 3 in 1 µm (Figure 3.2E).

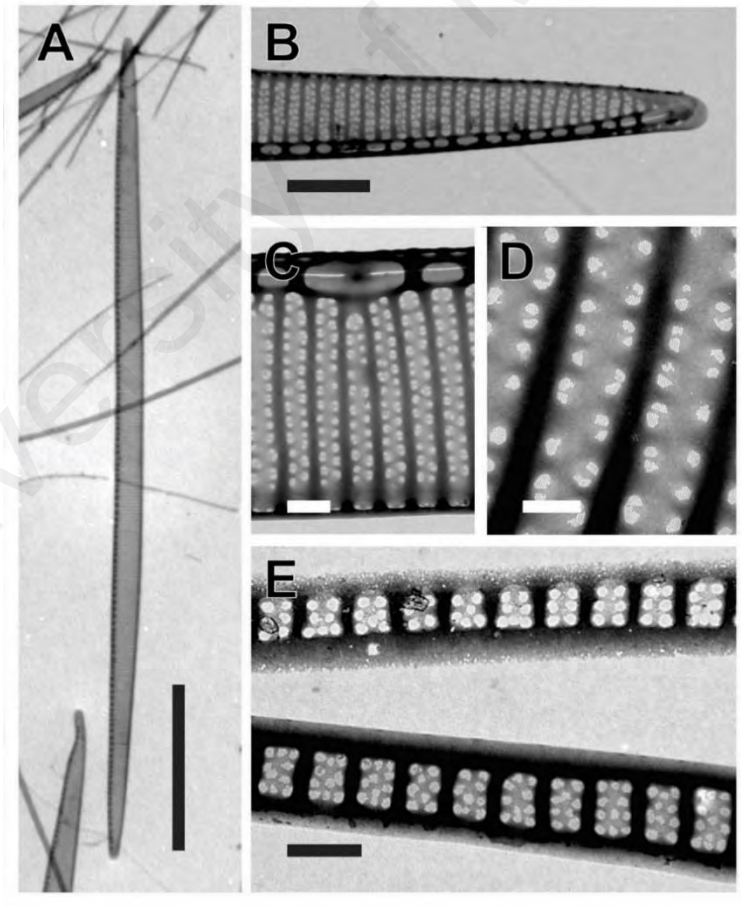

Figure 3.2: *Pseudo-nitzschia bipertita*. TEM. (A) Cell valve view, scale bar = 20 µm. (B) Valve ends, scale bar = 2 µm. (C) Striae, poroid structure of valve and mantle, central interspace present, scale bar = 0.5 µm. (D) Detail of poroid hymen, scale bar = 0.5 µm. (E) Details of cingulum. Valvocopula and second band, scale bar = 0.5 µm.

3.4.1.3 *Pseudo-nitzschia brasiliana*

Morphology

Cells are lanceolate in valve view, (Figure 3.3A), 40.01–41.53 µm long and 2.14–2.36 µm wide (Table 3.2). Valve apices are broadly rounded (Figure 3.3B). Central interspace is absent (Figure 3.3C). Densities of fibulae (21–23) and striae (23–24) are almost equal in 10 µm. Each stria consists of two rows of poroids (Figure 3.3C), with 7–8 poroids in 1 µm. The density of band striae in the valvocopula is 5 in 1 µm (Figure 3.3D).

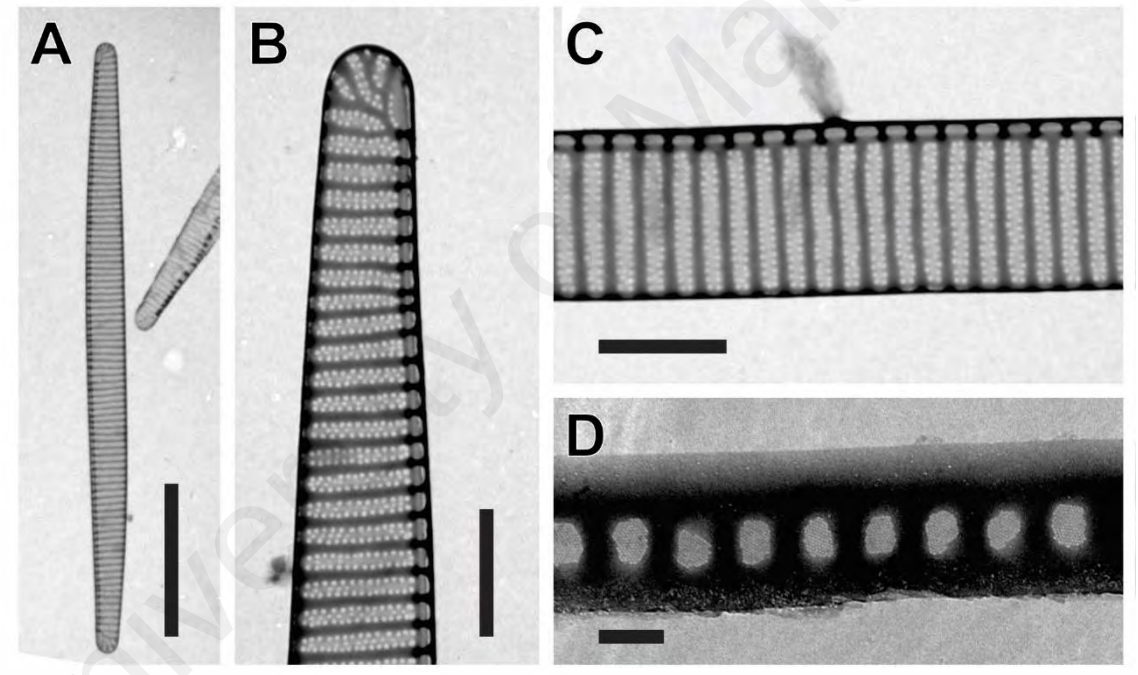

Figure 3.3: *Pseudo-nitzschia brasiliana*. TEM. (A) Cleaned valve showing the striae and fibulae, scale bar = 10 µm. (B) Apices, scale bar = 2 µm. (C) Central part of valve showing fibulae, each striae with two rows of poroids, and absent of central interspace, scale bar = 2 µm. (D) Valvocopula band striae, scale bar = 0.2 µm.

3.4.1.4 *Pseudo-nitzschia circumpora*

Morphology

Cells are asymmetrical and lanceolate in valve view (Figure 3.4A), with the presence of central interspace (Figure 3.4C). Transapical axis length is 42.35–47.03 µm and apical axis is 2.14–2.36 µm (Table 3.2). Valve apices are round (Figure 3.4B). The densities of fibulae and interstriae in 10 µm are 18–19 and 33–36, respectively. Each stria consists of one row of poroids, with inconsistent numbers of poroids (5–7) in 1 µm (Figure 3.4C). The poroids are round or rectangular, the dividing sectors are found arranged at the circumstance of each poroid in the striae (Figure 3.4C–3.4D). The cingular bands have 4-poroid high biseriate striae in 1 µm (Figure 3.4E–3.4F).

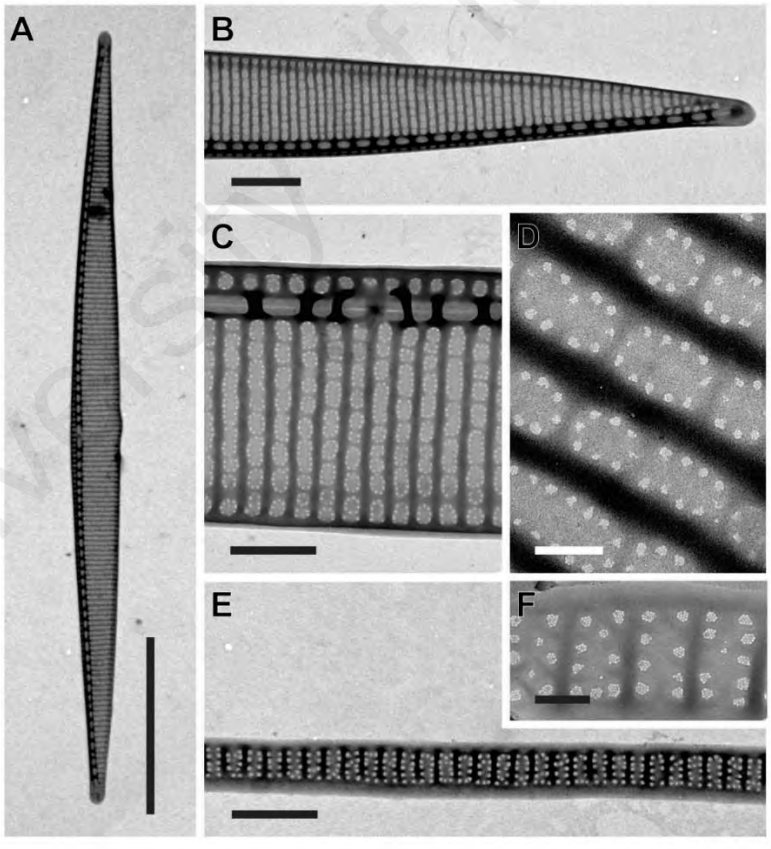

Figure 3.4: *Pseudo-nitzschia circumpora*. TEM. (A) Cell valve view, scale bar = 10 µm. (B) Valve ends, scale bar = 2 µm. (C) Central part of valve showing presence of central interspace, fibulae, mantle, striae, and rows of poroids, scale bar = 1 µm. (D) Detail of poroids with hexagonal pattern on the hymens, scale bar = 0.2 µm. (E) Details of valvocopula, scale bar = 1 µm. (F) Close up of poroids of valvocopula, scale bar = 0.2 µm.

3.4.1.5 *Pseudo-nitzschia cuspidata*

Morphology

Cells are lanceolate in valve view, with the presence of central interspace (Figure 3.5A). Transapical axis length is 32.51–45.95 µm and apical axis is 1.33–1.51 µm (Table 3.2). Valve apices are round (Figure 3.5B). The densities of fibulae and interstriae in 10 µm are 17–19 and 34–37, respectively. Each stria consists of one row of poroids, with the poroids of 5–6 in 1 µm (Figure 3.5C–3.5D). The poroid hymen is divided into 2–3 sectors, but most of the poroids are divided into 2 sectors (Figure 3.5D). The density of band striae in the valvocopula (first row from top) is 5 in 1 µm (Figure 3.5E).

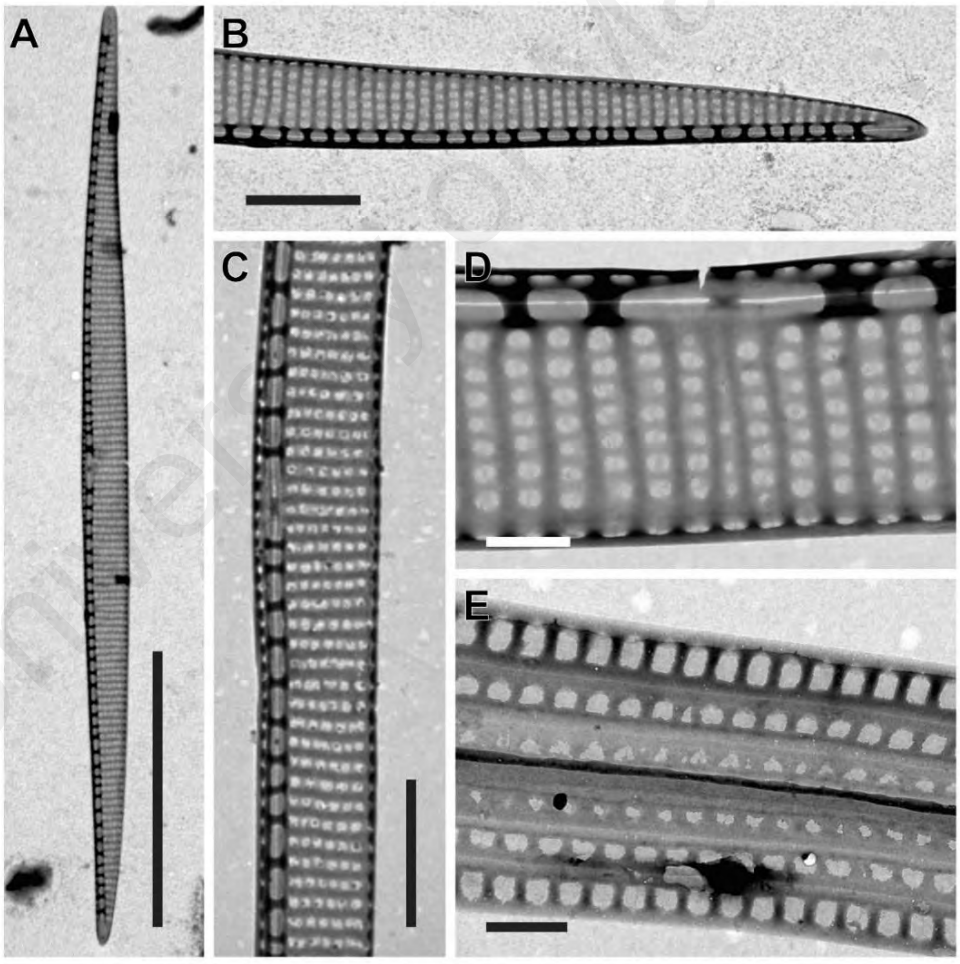

Figure 3.5: *Pseudo-nitzschia cuspidata*. TEM. (A) Cell valve view, scale bar = 10 µm. (B) Valve ends, scale bar = 2 µm. (C) Central part of valve showing presence of central interspace, fibulae, mantle, striae, and rows of poroids, scale bar = 2 µm. (D) Close up of central interspace and detail of poroids, scale bar = 0.5 µm. (E) Details of cingular bands, scale bar = 0.5 µm.

3.4.1.6 *Pseudo-nitzschia fukuyoi*

Morphology

Cells are symmetrical and linear to lanceolate and in valve view and slightly sigmoid in girdle view with pointed ends (Figure 3.6A). Transapical axis length is 90.46–93.58 µm and apical axis is 1.66–2.04 µm (Table 3.2). Valve apices are rounded (Figure 3.6B). A large central interspace with a central nodule is present (Figure 3.6C). Fibulae are irregularly spaced. The densities of fibulae and interstriae are 17–18 and 32–34 in 10 µm, respectively. Each stria contains one row of round-square poroids and divided into two to five sectors, with a density of 5–6 in 1 µm (Figure 3.6C–3.6D). Cingulum comprises three bands, with valvocopula contain 4 band striae in 1 µm (Figure 3.6E). Each band stria of valvocopula is two poroids wide and three to four poroids high (Figure 3.6E). The striae of the second band is two poroids wide and two poroids high, while third band structure only contain one row of longitudinal poroids (Figure 3.6E).

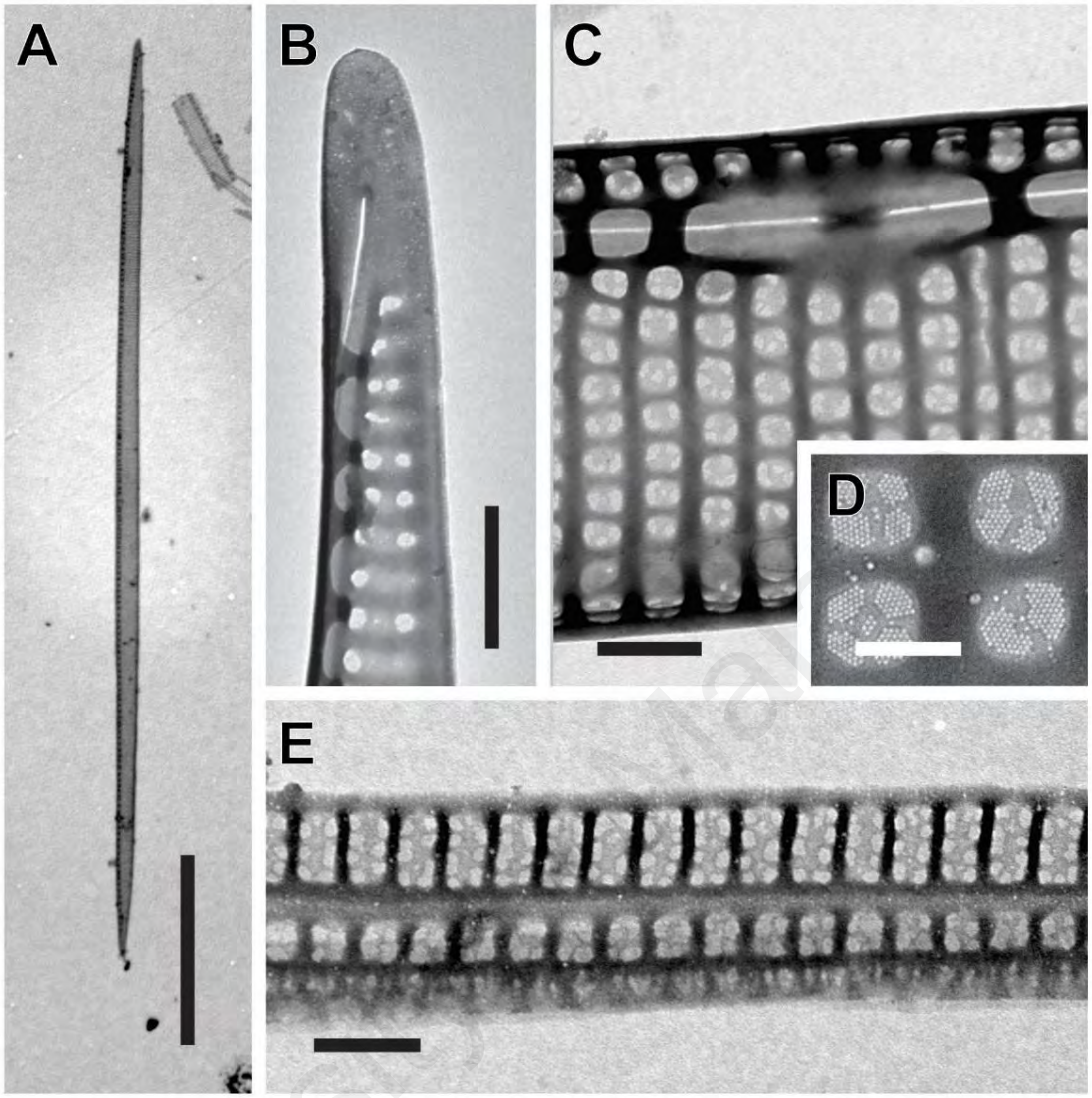

Figure 3.6: *Pseudo-nitzschia fukuyoi*. TEM. (A) Cell valve view, scale bar = 20 µm. (B) Valve ends, scale bar = 1 µm. (C) Central part of valve showing presence of central interspace, fibulae, mantle, striae, and rows of poroids, scale bar = 0.5 µm. (D) Detail of poroids and the divison of poroids hymens, scale bar = 0.2 µm. (E) Details of cingular bands, valvocopula (upper row) and band II and band III (second and third rows), scale bar = 0.5 µm.

3.4.1.7 *Pseudo-nitzschia pungens*

Morphology

Cells are linear to lanceolate in valve view, symmetrical along the apical axis, with pointed apices (Figure 3.7A and 3.7B). Transapical axis length is 69.36–81.06 µm and apical axis is 3.04–3.30 µm (Table 3.2). Central interspace is absent (Figure 3.7C). The densities of fibulae and interstriae are 10–13 and 10–14 in 10 µm, respectively.Each stria consists of two rows of round and simple poroids, with three to four poroids in 1 µm (Figure 3.7B–3.7D). The density of band striae in the valvocopula is 2–3 in 1 µm (Figure 3.7E).

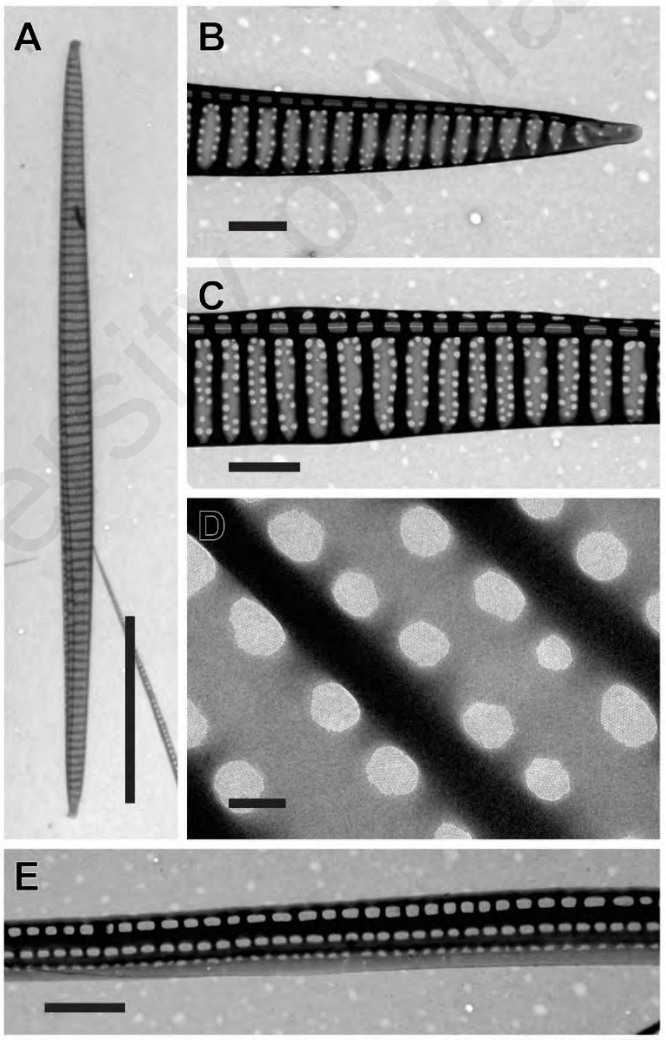

Figure 3.7: *Pseudo-nitzschia pungens*. TEM. (A) Cell valve view, scale bar = 20 µm. (B) Valve ends, scale bar = 2 µm. (C) Central part of valve showing absent of central interspace, fibulae, and interstriae, scale bar = 2 µm. (D) Close up of poroids, scale bar = 0.2 µm. (E) Details of valvocopula, scale bar = 0.2 µm.

3.4.2 *In silico* cox1 oligonucleotide primer design

The primer pair of *cox*1 was selected *in silico* considering the parameters of oligonucleotide length, Tm, GC contents, and *E*-values as shown in Table 3.3 and sequence logos of the signature regions of COX1F and COX1R were shown in Figure 3.8. The formation of hairpin structures, self-primer and primer-dimer of COX1F and COX1R were predicted based on their Gibbs free energy G (ΔG) (Appendix C).

Table 3.3: Primers used in *Pseudo-nitzschia cox*1 amplification, with their melting temperature (Tm), GC contents, length and *E*-values.

***cox*1 Primer**	**Position*** **(5′–3′)**	**Sequences (5′–3′)**	**T_m (°C)**	**GC (%)**	**Length**	***E*-value**
COX1F	29–51	GGG ATT GCD GGA ACA GCK TTA TC	58.0	51.4	23	2.0
COX1R	616–642	ACT GGA TCT CCT CCA CCA GCA GGA TC	63.3	57.7	26	2e-04

* Primers' positions refer to the nucleotide positions of *Pseudo-nitzschia cuspidata*, strain NWFSC 194, accession JN050306.

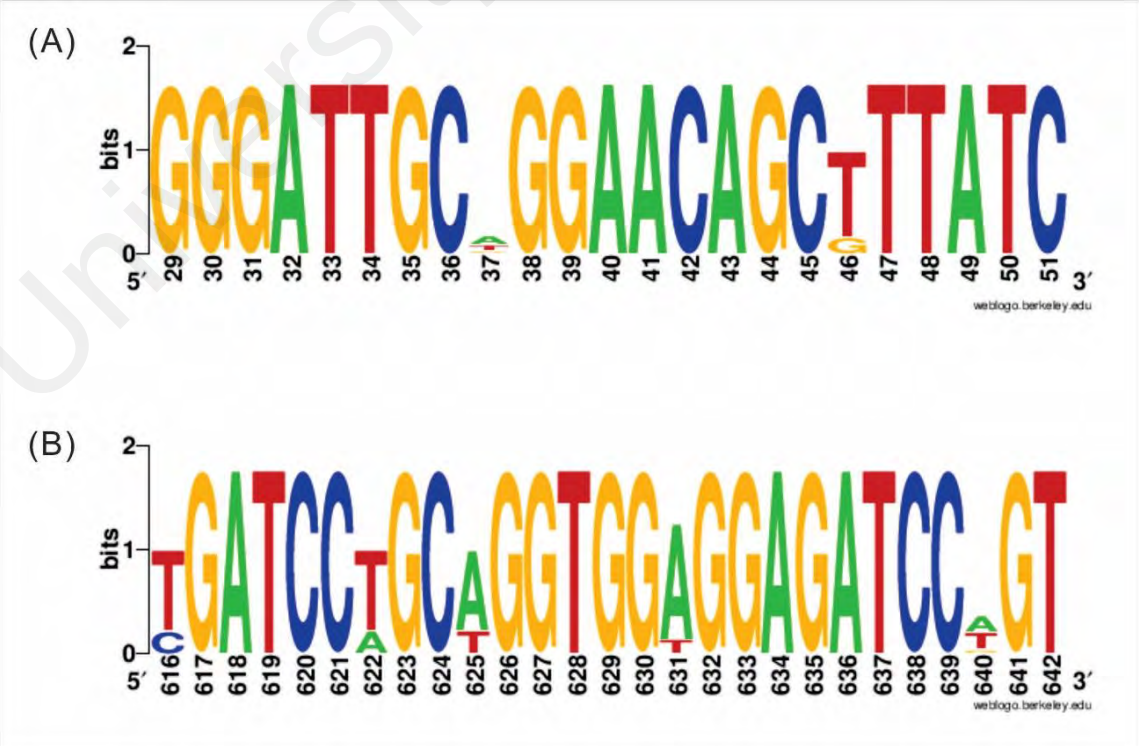

Figure 3.8: Sequences logos of signature regions. (A) Forward primer, COX1F. (B) Reverse primer, COX1R.

3.4.3 Phylogenetic analyses

A total of 55 nucleotide sequences were obtained in this study, and added to the 317 available sequences from GenBank to form the dataset. The datasets yielded 542 and 709 characters, with 218 and 145 parsimony informative sites for *cox1* and LSU, respectively. The final sequence-structure alignment of ITS2 yielded 654 characters. The best evolutionary models calculated for both ML and BI analyses were as follows: *cox1* dataset: TIM1+I+G; LSU dataset: TVM+I+G and ITS2 datasets: GTR+I+G.

The *cox1*, the LSU and the ITS2 analyses included 19 (38.8%), 36 (73.5%) and 41 (83.7%), respectively, of the presently described 49 *Pseudo-nitzschia* species (Appendix A). A phylogenetic tree is illustrated for each of the three genetic markers: mitochondrial *cox1* (Figure 3.9), LSU (Figure 3.10) and ITS2 (Figure 3.11). *Pseudo-nitzschia*/*Fragilariopsis* formed a cluster in the LSU and ITS2 analyses, but not in the *cox1* tree (Figures 3.9–3.11). The overall topology of the *cox1* tree is comparable to that of the LSU and ITS2 trees. The position of *Fragilariopsis* in the *cox1* tree is tentative, as there were only a few representatives of the *P. americana* complex sensu Lundholm et al. (2002b) and the *P. seriata* complex sensu Hasle et al. (1996).

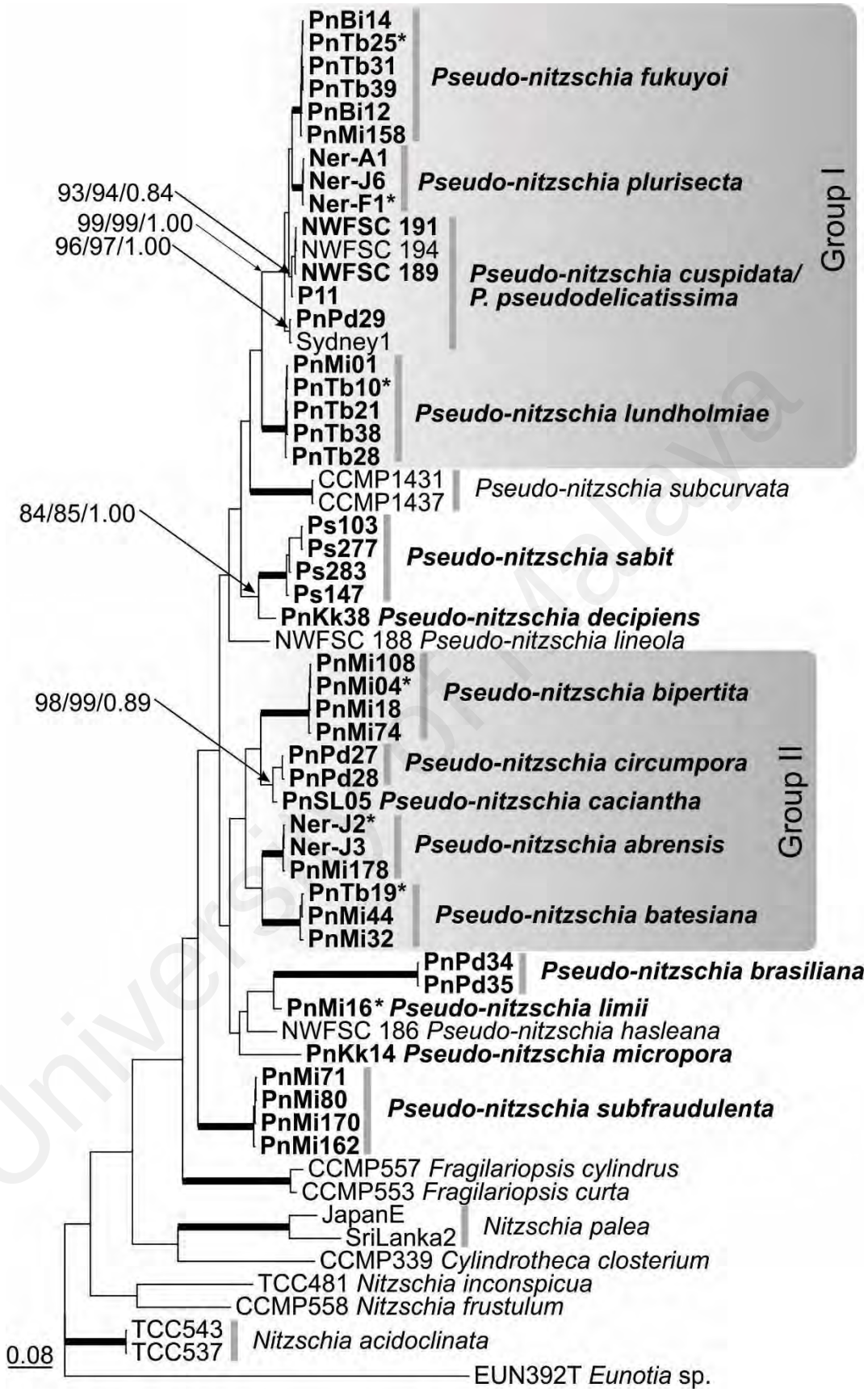

Figure 3.9: *Pseudo-nitzschia* Bayesian tree base on *cox1* gene. Nodes are annotated with MP/ML bootstraps values ≥80%, and BI posterior probabilities (PP) ≥0.80. Thick lines indicate MP/ML bootstrap values of 100% and a PP of 1.00. Strains in bold indicate sequences obtained in this study. Strains marked with a * indicate sequence obtained from holotype.

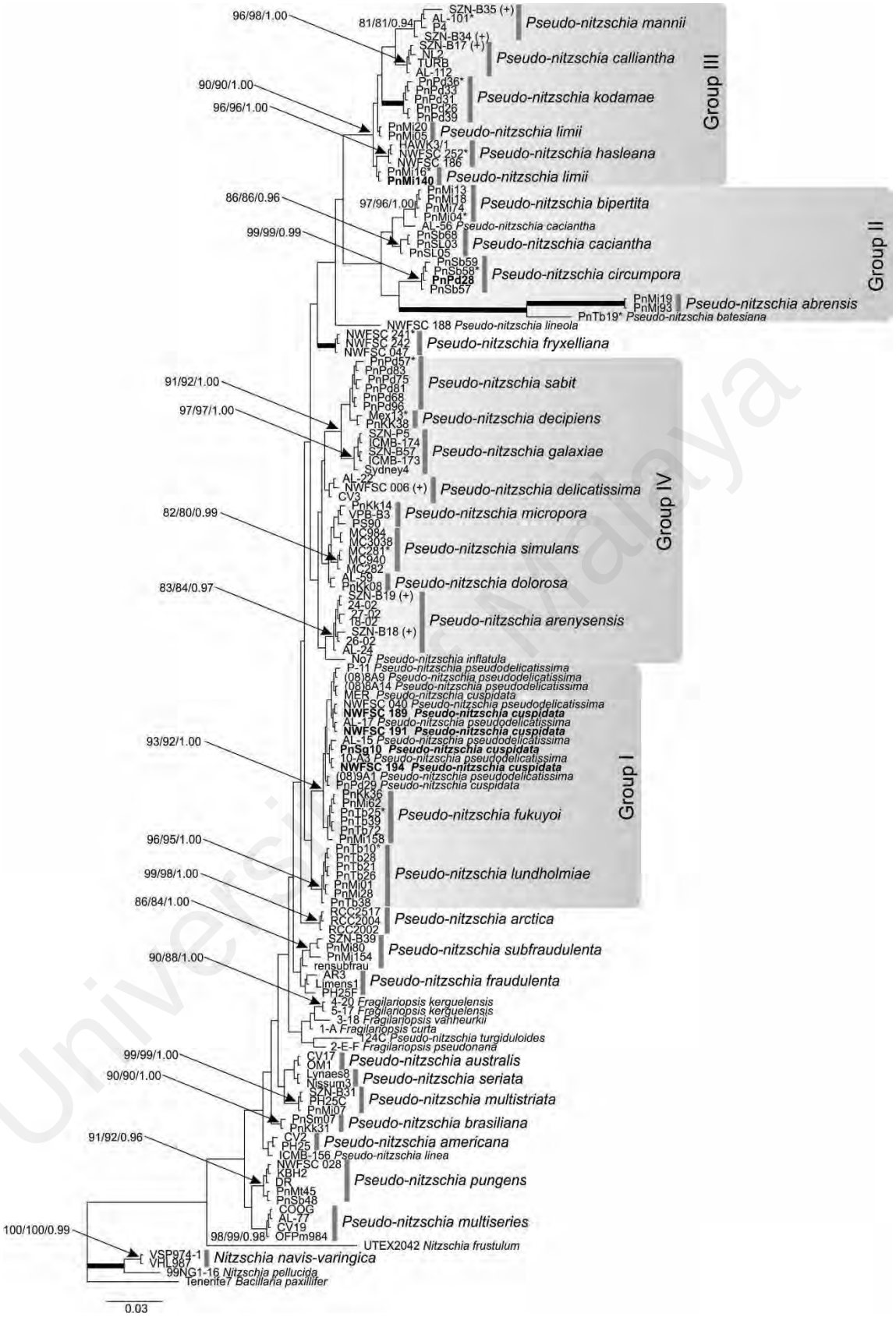

Figure 3.10: *Pseudo-nitzschia* Bayesian tree based on LSU D1-D3 sequences. MP/ML bootstraps values ≥80%, and BI posterior probabilities (PP) ≥0.80 are shown. Thick lines indicate MP/ML bootstrap values of 100% and a PP of 1.00. Strains in bold indicate sequences obtained in this study. The seven strains labelled with "(+)" indicate that they are amended from previously identified species (see text). Strains marked with a * indicate sequence obtained from holotype.

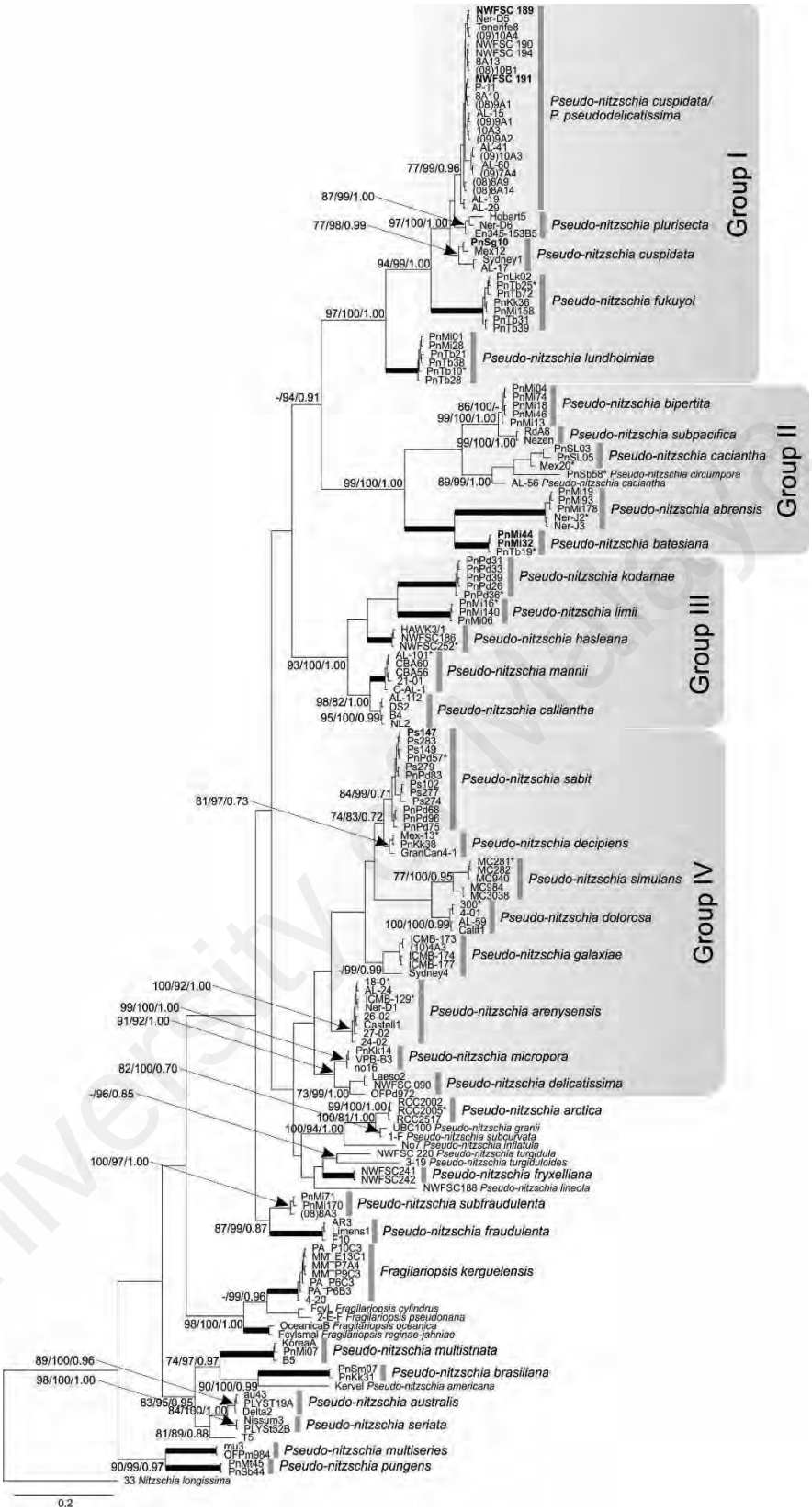

Figure 3.11: *Pseudo-nitzschia* Bayesian tree based on the sequence part as obtained from the ITS2 sequence-structure information. MP/ML bootstraps values (obtained from the 12-letter encoded ITS2 sequence-structure information) ≥70%, and BI posterior probabilities (PP) ≥0.70 are shown. Thick lines indicate MP/ML bootstrap values of 100% and a PP of 1.00. Strains in bold indicate sequences obtained in this study. Strains marked with a * indicate sequence obtained from holotype.

The monophyletic Groups I–III, recovered in the LSU and the ITS2 trees (Figures 3.10–3.11), comprised members of the *P. pseudodelicatissima* complex, along with a few other sequences (*P. bipertita* and *P. subpacifica*). Group IV was constituted mainly by sequences of the *P. delicatissima* complex (except *P. micropora* and *P. simulans* [in both the LSU and ITS2 trees] and *P. inflatula* [in the LSU tree]; Figures 3.9–3.11). Groups III and IV, however, were not recovered in the *cox1* tree, probably due to the current limited availability of sequences from the remaining 30 *Pseudo-nitzschia* species that have yet to be sequenced. Strong nodal supports were seen only in the ITS2 tree for the *P. pseudodelicatissima* complex Groups I–III and Group III in LSU tree, with >90% of bootstrap (MP/ML) and 1.00 posterior probabilities (BI; Figures 3.10–3.11). In comparing the *p*-distances using heatmap (Figure 3.12), ITS2 showed the greatest distances, followed by *cox1* and LSU, even though the sequence length of ITS2 was half that of *cox1*.

Group I, comprising sequences of *P. fukuyoi*, *P. plurisecta*, *P. cuspidata/P. pseudodelicatissima* and *P. lundholmiae*, was recovered in all three trees and was strongly supported in the ITS2 analyses (MP/ML/BI, 97/100/1.00; Figure 3.11). *Pseudo-nitzschia cuspidata*/*P. pseudodelicatissima* was polyphyletic in all trees. The two *P. plurisecta* sequences in GenBank could not be included in the LSU dataset (Figure 3.10) due to the presence of ambiguous nucleotides (for Hobart 5, AF417641) and short sequence, i.e., 505 bp (for En345-153B5, KF006835); our dataset required >700 bp.

Group II, recovered in all three trees, comprised sequences of *P. bipertita*, *P. circumpora*, *P. caciantha*, *P. abrensis* and *P. batesiana*, with strong support in the ITS2 (99/100/1.00) analyses (Figure 3.11). Only ITS2 sequences were available for *P. subpacifica*, and analyses showed that it clustered in Group II as a sister taxon to *P. bipertita*, along with other members of the *P. pseudodelicatissima* complex. One strain, AL-56, clustered outside the *P. caciantha* clade in both the LSU and ITS2 trees (Figures 3.10–3.11); no *cox1* sequence was available.

Some strains were re-identified based on genetic similarities (Appendix A; Figure 3.10). Our analyses allowed the amendment of previously identified strains as follows. Strains SZN-B34 and SZN-B35 (previously *P. pseudodelicatissima*; Orsini et al., 2002) are genetically close to *P. mannii*; strain SZN-B17 (previously *P. pseudodelicatissima*; Orsini et al., 2002) is *P. calliantha*; strains SZN-B18 and SZN-B19 (previously *P. delicatissima*; Orsini et al., 2002) are *P. arenysensis* (Appendix A). Strain NWFSC-006 (previously *P. pseudodelicatissima*; Stehr et al., 2002) clustered with *P. delicatissima* without bootstrap support (Figure 3.10).

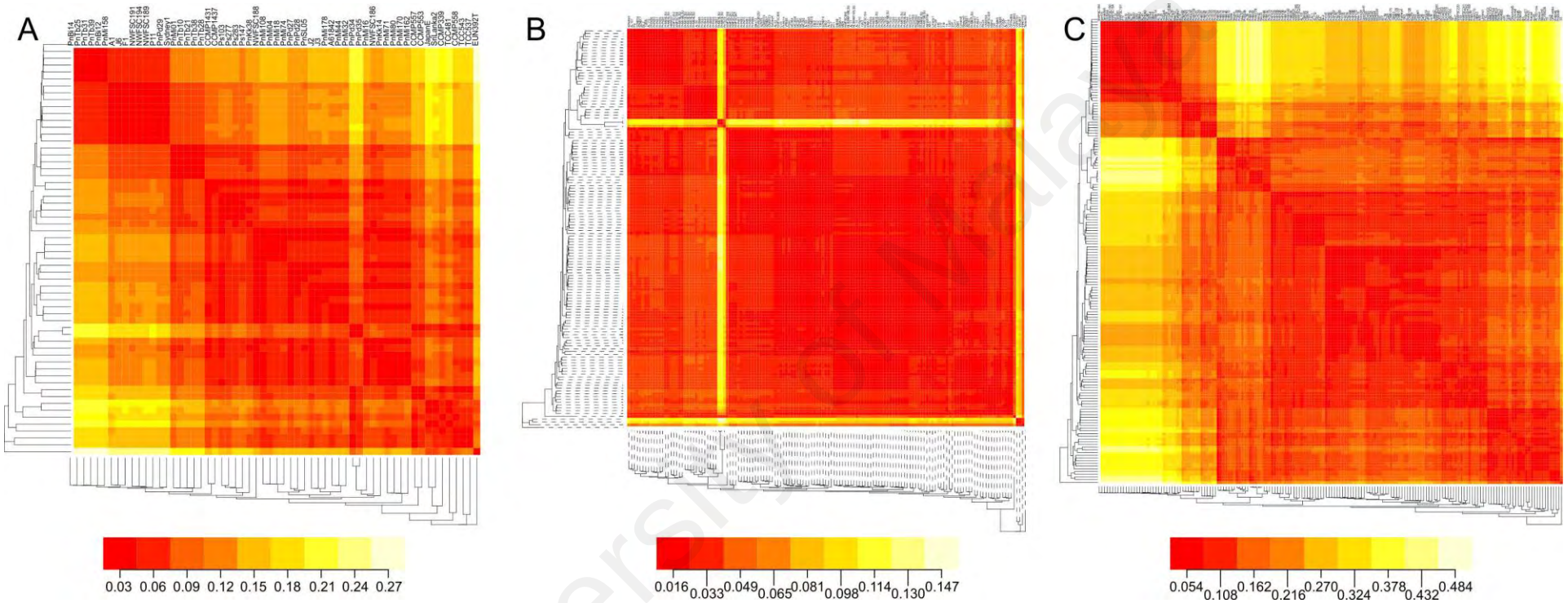

Figure 3.12: Color heatmap showing distribution of pairwise genetic distance estimated from (A) *cox1*, (B) LSU and (C) ITS2 based on p-distances. Refer to Figs. 1–3 for the detailed tree topology. The color bars indicate the p-distances range of each gene markers. Axis x/y shared the same legend.

3.4.4 Character-state evolution

Overall, the patterns of character-state distribution mapped on the ITS2 tree corresponded to the grouping of *Pseudo-nitzschia* species in morphological species complexes (Figure 3.13). Exceptions were *P. arctica*, *P. fryxelliana,* and *P. simulans*, which grouped outside of the *P. pseudodelicatissima* complex (Groups I–III; Figure 3.11). The absence of a central nodule on the raphe (Figure 3.13A) supported the grouping of species in the *P. americana* and *P. seriata* complexes, along with *Fragilariopsis* spp., which split from the rest of the *Pseudo-nitzschia* species. The basal clade of the *Pseudo-nitzschia* ITS2 tree was constituted mainly by species from the *P. seriata* group, i.e., *P. australis*, *P. multiseries*, *P. multistriata*, *P. obtusa*, *P. pungens,* and *P. seriata*, as well as *P. americana* and *P. brasiliana* (Figure 3.11). Exceptions were *P. granii*, *P. subcurvata,* and *P. micropora*; although they lack a central nodule, they did not group with the other species having this absence. Interestingly, two *Fragilariopsis* species possessing a central nodule (i.e., *F. oceanica* and *F. reginae-jahniae*) grouped with the other *Fragilariopsis* species lacking it.

One row of poroids (Figure 3.13B) was found to be common in the *P. pseudodelicatissima* complex (Groups I–III). Although both *P. bipertita* and *P. subpacifica* have two rows of poroids, they clustered inside Group II, which also includes four members of the *P. pseudodelicatissima* complex. Another anomaly was *P. kodamae* in Group III, which sometimes has an incomplete second row of poroids in some of the striae (Teng et al., 2014). Having two rows of poroids is common in the *P. delicatissima* complex (Group IV), except for *P. galaxiae*, which has the autapomorphic character, i.e., an absence of poroids in the striae, *P. simulans* with one row of poroids and *P. dolorosa*, with 1–2 rows of poroids (Figure 3.13B). *Pseudo-nitzschia lineola*,

which clustered outside of any of the complex groups, also has 1–2 rows of poroids (Figure 3.13B).

With respect to the number of sectors in poroids (Figure 3.13C), the *P. pseudodelicatissima* complex is diverse: from 1 to <5 sectors, 2 sectors, 2 to <10 sectors, and >10 sectors. Likewise, *P. subcurvata*, *P. granii* and *P. inflatula* have a diversity of sectors: 1 to <5; and, *P. fraudulenta*/*P. subfraudulenta* has 2 to <10 sectors. The other species, including those in the *P. delicatissima* complex, possess simple poroids, i.e., without division into sectors. Most *Pseudo-nitzschia* species have fewer fibulae vs. striae in 10 µm (Figure 3.13D), with the exception of *Fragilariopsis* spp., *P. fraudulenta*, *P. brasiliana*, *P. australis*, *P. obtusa*, *P. seriata*, *P. multiseries* and *P. pungens* that have an equal number of fibulae vs. striae in 10 µm. The shape of the apices (Figure 3.13E) was informative. Except for *P. galaxiae*, which has thin rostrae, and *P. americana* and *P. brasiliana*, which have broad, rounded apices, the rest of the *Pseudo-nitzschia* species have tapering apices. The density of the band striae in the valvocopula (Figure 3.13E) did not show a clear trend when the character was mapped. Likewise, other morphological characters that did not show a clear trend (e.g., the shape of valves) and those characters with overlapping morphometric measurements (e.g., valve width, transapical width, poroids in 10 µm and characters like girdle view and structure of valvocopula), were not considered.

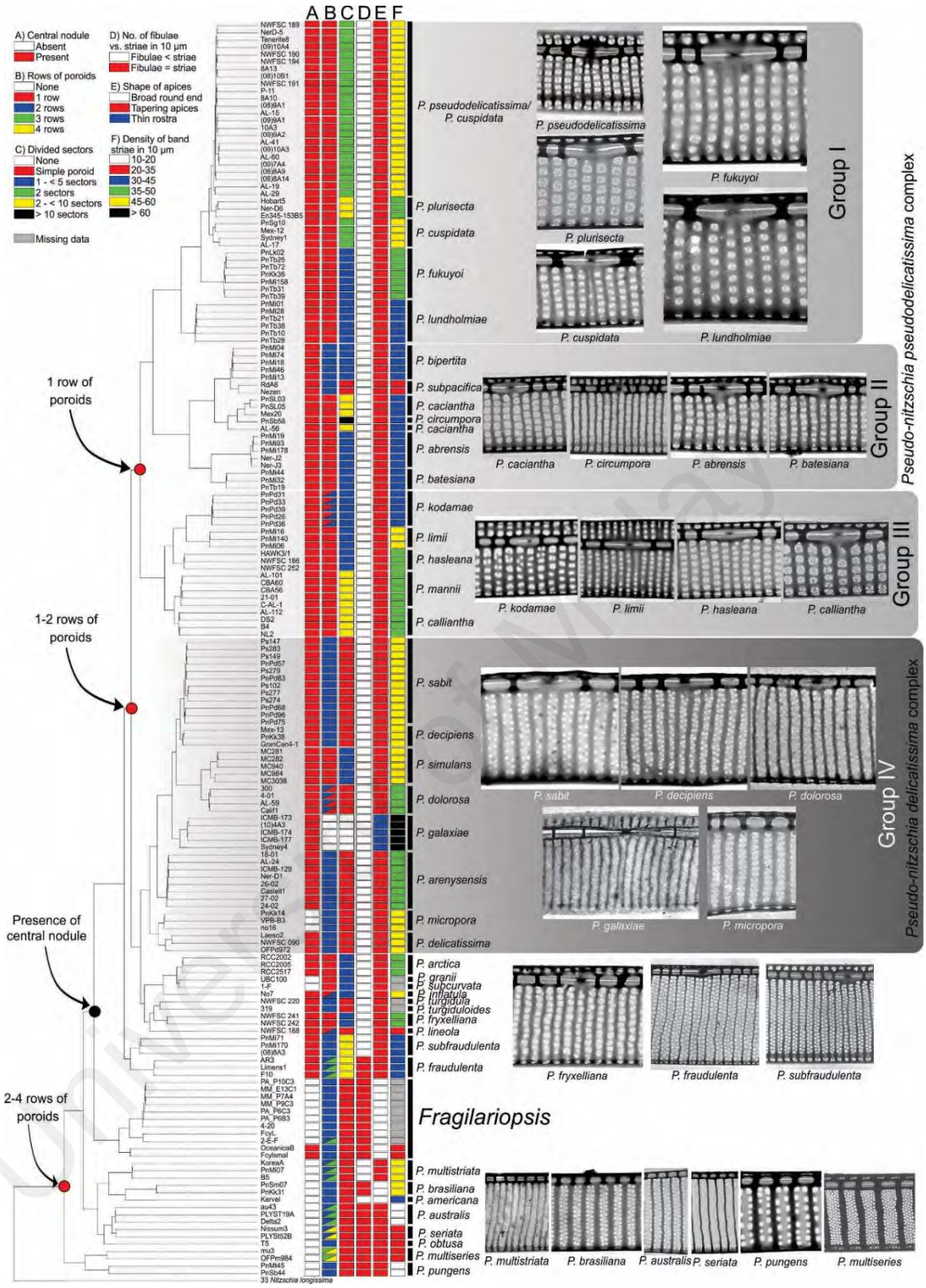

Figure 3.13: ITS2 Bayesian tree of *Pseudo-nitzschia*, with the inclusion of morphological characters (A) presence/absence of central nodule, (B) number of rows of poroids, (C) divided sectors of poroids, (D) number of fibulae and striae in 10 µm, (E) shape of apices and (F) density of band straie in 10 µm. TEM micrographs of *Pseudo-nitzschia* spp. showing the central part of valve; note the poroid structure, rows of poroids and central nodule.

3.5 Discussion

This study explored the phylogenetic resolution of the genus *Pseudo-nitzschia* based on three genetic markers (*cox1*, LSU and ITS2 rRNA) from two cellular compartments (mitochondrial and nuclear ribosomal genes). It also explored intrageneric relationships and identified sequences that represent taxonomically unresolved issues. The relevance of morphologically based species complexes in *Pseudo-nitzschia* phylogeny is assessed.

3.5.1 Phylogeny and species delineation of *Pseudo-nitzschia*

Numerous studies indicate that sufficient taxon sequence sampling is one of the most feasible and practical ways to infer evolutionary relationships more accurately (Zwickl & Hillis, 2002; Hedtke et al., 2006l; Heath et al., 2008). By increasing the sequencing effort, the ITS2 analysis included 85.7% (42/49) of the current taxonomically accepted *Pseudo-nitzschia* species, with 172 sequences in the tree; 75.5% (37/49) were included in LSU analysis (142 sequences), and 38.8% (19/49) in the *cox1* analysis (60 sequences). The remaining seven species that have yet to have the ITS2 sequenced include *P. antarctica*, *P. heimii*, *P. linea*, *P. prolongatoides*, *P. pungiformis*, *P. roundii* and *P. sinica*. Clearly, this more comprehensive sequence sampling to include more species improved the phylogenetic resolution in the *Pseudo-nitzschia cox1* phylogeny, providing a better grouping compared to what was achieved by Tan et al. (2015), which did not resolve the *P. pseudodelicatissima* complex into two groups, in contrast to the present study (Figure 3.9). As a comparison to other gene markers, the previously analyzed *rbcL* (Lundholm et al., 2012) and 18S rRNA genes (Lim et al., 2016) included only 20.4% (10/49; 22 sequences in the tree) and 26.5% (13/49; 48 sequences in the tree), respectively, from the 49 currently known *Pseudo-nitzschia* species in the phylogenetic analyses. The *rbcL* dataset did not resolve the *Pseudo-*

nitzschia species into groups (Lundholm et al., 2012). Similarly, the 18S rRNA dataset resolved the *P. pseudodelicatissima* and *P. delicatissima* complexes into only one clade (Clade II; Lim et al., 2016). A greater sequencing effort is required in order to compare the robustness of *rbcL* and 18S rRNA, in contrast to other gene markers, for constructing phylogenetic trees.

Generally, the support values for Groups I–IV are low, especially in the *cox1* and LSU trees. It is only in the ITS2 tree that members of the *P. pseudodelicatissima* complex are well represented in Groups I–III, with strong support at the branches. Both *P. bipertita* and *P. subpacifica* are morphologically different from any other members in the *P. pseudodelicatissima* complex, but they formed a strong subclade Group II in the complex.

Looking specifically at strains originally identified as *P. caciantha* in the LSU tree (Figure 3.10), it is seen that strain AL-56 from Italy (Mediterranean Sea) grouped with *P. bipertita*, and not with the *P. caciantha* strains from Malaysia (PnSL03, PnSL05 and PnSb68). Furthermore, in the ITS2 tree (Figure 3.11), it does not cluster with the other strains of *P. caciantha*, including the type material (Strain Mex20; Lundholm et al., 2003). Strain AL-56 possess a greater number of fibulae and striae in 10 µm (18–23 and 33–37, respectively) (Amato et al., 2007), in contrast to the original description of *P. caciantha* in Lundholm et al. (2003; 15–19 and 28–31, respectively); these ranges are not close, and the number of striae in 10 µm does not even overlap. The lack of evidence of monophyly for *P. caciantha* and the non-matching morphological characters suggest that strain AL-56 is not *P. caciantha*, but another undescribed species. More strains, to provide additional morphological and molecular evidence, are required to clarify the taxonomic status of strain AL-56.

Morphologically, both *P. subpacifica* and *P. heimii* share overlapping characters

(Hasle et al., 1996) and are genetically close in the ITS phylogenetic tree (91/0.99, ML/BI; Orive et al., 2013). The phylogenetic relationship between the sister taxa of *P. subpacifica*/*P. heimii* (not included in the present study), as seen in Teng et al. (2016) and Orive et al. (2013), warrant further verification, especially regarding species identity. In this respect, strains collected from type locality Terre Adélie, in the Antarctic (for *P. heimii*, Manguin, 1957), and northwest African waters (for *P. subpacifica*, Hasle, 1974), could be tested for mating compatibility and their molecular data compared.

Interestingly, long branches in the LSU trees lead to *P. abrensis* and *P. batesiana* (Figure 3.10). Coincidentally, both are in Group II of the *P. pseudodelicatissima* complex and the long branches do not affect the branching of these two species, nor the topology of the entire LSU tree (Lim et al., 2013; Orive et al., 2013). This is supported by the two sequences also being recovered as sister taxa in the *cox1* and ITS2 trees, where the branches are not long (Figures 3.9, 3.11). The long branches indicate that the LSU sequences of both *P. abrensis* and *P. batesiana* are divergent compared to other species in the genus. This is illustrated by the genetic distance of LSU between *P. abrensis* and *P. batesiana* being at least two-fold greater than that between *P. caciantha* and *P. circumpora* in the same *P. pseudodelicatissima* complex Group II (Figure 3.10).

In general, the ITS2 dataset indicates the highest genetic divergences, followed by *cox1* and LSU (Figure 3.12). As the sequence divergence for ITS2 is highly variable, several sequences of *Nitzschia* species (including *N. pusilla*, *N. alexandrina*, *N. laevis* Frenguelli, *N. navis-varingica*) were screened from the GenBank through secondary structure modelling. Only the *N. longissima* sequence fit the model, which was then used as outgroup to guide the sequence-structure alignment using 4SALE. In this

context, the complete sequences for the whole ITS2 region, confirmed through 5.8S-28S interaction/proximal stem (Lim et al., 2012, 2013) have been included in the analyses (for all *Pseudo-nitzschia*, *Fragilariopsis* and *Nitzschia* species). The alignment for this highly variable region is extremely difficult (Lim et al., 2013). Therefore, information from the secondary structure was further used to guide the orthologous sequence-structure alignment, followed by phylogenetic analyses. The complete hypervariable region of ITS2 increased the phylogenetically informative characters, providing a better resolution compared to the *cox1* and LSU datasets.

3.5.2 Character evolution

Both the *P. pseudodelicatissima* and *P. delicatissima* complexes share common morphological characters, i.e., the presence of a central nodule and fewer fibulae than striae in 10 µm. However, the number of rows of poroids and the structure of poroids can readily differentiate them. All members in the *P. pseudodelicatissima* complex possess only one row of poroids and the poroids are divided into several sectors. In contrast, all species in the *P. delicatissima* complex possess only two rows of poroids and the poroids have a simple structure (Figure 3.13). For comparison, species in the *P. seriata* and *P. americana* complexes share common morphological characters, i.e., simple poroids and an absence of a central nodule. Furthermore, members in the *P. seriata* complex have a transapical width of >3 µm and a strongly silicified frustule (Hasle et al., 1996), while those in the *P. americana* complex have broadly rounded apices and also a rectangular shape in valve view (Lundholm et al., 2002b).

Our analyses revealed that members of the *P. pseudodelicatissima* complex are found in three groups (I–III), with the exception of *P. arctica*, *P. fryxelliana* and *P. inflatula* (which belong to the *P. pseudodelicatissima* complex but grouped outside of Group I–III), and *P. bipertita* and *P. subpacifica* (which do not belong to the *P.*

pseudodelicatissima complex but grouped in Group II). Both *P. bipertita* and *P. subpacifica* have diverged from species in *P. pseudodelicatissima* complex, as they possess two rows of poroids and have a relatively large transapical width (5–6 µm and 2.6–4.2 µm, respectively; Hasle et al., 1996; Teng et al., 2016). This readily distinguishes them from other species in the *P. pseudodelicatissima* complex that have one row of poroids and a transapical width of <3 µm.

The *P. delicatissima* complex makes up a paraphyletic group, as Group IV comprises all morphologically closely related species of the *P. delicatissima* complex in addition to *P. simulans* (a member in the *P. pseudodelicatissima* complex) and *P. galaxiae* (Figures 3.10–3.12). *Pseudo-nitzschia simulans* represents an example of parallel evolution. In spite of the fact that it clusters in Group IV with other members of the *P. delicatissima* complex, it should be maintained as a member of the *P. pseudodelicatissima* complex, given that it possesses one row of poroids with 2–3 divided sectors (Li et al., 2017). *Pseudo-nitzschia galaxiae* is unique to the whole *Pseudo-nitzschia* genus by having lost the ability to form poroids in the interstriae (Lundholm & Moestrup, 2002; Cerino et al., 2005; Figure 3.13B).

The number of rows of poroids has previously been evaluated as a morphological character, but it did not show morphological congruency with the character-state evolution (Lim et al., 2013), in contrast to the present study. This might be due to a less comprehensive taxon sampling, covering only 32 of the *Pseudo-nitzschia* species known at that time. When more sequences are included, the morphologically based species complexes are shown to have some evolutionary relevance in the ITS2 tree due to its better resolved phylogenetic framework, in contrast to the *cox1* and LSU trees. When mapped on the ITS2 tree, the four morpho-characters (i.e., the presence/absence of a central nodule, the number of rows of poroids, number

of sectors, and number of fibulae vs. striae in 10 μm) make sense in an evolutionary context (Figure 3.13). For example, *P. pungens*, *P. multiseries*, *P. obtusa*, *P. seriata*, *P. australis*, *P. americana*, *P. brasiliana* and *P. multistriata* are united by pleisiomorphic characters, all possessing 2–4 rows of poroids and lacking a central nodule (Figure 3.13). Although the sister taxa *P. fraudulenta*/*P. subfraudulenta*, *P. turgidula*, *P. turgiduloides*, the entire *P. delicatissima* complex (Group IV), *F. oceanica* and *F. reginae-jahniae* retained the character of 2–3 rows of poroids (Figure 3.13), they evolved independently, as they possess a central nodule (Figure 3.13). By lacking a central nodule, *P. micropora* (Priisholm et al., 2002), *P. granii*, *P. subcurvata* and some *Fragilariopsis* species (*F. kerguelensis*, *F. cylindrus* and *F. pseudonana*) secondarily lost this apomorphic character (Figure 3.13A).

According to the ITS2 analysis, neither *P. arctica* nor *P. fryxelliana* and *P. inflatula* formed a clade with any of the *P. pseudodelicatissima* complex species (Groups I–III), even though they possess one row of poroids (incomplete 1–2 rows for *P. inflatula* and *P. kodamae*). This synapomorphy (one row of poroids) is shared by all members of the *P. pseudodelicatissima* complex. The entire *P. pseudodelicatissima* complex evolved independently as distinct groups (I–III; Figure 3.11), making species in this complex the most recently evolved descendants. Interestingly, some species in Group III, are characterized by having a proximal mantle bearing >2 poroids aligned to the fibula, as can be seen at the valve face; others bear only 1 poroid (Figure 3.13). Examples include *P. hasleana* (2–3 poroids; Lundholm et al., 2012), *P. kodamae* (2–4 poroids; Teng et al., 2014) and *P. limii* (3–4 poroids; Teng et al., 2016), which are unique in the *P. pseudodelicatissima* complex and thus represent an autapomorphy.

The *P. pseudodelicatissima* complex exhibits a wide variety with respect to divided sectors, while most other *Pseudo-nitzschia* species possess simple poroids

without divided sectors (Figure 3.13C). Apart from the *P. pseudodelicatissima* complex, poroids with divided sectors appear in *P. fraudulenta*/*P. subfraudulenta* (2 to <10 divided sectors), *P. arctica*, *P. fryxelliana*, *P. granii*, *P. inflatula* and *P. subcurvata* (each with 1 to >5 divided sectors; Figure 3.13C). *Pseudo-nitzschia simulans*, *P. fryxelliana* and *P. arctica* are species in the *P. pseudodelicatissima* complex that have poroids with divided sectors, but are grouped outside the complex (Groups I–III). Again, *P. galaxiae* is unique, as it does not possess poroids in the striae (Figure 3.13C).

The *Pseudo-nitzschia* species at the base of the ITS2 tree (mostly the *P. seriata* group) have an equal number of fibulae vs. striae in 10 µm, whereas *P. americana*, *P. multistriata*, *P. subfraudulenta* and the remaining species in the genus have a lower number of fibulae vs. striae in 10 µm (Figure 3.13D). All of the *Pseudo-nitzschia* species that possess tapering apices represent a pleisiomorphic character. Autapomorphic characters are found in *P. galaxiae* (thin rostrae) and *P. americana* and *P. brasiliana* (broad, round apices; Figure 3.13E).

Even though *Fragilariopsis* forms an ingroup within *Pseudo-nitzschia*, the genus *Fragilariopsis* can be readily differentiated from *Pseudo-nitzschia* by its flat, ribbon-like colonies, compared to the stepped chains in the latter (Hasle, 1994; Cefarelli et al., 2010). Other than that, the two genera are similar morphologically and genetically, except that some species of *Pseudo-nitzschia* produce domoic acid, as discussed in Lundholm et al. (2002b). Currently, 26 of the 49 species of *Pseudo-nitzschia* are documented to produce domoic acid (Lundholm, 2017; Wadt et al., 2017). Our analysis shows that the toxic *Pseudo-nitzschia* species are distributed across the entire ITS2 tree, and thus no clear trend can be seen. Furthermore, some strains of the same species have been proven to be toxic, and others not. Hence, the distribution of toxigenic species are not shown in Figure 3.13. The genera *Pseudo-nitzschia* and

Fragilariopsis are closely related but evolved divergently, and therefore have different traits. The phylogenetic relatedness can be seen in present study (Figures 3.9–3.11), where *Fragilariopsis* spp. tend to form as ingroup to *Pseudo-nitzschia* spp., regardless of what gene markers (*cox1*, LSU, ITS2) or outgroup are assigned. This supports an LSU phylogeny of the Bacillariaceae comprising an outgroup of araphid taxa and with the ingroup containing several Bacillariaceae genera (19 taxa; Lundholm et al., 2002a). It is similar to an SSU *Pseudo-nitzschia* phylogeny, which used an outgroup from genera in Bacillariaceae, i.e., *Nitzschia*, *Cylindrotheca*, *Tryblionella*, *Achnanthes*, *Bacillaria* and *Eutonia* (Lim et al., 2016). Whether *Pseudo-nitzschia* and *Fragilariopsis* should be congeneric remains a subject for scientific debate. It is noteworthy that some species of *Fragilariopsis* also possess a central nodule, e.g., *F. oceanica*, *F. reginae-jahniae*, *F. atlantica*, and *F. pacifica* (Lundholm & Hasle, 2010). Similarly, several *Nitzschia* species, e.g., *N. bizertensis* (Smida et al., 2014), *N. longissima* (Kaczmarska et al., 2007), *N. navis-varingica* (Lundholm & Moestrup, 2000), also possess a central nodule. Although the number of ITS sequences for *Fragilariopsis* (with ~25 species) in the GenBank database is currently limited, it would still be worthwhile to explore more thoroughly the relationships between *Pseudo-nitzschia* and *Fragilariopsis*. Furthermore, research is warranted to study their relationship to *Nitzschia*, although this would be a greater challenge because of the huge number of species (~775; Guiry & Guiry, 2017).

Based on our results, the presence/absence of a central nodule and the number of rows of poroids are useful morphological characters in an evolutionary context for *Pseudo-nitzschia*. Other morphological characters that have overlapping morphometric measurements or that did not show a clear trend (e.g., valve width, transapical width, shape of valve, valve girdle view, poroids in 10 μm, and structure of valvocopula) are not shown in Figure 3.13.

3.5.3 Taxonomic status of *P. cuspidata* and *P. pseudodelicatissima*

The separation of the cryptic *P. cuspidata* and *P. pseudodelicatissima* in all morphological and molecular analyses remained unresolved when using the genetic markers LSU, ITS1-5.8S-ITS2 and *rbcL* (Lundholm et al., 2003, 2012). Previously, it was considered possible to separate *P. cuspidata* and *P. pseudodelicatissima* using ITS2 plus secondary structure information (Lim et al., 2013; Teng et al., 2014, 2015, 2016). However, the delineation became uncertain as the number of sequences increased (as shown in Figures 3.9–3.11). The taxonomic uncertainty of these two species thus remains and requires examination of *P. pseudodelicatissima* from the type locality.

The holotype of *P. cuspidata* is from Las Palmas, Gran Canaria (Canary Islands), while that of *P. pseudodelicatissima* is from the Denmark Strait, North Atlantic (60°18' N, 31°0' W; Lundholm et al., 2003). Strain Tenerife8 (from Tenerife, Canary Islands; Lundholm et al., 2012) can thus represent an epitype of *P. cuspidata* and serve to define to which clade *P. cuspidata* belongs. Unfortunately, a representative strain for *P. pseudodelicatissima* from its type locality is currently unavailable, and further clarification is required by obtaining a live strain from the type locality. Given that species composition changes over decadal to multi-decadal time scales (e.g., Lundholm et al., 2010), it may not be possible to recover the representative strain. Currently, the available sequences of *P. pseudodelicatissima* were obtained from other biogeographic regions, i.e., northern Spain and Portugal, and the Tyrrhenian and Mediterranean Seas (Appendix A). Until a live strain from the type locality can be obtained, two possible scenarios remain: (1) *P. cuspidata* will be a synonym of *P. pseudodelicatissima* if the representative strain from the holotype area (i.e., Denmark Strait) falls in the same clade of *P. pseudodelicatissima*/*P. cuspidata*; (2) *P. pseudodelicatissima* will become the name of another clade if a representative strain

from the holotype area appears in another clade. *Pseudo-nitzschia pseudodelicatissima* was originally described on 24 May 1898, while *P. cuspidata* was described much later, on 6 January 1960 (Lundholm et al., 2003). Hence, *P. pseudodelicatissima* would be the valid species name in scenario #1.

3.5.4 *cox*1, LSU and ITS2 of *Pseudo-nitzschia*

Most often morphological and molecular evidence is used as indicators of speciation. Breeding experiments have provided valuable information on species boundaries and have helped to separate the pseudo-cryptic *P. mannii* within the *P. pseudodelicatissima* complex (Amato & Montresor, 2008), as well as the cryptic *P. arenysensis* and *P. dolorosa* within the *P. delicatissima* complex (Quijano-Scheggia et al., 2009). The phylogenetic approach to character interpretation (Patterson, 1988) is reflected in our ITS2 phylogeny, which is inferred from sequence structure data (Figure 3.11). Indeed, both morphological (i.e., features of the siliceous cell wall) and molecular (i.e., DNA sequences) characters can be treated equally to support species delineation under the phylogenetic species concept.

The complete sequence length of *cox1* in diatoms varies from ~1,000 to 6,500 bp, e.g., *Berkeleya fennica* (1,434 bp; An et al., 2016), *Thalassiosira pseudonana* (3,838 bp; Armbrust et al., 2004), *Phaeodactylum tricornutum* (6,295 bp; Outdot-Le Secq & Green, 2011), *Synedra acus* (6,468 bp; Ravin et al., 2010), and *Pseudo-nitzschia multiseries* (6,111 bp; Cao et al., 2016). Similarly, the number and length of introns in *cox1* varies among different species. For example, *Phaeodactylum tricornutum*, *Pseudo-nitzschia multiseries* and *Synedra acus* possess two introns (4,000–5,000 bp), while there is only one in *Thalassiosira pseudonana* (~2,000 bp) and none in *Berkeleya fennica*. Due to the presence of introns in *cox1* (Ehara et al., 2000), it can be relatively difficult to amplify and sequence the region (Moniz & Kaczmarska, 2009; Hamsher et

al., 2011), as also demonstrated in the *Sellaphora* (Evans et al., 2007) and *Nitzschia palea* (Troboja et al., 2010) complexes. Indeed, amplification of *cox1* sequences in *Pseudo-nitzschia* often resulted in multiple bands from PCR.

The alignment of datasets affects the robustness of a phylogeny other than sample density. In contrast to LSU and ITS2 rRNA genes, the mitochondrial *cox1* gene comprises few indels, and can thus readily be aligned for analyses (Evans et al., 2007; present study). ITS2 is especially difficult to align and requires an advanced understanding of bioinformatics tools. As a result, the prediction of secondary structure has sometimes differed among research groups (Moschandreou et al., 2012; Orive et al., 2013; Percopo et al., 2016). Compared to ITS2, the alignment of *cox1* is easier, more straightforward, and has a higher repeatability.

According to Evans et al. (2007), *cox1* sequences are more divergent than *rbcL* sequences, and are therefore more useful in resolving low-level, intra- and inter-specific relationships, e.g., in the diatom *Sellaphora*. Currently, the main drawback for applying *cox1* to diatoms (Bacillariophyta) is the restricted availability of entries in the GenBank database (~400), compared to a ~6-fold greater number for ITS. However, the ability of *cox1* to delimit species and its low intra-genomic variation make it worthy of further exploration, e.g., through the development of better primers (Troboja et al., 2010) or cloning. The ITS region of diatoms is complex, in particular because multiple divergent copies can be found within a single clonal culture (Behnke et al., 2004; Casteleyn et al., 2009). As ITS2 is a rapidly evolving gene, it is normal to have highly divergent polymorphisms in the sequences, because they evolved significantly faster than other genes. However, for *Pseudo-nitzschia*, it has been shown that evolution most often keeps the multiple divergent copies uniform (D'Alelio et al., 2009).

3.6 Conclusion

Comprehensive sequence sampling in this study has been shown to be a useful criterion in improving the accuracy of phylogenetic estimation by recovering the species complex groupings. The phylogenetic tree inferred from ITS2 sequence-structure analyses indicates that the morphologically based species complexes have an evolutionary relevance that agrees with molecular phylogeny. Currently, *cox1* sequences have only been recovered from 19 of the 49 described *Pseudo-nitzschia* species, whereas there are 36 and 41 sequences for LSU and ITS2, respectively. Thus, more sequences are required from each marker to make an adequate comparison of the relative usefulness of these markers. The data presented here contribute to the hypothetical framework of character evolution in *Pseudo-nitzschia*. The status of *P. cuspidata* and *P. pseudodelicatissima* remains unresolved and requires examination of material from the type localities.

CHAPTER 4: DIATOM *NITZSCHIA NAVIS-VARINGICA* (BACILLARIOPHYCEAE) AND ITS DOMOIC ACID PRODUCTION FROM THE MANGROVE ENVIRONMENTS OF MALAYSIA

4.1 Introduction

Domoic acid (DA), a neurotoxin that binds irreversibly to the glutamate receptor in the vertebrate central nervous system (Pulido, 2008), was first discovered from the red alga *Chondria armata* (Kützing) Okamura (Takemoto & Daigo, 1958). The toxin was responsible for amnesic shellfish poisoning (ASP) (reviewed in Lelong et al., 2012; Fernandes et al., 2014) that can be fatal to humans after consuming DA-contaminated fishery products. The source of DA contamination was diatoms of the genus *Pseudo-nitzschia* (e.g., Bates et al., 1989; Lelong et al., 2012; Dao et al., 2014). The massive bloom of *Pseudo-nitzschia* along the west coast of North America in 2015 caused a closure of crab and molluscan shellfisheries for an unprecedented time. This affected not only the local economy but also the fishing communities (McCabe et al., 2016). DA has also disrupted the marine food web, resulting in mass mortalities of marine mammals (sea lions and whales) at higher trophic levels (Lefebvre et al., 2016).

Diatoms of the genus *Nitzschia*, on the other hand, have so far never been associated with any human poisonings, even though two species have been confirmed to produce DA: *N. navis-varingica* Lundholm and Moestrup (Lundholm & Moestrup, 2000) and *N. bizertensis* Bouchouicha Smida, Lundholm, Sakka and Hadj Mabrouk (Bouchouicha Smida et al., 2014). The toxigenic *N. navis-varingica* was discovered for the first time from shrimp-culture ponds in Vietnam (Kotaki et al., 2000), and subsequently was found in brackish waters and estuaries throughout the Southeast Asian region (Kotaki et al., 2004, 2005, 2006, 2008; Bajarias et al., 2006; Romero et al., 2008, 2011, 2012; Takata et al., 2009; Thoha et al., 2012; Suriyanti and Usup, 2015).

Conversely, the distribution of *N. bizertensis* was limited to Bizerte Lagoon, Tunisia, the type locality (Bouchouicha Smida et al., 2014).

While most toxigenic *Pseudo-nitzschia* species are planktonic, *N. navis-varingica* was frequently found in the benthic brackish ecosystem (e.g., Kotaki et al., 2004, 2005; Romero et al., 2012). Mangroves are one of the tropical-substropical brackish ecosystems that play an important role as shelters for marine life. They often host many commercially valuable molluscan shellfish (e.g., benthic clams: *Polymesoda*; rock oysters: *Crassostrea*; razor clams: *Solen*) and crustacean species (mud crabs: *Scylla serrata*) (Rönnbäck, 1999; Honculada-Primavera, 2000), which may serve as vectors of DA (W.N. Noordin and P.T. Lim, per. comm.).

In the Western Pacific region, DA contamination in bivalves was limited to Vietnam (Dao et al., 2006, 2009; Huyen et al., 2006; Takata et al., 2009), Philippines and Japan (Takata et al., 2009). Only studies from Vietnam confirmed that DA contamination in bivalves was attributed to DA-producing *Pseudo-nitzschia* species (Dao et al., 2014, 2015). *Pseudo-nitzschia* species, including several novel and toxic ones, have been widely reported from coastal waters of the Straits of Malacca and South China Sea (e.g., Lim et al., 2013, 2014; Teng et al., 2014, 2015). Conversely, information on the occurrence and distribution of toxigenic *Nitzschia* species is very scattered. The aim of this study was to document the presence of toxigenic *N. navis-varingica* from the mangrove habitats of Peninsular Malaysia and collect the information about DA accumulated in bivalve shellfish. Morphological characters of *Nitzschia* species were based on wild and cultured specimens, using light and electron microscopy. The phylogenetic relationship of *N. navis-varingica* was inferred based on the nuclear-encoded ribosomal DNA (rDNA) in the large subunit (LSU) and the internal transcript spacer (ITS) regions. Toxicity of some strains and bivalve shellfish was

analyzed by liquid chromatography (FMOC-LC-FLD) and further confirmed by mass spectrometry (LC-MS/MS).

4.2 Literature Review

4.2.1 *Nitzschia navis-varingica* Lundholm et Moestrup

Diatom *N. navis-varingica* was first found in the shrimp pond in Vietnam, subsequently the species was found throughout the Southeast Asian region [Philippines (Kotaki et al., 2004, 2005, 2006, 2008; Bajarias et al., 2006; Romero et al., 2011), Thailand (Romero et al., 2008), Malaysia (Suriyanti & Usup, 2015), Indonesia (Romero et al., 2011)] and Japan (Kotaki et al., 2004, 2008). According to Lundholm and Moestrup (2000), *N. navis-varingica* has several characteristics when observed under LM: yellow-brown, two chloroplasts, rectangular in girdle view, lanceolate in valve view, and pervalvar axis wider than the transapical axis. The raphe is moderately eccentric. In molecular data, only LSU rDNA sequences have been used in the study of *N. navis-varingica* phylogeny for identification (Lundholm et al., 2002; Trobajo et al., 2006; Bouchouicha-Smida et al., 2014; Carballeira et al., 2017). No study of phylogeny of *N. navis-varingica* using the region of ITS2 as a genetic marker. In toxicity data, the cellular DA content of *N. navis-varingica* strains was in the range from 0.04 to 15.3 pg DA/cell (Kotaki et al., 2000, 2004, 2005, 2006, 2008 Bajarias et al., 2006; Romero et al., 2008, 2011).

4.2.2 Mass spectrometry fragmentation of DA

For DA, a typical mass spectrum of DA molecule in the positive ion mode shown molecular ion $[M+H]^+$ at the base peak of *m*/*z* 312 (Figure 4.1). Two prominent peaks, at *m*/*z* 266 and 294 formed from the loss of water $[M+H-H_2O]^+$ and formic acid molecule $[M+H-HCOOH]^+$, respectively. The ions at *m*/*z* 266 and 294 continuosly separated by removing formic acid, water molecule or $[C_2H_4O_2N]$ and resulted as peaks at *m*/*z* 276, and 248 for *m*/*z* 266; peaks at *m*/*z* 266 gave three prominent fragment ions at *m*/*z* 248, 220 and 193. The following daughter ions namely *m*/*z* 230, 202, 174, 119 and 175 were shown due to the loss of water or formic acid molecules (Figure 4.1) (Furey et al., 2001; La Barre et al., 2014).

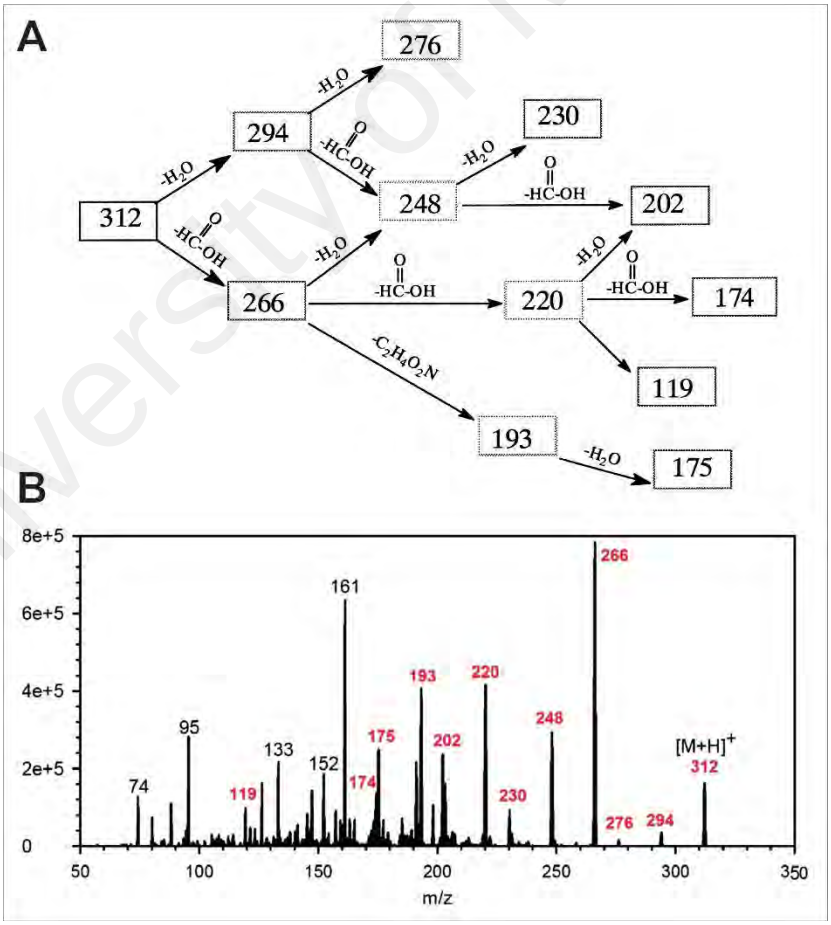

Figure 4.1: (A–B) Characteristic fragmentation pathway of domoic acid (DA) in positive ion mode. (B) The peaks in red correspond to species resulting from fragmentation pattern. (Source: La Barre et al., 2014).

4.3 Methodology

4.3.1 Sampling sites, sample collection and algal cultures

For culture collection, sampling was undertaken at four mangrove areas (Figure 4.2) where bivalve shellfish and crabs have been harvested by local populations for trading and personal consumption. Tok Bali (Kelantan; 5.8611° N, 102.5149° E), located at north-eastern Peninsular Malaysia, is known for the production of benthic clams (*Polymesoda similis*) and rock oysters (*Crassostrea iredalei*); Linggi River (Negeri Sembilan; 2.3970° N, 101.9825° E and Malacca; 2.3883° N, 101.9713° E), on the west coast of the Peninsula, is an important site for the collection of mussels by artisanal fishermen; Muar (Johor; 2.0669° N, 102.5586° E), located at the south-western coast of the Peninsula, is well known for oyster harvesting; Pendas, situated at the Tebrau Strait (Johor; 1.3759° N, 103.6388° E), is a fishing village.

Plankton samples were collected with a 20-µm mesh plankton net using the kick-net sampling method (Kotaki et al., 2000). Live samples were transferred into 500-ml bottles and brought back to the laboratory to establish cultures. Single cells were isolated using a finely drawn Pasteur pipette under a Leica DM3000 microscope (Leica, Germany). Generally, *Nitzschia* appeared at low densities; thus, the field samples were first enriched (see below) and incubated in continuous light for 24–48 hr prior to cell isolation.

Cultures were established and grown in f/2 medium (Guillard & Ryther, 1962), at 25 ± 0.5 °C, the salinity of 27, and a light intensity of 100 µmol photons m^{-2} s^{-1} under 12:12 h light:dark photoperiod. Clonal cultures of *N. navis-varingica* established and used in this study are shown in Appendix D. Bivalve shellfish (e.g. cockles, clams, razor shell, scallop, mussel) were collected for toxin analysis (Figure 4.2).

Figure 4.2: Map of Peninsular Malaysia showing sampling sites of *Nitzschia* species (blue dots on map) and collection of bivalve shellfish (red dots on map).

4.3.2 Morphological observation

Live cells of *Nitzschia* (8–12 days after inoculation) were observed under a Leica DM3000 microscope (Leica, Germany), with a 400× magnification. For TEM, samples were acid-cleaned as described in Teng et al. (2013). A drop of the acid-cleaned cells was then transferred onto a Formvar-coated copper grid. Samples were observed under a JEOL JEM-1230 TEM (JEOL, Tokyo, Japan). Morphometric measurements of valve length and width, the density of interstriae, fibulae, and areolae of >30 cells were obtained.

4.3.3 DNA extraction, gene amplifications, and sequencing

Cultures at mid-exponential phase were harvested by centrifugation (2600 ×*g*, 10 min), lysed by adding 2× Cetyl-trimetyl-ammonium-bromide (CTAB) lysis buffer, and the genomic DNA was extracted as described in Lim et al. (2012). Large subunit ribosomal DNA (LSU rDNA) in the domain D1–D3 was amplified using the primer pair DIR and D3Ca (Scholin et al., 1994), and the internal transcribed spacer (ITS) region was amplified using ITS1 and ITS4 (White et al., 1990). PCR was performed in a peqSTAR 96X universal gradient thermocycler (Erlangen, Germany) with the following PCR conditions: 94°C for 5 min for the initial denaturation, followed by 35 cycles of denaturation (94°C for 45 s), annealing (52°C for 30 s) and elongation (72°C for 90 s), and completed with a final extension at 72°C 8 min. The amplicons were purified using the QIAquick DNA purification kit (Qiagen, Hilden, Germany). DNA sequencing was performed on an ABI 3770XL automated sequencer (PE Applied Biosystems, Foster City, CA) on both strands.

4.3.4 LSU rDNA analyses and phylogenetic reconstruction

For the LSU rDNA dataset, 16 nucleotide sequences of *Nitzschia* were obtained in this study. These sequences, and 11 of *Nitzschia* retrieved from NCBI GenBank nucleotide database (Appendix E) were multiple-aligned using MUSCLE (Edgar, 2004b). *Navicula* cf. *erifuga* and *Halamphora coffeiformis* (C.Agardh) Levkov (previously known as *Amphora coffeaeformis*) were chosen as outgroup taxa. Maximum Parsimony (MP) and Maximum Likelihood (ML) were performed using PAUP* ver. 4.0b.10 (Swofford, 2001), and Bayesian analysis (BI) was run by MrBayes 3.2.2 (Ronquist et al., 2012) as detailed in Teng et al. (2015).

4.3.5 ITS2 secondary structure modeling and phylogenetic analyses

For the ITS2 dataset, 38 ITS2 secondary structures of newly obtained sequences and those retrieved from Genbank were modeled. The universal motifs of ITS2 secondary structure were based on previous studies (Coleman, 2003, 2009; Keller et al., 2009; Koetschan et al., 2010). Structures of ITS2 were illustrated using VARNA (Darty et al., 2009).

To construct the ITS2 sequence-structure phylogenetic tree, *Amphora* sp. [accession: JF834543] and *Navicula trivialis* Lange-Bertalot [accessions: FN397610 and FN397614] were chosen as outgroups (Appendix E). 4SALE v1.5 was used to perform the sequence-structure alignment with the ITS2 specific scoring matrix (Seibel et al. 2006, 2008; Wolf et al., 2014). Trees were reconstructed by the neighbour-joining (NJ) method, using ProfDistS v0.9.9 (Qt version) (Friedrich et al., 2005; Wolf et al., 2008) and by sequence-structure ML, using phangorn (Schliep, 2011) in R (R Core Team, 2014) as detailed in Teng et al. (2015). Genetic divergences among *Nitzschia* taxa were calculated using MEGA5 (Tamura et al., 2011).

4.3.6 Domoic acid analyses culture

Late exponential phase-cultures (21–28 d after inoculation) of 48 strains of *N. navis-varingica* (10 ml, cells plus medium) were extracted by ultra-sonication (2 min), and ultra-filtrated using a 10,000 cut-off Ultrafree-MC centrifugal filter unit (Millipore, MA, USA). DA analysis was performed by HPLC with pre-column derivataization using 9-fluorenylmethylchloroformate (FMOC) and fluorescence detection (FMOC-LC-FLD) (Pocklington et al., 1990; Kotaki et al., 2005). Extract from some strains were further analysed by LC-MS/MS, using a Triple TOF® 5600+ system, a hybrid triple quadrupole time-of-flight (TOF) mass spectrometer (AB SCIEX, US), with the conditions as described in Romero et al. (2011). Calibration was performed using a DA standard (National Research Council of Canada, Halifax, NS, Canada) and purified isodomoic acid B (IB; Kotaki et al., 2005). Multiple reaction monitoring (MRM) was performed by selecting the transitions at *m/z* 312.1→266.1, 312.1→248.1 and 312.1→202.1, respectively (Furey et al., 2001). Cellular DA (pg cell^{-1}) was calculated by attributing the total DA produced in the culture to the total cell number, as detailed in Bates et al. (1991).

4.3.7 Toxin production of strain NTB02 over the growth cycle

Growth of *N. navis-varingica* strain NTB02 was monitored by subsampling for cell counts. Subsamples were fixed in Lugol's solution and counted microscopically using a Sedgewick-Rafter slide (1 ml, in triplicate). Samples were collected at 3-day intervals over the 24-days growth cycle (day 7, 10, 13, 16, 19 and 24). Toxins were analysed by FMOC-LC-FLD as described above.

4.3.8 Domoic acid analyses on bivalve shellfish

Shellfish tissue were homogenized and freeze-dried. A total of 0.5 g of freeze-dried samples were placed into a 15 mL centrifuge tube. 10 µL of surrogate solutions was added to the samples before extracting with 4 mL of methanol. The sample was mixed and vortex for 1 min and centrifuged at 4000 rpm for 10 min. The supernatant was collected into another 15mL centrifuge tube. Step on methanol extraction was repeated. A total of 8 mL of supernatant were collected. A C18-ODS (200 mg/3 mL) column was placed on a SPE Vacuum manifold (ANPEL Scientific Instrument) and conditioned with 6 mL of methanol. 1 mL of supernatant was applied and eluted with 0.5 mL of methanol. The supernatant of the sample was added to 2 mL by adding methanol. A portion of 1 mL of solution was filtered using a 0.22 µm Polyethersulfone resin (PES) membrane filter before LC-MS/MS analysis.

4.4 Results

4.4.1 Morphology of *N. navis-varingica*

A total of 82 clonal cultures of *Nitzschia* were established from Malaysia (Appendix D). Here, we present the morphology of *N. navis-varingica* (strains NTB02, NTB23, NLN01, NLN08 and NLN29) from Malaysian mangroves (Table 4.1; Figures 4.3–4.4). The nucleus is located in the central gap between the two yellow-brown discoidal chloroplasts. Cells are lanceolate and symmetrical in valve view (Figure 4.2A) and rectangular in girdle view (Figure 4.2B). Cells were solitary and sometimes appeared as doublets (Fig. 2B). The incompletely separated cells are merely adhered to each other and are frequently observed in the exponential phase (Figure 4.2C). Cell valve is 88.5 ± 5.3 µm long and 5.7 ± 1.1 µm wide (Table 4.1).

The raphe is positioned eccentrically and raised on a keel, where striae are raised on the valve (supported by the fibulae) (Figure 4.3A–D). Fibulae and interstriae are visible under TEM (Figure 4.3D–F). Densities of fibulae and interstriae in 10 µm are 10–14 and 26–29, respectively (Table 4.1). Each stria consists of one row of circular areolae (4–7 areolae in 1 µm) (Figure 4.3F and 4.3G). The cingulum comprises few rows of areolae (Figure 4.3H). The density of areolae in cingular band is 2–5 in 1 µm (Figure 4.3I).

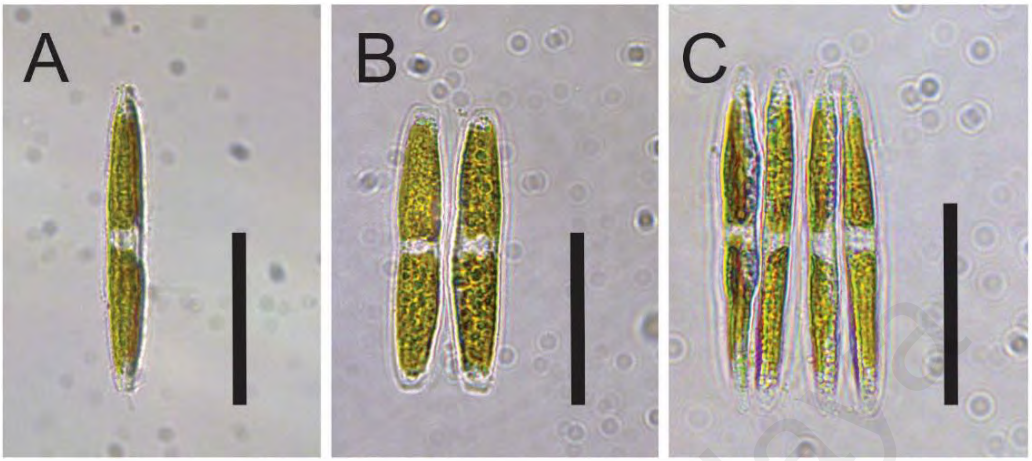

Figure 4.3: *Nitzschia navis-varingica*, strain NTB02. Live cells. LM. (A) Valve view, single cell. (B) Girdle view, cells adhering valve to valve. (C) Valve view, cells adhering girdle to girdle. Scale bars, 50 µm.

Table 4.1: Frustule morphometric measurements of *Nitzschia navis-varingica* obtained in this study, compared to the type specimen (VSP974-1). *n*, number of cells observed. n.d., not detected.

Strain	Length (µm)	Width (µm)	Fibulae in 10 µm	Striae in 10 µm	Areolae in 1 µm	Rows of areolae	Band areolae in 1 µm	Reference
NTB02	86.27–91.89 89.08±2.81 (*n*=30)	4.24–5.26 4.75±0.51 (*n*=30)	11–13	26–29	4–6	1	3–5	This chapter
NTB23	89.26–93.98 91.62±2.36 (*n*=30)	5.40–6.18 5.79±0.39 (*n*=30)	10–12	26–28	4–5	1	3–4	This chapter
NLN01	88.93–92.89 90.91±1.98 (*n*=30)	4.67–5.47 5.07±0.40 (*n*=30)	10–12	26–28	4–5	1	3–4	This chapter
NLN08	74.14–87.46 80.80±6.66 (*n*=30)	5.49–8.19 6.84±1.35 (*n*=30)	10–12	26–28	4	1	2–4	This chapter
NLN29	88.26–92.64 89.83±2.81 (*n*=30)	5.69–6.77 6.23±0.54 (*n*=30)	12–14	26–28	4–7	1	n.d.	This chapter
VSP974-1	45.00–55.00	9.00–11.00	10–12	26–30	3–4	1	2–3	Lundholm & Moestrup (2000)

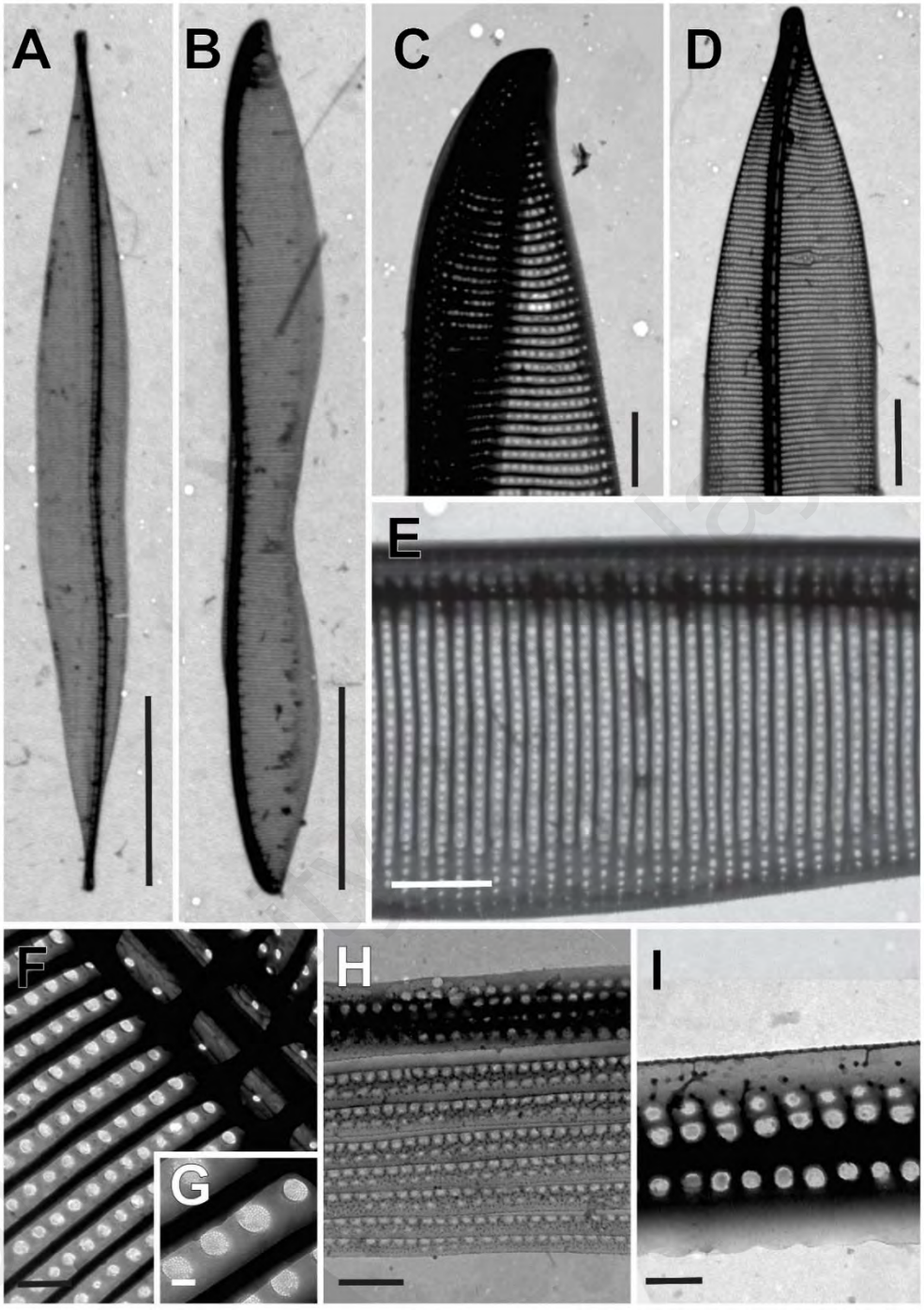

Figure 4.4: ***Nitzschia navis-varingica*****, strain NTB02. TEM. (A–B) Valve and girdle view of frustule. The raphe slits are positioned along one edge of the valve face, raised along the keel and spanned internally by fibulae. (C) Apices of valve curved inward. (D) Tips of valve with visible fibulae from the canals. (E) View of valve near the central nodule. (F) Distinct and regularly spaced fibulae and the wall of raphe canal, showing pattern of silica ridges on the wall of the raphe canal. (G) Round areolae. (H) Cingulum comprises varying rows of areolae. (I) Single band, part of the girdle showing three rows of areolae at valvocopula. Scale bars: 20 µm (A, B); 2 µm (C, E, H); 5 µm (D); 0.5 µm (F, I); 0.1 µm (G).**

4.4.2 Molecular phylogenetic inferences and genetic divergences

The LSU dataset yielded a final alignment consisting of 798 characters, of which 572 characters are constant, 123 are parsimony informative, and 103 are parsimony uninformative. All MP, ML and BI yielded identical tree topologies; only the BI tree is shown (Figure 4.5). The trees revealed a group comprising *N. navis-varingica* strains from Malaysia, Vietnam (VSP9741 and VHL987) and Philippines (BCEA0342, SREA033 and BLEC03172) (Lundholm et al., 2002; Kotaki et al., 2005) with strong bootstrap supports (MP/ML/BI: 93/94/0.87) and low sequence divergences (*p*-distances, <0.3%; Table 4.2). *Nitzschia laevis* Hustedt, *N.* cf. *promare* and *N. pellucida* Grunow formed a highly supported branch to *N. navis-varingica* (MP/ML/BI: 100/100/1.0).

The ITS2 secondary structure of *N. navis-varingica* showed a common feature of the eukaryotic ITS2 transcript, with four main helices and a pseudo-helix, IIa. The consensus structure revealed high structural conservation among strains of *N. navis-varingica* (Figure 4.6). The ITS2 sequence-structure alignment contained 701 columns; trees constructed were congruent, and only the NJ tree is shown (Figure 4.6). Strains of *N. navis-varingica*, as previously revealed by the LSU rDNA dataset, formed a strong monophyletic lineage (NJ/MP/ML: 94/80/70), with three subclades resolved, namely A, B, and C. Sequence divergences within subclades are 0–1.5%; the pair-wise uncorrected *p*-distances among groups ranged between 2.5–7.4% (Figure 4.6; Table 4.3).

.

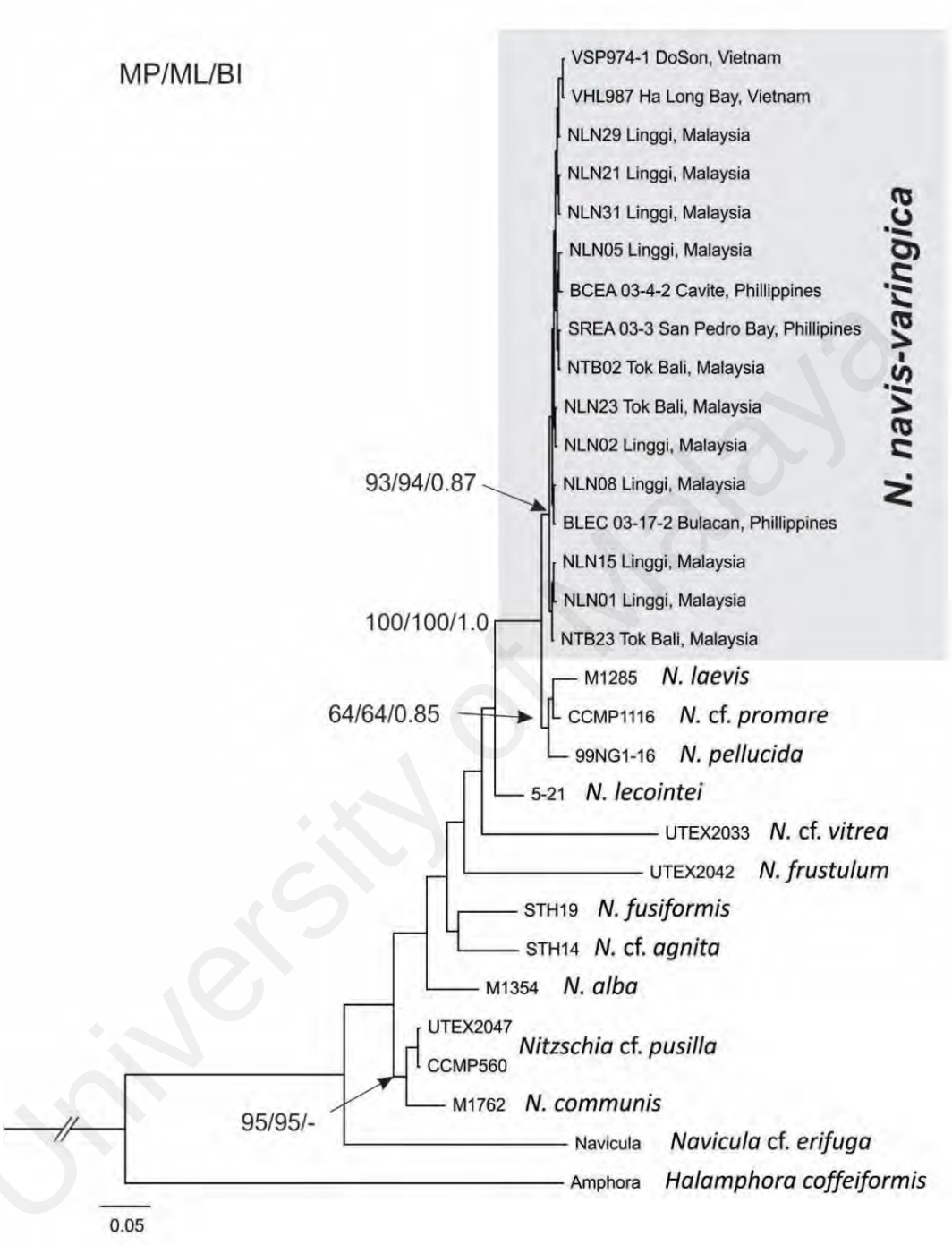

Figure 4.5: Bayesian tree of *Nitzschia navis-varingica* and its sister species inferred from the LSU rDNA dataset. Values on nodes represent bootstrap supports of MP and ML, and posterior probabilities of BI.

Table 4.2. Pairwise LSU rDNA genetic distances of *Nitzschia* species (uncorrected *p*-distances). Shaded diagonal, intraspecific sequence divergences (in percent, %).

Species	1	2	3	4	5	6	7	8	9	10	11	12
1. *Nitzschia* cf. *vitrea*	0											
2. *N. frustulum*	10.5	0										
3. *N. alba*	10.5	9.3	0									
4. *N. communis*	9.2	10.4	6.2	0								
5. *N. pusilla*	8.4	8.5	5.0	3.1	0							
6. *N. fusiformis*	9.4	8.4	6.2	6.2	5.5	0						
7. *N. agnita*	9.6	8.5	6.2	5.8	5.1	5.3	0					
8. *N. lecointei*	9.0	8.8	5.4	5.8	4.9	6.5	5.1	0				
9. *N. laevis*	8.5	8.8	7.0	7.3	6.1	6.1	6.6	5.0	0			
10. *N. pellucida*	9.8	10.0	7.3	7.5	6.5	5.9	7.0	5.0	2.2	0		
11. *N. promare*	8.8	8.8	7.0	7.0	5.5	5.8	6.5	4.3	1.6	1.9	0	
12. *N. navis-varingica*	8.2–8.5	8.8–8.9	6.6–6.9	7.1–7.4	5.9–6.2	5.7–5.9	6.2–6.3	3.8–4.0	1.9–2.0	2.0–2.3	1.2–1.5	0–0.3

Table 4.3. Pairwise ITS2 genetic distances of *Nitzschia* species (uncorrected *p*-distances). Shaded diagonal, intraspecific divergence (in percent, %).

Species	1	2	3	4	5
1. *Nitzschia navis-varingica*	0–7.4				
2. *N. closterium* f. *minutissima*	30.9–31.9	0			
3. *N. longissima*	28.9–33.3	38.2	0		
4. *N. palea*	48.5–51.0	54.4	47.1	0	
5. *N. microcephala*	32.4–32.8	37.7	40.2	50.0	0

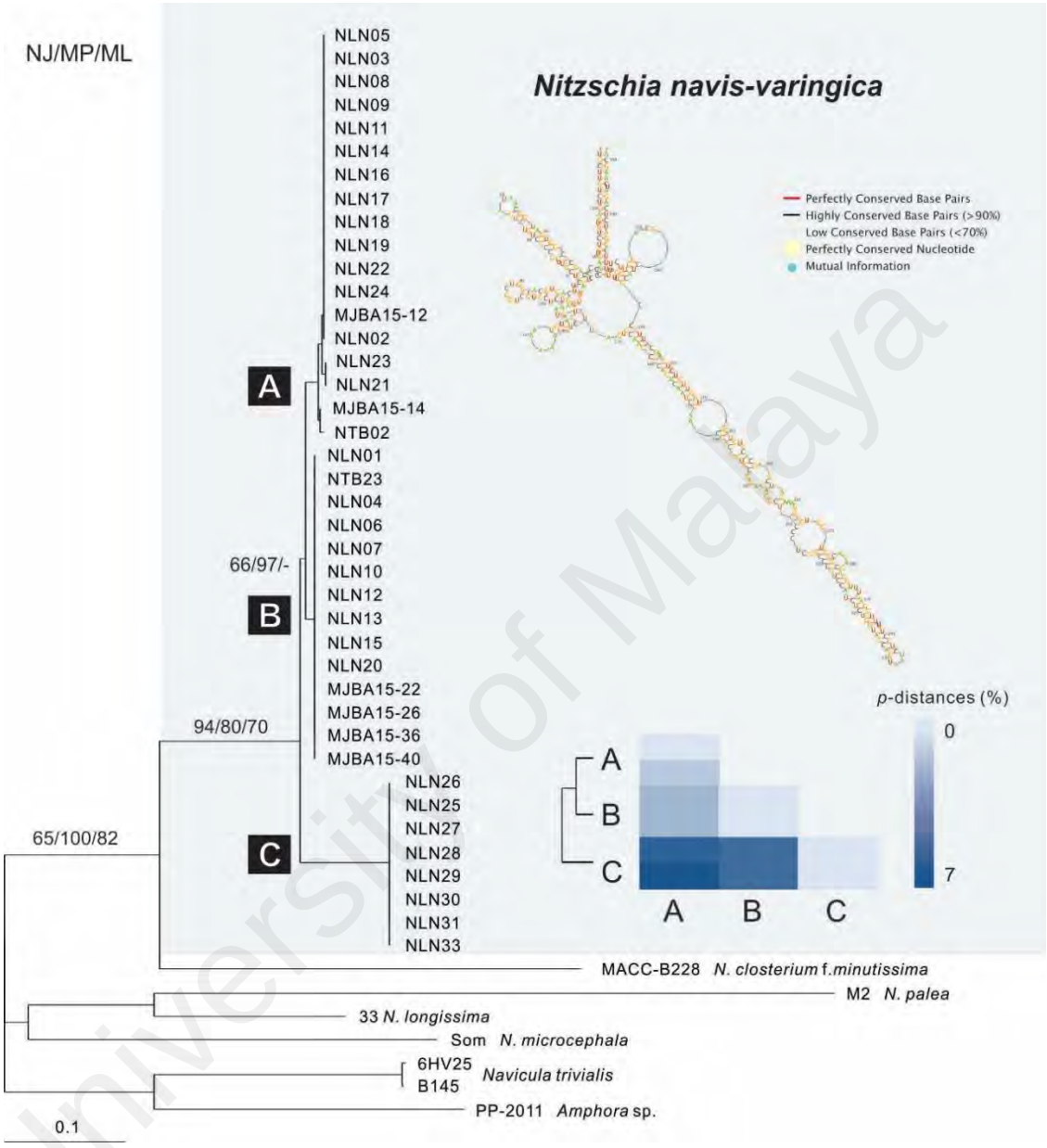

Figure 4.6: NJ tree of *Nitzschia navis-varingica* based on ITS2 sequence-structure alignment. Values on nodes represent bootstrap supports of NJ, MP and ML. Three subgroups are revealed in the *N. navis-varingica* clade (A, B, and C). The heatmap presents the pair-wise uncorrected *p*-distances among subgroup A, B and C. A consensus ITS2 transcript of *N. navis-varingica* showing four common helices and one pseudo-helix.

4.4.3 Domoic acid production

DA was detected in 48 strains of *N. navis-varingica* by FMOC-HPLC-FLD (Figure 4.7A–B). TOF LC-MS/MS confirmed the presence of DA in four strains (NTB02, MJBA15-10, MJBA15-25 and MLGB15-9); LC-MS/MS chromatrograms of the NTB02 extract are shown in Figure 4.7C–J. Full scan MS in the positive ion mode gave three dominant peaks at $[M+H]^+$ *m/z* 312, corresponding to isodomoic acid A (IA), domoic acid (DA) and isodomoic acid B (IB), respectively (Figure 4.7C). The following characteristic MRM mass transitions were observed: $[M+H]^+$ *m/z* 312 to *m/z* 266, due to loss of the formic acid molecule $[M+H–CH_2O_2]^+$ or water and carbon dioxide $[M+H–H_2O–CO_2]^+$ (Figure 4.7D), followed by loss of water molecules $[M+H–CH_2O_2–H_2O]^+$ to *m/z* 248 (Figure 4.7E). The ion at *m/z* 202 was due to the loss of formic acid or carbon dioxide and water (Figure 4.7F). Extracts of strain NTB02 (on day 24) showed the presence of two dominant peaks, DA and IB (Figure 4.7E). The fragmentation pattern of algal extracts (Figure 4.7H–J) was identical to the standards of DA and its isomers (Figure 4.7D–F).

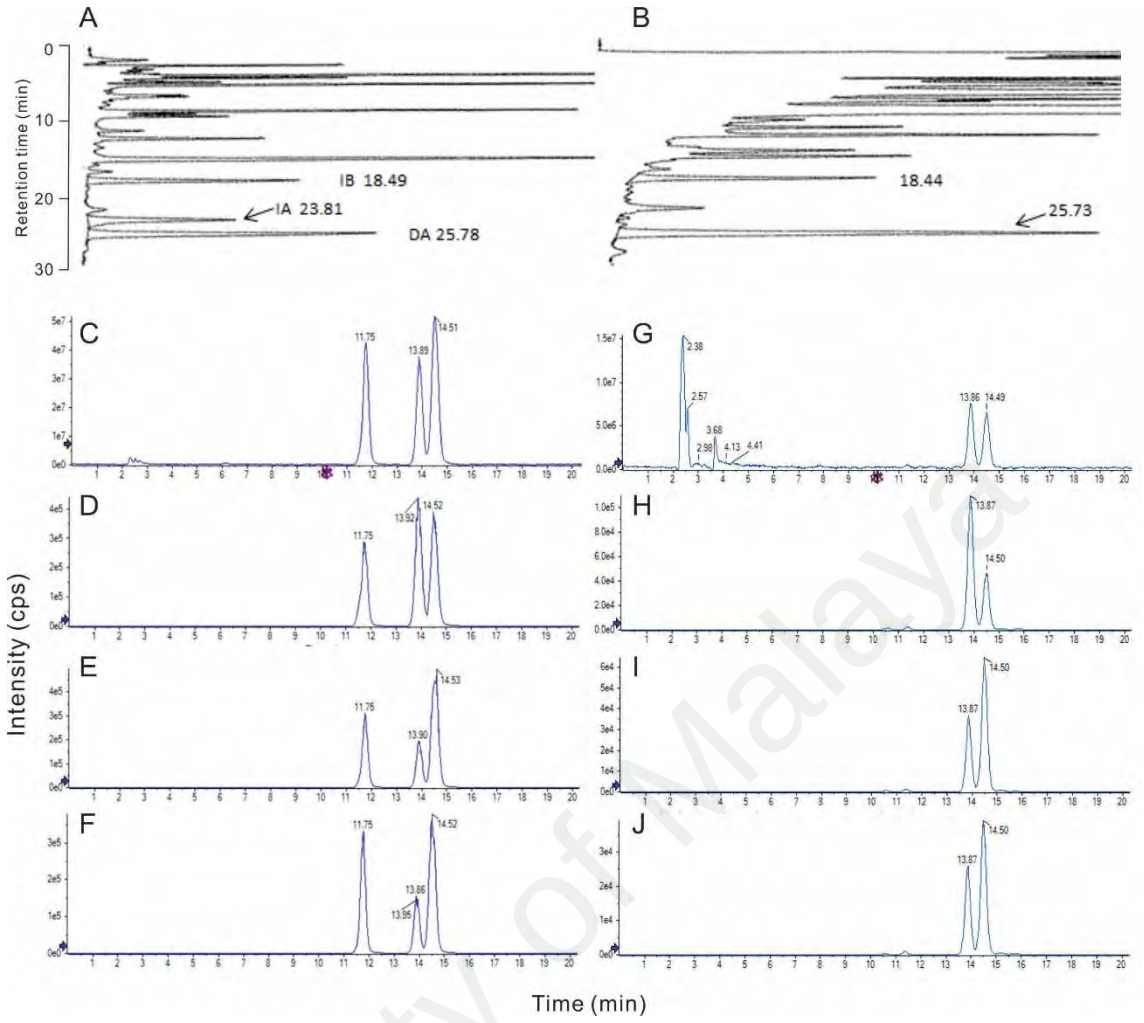

Figure 4.7: FMOC HPLC-FLD (A–B) and LC-MS/MS selected ion monitoring (SIM) chromatograms (C–J) of *Nitzschia navis-varingica*, strain NTB02. (A) Toxin standard, DAKS13A-3; domoic acid (DA), 35.9 ng ml^{-1}; isodomoic acid A (IA), 16.0 ng ml^{-1}; isodomoic acid B (IB), 26.4 ng ml^{-1}. (B) Toxin extract on day 24. (C–F) Toxin standard, DAKS 13A×15; DA, 15.2 μg ml^{-1}; IA, 24.6 ppm; IB, 25.8 μg ml^{-1}. (G–J) strain NTB02 extract on day 24 (DA, 2.7 μg ml^{-1}; IB, 1.2 μg ml^{-1}). Total ion monitoring (C, F) and multiple reaction monitoring (MRM) of protonated DA, IA and IB at *m/z* 312.1→266.1 (D, H), 312.1→248.1 (E, I), and 312.1→202.1 (F, J).

DA was detected as the major congener in all strains, comprising at least 61% of the DA plus isomers, with the exception of MJBA15-12. That strain contained IB as the major congener, comprising 73% of the total toxin content. While IB was detected as the second major congener in most strains, it was not detected in strain MJBA15-13. IA was detected in trace amounts in some strains (<2.5%), and as a minor constituent in seven strains (MJBA15-12, MLGB15-10, MLGB15-9, MLGB15-8, MJBA15-9,

MJBA15-13 and MJBA15-10), comprising 3.8–7.0% of the total toxin content (Figure 4.8). However, IA concentrations of these strains never reached more than 0.2 pg cell^{-1}. Only two strains from Linggi contained a high proportion of IA: MLGB15-6 (12.7%) and MLGB15-1 (23.5%). Four strains from Pendas and a strain from Linggi were detected with only DA, but the concentration varied between 0.48 and 5.94 pg cell^{-1}. Considerable variability in the total DA concentration of all strains was observed, ranging from 0.37 pg cell^{-1} (strain MLGB15-1, Linggi) to 11.06 pg cell^{-1} (strain MMAD15-7, Muar) (Figure 4.8). Generally, strains from Linggi (0.37–0.98 pg cell^{-1}, *n* = 10) were less toxic than those from Muar (0.92–11.06 pg cell^{-1}, *n* = 10) and Pendas (0.82–10.79 pg cell^{-1}, *n* = 27).

The result of Ward's cluster analysis performed using the compositions (%) of DA found in all *N. navis-varinginca* strains tested in this study revealed two main groups separated by the composition of the major constituent, DA: strains containing DA >80% and those with DA <80%. No clear separation with geographical origins was observed (Figure 4.8).

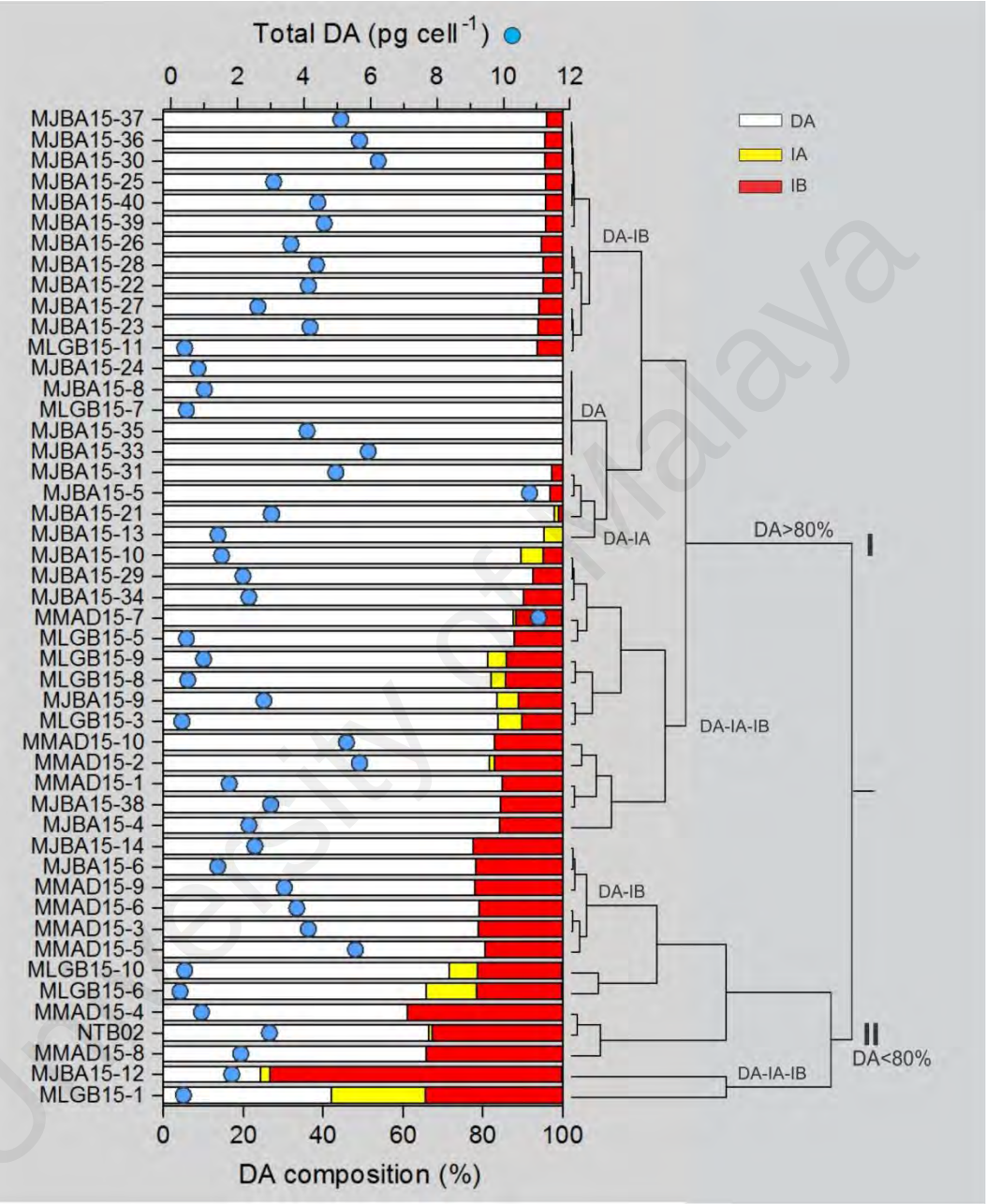

Figure 4.8: Total domoic acid (DA) concentration (pg cell^{-1}; open circles) and toxin composition (%; bars) of *Nitzschia navis-varingica* strains from Malaysia. The Ward's dendrogram is constructed based on the toxin composition of all strains. The cluster reveals two major toxin groups: (I) strains containing DA >80% and (II) strains with DA <80%.

The growth of strain NTB02 was studied with respect to the production of DA and its isomers. Cell numbers did not increase between days 7 (the first sampling) and 16, but then a short period of exponential growth was observed between days 16 and 19 (specific growth rate, μ = 0.25 d^{-1}), followed by the beginning of the stationary phase (Table 4.4; Figure 4.9). The toxin profile of strain NTB02 was stable throughout the growth cycle, predominantly contributed by DA and IB (~99–100%) (Table 4.4; Figure 4.9). Even though the profile is stable, the composition was notably different at the beginning of culture cycle (day 7), when the relative proportion of IB was considerably higher than DA (DA:IB, 45:55). The proportion of DA increased after day 7, and remained almost constant throughout the culture cycle (mean ratios of DA:IB, 71:29). Trace amounts of IA were detected only on day 13 onward (<0.5%, <0.03 pg $cell^{-1}$). Concentrations of total DA increased gradually from 0.54 to 2.23 pg $cell^{-1}$ between days 7 and 16 (Table 4.4; Figure 4.9), even though no cell growth was observed during this period. The concentration of total DA per cell declined by almost half (to 1.41 pg $cell^{-1}$) from day 16 to 19, coinciding with a 2-fold increase in cell density (Table 4.4; Figure 4.9).

Table 4.4: Growth and toxin profile of *Nitzschia navis-varingica* strain NTB02, domoic acid (DA), isodomoic acid A (IA) and isodomoic acid B (IB).

Day of sampling	Cell density, 10^3 cells ml^{-1} (±SD)	DA, ng $cell^{-1}$ (%)	IA, ng $cell^{-1}$ (%)	IB, ng $cell^{-1}$ (%)	Total DA, ng $cell^{-1}$
7	16.4±1.5	0.24 (44.9)	0 (0)	0.29 (55.1)	0.54
10	19.1±7.0	0.80 (77.2)	0 (0)	0.24 (22.8)	1.03
13	18.2±1.1	1.21 (67.4)	0.01 (0.4)	0.58 (32.2)	1.80
16	14.7±7.3	1.51 (67.9)	0.01 (0.5)	0.70 (31.6)	2.23
19	31.1±6.8	1.01 (71.3)	0.01 (0.5)	0.40 (28.2)	1.41
24	32.1±12.3	1.97 (86.4)	0.03 (0.8)	0.97 (32.8)	2.96

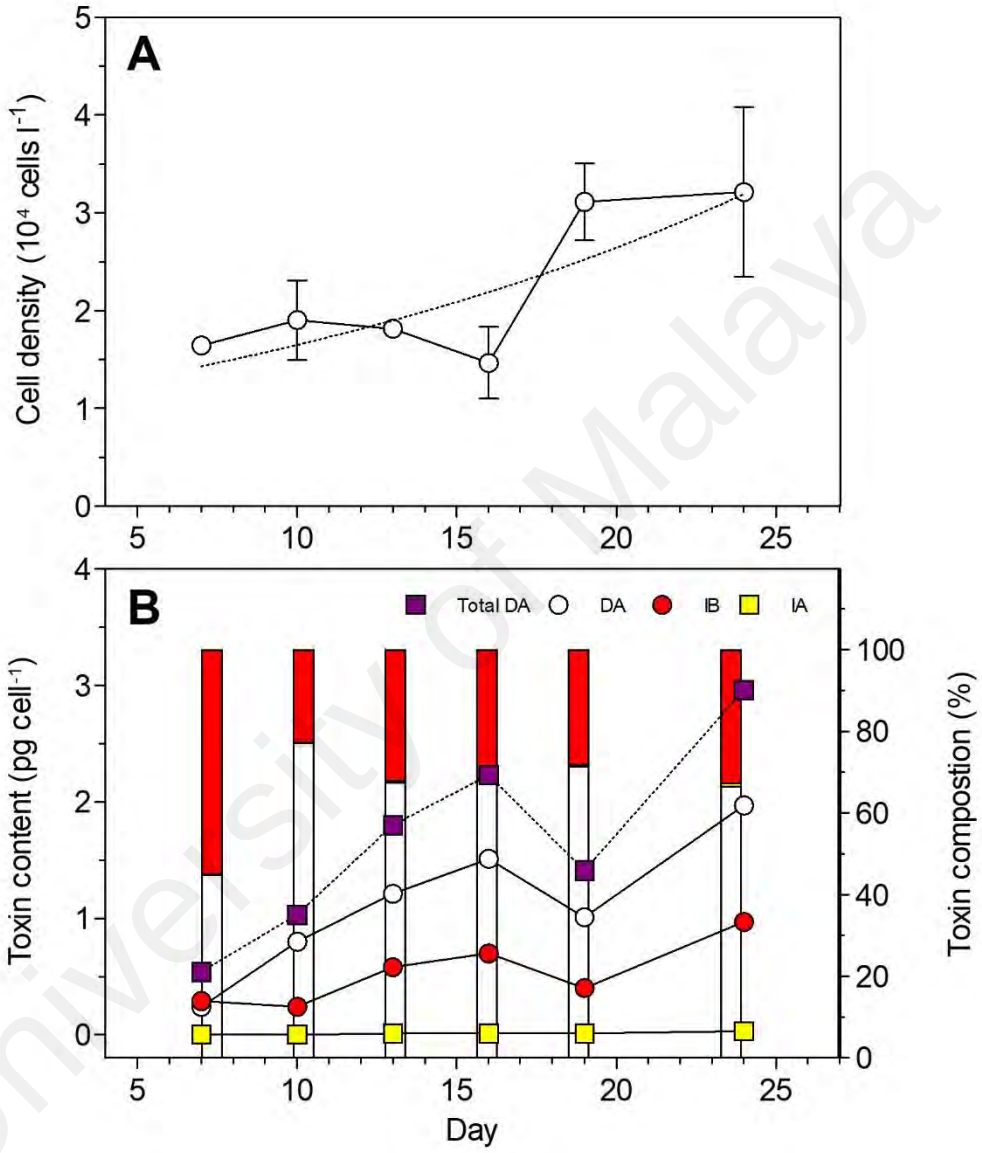

Figure 4.9: Growth (A) and changes in terms of toxin composition of *Nitzschia navis-varingica*, strain NTB02 (B).

4.4.4 Domoic acid analyses on bivalve shellfish

Table 4.5 shows the results of analyses of bivalve shellfish collected between June 2016 and February 2017. In the analysis of DA in 26 specimens, only two cockles' samples collected from Asajaya, Sarawak showed trace amount of DA (465.04 µg/kg DW and 283.72 µg/kg DW, Table 4.5; Figure 4.10).

Table 4.5: Details of shellfish samples collected and analyzed in this study. n.d., not detected.

Figure 4.10	Types of shellfish	Scientific Names	Location	Date of collection	Wet Weight (g)	Dry Weight (g)	DA (µg/kg DW)
A	Cockles	*Anadara granosa*	Kuching, Sarawak	26th June 2016	10.049	1.867	n.d.
B	Cockles	*Anadara granosa*	Kota Kinabalu, Sabah	9th July 2016	11.347	2.425	n.d.
C	Cockles	*Anadara granosa*	Pantai Remis, Perak	6th September 2016	10.517	1.838	n.d.
D	Cockles	*Anadara granosa*	Kuala Kubang Rotan, Kedah	4th September 2016	11.685	1.97	n.d.
E	Cockles	*Anadara granosa*	Sekinchan, Selangor	7th September 2016	12.289	2.239	n.d.
F	**Cockles**	***Anadara granosa***	**Asajaya, Sarawak**	**24th January 2017**	11.157	1.774	**465.04****
G	**Cockles**	***Anadara granosa***	**Asajaya, Sarawak**	**10th February 2017**	11.253	1.893	**283.72****
H	Cockles	*Anadara granosa*	Bako, Sarawak	21st February 2017	10.256	1.307	n.d.
I	Venus Clam	*Paratapes undulatus*	Kuala Kubang Rotan, Kedah	4th September 2016	10.734	1.247	n.d.
J	Venus Clam	*Paratapes undulatus*	Kuala Kubang Rotan, Kedah	4th September 2016	10.533	1.047	n.d.
K	Venus Clam	*Meretrix lamarck*	Pantai Melawi, Kelantan	8th July 2016	11.338	1.111	n.d.
L	Venus Clam	*Meretrix lamarck*	Kuala Kubang Rotan, Kedah	4th September 2016	10.299	1.198	n.d.
M	Venus Clam	*Meretrix lamarck*	Sekinchan, Selangor	7th September 2016	10.247	2.006	n.d.
N	Hard Clams	*Polymesoda* species	Tanjung Manis Port, Sarawak	28th June 2016	11.741	0.812	n.d.

Table 4.5, continued.

Figure 4.10	Types of shellfish	Scientific Names	Location	Date of collection	Wet Weight (g)	Dry Weight (g)	DA (µg/kg DW)
O	Hard Clams	*Polymesoda* sp.	Asajaya, Sarawak	10th February 2017	11.288	0.844	n.d.
P	Hard Clams	*Polymesoda* sp	Sampadi, Sarawak	22nd February 2017	11.559	1.138	n.d.
Q	Green mussel	*Perna canaliculus*	Lumut, Perak	6th September 2016	10.717	1.536	n.d.
R	Gould's razor shell	*Solen strictus*	Kuching, Sarawak	9th July 2016	11.169	1.977	n.d.
S	Gould's razor shell	*Solen regularis*	Asajaya, Sarawak	12th January 2017	10.158	1.486	n.d.
T	Gould's razor shell	*Solen regularis*	Asajaya, Sarawak	18th January 2017	10.213	1.397	n.d.
U	Sea snail	*Babylonia* species	Kuala Perlis, Perlis	4th September 2016	11.435	2.268	n.d.
V	Sea snail	*Cerithidea obtusa*	Bako, Sarawak	21st February 2017	10.088	1.558	n.d.
W	Sea snail	*Cerithidea obtusa*	Sampadi, Sarawak	22nd February 2017	10.621	1.719	n.d.
X	Sea snail	*Nerita articulata*	Sampadi, Sarawak	22nd February 2017	10.443	1.782	n.d.
Y	Sea snail	Melongenidae	Kuala Perlis, Perlis	4th September 2016	12.399	3.574	n.d.

** Regulatory limit (20 mg/kg) (Wekell et al., 2004).

Figure 4.10: Shellfish samples collected in different sampling location in Malaysia. (A–H) Cockles. (I–M) Venus clams. (M–P) Hard clam. (Q) Green mussel. (R–T) Gould's razor shell. (U–Y) Sea snails.

4.5 Discussion

4.5.1 Update on the distribution of *N. navis-varingica*

This is the first comprehensive assessment of the distribution and toxicity of *N. navis-varingica* on Peninsular Malaysia. Four locations on the Malaysian coast were surveyed for the occurrence of toxic *N. navis-varinginca*. In this study, the "kick-net" sampling method adopted was effective in collecting benthic diatoms, as the organisms tend to adhere weakly onto the mangrove roots.

Strains of *N. navis-varingica* were collected from the brackish-water mangrove swamps that experience extreme changes in salinity, indicating the halotolerance of this *Nitzschia* species. This is not surprising, as *Nitzschia* species have been found in diverse intertidal environments, from estuaries, to mangroves and artificial reservoirs such as shrimp ponds. This species is also widely distributed in the Western Pacific region, from Vietnam (Kotaki et al., 2000, 2008; Takata et al., 2009), Japan (Kotaki et al., 2004, 2008), Philippines (Kotaki et al., 2004, 2005, 2006; Bajarias et al., 2006; Romero et al., 2011, 2012), Thailand (Romero et al., 2008), and Indonesia (Romero et al., 2011; Thoha et al., 2012). This study provides an update on the distribution of toxigenic *N. navis-varingica* in the region (Figure 4.8).

The frustule morphological characteristics of the observed strains are generally in good agreement with the type species of *N. navis-varingica* (Lundholm & Moestrup, 2000). Valve lengths (45–94 μm, culture specimens) are comparable to those reported from Philippines, Thailand, and Indonesia (38–110 μm) (Kotaki et al., 2006; Romero et al., 2008, 2011, 2012), but longer than the type specimens from Vietnam (45–55 μm) (Lundholm & Moestrup, 2000) and Johor, Malaysia (44–76 μm) (Suriyanti & Usup, 2015). However, valve length is regarded as the least realiable character in diatom taxonomy (e.g., *Pseudo-nitzschia*, Lelong et al., 2012; Teng et al., 2015), as the length

decreases with each successive cell division. The number of areolae (in 1 μm) observed in Malaysian strains (4–7) is higher compared to the type specimen (3–4) (Lundholm & Moestrup, 2000). A similar finding was reported for the *N. navis-varingica* strain established from the Johor Strait (5–7) (Suriyanti & Usup, 2015).

The identity of *N. navis-varingica* in this study was well supported by the phylogenetic inferences of LSU and ITS2 rDNAs (Figures 4.5 and 4.6). ITS rDNA has been applied widely to resolve the phylogenetic relationship of diatoms (e.g., *Pseudo-nitzschia*). However, to our knowledge this is the first study that presents ITS nucleotide sequences of *N. navis-varingica*, and applies the ITS2 transcript in a phylogenetic assessment of *N. navis-varingica*, by incorporating its secondary structure information.

4.5.2 DA production by *N. navis-varingica*

DA production by *N. navis-varingica* from Malaysian mangroves was confirmed by both FMOC-LC-FLD and LC-MS/MS (Figure 4.7). The content of total DA in Malaysian strains (0.37–11.06 pg cell^{-1}, n = 48), even though showing high variability, was comparable to that of other strains from the region: Japan: 0.1–9.8 pg cell^{-1} (Kotaki et al., 2004, 2008); Vietnam: 0.5–11.3 pg cell^{-1} (Kotaki et al., 2000, 2008); Philippines: 0.04–15.3 pg cell^{-1} (Kotaki et al., 2004, 2005, 2006; Bajarias et al., 2006; Romero et al., 2011, 2012); Thailand: 0.3–4.3 pg cell^{-1} (Romero et al., 2008); Indonesia: 2.44 pg cell^{-1} (Romero et al., 2011; Thoha et al., 2012); Johor, Malaysia: 1.8 pg cell^{-1} (Suriyanti & Usup, 2015).

In the LC-MS/MS analysis, fragmentation yielded a parent ion at $[M+H]^+$ *m/z* 312 and daughter ions that corresponding to DA (Furey et al., 2001), thus confirming structurally the presence of DA, isodomoic acid A (IA) and isodomoic acid B (IB) in the cultures. This is in agreement with previous studies of Kotaki et al. (2005) and Romero et al. (2008, 2011). Suriyanti & Usup (2015) reported that only DA was present

in their *N. navis-varingica* strains from Johor, Malaysia. However, they did not analyze for other isomers, thus their presence cannot be ruled out. Non-toxic strains of *Nitzschia*-like diatoms have been reported in previous studies (Kotaki et al. 2004, 2005, 2006, 2008; Thoha et al., 2012). The ability to produce DA in *N. navis-varinginca* may vary among strains, as has been shown in the DA-producing *Pseudo-nitzschia* species (Trainer et al., 2012). However, all of the strains isolated for this study were toxigenic.

Generally, toxin profiles of *N. navis-varingica* revealed DA and/or IB as the major toxin constituents, and IA as a minor constituent; other minor isomers (isodomoic acid D, ID; isodomoic acid E, IE; diastereoisomer epi-domoic acid, epi-DA) were also reported to occur in *N. navis-varingica* (Kotaki et al., 2005; Romero et al., 2011), but were not detected in our strains. DA is the most potent form among its geometrical isomers, while IB is the least potent form (Sawant et al., 2008, 2010; reviewed in Lelong et al., 2012). Even though IA was found to be functionally equipotent to DA (Sawant et al., 2010), the intraperitoneal toxicity to mice of IA, IB, and isodomoic acid C is much lower than that of DA (Munday et al., 2008). In our batch culture experiment, the toxin composition changed over time, with a proportional change from the least potent IB to the highly potent DA. The toxin profile of strain NTB02 was relatively stable, although trace amounts of IA were detected at the later stage of the culture cycle (>day 13).

DA production by *N. navis varingica* (NTB02) was observed during the early stage of our batch culture, when the cells were not growing. This may at first seem as a contradiction to the previous study of Kotaki et al. (2000), as well to studies of most other DA-producing *Pseudo-nitzschia* species (summarized in Lelong et al., 2012), where most DA is produced during the late-exponential to stationary phases. However, our experiment used an inoculum from a stationary phase-culture (of at least 3-weeks old), instead of from an exponentially growing culture. This may have accounted for the

unusually long lag phase (16 days), during which time the DA quota increased steadily. A similar result was reported by Douglas & Bates (1992), for *P. multiseries*. This finding is consistent with cells being arrested at the G1 or G_0 phase, when they are still metabolically active, so that the DA can accumulate because cell division is stalled (Bates, 1998). In the toxic dinoflagellate *Alexandrium fundyense*, saxitoxins were produced during the G1 phase (Taroncher-Oldenburg et al., 1997). Cell growth accelarated after day 16, and the cell concentration doubled on day 19. During that time, the DA quota decreased to almost half, indicating that the toxin quota was bisected during the cell division. Further studies to explore growth and nutrient stoichiometry in relation to DA production are required to understand the physiology and factors triggering DA biosynthesis by *N. navis-variginca*.

To address whether the DA profile is a stable character in *N. navis-varingica*, we compared the toxin composition of *N. navis-varingica* strains from the Western Pacific (Figure 4.11), summarized from this study, Kotaki et al. (2005, 2008), Bajarias et al. (2006) and Romero et al. (2008). Earlier studies (Kotaki et al., 2000, 2004) only analyzed for DA, and not the isomers. Subsequent studies, however, included isomers (Kotaki et al., 2005, 2006, 2008; Romero et al., 2008, 2011; Thoha et al., 2012). It is thus possible to describe five types of toxin profiles in *N. navis-varingica* strains: DA, DA-IB, IA-IB, IB and DA-IA-IB. Our analysis shows that the DA profiles of *N. navis-varingica* exhibit high inter- and intrapopulation heterogeneity. The Malaysian strains belong to the toxin profile types: DA, DA-IB, DA-IA-IB and DA-IA; the Philippines strains exhibited types DA-IB, DA-IA-IB, IB and IA-IB; strains from Japan, Indonesia, Thailand and Vietnam exhibited only type DA-IB. Interestingly, the DA-IA type, which had not previously been detected in any strains, was first discovered in this study, from a strain from Pendas (Johor, Malaysia). A degree of similarity in the toxin profiles and compositions was observed in strains from different localities, e.g., DA-IB type in

strains from Pendas, South Sulawasi, Bangkok and Iwate. Nonetheless, some strains with similar toxin profiles possessed a great variation in their compositions. For example, in a strain from Tok Bali, Malaysia (NTB 02), DA>IB>IA (DA:IA:IB, 66:1:33), but a strain from Cavite, Luzon Island, Philippines (PCAVA 07), IB>DA>IA (DA:IA:IB, 33:14:53). These isomers occur naturally in *N. navis-varingica* cells.

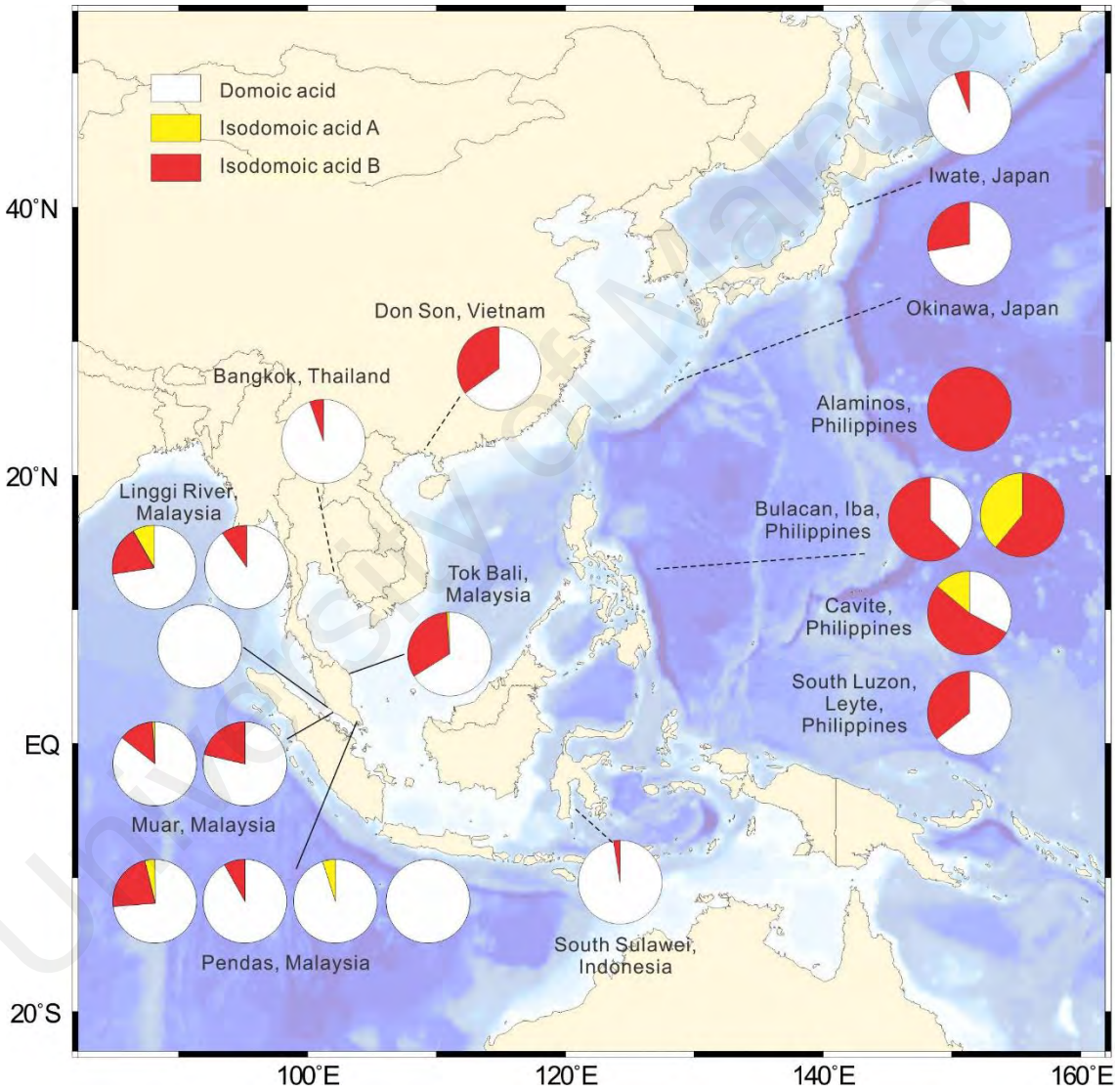

Figure 4.11: Distribution of *Nitzschia navis-varingica* in the Western Pacific region, with their toxin compositions as shown in the pie charts. Lines point to the geographical locations of strains isolated; solid lines on Peninsular Malaysia indicate data from this study, dashed lines from the other locations indicate data obtained from the literature (Kotaki et al., 2005, 2008; Bajarias et al., 2006; Romero et al., 2008, 2011).

4.5.3 DA production by shellfish

In this study, two batches of cockle specimen collected from Asajaya, Sarawak were comfirmed to be DA contamination; with the trace amount of 283.72 and 465.04 µg/kg, respectively (Table 4.5; Figure 4.10F–G). Accumulation of DA in bivalves has also reported throughout the Western Pacifc region, e.g. Vietnam (Dao et al., 2006, 2009; Huyen et al., 2006; Takata et al., 2009), Thailand, Japan and Philippines (Takata et al., 2009). Recently, DA was detected in molluscan shellfish collected from shellfish farming areas of Peninsular Malaysia during a survey conducted by the Fisheries Department of Malaysia (W.N. Noordin and P.T. Lim, per. comm.). High DA contamination in shellfish can cause the closures of shellfish harvest areas.

Over the past two decades, DA contamination on shellfish and massive DA bloom have been reported on the Pacific coast of the United States. The outbreaks of toxicity which responsible from high levels of DA had affecting the mortality of marine mammals and closures of shellfish harvest areas especially in Oregon, California, and Washington (Fritz et al., 1992; Work et al., 1993; Wekell et al., 1994; Sierra Beltran et al., 1997; Lefebvre et al., 1999, 2002; Scholin et al., 2000; Trainer et al., 2000, 2007; Gulland et al., 2002; Silvagni et al., 2005; Goldstein et al., 2008; Fire et al., 2009, 2010, 2011; Schwacke et al., 2010; Bargu et al., 2012). For the past few years, DA contamination in shellfish and crabs had subsequently increased and caused major problems especially to marine mammals' ecosystem and public health (Grattan et al., 2018).

DA and its geometrical isomers (IA and IB) were detected in *N. navis-varingica* in Malaysian water. Only DA component was tested in the shellfish samples because DA itself is more toxic and has been shown to harm marine mammals and cause risk to human health but the isomers pose relatively little risk to human or animal health

(Holland et al., 2005; Sawant et al., 2007; Munday et al., 2008). Interestingly, DA and isomers of DA (e.g. IA, IB, isodomoic acid D, isodomoic acid E and 5'-epidomoic acid) were detected in bivalves from tropical areas in Philippines, Vietnam, Japan, and Thailand (Takata et al., 2009). In contrast, bivalves from the Philippines only contained DA (e.g. *Perna viridis*, *Anadara antiquate*, *Chama iostoma*, *Chama lazarus*, and *Hyotissa hyotis*) (Takata et al., 2009).

In this study, toxigenic *N. navis-varingica* was mainly found in brackish waters and DA contaminated cockles samples. This DA producer has potential risk to interrupt food chain and become the primary source for filter-feeding organisms as cockles can be found in mudflats on mangrove strands or in the sediment of brackish water (Boyden and Russell, 1972). Kottè-Mapoko et al. (2017) reported that filter-feeding organisms such as clams, mussels, and oyster are often found on mangrove roots and lower parts of trunks and all these shellfish able to accumulate DA toxins. Although there is no ASP case reported in Malaysian waters and the DA content in shellfish samples were less than the regulatory limit (20 mg/kg) (Wekell et al., 2004), but the results of this study served as a baseline data in the country. Therefore, DA accumulation and depuration in shellfish together with routine sampling and analysis on coastal and shellfish along the Malaysian waters should be included in monitoring program in our country to ensure seafood products meet the safety requirements for human consumption.

4.6 Conclusion

This study demonstrates that the toxigenic euryhaline diatom, *N. navis-varingica* is widely distributed in Malaysian mangrove swamps and presence of DA in the mangrove-related fisheries products were found even though DA content of our samples were much lower than the regulatory limit (20 mg/kg) and *Nitzchia navis-varingica* could become the DA source for shellfish mollusks as *Nitzchia navis-varingica* was found in mangrove waters in Malaysian waters. This study suggesting the possibility of amnesic shellfish poisoning in future and further study on their biosynthesis and bio-transformation in the diatom cells, as well as the mechanism of bioaccumulation in molluscan shellfish and other vectors (e.g., crab, cutterfish; Costa et al., 2003, 2005) is needed for public health concern and also health of ecosystems with their trophic structure.

CHAPTER 5: GENETIC DIVERSITY OF *NITZSCHIA NAVIS-VARINGICA* (BACILLARIOPHYCEAE) IN MALAYSIAN WATERS

5.1 Introduction

The pennate benthic diatom *Nitzschia navis-varingica* Lundholm et Moestrup has so far never been associated with any human poisonings, but the species is able to produce domoic acid (DA), a neuro-excitatory amino acid that binds irreversibly to the glutamate receptor of the vertebrate nervous system, and responsible for amnesic shellfish poisoning (ASP). *Nitzschia navis-varingica*, the first DA-producing *Nitzschia* species was discovered from shrimp-culture ponds in Do Son, Vietnam (Kotaki et al., 2000). This toxigenic species was subsequently found in estuary areas or brackish waters in the Western Pacific regions: Japan (Kotaki et al., 2004, 2008), Philippines (Kotaki et al., 2004, 2005, 2006, 2008; Bajarias et al., 2006; Romero et al., 2011, 2012), Thailand (Romero et al., 2008), Vietnam (Kotaki et al., 2008; Takata et al., 2009), Indonesia (Romero et al., 2011; Thoha et al., 2012), and Malaysia (Suriyanti & Usup, 2015; Tan et al., 2016). This species also found in marine sea water in Australia: Western Port Bay Victoria (Higgins et al., 2003) and Mediterranean Sea (Ayaz et al., 2018). Toxin profile type can be classified as DA, DA-IB, IA-IB, IB, DA-IA-IB, and DA-IA. Interestingly, DA-IA type only found in Malaysian water (Tan et al., 2016).

The taxonomy of *Nitzschia* species is always challenging in terms of morphology and requires well-trained taxonomists and skills in electron microscopy. The application of molecular markers as DNA barcoding was used to aid species identification and has the potential to be faster than morphology-based approaches (Lundholm et al., 2002; Trobajo et al., 2006; Bouchouicha-Smida et al., 2014; Carballeira et al., 2017). In the early 2000s, the nuclear-encoded large subunit ribosomal DNA (LSU rDNA) was first applied in *Nitzschia* species (Lundholm et al., 2002;

Trobajo et al., 2006, 2009, 2010). Later, *Nitzschia* species were inferred from small subunit ribosomal DNA (SSU rDNA) (Trobajo et al., 2006; Bouchouicha-Smida et al., 2014), cox1 (Trobajo et al., 2010), 18 rDNA (Rimet et al., 2011), and the chloroplast-encoded RUBISCO (rbcL) gene (Trobajo et al., 2014; Rovira et al., 2015; Carballeira et al., 2017). Internal transcribed spacer 2 (ITS2) region has been applied in different groups in eukaryote due to its potential as a DNA barcoding for taxonomic classification and phylogenetic reconstruction, such as fungi (Coleman, 2007; Kelly et al., 2011; Heinrichs et al., 2012), animals (Coleman & Vacquier, 2002; Wiemers et al., 2009; Li et al., 2010; Yao et al., 2010), algae (Hunter et al., 2007; Sorhannus et al., 2010; Buchheim et al., 2011, 2012, 2013; Lim et al., 2018; Tan et al., 2016) and plants (Coleman, 2003, 2007, 2009; Chen et al., 2010; Gao et al., 2010a, 2010b; Yao et al., 2010; Kuzima et al., 2012; Pang et al., 2012; Garcia-Robledo et al., 2013; Gu et al., 2013; Hassel et al., 2013).

In recent years, studies on population genetics for diatom are sparse; majority studies only focus on *Pseudo-nitzschia pungens* (planktonic) but no study on *Nitzschia* (benthic) (Evans et al., 2005; Adams et al., 2009; Casteleyn et al., 2009; 2010; Lim et al., 2014). Little known about the distribution of *N. navis-varingica* in the South China Sea and Strait of Malacca, particularly in the Malaysian waters (Suriyanti & Usup, 2015; Tan et al., 2016) and genetic relationships among the *N. navis-varingica* populations throughout this large geographic locality have not been assessed. This study aims to investigate the intraspecific genetic variation and geographic distribution patterns of Malaysian *N. navis-varingica*. In this study, clonal cultures of *N. navis-varingica* were established from different locations in Malaysian waters. The morphology characteristics of *N. navis-varingica* were observed under electron microscopy. Phylogenetic relationship of *N. navis-varingica* was inferred based on the LSU rDNA and the ITS2 regions. The genetic diversity of the species was examined

using the ITS2 rDNA with the inference of its secondary structure. This is the first report to elucidate the population genetic structure and biogeography of the toxigenic benthic diatom in the Western Pacific region.

5.2 Literature Review

The DA-producing pennate diatom *N. navis-varingica* was first discovered in 1997 in Vietnam (Kotaki et al., 2000) and was subsequently found in several countries; Vietnam (101 isolates), Japan (158 isolates), Philippines (95 isolates), Thailand (18 isolates), Indonesia (15 isolates), Malaysia (2 isolates and in this study) and Australia (Table 5.1) (Kotaki et al., 2000, 2004, 2005, 2006, 2008; Takata et al., 2009; Bajarias et al., 2006; Higgins et al., 2003; Romero et al., 2008, 2011, 2012; Thoha et al., 2012; Suriyanti & Usup, 2015; Ayaz et al., 2018). In *N. navis-varingica*, DA production had been confirmed by FMOC-LC-FLCD (Kotaki et al., 2000, 2005, 2008; Bajarias et al., 2006; Romero et al., 2011, 2012), LC/ESI-MS (Kotaki et al., 2000, 2004), and LC-MS/MS (Romero et al., 2011, 2012; Thoha et al., 2012). Early studies of DA production of *N. navis-varingica* only included analyses for DA (Kotaki et al., 2000, 2004) but DA isomers (IA and/or IB) was then detected in *N. navis-varingica*, rather than DA itself (Kotaki et al., 2005).

Table 5.1: Geographical distribution of toxigenic *N. navis-varingica* and levels of domoic acid and geometrical isomers (* didn't test on the DA derivative).

Country	Sampling Sites	Number of strains	Toxin level (pg/cell)	Toxin type	References
Vietnam	Do Son	1	1.7	DA*	Kotaki et al., 2000
		1	2.1271	DA–IB (DA:IA:IB:ID:IE:Epi-DA; 74.5:0.4:19.1:1.7:3.2:1.1)	Takata et al., 2009
	Haiphong	99	0.5–11.3	–	Kotaki et al., 2008
Japan	Ishigaki Island, Okinawa	88	0.1–15.3	DA*	Kotaki et al., 2004
	Tohoku district	14	0.4–2.9	DA–IB	Kotaki et al., 2008
	Okinawa	56	0.1–9.8	DA–IB	
Philippines	Bacoor Estuary	10	1.4–15.3	DA*	Kotaki et al., 2004
		5	3.1–5.3	DA–IB	Kotaki et al., 2005, 2006
	Tanauan	15	0.04–3.7	DA–IB	
	Bulacan	21	–	IA–IB	
		7	1.86	DA–IB	Romero et al., 2011, 2012
	San Roque	15	1.3–5.3	DA–IB	Kotaki et al., 2006
	Alaminos	10	3.05(average)	IB	Romero et al., 2011, 2012
	Cavite	7	1.7	DA–IA–IB	
	Iba, Zambales	5	0.9–19.0	DA–IA–IB	Bajarias et al., 2006
Thailand	Bangkok	18	0.3–4.3	DA–IB	Romero et al., 2008
Indonesia	South Sulawei	15	2.44	DA–IB	Romero et al., 2011; Thoha et al., 2012
Malaysia	Pendas	2	1.8	DA*	Suriyanti & Usup, 2015
Australia	Victoria	1	–	–	Higgins et al., 2003
	North eastern Mediterranean Sea	–	–	–	Ayaz et al., 2018

5.3 Methodology

5.3.1 Field sampling, sampling collection and algae cultures

Sampling was undertaken along the coastal waters to brackish waters of Malaysia from September 2014 to August 2017 (Figure 5.1, Appendix F). Plankton samples were collected with a 20-µm mesh plankton net using the kick-net sampling method (Kotaki et al., 2000). Salinity at the sampling sites ranged from 0–31 (Appendix F). Live samples were transferred into 500-ml bottles and brought back to the laboratory to establish cultures. Single cells were isolated using a finely drawn Pasteur pipette under a Leica DM3000 microscope (Leica, Germany). Enrichment of field samples was performed as described in Tan et al. (2016) due to the appearance of *Nitzschia* (low densities). Cultures were established and grown in f/2 medium (Guillard and Ryther, 1962), with a salinity of 27. The cultures were maintained at 25 ± 0.5 °C, and a light intensity of 100 µmol photons m^{-2} s^{-1} under 12:12 h light:dark (L:D) photoperiod. Detailed information on the strains established and used in this study are listed in Appendix F.

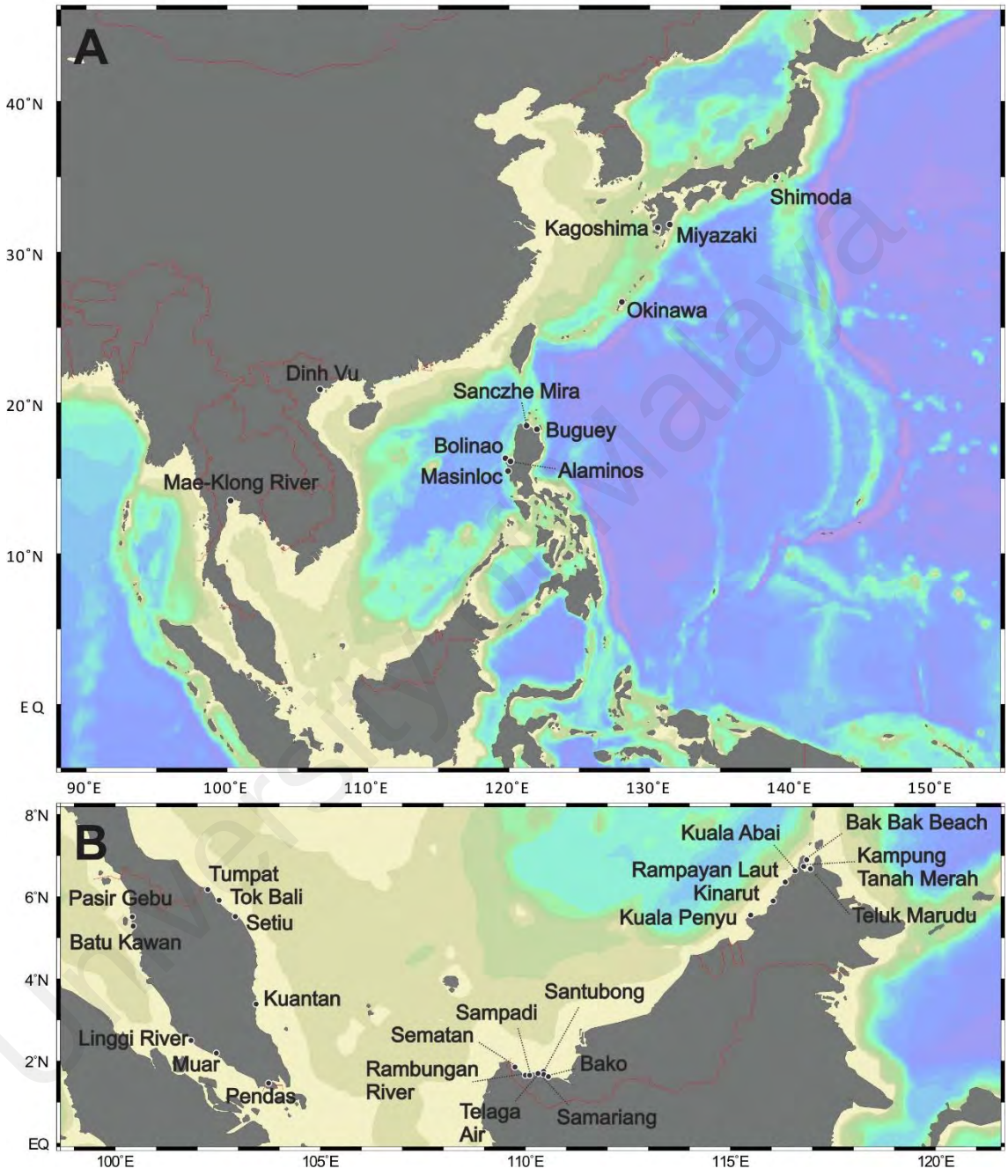

Figure 5.1: Maps showing sampling stations. (A) Location of stations in Western Pacific region. (B) Location of stations in Malaysia.

5.3.2 Morphological observation

For species identification, samples were treated with saturated $KMnO_4$, 37% HCl and 10% oxalic acid as described in Teng et al. (2013). Prior to scanning electron microscopic (SEM) observation, the acid-cleaned samples were mounted onto a track-etched polycarbonate membrane filter (pore size, 0.2 μm), attached to a stub with carbon tape, and sputter-coated with gold-palladium. Samples were observed under a LEO 1530 Gemini SEM (Zeiss/LEO, Oberkochen, Germany). For transmission electron microscopy (TEM), cleaned samples were transferred onto a Formvar-coated copper grid and air-dried overnight. Samples were examined under a JEOL JEM-1230 TEM (JEOL, Tokyo, Japan). Morphometric measurements of valve length and width, the density of fibulae and striae, areolae and band areolae of >20 cells were obtained (Table 5.2).

5.3.3 DNA extraction, PCR amplification and sequencing

Cultures of *N. navis-varingica* at mid-exponential phase were harvested by centrifugation (2600 ×*g*, 10 min). Genomic DNA of *N. navis-varingica* was extracted with 2× Cetyl-trimethyl-ammonium-bromide (CTAB) lysis buffer and precipitated with ethanol. The large subunit ribosomal DNA (LSU rDNA) in the domain D1–D3 was amplified using the primer pair DIR and D3Ca (Scholin et al., 1994) and internal transcribed spacer (ITS1-5.8S-ITS2) region was amplified using the primer set ITS1 and ITS4 (White et al., 1990).

To obtain sequences of LSU and ITS rDNA, gene amplification was performed using a peqSTAR 96X universal gradient thermocycler (Erlangen, Germany). The PCR running conditions was pre-denaturation at 94°C for 5 min, followed by 35 cycles of denaturation at 94°C for 45 s, annealing at 52°C for 30 s and elongation at 72°C for 90 s, and completed with a final extension at 72°C for 8 min. The amplicons were purified

using the QIAquick DNA purification kit (Qiagen, Hilden, Germany). The purified PCR amplicons were directly sequenced for both strands by First Base Laboratories (Selangor, Malaysia). DNA sequencing was performed on an ABI 3770XL automated sequencer (PE Applied Biosystems, Foster City, CA) on both strands.

5.3.4 LSU rDNA analyses and phylogenetic reconstruction

For the LSU rDNA dataset, 43 nucleotide sequences of *N. navis-varingica* and two *N. pellucida* were obtained in this study. These sequences, 11 of *N. navis-varingica* from a previous study (Tan et al., 2016), 18 of *Nitzschia* sequences and two sequences for outgroups from NCBI Genbank nucleotide database (Appendix G), were multiple-aligned using MUSCLE (Multiple Sequence Comparison by Log-Expectation) (Edgar, 2004b). *Navicula* cf. *erifuga* [accessions: AF417679] and *Halamphora coffeiformis* (C.Agardh) Levkov [accessions:AF417682] were chosen as outgroup taxa.

Maximum parsimony (MP), maximum likelihood (ML) and Bayesian inference (BI) were used for LSU rDNA phylogeny. MP and ML were performed using PAUP* ver. 4.0b.10 (Swofford, 2001). MP tree were carried out using stepwise addition (SA), branch-swapping tree bisection-reconnection (TBR), heuristic searches with random addition of sequences (1,000 replications), and 1,000 bootstrap replicate (10 random addition of sequence run per bootstrap replicate). To obtain the optimal substitution and rate heterogeneity model for ML and BI analyses, Akaike information criterion (AIC) was used as implemented in jModelTest 2 (Posada, 2008; Darriba et al., 2012). The best substitution and rate heterogeneity model selected for ML and BI analysis was as follow: TIM3+I+G (parameter values set: rAC = 0.4980, rAG = 1.6467, rAT = 1.0000, rCG = 0.4980, rCT = 5.1757, rGT = 1.0000; A = 0.2424, C =0.2125, G = 0.3066; I = 0.4090; γ = 0.3960).

ML was performed with the selected model using PAUP, starting with 10 random-addition replications; a heuristic search was made using nearest neighbour interchange (NNI) and branching swapping. Bootstrap replications of 100 with 10 random addition of sequence run per bootstrap replicate were set. BI was performed using MrBayes 3.2.5 (Ronquist and Huelsenbeck, 2003) with 10,000,000 generations and tree were sampled every 100 generations. Bayesian Evolutionary Analysis Utility (BEAUti), Bayesian Evolutionary Analysis Sampling Trees (BEAST) (Drummond et al., 2012) and Tracer (Rambaut et al., 2018) were used to obtain the effective sample size and burn-in value of 10%.

5.3.5 ITS2 secondary structure modeling and phylogenetic analyses

Only ITS2 of the ITS region was used in this study. The ITS2 transcripts from previous study, *N. navis-varingica*, NTB 02 (KX353643) was used as a template (Tan et al., 2016) in the ITS2 database (http://its2-old.bioapps.biozentrum.uni-wuerzburg.de/cgi-bin/index.pl?custom; Schultz et al., 2006; Selig et al., 2008; Koetschan et al., 2010) for homology modeling folding of newly obtained *Nitzschia* ITS2 sequences in this study. The suboptimal helices were manually refolded using RNAStructure ver. 5.6 (Mathews, 2014) and the structures of ITS2 were illustrated using VARNA (Darty et al., 2009). For the ITS2 dataset, 355 ITS2 secondary structures sequences (included Tan et al., 2016 in chapter 4; Romero et al., in prep) and those retrieved from Genbank, as well as for outgroup sequences (obtained from GenBank) were modeled.

To construct the ITS2 sequence-structure phylogenetic tree, *Amphora* sp. [accession: JF834543] and *Navicula trivialis* Lange-Bertalot [accessions: FN397610 and FN397614] were chosen as outgroups (Appendix G). The ITS2 sequences together with structural information were unambiguously aligned using 4SALE v1.7 (Seibel et

al. 2006, 2008; Wolf et al., 2014). The aligned sequences with secondary structure information were saved in ".xfasta" extension for analysis in ProfDistS v0.9.9 (Qt version) (Friedrich et al., 2005; Wolf et al., 2008) and aligned sequences with one letter encoded by sequence-structure ML, using phangorn (Schliep, 2011) in R (R Core Team, 2014). The parameters set as: number of bootstraps=1,000, distance correction model=General Time Reversible, and Ratematrix Q=Q_ITS2. The CBC Analyzer option in 4SALE was used to analyze compensatory base changes (CBCs). All the phylogenetic trees were visualized using a graphical tree viewer, FigTree v.1.4.2 (http://tree.bio.ed.ac.uk/software/figtree/). Genetics divergences among *N. navis-varingica* were calculated using MEGA5 (Tamura et al., 2011).

5.3.6 Population genetic analyses

Haplotype analysis was performed using DnaSP v5 (Librado & Rozas, 2009). The aligned sequence-structural data was used, the sites with alignment gaps were included in the analysis and the sequence sets were shown based on the localities for each strain. Haplotype data files were generated in both NEXUS (.nex) and Arlequin (.arp) format. Population pairwise *F*-statistic was calculated using the program Arlequin 3.5.1.2 (Excoffier & Lischer, 2010), to estimate the gene flow based on the analysis of AMOVA (analysis of molecular variance) (Weir & Cockerham, 1984). A median-joining network was reconstructed using Network 4.6.1.0 to infer haplotype relationship (Bandelt et al., 1999).

5.4 Results

5.4.1 Morphological observation of *N. navis-varingica*

A total of 299 strains of *N. navis-varingica* were established from Malaysian waters and confirmed morphologically by electron microscopy (Appendix F). Details morphometric measurements of *N. navis-varingica* were present into eight clades (Clade A–H), together with the data in Tan et al. (2016) and Romero et al. (in prep) (Table 5.2; Figure 5.2–5.10). The detailed morphometric data of *N. navis-varingica* obtained in this study is shown in Table 5.2 and Figure 5.2. Cell shape, cell apex, central interspace, fibulae, interstriae, areolae and band striae for each clade were shown in Figure 5.3 to Figure 5.10, separately.

Cells were observed in girdle view (Figure 5.3A, 5.4A, 5.5A–B, 5.6A, 5.7A–B, 5.8A–B, 5.9C–D, and 5.10A–B) and valve view (Figure 5.3B, 5.5C, 5.6B–C, 5.7C, 5.8C, and 5.9A–B) under electron microscopy. Cells are usually observed in girdle view due to the size of pervalvar axis is wider than the transapical axis (Figure 5.5A, 5.10A). Overall, the cell valve is 54.51–215.95 µm long and 4.00–15.86 µm wide (Table 5.2; Figure 5.2). Cell raphe is raised on a keel and positioned eccentrically, where supported by the fibulae and striae are raised on the valve (Figure 5.3A–E, 5.4A–B, 5.5A–F, 5.6A–G, 5.7A–E, 5.8A–G, 5.9A–H, and 5.10A–D). Cell apex and tip of the valve showing the terminal fissure curving toward the distal side were observed under SEM and TEM (Figure 5.3C–E, 5.4B, 5.5D–F, 5.6D–I, 5.7D–E, 5.8D–G, 5.9E–I, and 5.10C–E). Central interspace is visible under SEM and TEM (Figure 5.3F–G, 5.4C–D, 5.5G–H, 5.6J–K, 5.7F, 5.8H–I, 5.9J–L, and 5.10F). Densities of fibulae and interstriae in 10 µm 6–12 and 19–31, respectively (Table 5.2; Figure 5.2). One row of circular areolae present in each stria (Figure 5.3H, 5.4E, 5.5I–J, 5.6L, 5.7G, 5.8J, 5.9M, and 5.10G–H). The cingulum comprises few rows of areolae (Figure 5.3I, 5.4F, 5.5K, 5.6M–O, 5.7H, 5.8K, 5.9N–O, and 5.10I–J), with the density of areolae in between two to 5 per 1 µm .

Table 5.2: Frustule morphometric measurements of *Nitzschia navis-varingica* obtained in this study, compared to the type specimen (VSP974-1). *n*, number of cells observed. n.d., not detected.

Clade	Strain	Length (µm)	Width (µm)	Fibulae in 10 µm	Striae in 10 µm	Areolae in 1 µm	Rows of areolae	Band areolae in 1 µm	Reference
A	NTB02	83.73–94.20 89.08±2.81 (*n*=30)	4.00–5.89 4.75±0.51 (*n*=30)	11–13	26–29	4–6	1	3–5	Tan et al. 2016 (in chapter 4)
	NLN 05	67.77–76.90 73.55±2.61 (*n*=20)	5.05–6.72 5.69±0.50 (*n*=20)	7–13	26–28	5–6	1	3–4	In this chapter
	NLN 08	69.08–89.97 80.80±6.66 (*n*=30)	5.11–8.98 6.84±1.35 (*n*=30)	10–12	26–28	4	1	2–4	Tan et al. 2016 (in chapter 4)
	NPg 67	106.27–123.99 116.13±5.50 (*n*=20)	6.58–8.16 7.40±0.61 (*n*=20)	9–11	24–28	4–5	1	3	In this chapter
	NPg 72	109.14–125.19 116.43±5.52 (*n*=20)	6.14–7.68 6.98±0.37 (*n*=25)	10–12	25–28	4–5	1	3–4	In this chapter
	NBk 02	58.96–64.83 62.21±1.82 (*n*=20)	4.62–6.13 5.48±0.43 (*n*=20)	10–12	26–28	5–7	1	n.d.	In this chapter
	NSt 07	104.84–114.19 108.18±2.47 (*n*=20)	4.28–5.36 4.83±0.45 (*n*=20)	10–13	25–28	5–6	1	3–4	In this chapter
Average for Clade A		58.96–125.19 91.41±19.48 (*n*=160)	4.00–8.98 6.00±1.23 (*n*=165)	7–13	24–29	4–7	1	2–5	

Table 5.2, continued.

Clade	Strain	Length (µm)	Width (µm)	Fibulae in 10 µm	Striae in 10 µm	Areolae in 1 µm	Rows of areolae	Band areolae in 1 µm	Reference
B	NTB23	88.37–97.11 91.62±2.36 (*n*=30)	4.93–6.42 5.79±0.39 (*n*=30)	10–12	26–28	4–5	1	3–4	Tan et al. 2016 (in chapter 4)
	NLN01	87.32–94.36 90.91±1.98 (*n*=30)	4.47–5.85 5.07±0.40 (*n*=30)	10–12	26–28	4–5	1	3–4	Tan et al. 2016 (in chapter 4)
	NTa 01	61.97–72.61 67.27±2.83 (*n*=21)	5.21–6.52 5.77±0.41 (*n*=21)	8–11	26–28	4–6	1	4	In this chapter
Average for Clade B		61.97–97.11 85.04±10.84 (*n*=81)	4.47–6.52 5.52±0.53 (*n*=81)	8–12	26–28	4–6	1	3–4	
C	NLN 27	84.78–113.14 98.68±10.32 (*n*=20)	5.72–8.52 7.27±0.68 (*n*=20)	10–12	25–29	4–5	1	4	In this chapter
	NLN29	88.67–92.32 89.83±2.81 (*n*=30)	5.15–7.01 6.23±0.54 (*n*=30)	12–14	26–28	4–7	1	n.d.	Tan et al. 2016 (in chapter 4)
	NTm 09	109.13–127.55 120.03±5.93 (*n*=20)	5.45–6.20 5.68±0.19 (*n*=20)	11–14	25–29	4–5	1	3–4	In this chapter
	NSm 02	74.04–85.32 80.10±3.15 (*n*=22)	7.14–9.77 8.36±0.85 (*n*=20)	9–11	26–29	4–5	1	4	In this chapter
Average for Clade C		74.04–127.55 95.99±15.33 (*n*=92)	5.15–9.77 6.81±1.16 (*n*=90)	9–14	25–29	4–7	1	3–4	

Table 5.2, continued.

Clade	Strain	Length (µm)	Width (µm)	Fibulae in 10 µm	Striae in 10 µm	Areolae in 1 µm	Rows of areolae	Band areolae in 1 µm	Reference
D	NKp 06	69.22–84.32 78.17±4.25 (*n*=25)	5.55–6.59 6.00±0.37 (*n*=25)	9–11	25–31	4–5	1	3–4	In this chapter
	NStb 01	79.74–94.10 88.11±3.63 (*n*=22)	5.42–6.39 5.92±0.32 (*n*=22)	7–11	25–28	4–5	1	3–4	In this chapter
	NStb 06	72.20–93.30 85.32±5.03 (*n*=24)	5.18–6.00 5.52±0.23 (*n*=24)	8–12	25–28	4–5	1	3–4	In this chapter
Average for Clade D		69.22–94.10 83.82±5.85 (*n*=71)	5.18–6.59 5.81±0.38 (*n*=71)	7–12	25–31	4–5	1	3–4	
E	MLGB 15–4	73.60–87.17 80.22±4.99 (*n*=20)	4.73–7.25 5.58±0.52 (*n*=20)	7–9	25–28	4–5	1	n.d.	In this chapter
	NTg 02	121.11–133.50 126.93±4.53 (*n*=20)	5.54–6.38 5.97±0.26 (*n*=20)	10–12	25–26	4–5	1	3–4	In this chapter
	VSP974-1	45.00–55.00	9.00–11.00	10–12	26–30	3–4	1	2–3	Lundholm & Moestrup (2000)
Average for Clade E		73.60–133.50 103.57±24.11 (*n*=40)	4.73–7.25 5.77±0.45 (*n*=40)	7–12	25–28	3–5	1	2–4	

Table 5.2, continued.

Clade	Strain	Length (µm)	Width (µm)	Fibulae in 10 µm	Striae in 10 µm	Areolae in 1 µm	Rows of areolae	Band areolae in 1 µm	Reference
F	NTB 16	172.73–184.87 176.9±2.81 (*n*=20)	6.73–8.53 7.69±0.42 (*n*=20)	7–10	19–22	4–5	1	3	In this chapter
	PBOLA 16–1	129.65–147.02 138.45±4.98 (*n*=27)	6.25–7.38 6.79±0.32 (*n*=27)	9–11	22–24	4–5	1	3–4	In this chapter
	PBOLA 16–2	138.36–143.81 140.41±1.44 (*n*=20)	5.69–6.76 6.25±0.31 (*n*=20)	8–10	22–24	4–6	1	3–4	In this chapter
	PBOLB 16–5	109.08–129.9 116.76±4.59 (*n*=30)	5.15–8.00 6.73±0.74 (*n*=30)	9–12	22–26	4–6	1	3–4	In this chapter
Average for Clade F		109.08–184.87 140.07±21.64 (*n*=97)	5.15–8.53 6.84±0.68 (*n*=97)	7–12	19–26	4–6	1	3–4	
G	NTB 14	54.51–67.22 61.16±5.16 (*n*=20)	7.88–8.90 8.42±0.30 (*n*=20)	9–10	20–22	3–5	1	3	In this chapter
	NTB 35	78.73–96.4 89.17±4.53 (*n*=21)	6.07–9.49 7.59±1.19 (*n*=21)	8–9	20–23	3	1	2–3	In this chapter
	NTB 40	91.65–111.53 104.60±6.08 (*n*=20)	7.07–7.98 7.47±0.29 (*n*=20)	7–11	19–21	3–4	1	2–3	In this chapter
	NTB 45	173.02–215.95 194.07±14.01 (*n*=20)	13.58–15.86 14.93±0.65 (*n*=20)	6–8	20–22	4–5	1	3–4	In this chapter

Table 5.2, continued.

Clade	Strain	Length (µm)	Width (µm)	Fibulae in 10 µm	Striae in 10 µm	Areolae in 1 µm	Rows of areolae	Band areolae in 1 µm	Reference
G	NPg 44	98.20–121.14 109.71±7.48 (*n*=20)	6.80–9.06 8.37±0.66 (*n*=20)	6–8	19–21	3–4	1	3	In this chapter
Average for Clade G		54.51–215.95 111.52±45.27 (*n*=101)	6.07–15.86 9.34±2.90 (*n*=101)	6–11	19–23	3–5	1	2–4	
H	NStb 07	68.78–73.59 71.12±1.27 (*n*=21)	6.12–8.21 7.45±0.61 (*n*=21)	9–11	23–25	4–5	1	3–4	In this chapter
	NSt 03	79.76–97.41 89.63±4.87 (*n*=20)	6.34–7.97 6.90±0.44 (*n*=20)	10–12	25–27	5–6	1	3–4	In this chapter
	NSt 05	87.69–92.62 90.45±1.30 (*n*=23)	5.96–7.63 6.73±0.55 (*n*=23)	9–10	24–25	4–5	1	3–4	In this chapter
	NSt 06	83.67–92.86 89.99±2.02 (*n*=23)	5.55–8.96 7.21±1.25 (*n*=23)	8–11	23–28	4–5	1	3–4	In this chapter
Average for Clade H		68.78–97.41 85.47±8.57 (*n*=87)	5.55–8.96 7.07±0.83 (*n*=87)	8–12	23–28	4–6	1	3–4	

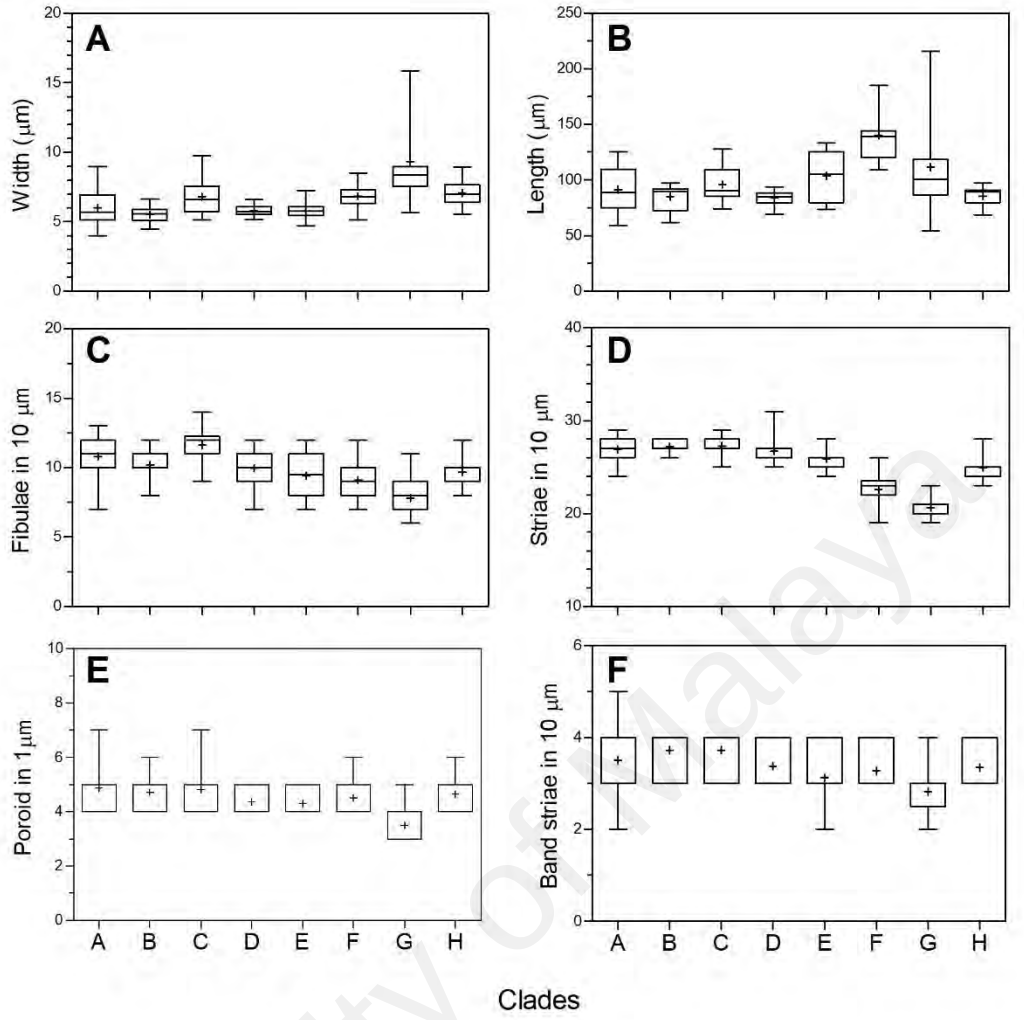

Figure 5.2: Morphometric data on valve width (A), length (B), fibulae (C), striae (D), poroid/areolae (E), and band striae (F) of each clade of *N. navis-varingica* in this study. The central rectangle shows the range between first and third quartiles, a segment inside the rectangle is the media, plus sign is the mean, whiskers above and below the rectangle are the minimum and maximum values.

Frustule morphological characteristics of *N. navis-varingica* in this study are nearly identical to the description of *N. navis-varingica* in Lundholm and Moestrup (2000). However, SEM and TEM reveal that strains in clade G were slight difference compared to strains in other clades, where the cell length (54.51–215.95 µm) and cell width (6.07–15.86 µm) in clade G were longer and wider (Table 5.2; Figure 5.2). The densities of fibulae (6–11) in 10 µm , densities of interstriae (19–23) in 10 µm, number of areolae (3–5) in 1 µm and number of band stria in 10 µm are in the ranged compared to strains in other clades.

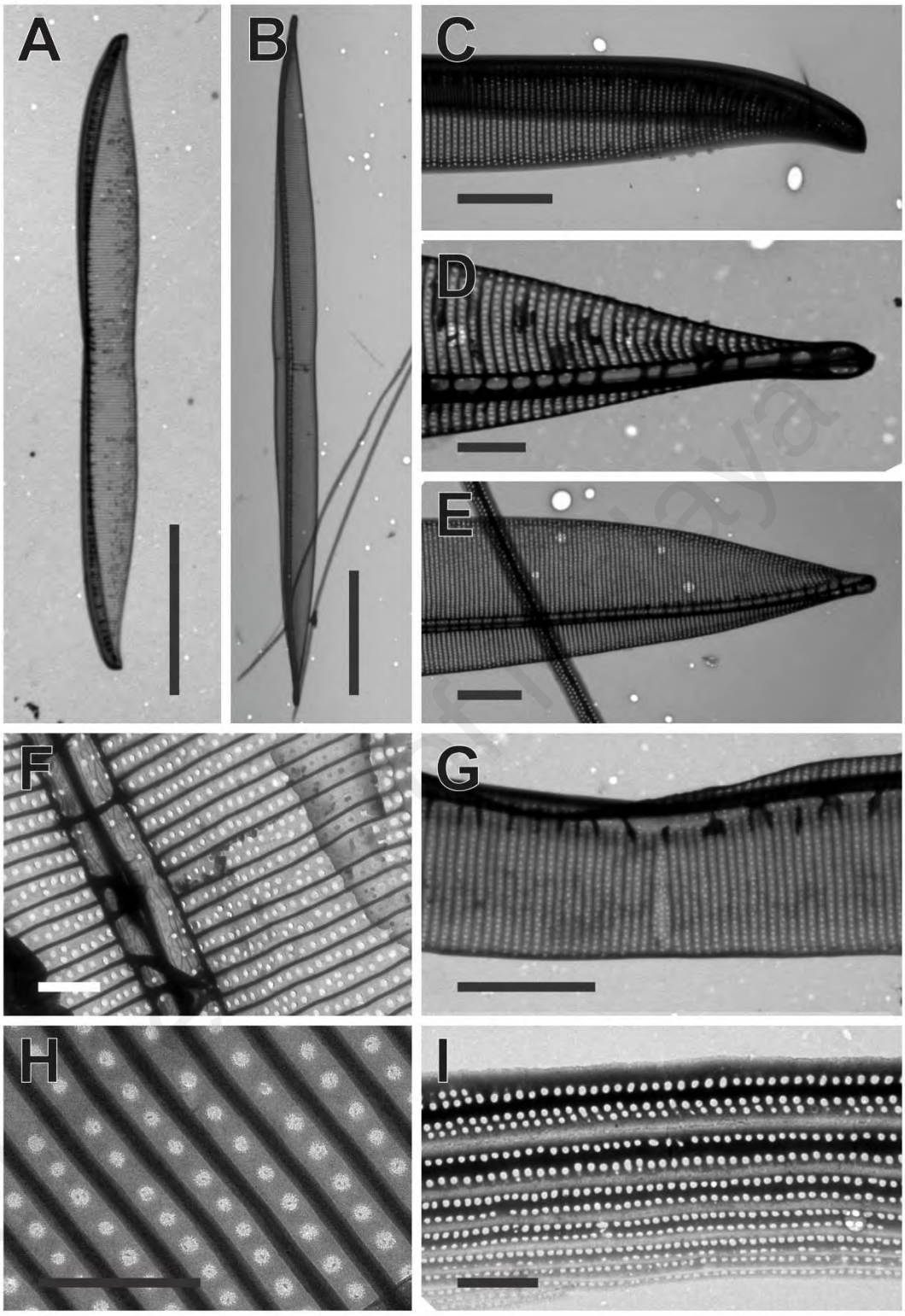

Figure 5.3: Valve shape and ultrastructure of *N. navis-varingica* in clade A. TEM micrographs. (A and B) Girdle and valve view of frustule. The raphe slits are positioned along one edge of the valve face, raised along the keel and spanned internally by fibulae. (C) Apices of valve curved inward. (D and E) Tips of valve with visible fibulae from the canals. (F) Central interspace is present. Distinct and regularly spaced fibulae and the wall of raphe canal, showing pattern of silica ridges on the wall of the raphe canal. (G) View of valve near the central nodule. (H) Round areolae. (I) Cingulum comprises varying rows of areolae. Scale bars: 20 µm (A, B); 5 µm (C, E, G); 2 µm (D, I); 1 µm (F, H).

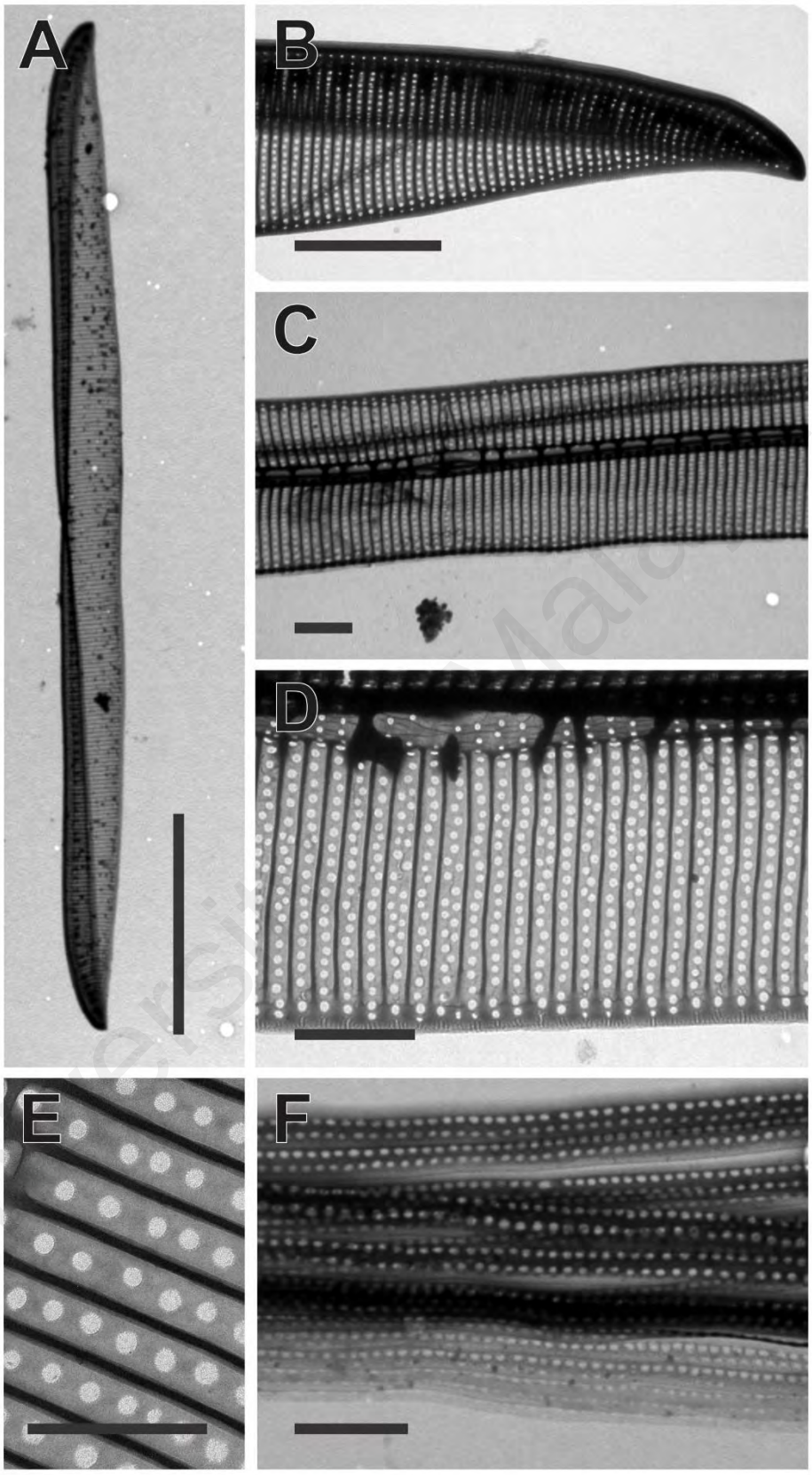

Figure 5.4: Valve shape and ultrastructure of *N. navis-varingica* in clade B. TEM micrographs. (A) Girdle view of frustule. The raphe slits are positioned along one edge of the valve face, raised along the keel and spanned internally by fibulae. (B) Apices of valve curved inward. (C and D) View of valve near the central nodule. (E) Round areolae. (F) Cingulum comprises varying rows of areolae. Scale bars: 20 µm (A); 5 µm (B); 2 µm (C, D, F); 1 µm (E).

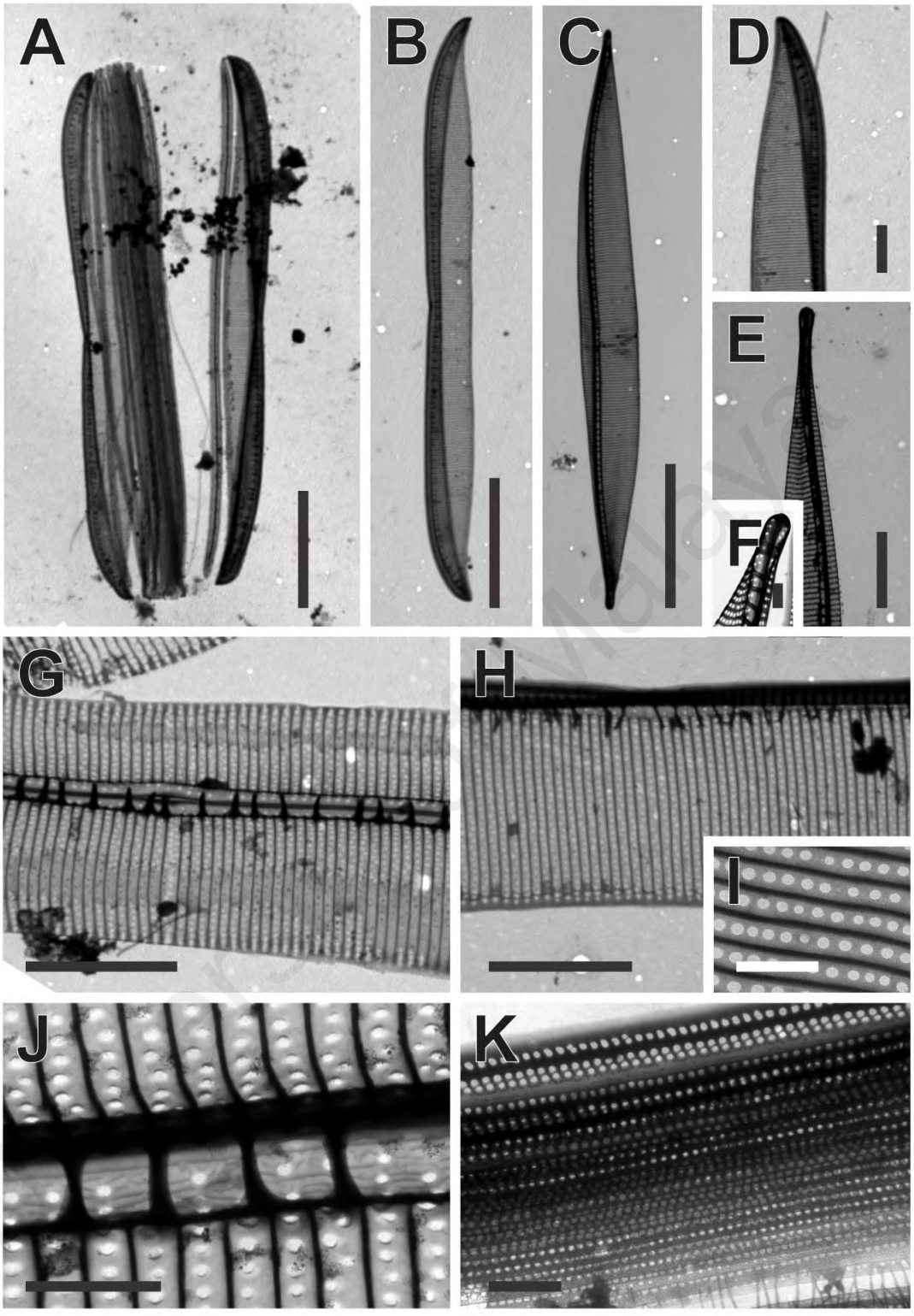

Figure 5.5: Valve shape and ultrastructure of *N. navis-varingica* in clade C. TEM micrographs. (A, B and C) Girdle and valve view of frustule. The raphe slits are positioned along one edge of the valve face, raised along the keel and spanned internally by fibulae. (D) Apices of valve curved inward. (E and F) Tips of valve with visible fibulae from the canals. (G and H) View of valve near the central nodule. (I) Round areolae. (J) Distinct and regularly spaced fibulae and the wall of raphe canal, showing pattern of silica ridges on the wall of the raphe canal. (K) Cingulum comprises varying rows of areolae. Scale bars: 20 µm (A, B, C); 5 µm (D, E, G, H); 1 µm (F, I, J); 2 µm (K).

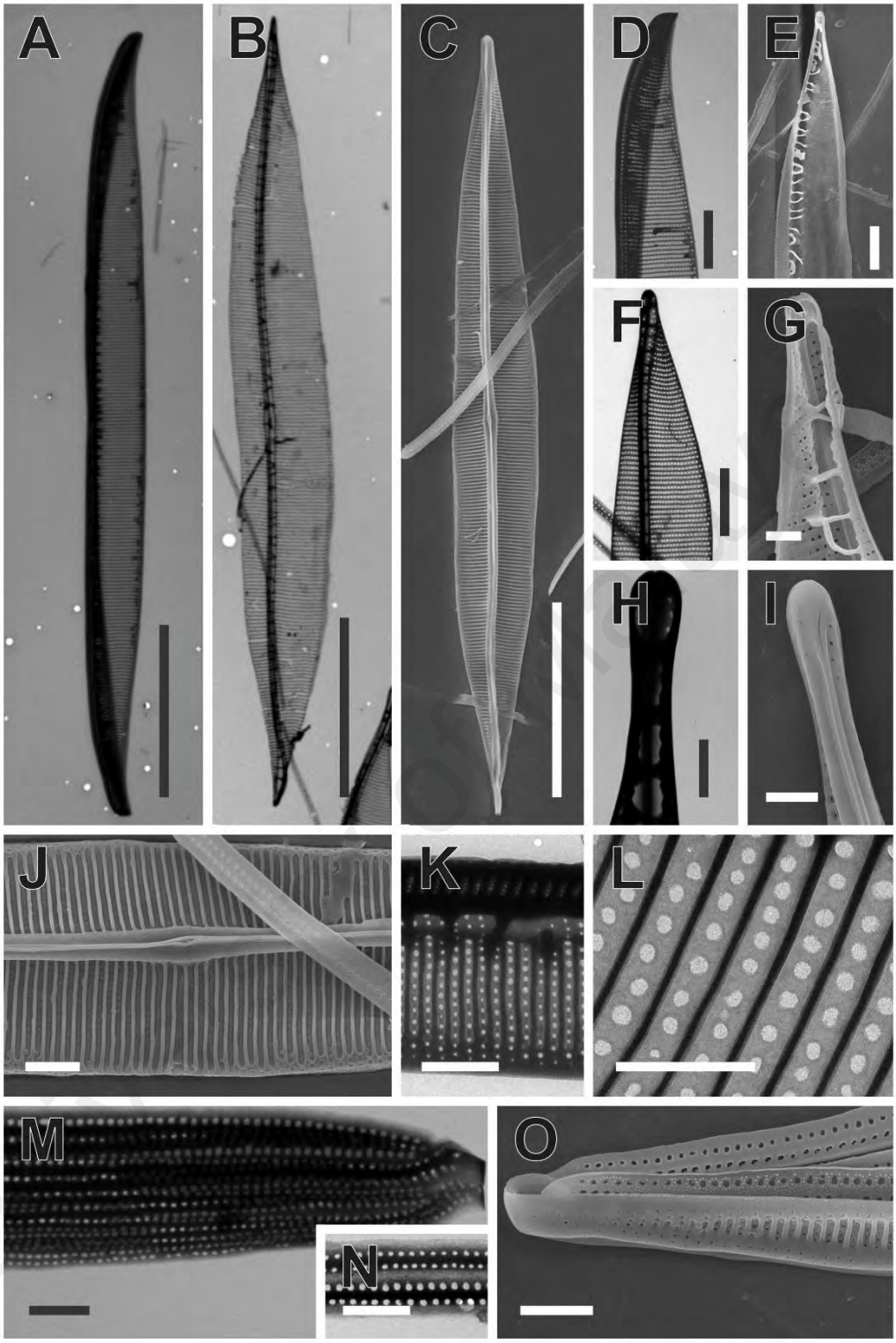

Figure 5.6: Valve shape and ultrastructure of *N. navis-varingica* in clade D. TEM micrographs, except for C, E, G, I, J and O, SEM. (A, B and C) Girdle and valve view of frustule. The raphe slits are positioned along one edge of the valve face, raised along the keel and spanned internally by fibulae. (D) Apices of valve curved inward. (E, F, G) Tips of valve with visible fibulae from the canals. (H and I) Tips of valve showing the terminal fissure curving toward the distal side. (J and K) View of valve near the central nodule. (L) Round areolae. (M and O) Cingulum comprises varying rows of areolae. (N) Single band, part of the girdle showing four rows of areolae at valvocopula. Scale bars: 20 µm (A, B, C); 5 µm (D, E, F); 1 µm (G, H, I, L); 2 µm (J, K, M, N, O).

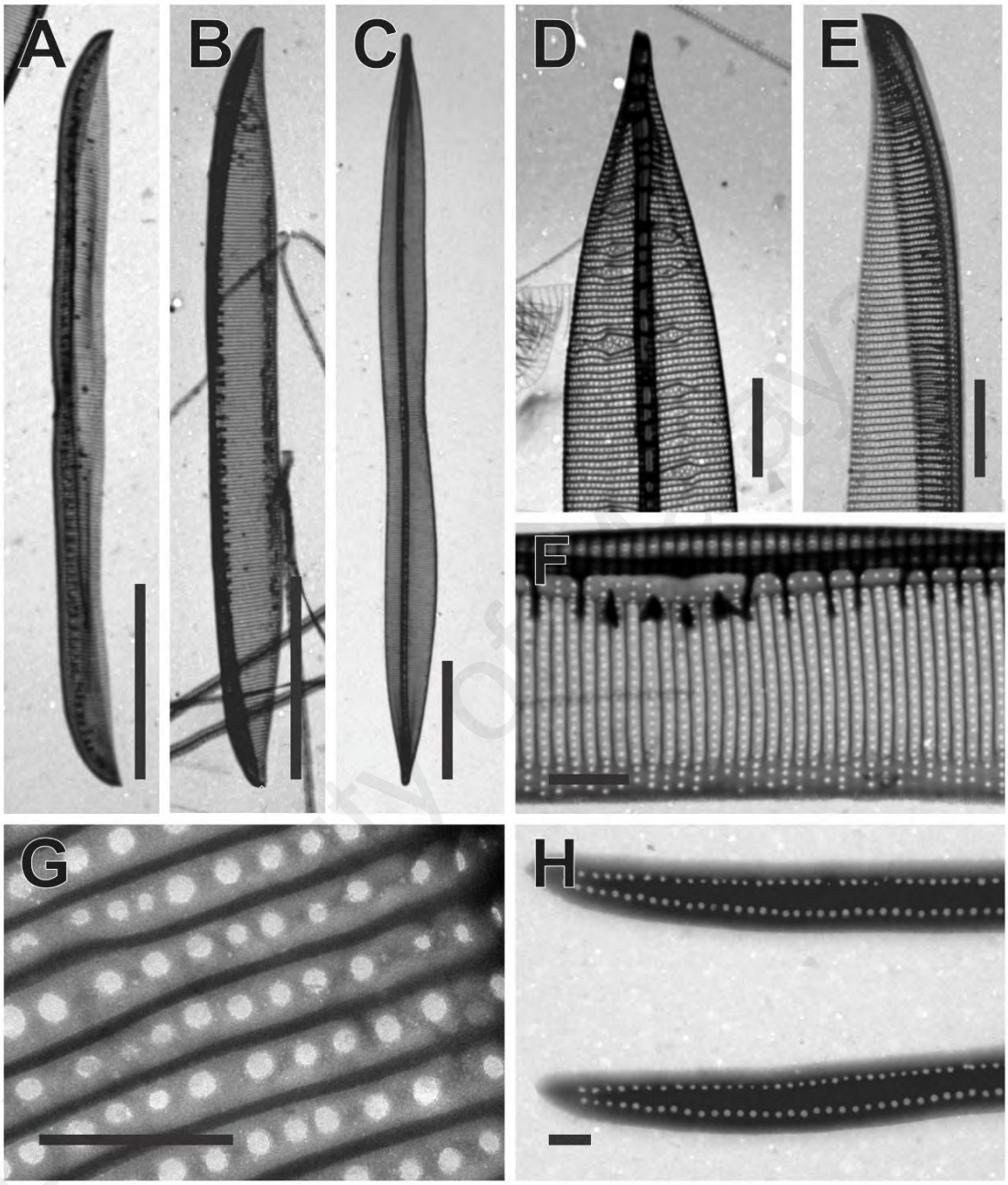

Figure 5.7: Valve shape and ultrastructure of *N. navis-varingica* in clade E. TEM micrographs. (A, B and C) Girdle and valve view of frustule. The raphe slits are positioned along one edge of the valve face, raised along the keel and spanned internally by fibulae. (D) Tips of valve with visible fibulae from the canals. (E) Apices of valve curved inward. (F) View of valve near the central nodule. (G) Round areolae. (H) Single band, part of the girdle showing four rows of areolae at valvocopula. Scale bars: 20 µm (A, B, C); 5 µm (D, E, F); 1 µm (G, H).

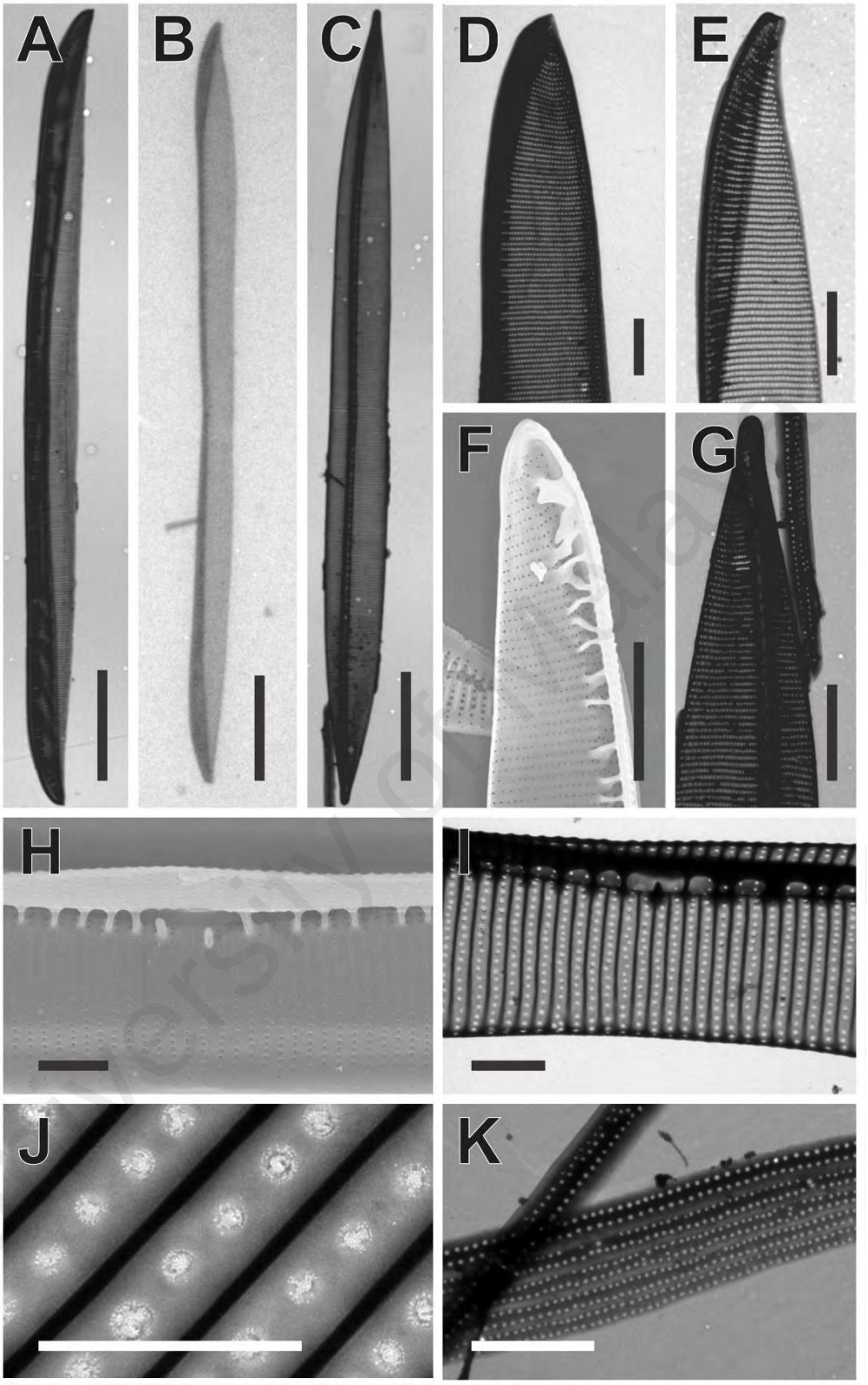

Figure 5.8: Valve shape and ultrastructure of *N. navis-varingica* in clade F. TEM micrographs, except for F and H, SEM. (A, B and C) Girdle and valve view of frustule. The raphe slits are positioned along one edge of the valve face, raised along the keel and spanned internally by fibulae. (D, E and F) Apices of valve curved inward. (G) Tips of valve with visible fibulae from the canals. (H and I) View of valve near the central nodule. (J) Round areolae. (K) Cingulum comprises varying rows of areolae. Scale bars: 20 µm (A, B, C); 5 µm (D, E, F, G, K); 2 µm (H, I); 1 µm (J).

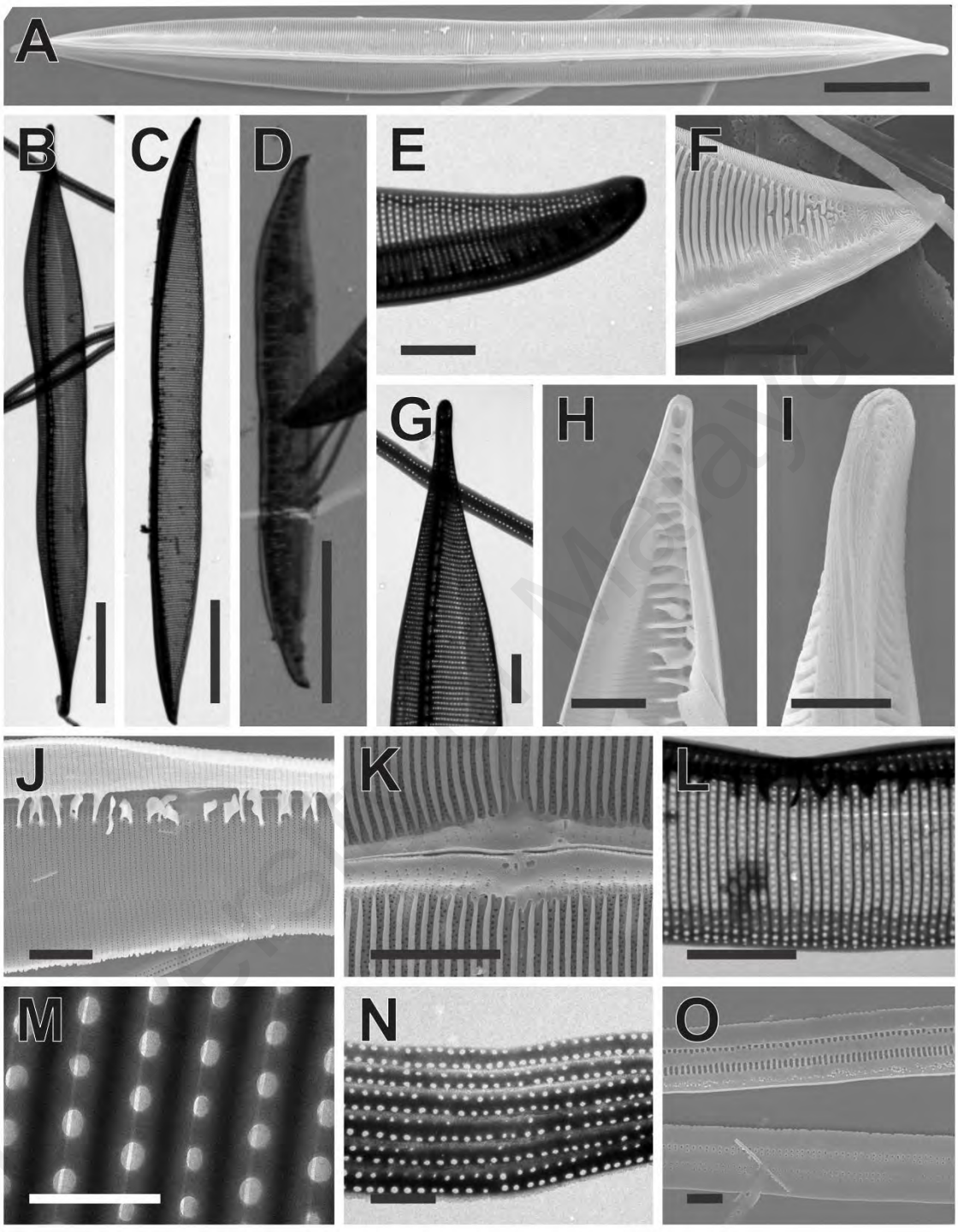

Figure 5.9: Valve shape and ultrastructure of *N. navis-varingica* in clade G. SEM micrographs, except for B, C, D, E, G, L, M and N, TEM. (A, B, C and D) Girdle and valve view of frustule. The raphe slits are positioned along one edge of the valve face, raised along the keel and spanned internally by fibulae. (E and F) Apices of valve curved inward. (G and H) Tips of valve with visible fibulae from the canals. (I) Tips of valve showing the terminal fissure curving toward the distal side. (J, K and L) View of valve near the central nodule. (M) Round areolae. (M and N) Cingulum comprises varying rows of areolae. Scale bars: 20 µm (A, B, C, D); 5 µm (E, G, L); 2 µm (F, H, I, J, K, N, O); 1 µm (M).

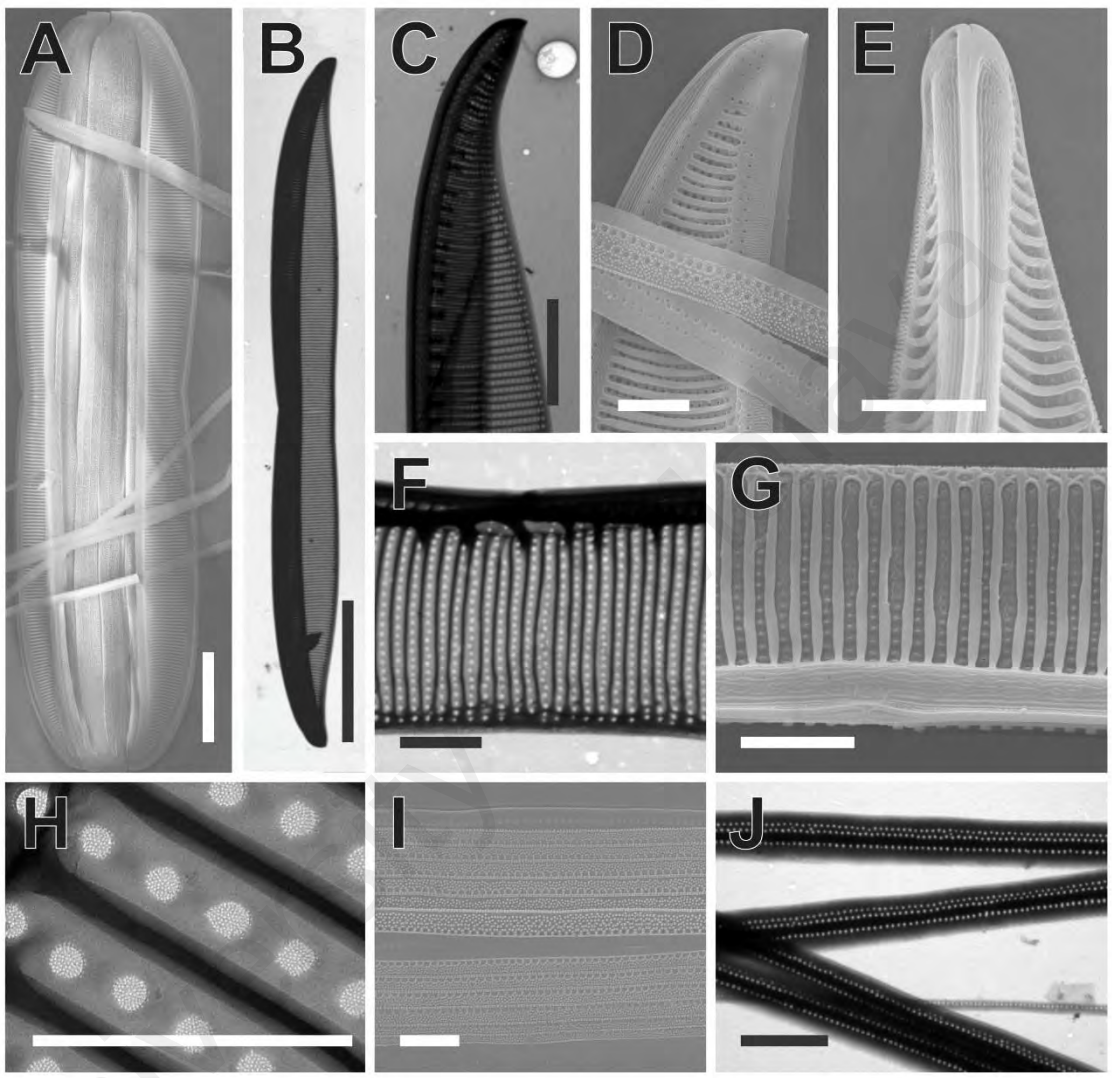

Figure 5.10: Valve shape and ultrastructure of *N. navis-varingica* in clade H. SEM micrographs, except for B, C, F, H and J, TEM. (A and B) Girdle view of frustule. The raphe slits are positioned along one edge of the valve face, raised along the keel and spanned internally by fibulae. (C and D) Apices of valve curved inward. (E) Tips of valve showing the terminal fissure curving toward the distal side. (F and G) View of valve near the central nodule. (H) Round areolae. (I and J) Cingulum comprises varying rows of areolae. Scale bars: 20 µm (A, B); 5 µm (C, J); 2 µm (D, E, F, G, I); 1 µm (H).

5.4.2 LSU rDNA phylogeny and sequence divergences

Multiple sequence alignments of LSU rDNA yielded 768 characters (including gaps), of which 552 characters are constant, 120 are parsimony-informative, and 96 are parsimony-uninformative. All MP, ML and BI yielded identical tree topologies; only the BI tree is shown (Figure 5.11). The phylogenetic inference showed a group comprising *N. navis-varingica* strains from Malaysia, Philippines and Vietnam (Lundholm et al., 2002; Kotaki et al., 2005; Appendix F–G) with strong bootstrap supports (MP/ML/BI: 80/79/0.55) and low sequence divergences (*p*-distances, <0.9%; Table 5.3). *Nitzschia pellucida* Grunow, *N. linearis* W. Smith, *N.* cf. *promare* and *N. laevis* Hustedt formed the sister clade to all *N. navis-varingica* with strong bootstrap value (MP/ML/BI: 98/100/1.00). All *N. navis-varingica* strains were grouped into eight subclades, namely clade A–H, followed the cladding of ITS2 phylogeny. Intra-specific divergences of LSU rDNA yielded 0–0.6 % and inter-specific divergences yielded 0–0.9 % (Table 5.3). Intra-specific divergences in clade G is 0–0.6 % and inter-specific divergences between clade B and clade G yielded highest sequence divergences (0.1–0.9 %).

5.4.3 ITS2 rDNA phylogeny and sequence divergences

The final dataset comprised of 359 including in-group and outgroup (Appendix F–G). The ITS2 transcript alignment yielded a total of 649 characters in the dataset. Neighbour-joining (NJ) analysis was conveyed on ITS2 with secondary structure inferences. Here, only the NJ tree is shown with NJ and ML bootstrap supports (Figure 5.12). The subclades in ITS2 phylogeny revealed a grouping similar to that of the LSU tree, except strains in clade A, C and G (Figure 5.11), which clade A, C, and G were separated in the different clade.

In ITS2 phylogeny, all *N. navis-varingica* taxa were clustered together and supported by high bootstrap values (NJ/ML: 98/100) (Figure 5.12). Clade A comprised strains from Malaysia, Thailand, Philippines and Japan (NJ/ML: 85/100); whereas *N. navis-varingica* in clade B, C, D, G and H comprised strains mainly from Malaysia. Strains in clade H majority from Sarawak (Santubong and Sematan). *N. navis-varingica* in clade E comprised strains mainly from Malaysia, the Philippines, followed by Japan and Vietnam (NJ/ML: 99/100); whereas *N. navis-varingica* in clade F comprised strains only from Tok Bali (one strain) (Malaysia) and Bolinao (Philippines) (nine strains). The intraspecific divergence of *N. navis-varingica* within eight subclades was in the value of 0–12.6% whereas the interspecific divergence between eight *N. navis-varingica* clades was 0.5–19.7% (Table 5.4).

Table 5.3: Pairwise LSU rDNA genetic distances (uncorrected *p*-distances) within and among the eight *N. navis-varingica* clades, shown as minimum-maximum. Shaded diagonal, intraspecific sequence divergence (in percent, %).

Clade	A	B	C	D	E	F	G	H
A (n=12)	0.0							
B (n=7)	0.1 − 0.6	0.0 − 0.4						
C (n=9)	0.0	0.1 − 0.6	0.0					
D (n=4)	0.6 − 0.7	0.4 − 1.0	0.6 − 0.7	0.0 − 0.1				
E (n=5)	0.1	0.3 − 0.7	0.1	0.4 − 0.6	0.0			
F (n=4)	0.1	0.3 − 0.7	0.1	0.4 − 0.6	0.0	0.0		
G (n=7)	0.0 − 0.6	0.1 − 0.9	0.0 − 0.6	0.4 − 0.7	0.1 − 0.4	0.1− 0.4	0.0 − 0.6	
H (n=1)	0.1	0.3 − 0.7	0.1	0.4 − 0.6	0.0	0.0	0.1 − 0.4	0.0

Table 5.4: Pairwise ITS2 rDNA genetic distances (uncorrected p-distances) within and among the eight *N. navis-varingica* clades, shown as minimum-maximum. Shaded diagonal, intraspecific sequence divergence (in percent, %).

Clade	A	B	C	D	E	F	G	H
A (n=145)	0.0 − 4.4							
B (n=105)	1.6 − 13.1	0.0 − 1.1						
C (n=30)	8.2 − 10.9	7.1 − 8.2	0.0					
D (n=4)	14.8 − 16.9	14.8 − 15.3	18.6	0.0				
E (n=46)	0.5 − 16.9	1.6 − 16.4	12.0 − 15.8	17.5 − 19.7	0.0 − 12.6			
F (n=10)	9.8 − 13.7	10.4 − 12.0	9.3 − 10.4	14.8 − 15.8	8.2 − 10.9	0.0 − 2.2		
G (n=9)	13.7 − 18.0	14.2 − 16.9	12.0 − 13.1	14.8 − 17.5	11.5 − 14.2	8.7 − 10.9	0.0 − 3.8	
H (n=6)	8.7 − 12.0	9.3 − 10.4	10.9 − 12.0	17.5 − 18.0	9.3 − 13.1	8.2 − 9.8	10.4 − 14.2	0.0 − 1.6

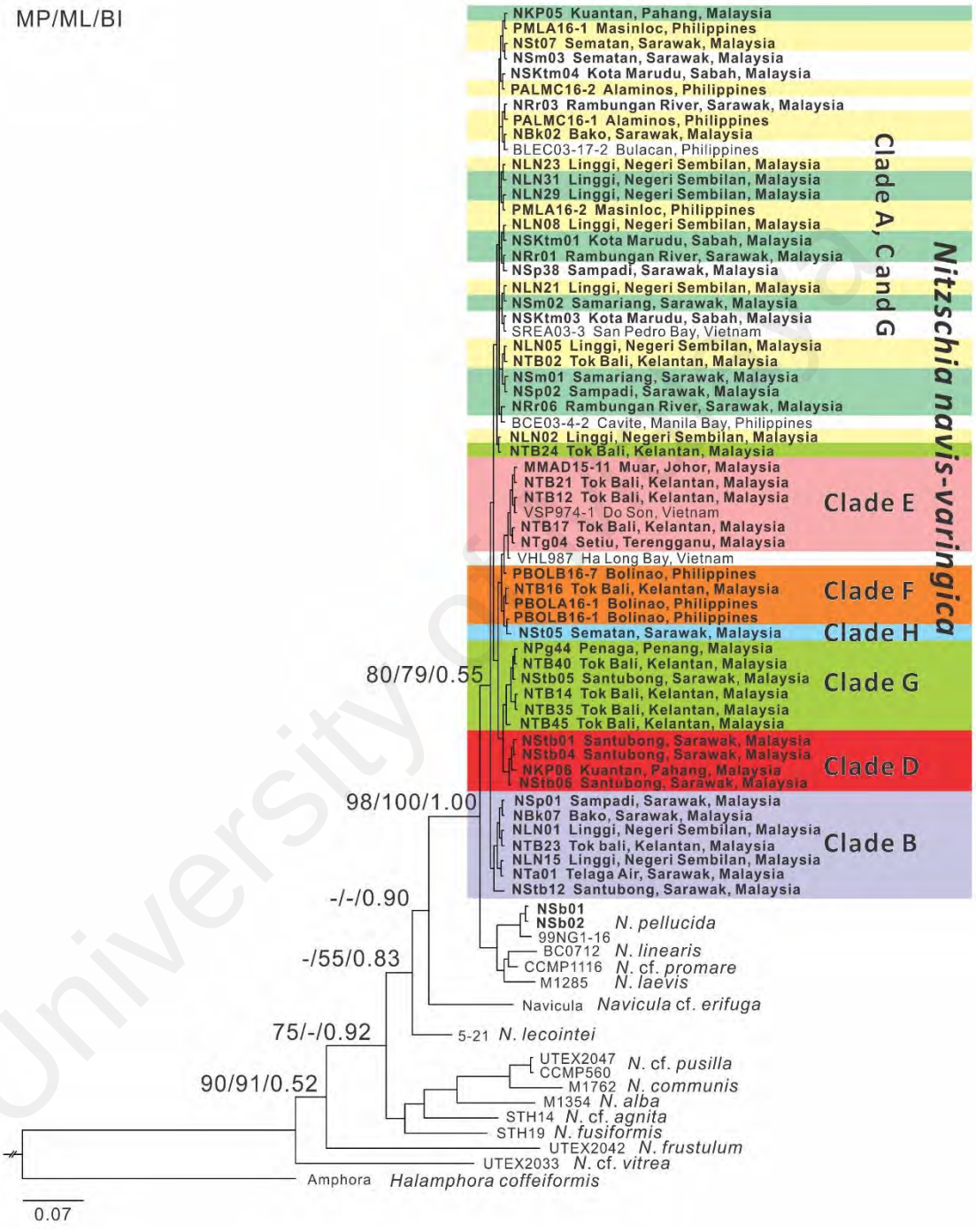

Figure 5.11: Tree topology inferred from Bayesian inference (BI), based on the *N. navis-varingica* LSU rDNA sequence. Values on nodes represent bootstrap supports of MP and ML, and posterior probabilities of BI.

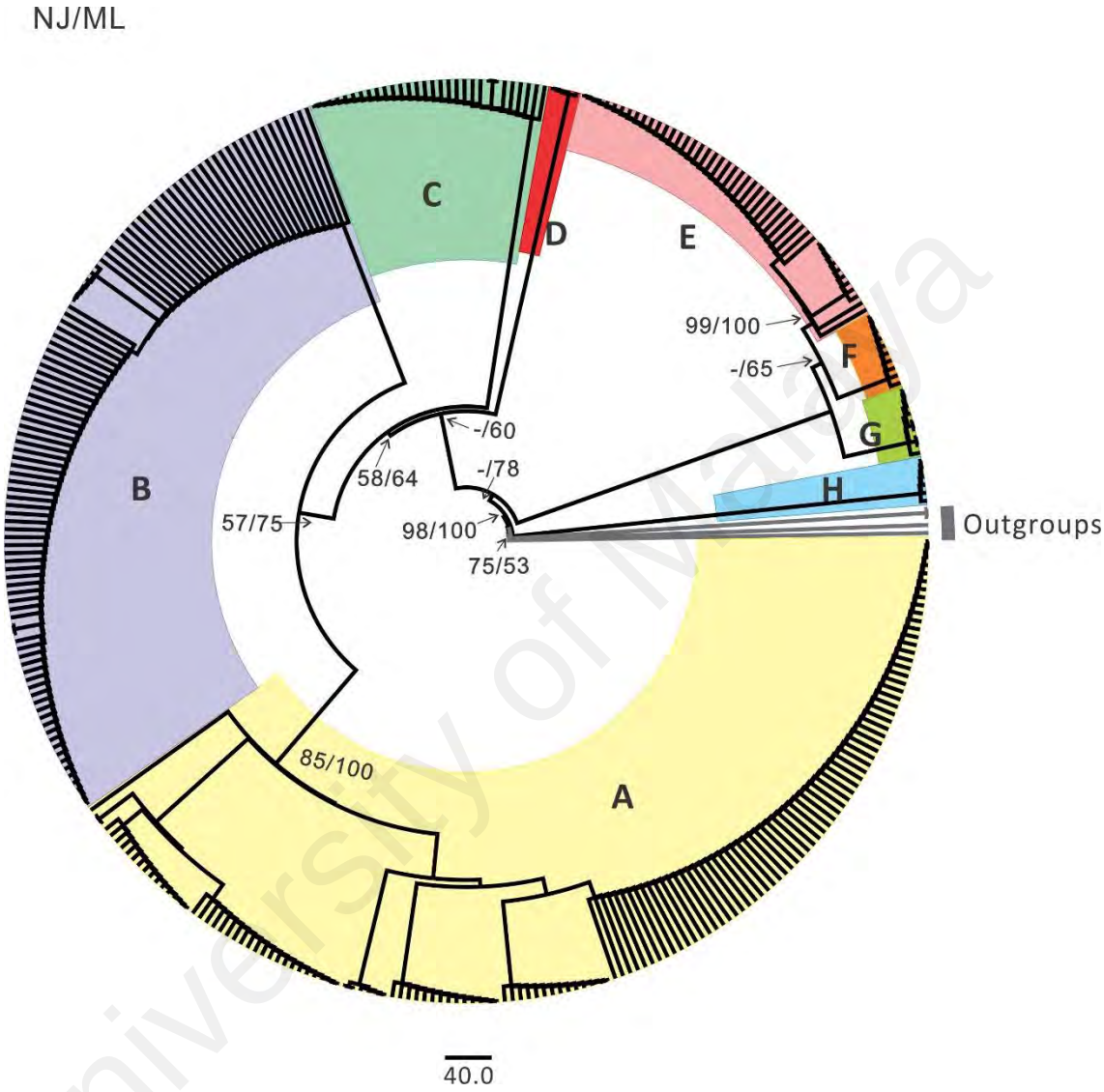

Figure 5.12: Tree topology based on sequence structure of *N. navis-varingica* ITS2 rDNA sequences inferred by neighbour-joining. Values on nodes represent bootstrap supports of NJ and ML. Eight subgroups are revealed in the *N. navis-varingica* clade (A–H).

5.4.4 Genetic diversity of *N. navis-varingica*

Sequence analysis revealed 44 unique haplotypes in 355 sequences from Western Pacific region. The region of ITS2 was highly variable, with 309 differing nucleotide sites; the details of each haplotype are listed in Appendix H. A median-joining network derived from ITS2 sequences of *N. navis-varingica* was shown in Figure 5.13. Based on median-joining network, *N. navis-varingica* grouped not only according to the haplotypes but also separated according to clades in ITS2 phylogeny (Figure 5.12). From the network, haplotype H2 shown the highest frequencies in clade B, followed by H7 in clade A, H5 in clade C and H4 in clade E (Figure 5.13).

N. navis-varingica in clade A comprised 21 haplotypes in 145 sequences from 20 geographical regions in Southeast Asian countries. For *N. navis-varingica* in clade B, this clade comprised only 6 haplotypes among 105 sequences from 12 locations (Figure 5.13; Appendix F). *N. navis-varingica* in clade C, H and G consisted only 3 haplotypes among 30, 6 and 9 sequences from 8, 2 and 4 sampling sites, respectively. Interestingly, haplotypes in clade H are unique and only found in Sarawak (Santubong and Sematan). Clade D only consisted of one haplotype (H21) among 4 sequences from Santubong and Kuantan. Clade E of *N. navis-varingica* comprised five haplotypes among 46 sequences from nine geographical regions, while *N. navis-varingica* in clade F only comprised of two haplotypes within 10 sequences from Tok Bali (H31) and Bolinao (H37). The grouping in this network is in agreement with the clustering in the NJ phylogenetic tree (Figure 5.12).

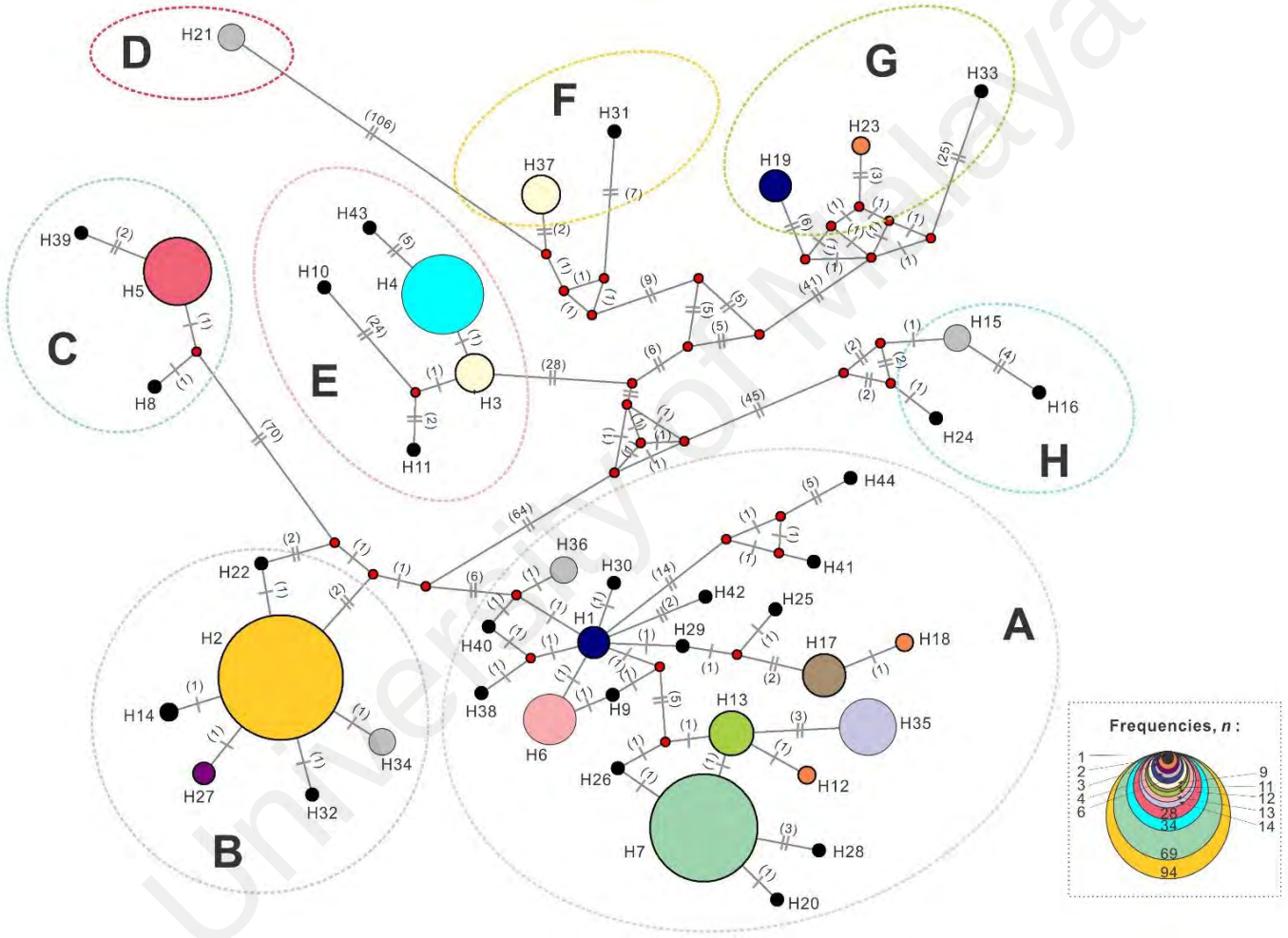

Figure 5.13: Median-joining network derived from *N. navis-varingica* ITS2 nucleotide sequences. Haplotypes are designated by numbers. Each tick and the number in bracket represents the mutational steps. The haplotypes are assigned from A to H, corresponds to subclades in ITS2 rDNA phylogeny in Figure 5.12. Each color of the circle represent the number of sequences within the haplotype.

Among the haplotypes in Western Pacific, Batu Kawan (Malaysia) showed the highest haplotypes diversity, with 8 haplotypes, H7, H17, H18, H20, H25, H26, H29, and H30 (Figure 5.13; Appendix I). Some haplotypes were common and shared between different sampling locations. Based on the network, H2 was the haplotype with the highest frequency among the 44 haplotypes, comprised a total of 94 strains from 10 different geographic locations in Malaysia: Samariang (Sarawak; 17 strains), Santubong (Sarawak ; 10 strains), Bako (Sarawak; 1 strain), Sampadi (Sarawak; 21 strains), Rambungan River (Sarawak; 23 strains), Telaga Air (Sarawak; 7 strains), Linggi River (Negeri Sembilan; 9 strains), Pendas (Johor Bahru; 4 strains), Rampayan Laut (Sabah ;1 strain) and Tok Bali (Kelantan; 1 strain) (Appendix I). Furthermore, different geographic locations among different countries also shared the same haplotype. Haplotype 3 comprised of 9 strains from four different geographic locations: Dinh Vu from Vietnam (3 strains), Do Son fromVietnam (1 strain), Kagoshima from Japan (2 strains) and Shimoda from Japan (3 strains).

Based on the median-joining network, clade A was separated from clade B with 7 mutational steps while clade B separated from clade C with 70 mutational steps (Figure 5.13). Clade D, E, F, G and H were separated from clade A with 94, 72, 93, 124 and 118 mutational steps, respectively. According to AMOVA, 48 % of the total ITS2 rDNA variation was found among the populations, and 52% within populations (Φ_{ST}=0.48095). The *F*-statistic values were very high for Malaysia strains from the west coast of Peninsula Malaysia (Malacca Strait) compared to other strains from east coast of Peninsula Malaysia (South China Sea), Thailand, Philippines, Japan and Vietnam; ranged from -0.00105–1.00. The F_{ST} between strains from Japan and Thailand were also comparably high at 1.00 (Table 5.5). The F_{ST} among strains in within Thailand and Vietnam were extremely low, given 0.00.

Table 5.5: Genetic divergence of the ITS2 region in *Nitzschia navis-varingica* populations. Upper diagonal: Average number of pairwise differences between population (PiXY); Diagonal element: Average number of pairwise differences within populations; lower diagonal: Population pairwise FSTs values.

Population	1	2	3	4	5	6	7	8	9	10	11	12	13	14	15	16
1 (n=6)	0.00000	1.00000	1.00000	1.00000	1.00000	1.00000	1.00000	1.00000	1.00000	1.00000	1.00000	1.00000	1.00000	1.00000	1.00000	1.00000
2 (n=22)	0.71563	0.38528	1.00000	1.00000	0.42879	0.74518	0.48485	1.00000	1.00000	0.81818	1.00000	0.81818	0.91414	1.00000	1.00000	0.81602
3 (n=3)	1.00000	0.68057	0.00000	1.00000	1.00000	1.00000	1.00000	1.00000	1.00000	1.00000	1.00000	1.00000	1.00000	1.00000	1.00000	1.00000
4 (n=26)	1.00000	0.82136	1.00000	0.00000	1.00000	1.00000	1.00000	1.00000	1.00000	1.00000	1.00000	1.00000	1.00000	1.00000	1.00000	1.00000
5 (n=30)	0.63188	-0.02402	0.59562	0.74020	0.49195	0.74242	0.52222	1.00000	0.96667	0.83333	0.97500	0.83333	0.86296	1.00000	0.98667	0.79444
6 (n=33)	0.48096	0.23811	0.43187	0.60705	0.17583	0.72917	0.75253	1.00000	0.80303	0.75758	0.85227	0.75758	0.61953	1.00000	0.92121	0.70996
7 (n=6)	0.70000	0.01324	0.60000	0.88092	-0.03324	0.09979	0.60000	1.00000	0.91667	1.00000	0.9375	1.00000	0.77778	1.00000	0.96667	0.74603
8 (n=1)	1.00000	0.61472	1.00000	1.00000	0.50805	0.27083	0.40000	0.00000	1.00000	1.00000	1.00000	1.00000	1.00000	1.00000	1.00000	1.00000
9 (n=10)	0.58758	0.49742	0.50187	0.78789	0.41557	0.11387	0.29049	0.31111	0.68889	1.00000	0.81250	1.00000	0.55556	1.00000	0.90000	0.71429
10 (n=1)	1.00000	0.5291	1.00000	1.00000	0.40966	0.03750	0.40000	1.00000	0.31111	0.00000	1.00000	0.00000	1.00000	1.00000	1.00000	1.00000
11 (n=8)	0.61984	0.51148	0.52450	0.82317	0.43002	0.16852	0.3146	0.32143	0.15822	0.32143	0.67857	1.00000	0.66667	1.00000	0.92500	0.78571
12 (n=2)	1.00000	0.59217	1.00000	1.00000	0.49639	0.23447	0.53846	1.00000	0.44840	0.00000	0.46573	0.00000	1.00000	1.00000	1.00000	1.00000
13 (n=9)	0.86580	0.63995	0.82898	0.94336	0.53309	0.16365	0.50701	0.77778	0.17167	0.77778	0.33543	0.80978	0.22222	1.00000	0.82222	0.46561
14 (n=3)	0.79310	0.55752	0.66667	0.93963	0.47083	0.28722	0.37600	0.33333	0.31804	0.33333	0.32538	0.57143	0.66220	0.66667	0.70000	1.00000
15 (n=20)	0.48034	0.42517	0.41586	0.64900	0.37120	0.18585	0.26746	0.22632	0.18240	0.22632	0.20691	0.36930	0.33453	-0.04957	0.77368	0.88571
16 (n=42)	0.53690	0.3634	0.49855	0.63886	0.29387	0.04897	0.17674	0.37747	0.08791	0.37747	0.17958	0.46911	0.04360	0.36717	0.22048	0.62253
17 (n=12)	0.73432	0.60525	0.68142	0.86558	0.53846	0.39476	0.51807	0.59091	0.29924	0.59091	0.47347	0.65217	0.67352	0.52542	0.38599	0.45277
18 (n=11)	0.77932	0.60205	0.73090	0.89447	0.50241	0.13982	0.44181	0.65455	0.12918	0.65455	0.27946	0.70491	-0.08400	0.57332	0.29956	0.02963
19 (n=7)	0.71906	0.55857	0.63449	0.88316	0.47291	0.31943	0.44017	0.47619	0.38498	0.38889	0.39556	0.52100	0.64266	0.42882	0.32215	0.39223
20 (n=34)	0.61450	-0.00934	0.57932	0.71820	-0.00955	0.19769	-0.00105	0.48841	0.42497	0.37879	0.43306	0.47197	0.54531	0.45535	0.37222	0.32152
21 (n=19)	0.47468	0.39506	0.40762	0.47181	0.34195	0.23215	0.25706	0.21053	0.25471	0.21053	0.25661	0.35927	0.43377	0.19114	0.21848	0.29098
22 (n=2)	1.00000	0.66060	1.00000	0.00000	0.57194	0.39362	0.53846	1.00000	0.44840	1.00000	0.46573	1.00000	0.80978	0.57143	0.36930	0.46911
23 (n=1)	1.00000	0.52910	1.00000	1.00000	0.40966	0.03750	0.40000	1.00000	0.31111	0.00000	0.32143	0.00000	0.77778	0.33333	0.22632	0.37747
24 (n=15)	0.90411	0.72174	0.88685	0.95132	0.64485	0.50446	0.71977	0.86667	0.63053	0.86667	0.65966	0.87882	0.83266	0.76562	0.51868	0.55110
25 (n=7)	1.00000	0.04819	1.00000	1.00000	0.06064	0.34300	0.13103	1.00000	0.60752	1.00000	0.64163	1.00000	0.85906	0.81579	0.49476	0.43186
26 (n=1)	1.00000	0.61472	0.00000	1.00000	0.50805	0.27083	0.40000	1.00000	0.31111	1.00000	0.32143	1.00000	0.77778	0.33333	0.22632	0.37747
27 (n=3)	1.00000	0.68057	1.00000	1.00000	0.59562	0.43187	0.60000	1.00000	0.50187	1.00000	0.52450	1.00000	0.82898	0.66667	0.41586	0.49855
28 (n=9)	1.00000	0.74005	1.00000	1.00000	0.65571	0.50921	0.75676	1.00000	0.64111	1.00000	0.67766	1.00000	0.88889	0.84874	0.51950	0.55927
29 (n=3)	0.67568	0.47671	0.50000	0.89811	0.38801	0.19253	0.25000	0.00000	0.20747	0.00000	0.20879	0.36842	0.56160	0.16667	0.15578	0.27967
30 (n=1)	1.00000	0.61472	1.00000	1.00000	0.50805	0.27083	0.40000	1.00000	0.31111	1.00000	0.32143	1.00000	0.77778	0.33333	0.22632	0.37747
31 (n=1)	1.00000	0.61472	1.00000	1.00000	0.50805	0.27083	0.40000	1.00000	0.31111	1.00000	0.32143	1.00000	0.77778	0.33333	0.22632	0.37747
32 (n=1)	1.00000	0.61472	1.00000	1.00000	0.50805	0.27083	0.40000	1.00000	0.31111	1.00000	0.32143	1.00000	0.77778	0.33333	0.22632	0.37747
33 (n=2)	1.00000	0.66060	0.00000	1.00000	0.57194	0.39362	0.53846	1.00000	0.44840	1.00000	0.46573	1.00000	0.80978	0.57143	0.36930	0.46911

Table 5.5, continued.

Population	1	2	3	4	5	6	7	8	9	10	11	12	13	14	15	16
34 (n=1)	1.00000	0.61472	1.00000	1.00000	0.50805	0.27083	0.40000	1.00000	0.31111	1.00000	0.32143	1.00000	0.77778	0.33333	0.22632	0.37747
35 (n=3)	1.00000	0.68057	0.00000	1.00000	0.59562	0.43187	0.60000	1.00000	0.50187	1.00000	0.52450	1.00000	0.82898	0.66667	0.41586	0.49855

Label	Population Name
1	Mae Klong River, Thailand
2	Samariang, Sarawak, Malaysia
3	Dinh Vu, Vietnam
4	Kuala Abai, Sabah, Malaysia
5	Sampadi, Sarawak, Malaysia
6	Linggi River, Negeri Sembilan, Malaysia
7	Pendas, Johor Bahru, Malaysia
8	Muar, Johor, Malaysia
9	Kinarut, Sabah, Malaysia
10	Kuala Penyu, Sabah, Malaysia
11	Sematan, Sarawak, Malaysia
12	Kampung Tanah Merah, Kota Marudu, Sabah, Malaysia
13	Rampayan Laut, Kota Belud, Sabah, Malaysia
14	Pasir Gebu, Penaga, Penang, Malaysia
15	Batu Kawan, Penang, Malaysia
16	Santubong, Sarawak, Malaysia
17	Teluk Marudu, Sabah, Malaysia
18	Bako, Sarawak, Malaysia

Label	Population Name
19	Kuantan, Pahang, Malaysia
20	Rambungan River, Sarawak, Malaysia
21	Tok Bali, Kelantan, Malaysia
22	Setiu River, Terengganu, Malaysia
23	Tumpat, Kelantan, Malaysia
24	Bak Bak Beach, Sabah, Malaysia
25	Telaga Air, Sarawak, Malaysia
26	Do Son, Vietnam
27	Masinloc, Philippines
28	Bolinao, Philippines
29	Alaminos, Philippines
30	Uruma, Okinawa, Japan
31	Sanchez Mira, Cagayan, Philippines
32	Buguey Cagayan, Philippines
33	Kagoshima, Japan
34	Miyazaki, Japan
35	Shimoda, Japan

Table 5.5, continued.

Population	17	18	19	20	21	22	23	24	25	26	27	28	29	30	31	32	33	34	35
1 (n=6)	1.00000	1.00000	1.00000	1.00000	1.00000	1.00000	1.00000	1.00000	1.00000	1.00000	1.00000	1.00000	1.00000	1.00000	1.00000	1.00000	1.00000	1.00000	1.00000
2 (n=22)	1.00000	0.92975	0.97403	0.44519	0.95933	1.00000	0.81818	1.00000	0.22727	1.00000	1.00000	1.00000	1.00000	1.00000	1.00000	1.00000	1.00000	1.00000	1.00000
3 (n=3)	1.00000	1.00000	1.00000	1.00000	1.00000	1.00000	1.00000	1.00000	1.00000	0.00000	1.00000	1.00000	1.00000	1.00000	1.00000	1.00000	0.00000	1.00000	0.00000
4 (n=26)	1.00000	1.00000	1.00000	1.00000	0.68421	0.00000	1.00000	1.00000	1.00000	1.00000	1.00000	1.00000	1.00000	1.00000	1.00000	1.00000	1.00000	1.00000	1.00000
5 (n=30)	1.00000	0.88182	0.95238	0.49706	0.95263	1.00000	0.83333	1.00000	0.30000	1.00000	1.00000	1.00000	1.00000	1.00000	1.00000	1.00000	1.00000	1.00000	1.00000
6 (n=33)	1.00000	0.65289	0.96537	0.77273	0.98565	1.00000	0.75758	1.00000	0.72727	1.00000	1.00000	1.00000	1.00000	1.00000	1.00000	1.00000	1.00000	1.00000	1.00000
7 (n=6)	1.00000	0.80303	1.00000	0.54902	0.96491	1.00000	1.00000	1.00000	0.33333	1.00000	1.00000	1.00000	1.00000	1.00000	1.00000	1.00000	1.00000	1.00000	1.00000
8 (n=1)	1.00000	1.00000	1.00000	1.00000	1.00000	1.00000	1.00000	1.00000	1.00000	1.00000	1.00000	1.00000	1.00000	1.00000	1.00000	1.00000	1.00000	1.00000	1.00000
9 (n=10)	0.77500	0.59091	1.00000	1.00000	1.00000	1.00000	1.00000	1.00000	1.00000	1.00000	1.00000	1.00000	1.00000	1.00000	1.00000	1.00000	1.00000	1.00000	1.00000
10 (n=1)	1.00000	1.00000	0.85714	0.82353	1.00000	1.00000	0.00000	1.00000	1.00000	1.00000	1.00000	1.00000	1.00000	1.00000	1.00000	1.00000	1.00000	1.00000	1.00000
11 (n=8)	1.00000	0.69318	1.00000	1.00000	1.00000	1.00000	1.00000	1.00000	1.00000	1.00000	1.00000	1.00000	1.00000	1.00000	1.00000	1.00000	1.00000	1.00000	1.00000
12 (n=2)	1.00000	1.00000	0.85714	0.82353	1.00000	1.00000	0.00000	1.00000	1.00000	1.00000	1.00000	1.00000	1.00000	1.00000	1.00000	1.00000	1.00000	1.00000	1.00000
13 (n=9)	1.00000	0.26263	1.00000	0.92484	0.99415	1.00000	1.00000	1.00000	0.88889	1.00000	1.00000	1.00000	1.00000	1.00000	1.00000	1.00000	1.00000	1.00000	1.00000
14 (n=3)	1.00000	1.00000	1.00000	1.00000	0.92982	1.00000	1.00000	0.97778	1.00000	1.00000	1.00000	1.00000	1.00000	1.00000	1.00000	1.00000	1.00000	1.00000	1.00000
15 (n=20)	1.00000	0.83636	1.00000	1.00000	1.00000	1.00000	1.00000	1.00000	1.00000	1.00000	1.00000	1.00000	1.00000	1.00000	1.00000	1.00000	1.00000	1.00000	1.00000
16 (n=42)	1.00000	0.51082	0.97279	0.83894	0.97995	1.00000	1.00000	1.00000	0.76190	1.00000	1.00000	1.00000	1.00000	1.00000	1.00000	1.00000	1.00000	1.00000	1.00000
17 (n=12)	0.40909	1.00000	1.00000	1.00000	1.00000	1.00000	1.00000	1.00000	1.00000	1.00000	1.00000	1.00000	1.00000	1.00000	1.00000	1.00000	1.00000	1.00000	1.00000
18 (n=11)	0.62169	0.34545	1.00000	0.9385	0.99522	1.00000	1.00000	1.00000	0.90909	1.00000	1.00000	1.00000	1.00000	1.00000	1.00000	1.00000	1.00000	1.00000	1.00000
19 (n=7)	0.54438	0.58037	0.52381	0.97479	0.77444	1.00000	0.85714	1.00000	1.00000	1.00000	1.00000	1.00000	1.00000	1.00000	1.00000	1.00000	1.00000	1.00000	1.00000
20 (n=34)	0.52487	0.51626	0.47134	0.51159	0.96440	1.00000	0.82353	1.00000	0.32353	1.00000	1.00000	1.00000	1.00000	1.00000	1.00000	1.00000	1.00000	1.00000	1.00000
21 (n=19)	0.37955	0.39906	0.12713	0.34220	0.78947	0.68421	1.00000	0.98596	0.94737	1.00000	1.00000	1.00000	1.00000	1.00000	1.00000	1.00000	1.00000	1.00000	1.00000
22 (n=2)	0.65217	0.70491	0.58435	0.55540	0.12165	0.00000	1.00000	1.00000	1.00000	1.00000	1.00000	1.00000	1.00000	1.00000	1.00000	1.00000	1.00000	1.00000	1.00000
23 (n=1)	0.59091	0.65455	0.38889	0.37879	0.21053	1.00000	0.00000	1.00000	1.00000	1.00000	1.00000	1.00000	1.00000	1.00000	1.00000	1.00000	1.00000	1.00000	1.00000
24 (n=15)	0.74168	0.77491	0.73283	0.62692	0.50851	0.87882	0.86667	0.13333	1.00000	1.00000	1.00000	1.00000	1.00000	1.00000	1.00000	1.00000	1.00000	1.00000	1.00000
25 (n=7)	0.74724	0.77098	0.73810	0.08065	0.46543	1.00000	1.00000	0.90862	0.00000	1.00000	1.00000	1.00000	1.00000	1.00000	1.00000	1.00000	1.00000	1.00000	1.00000
26 (n=1)	0.59091	0.65455	0.47619	0.48841	0.21053	1.00000	1.00000	0.86667	1.00000	0.00000	1.00000	1.00000	1.00000	1.00000	1.00000	1.00000	0.00000	1.00000	0.00000
27 (n=3)	0.68142	0.73090	0.63449	0.57932	0.40762	1.00000	1.00000	0.88685	1.00000	1.00000	0.00000	1.00000	0.66667	1.00000	1.00000	1.00000	1.00000	1.00000	1.00000
28 (n=9)	0.76923	0.81101	0.76892	0.63707	0.51540	1.00000	1.00000	0.91641	1.00000	1.00000	1.00000	0.00000	1.00000	1.00000	1.00000	1.00000	1.00000	1.00000	1.00000
29 (n=3)	0.42857	0.47619	0.31022	0.37271	0.14394	0.36842	0.00000	0.69708	0.70833	0.00000	0.25000	0.75676	1.00000	1.00000	1.00000	1.00000	1.00000	1.00000	1.00000
30 (n=1)	0.59091	0.65455	0.47619	0.48841	0.21053	1.00000	1.00000	0.86667	1.00000	1.00000	1.00000	1.00000	0.00000	0.00000	1.00000	1.00000	1.00000	1.00000	1.00000
31 (n=1)	0.59091	0.65455	0.47619	0.48841	0.21053	1.00000	1.00000	0.86667	1.00000	1.00000	1.00000	1.00000	0.00000	1.00000	0.00000	1.00000	1.00000	1.00000	1.00000
32 (n=1)	0.59091	0.65455	0.47619	0.48841	0.21053	1.00000	1.00000	0.86667	1.00000	1.00000	1.00000	1.00000	0.00000	1.00000	1.00000	0.00000	1.00000	1.00000	1.00000
33 (n=2)	0.65217	0.70491	0.58435	0.55540	0.35927	1.00000	1.00000	0.87882	1.00000	0.00000	1.00000	1.00000	0.36842	1.00000	1.00000	1.00000	0.00000	1.00000	0.00000
34 (n=1)	0.59091	0.65455	0.47619	0.48841	0.21053	1.00000	1.00000	0.86667	1.00000	1.00000	1.00000	1.00000	0.00000	1.00000	1.00000	1.00000	1.00000	0.00000	1.00000
35 (n=3)	0.68142	0.7309	0.63449	0.57932	0.40762	1.00000	1.00000	0.88685	1.00000	0.00000	1.00000	1.00000	0.50000	1.00000	1.00000	1.00000	0.00000	1.00000	0.00000

5.5 Discussion

This study confirmed that the species of *N. navis-varingica* is widely distributed in the mangrove areas of Malaysian waters. Morphological data obtained from observation using electron microscopy confirmed the species identities of *N. navis-varingica* isolates established in this study. *N. navis-varingica* isolates were morphologically identical to the type species (Lundholm & Moestrup, 2000) but minor different in the range of some morphometric characteristics (Table 5.2; Figure 5.2). Cell lengths and cell width of Malaysian *N. navis-varingica* (54.51–215.95 µm; 4.00–15.86 µm) are comparable to isolates reported from the Japan, Philippines and Thailand (38–110 µm; 9–13 µm) (Kotaki et al., 2004, 2005, 2006; Bajarias et al., 2006; Romero et al., 2008, 2011), but longer and wider than the type specimen discovered from Do Son, Vietnam in year 1997 (45–55 µm; 9–11 µm) (Lundholm & Moestrup, 2000). However, valve length and valve width commonly exclude for comparison as these characters tend to reduce during cylce of cell division.

Furthermore, the number of fibulae (in 10 µm) observed in Malaysia isolates (6–14) also comparable to those reported from Japan (10–12), Philippine (8–12) and Vietnam (10–12) (Lundholm & Moestrup, 2000; Kotaki et al., 2004, 2005, 2006; Bajarias et al., 2006; Romero et al., 2011). The range of number of striae of Malaysian isolates (6–14) are wider compared to Japan (10–12), Philippines (8–12), and Vietnam (10–12) (Lundholm & Moestrup, 2000; Kotaki et al., 2004, 2005, 2006; Bajarias et al., 2006; Romero et al., 2011). The number of areolae in 1 µm observed in Malaysian isolates (3–7) is higher than the type specimen (3–4) and isolates from Japan (3–4), and Philippines (3–5) (Lundholm & Moestrup, 2000; Kotaki et al., 2004, 2005, 2006; Bajarias et al., 2006; Romero et al., 2011). Additionally, isolates from Bolinao, Philippines (PBOLA 16–1, PBOLA 16–2 and PBOLB 16–5) (109.08–147.02 µm; 5–15.8 µm) are comparable to the type specimen but longer and wider than the type

specimen reported in Vietnam. The range of areolae (4–6) and band (3–4) in 1 µm are higher compared to the type specimen (areolae: 3–4; band: 2–3) (Lundholm & Moestrup, 2000) (Table 5.2; Figure 5.2).

The identity of *N. navis-varingica* in this study was well supported by the phylogenetic inferences of LSU and ITS2 rDNA (Figure 5.11–5.12). The LSU rDNA dataset revealed high sequence homogeneity among all strains examined (0–0.9%) (Table 5.3). The phylogenetic tree does not reveal group according to geographically structured but rather dispersed in different clusters. Our data show eight distinct ITS2 entities, additional five subclades compared to the previous study (Tan et al., 2016; chapter four) due to the additional of taxon sampling; with high sequence heterogeneity ranging from 0.5 to 19.7% (Table 5.4; Figure 5.12). The ITS2 tree revealed eight entities: clade A comprised strains from Malaysia, Thailand, Japan, and the Philippines; clade B, clade C, and clade G comprised strains from both South China Sea (SCS) and the Strait of Malacca (MS) along Malaysian waters; clade D comprised strains from Kuantan and Santubong; clade E comprised strains from Malaysia, Vietnam, Japan, and the Philippines; clade F comprised mainly from Bolinao and Tok Bali (SCS); and clade H comprised strains only from Sarawak (Santubong and Sematan) (SCS). This further supported in our analyses by high F_{ST} values, indicative of high genetic different and existence of barriers to gene flow. For example, there is a high degree of gene flow in clade A between strains from Thailand with isolates from Malaysian, Japan, and Philippines (F_{ST}= 0.47468–1.00) (Table 5.5; Figure 5.12; Appendix H).

To understand the population dynamics of *N. navis-varingica* in the Western Pacific region, genetic diversity of *N. navis-varingica* was investigated using the ITS2 rDNA marker because of its valuable characteristics especially on the variability to distinguish closely related species. The data revealed high gene flow among *N. navis-varingica* populations in the Western Pacific region (Φ_{ST} = 0.48095). Homogenous

populations were found within each environment (Figure 5.14). High gene flow reduces genetic differentiation and increases homogeneity, thus, we hypothesized that genetic exchange might occur within the populations. Genetic exchange of common haplotypes in short and long geographic distance might dispersal based on northeast monsoon period or southwest monsoon period. For example, H2 was dispersal among eight locations in SCS and two locations in MS (Figure 5.14). No genetic difference within a short geographic distance of common populations in Kuching, Sarawak could be explained by a sea surface current. Wind direction generated by monsoon forced the sea surface current passing through all the locations in Kuching. In contrast, for H2 that found in Pendas and Linggi Liver, the exchange could be due to the wind direction generated by the northeast monsoon and forced the sea surface current passing the MS through westward. Furthermore, common haplotypes in distanced population was found in this study. H4 only found in SCS region: Tok Bali (n=6), Setiu (n=2) and Kuala Abai (n=26); while H6 was found in Tok Bali (n=6), Kuantan (n=5), Sampadi (n=1) and Sampadi (n=1) (Figure 5.14). Thus, the wind direction and monsoon period play role in genetic exchange and enhance the gene flow of *N. navis-varingica* population in this study.

The dispersal capability in this benthic species is still poorly understood. It is hypothesized that the dispersal might occur via rafting on floating object. Microalgae might become the structure of epiphytic forms and act as assemblages on mangrove roots (Navarro, 1982; Siqueiros Beltrones & López Fuerte, 2003). In this study, a planktonic *N. navis-varingica*, NTm 09, was found in the surface waters nearby the aquaculture farm in Tumpat, Kelantan, Malaysia. Recently, *N. navis-varingica* was also found in the surface water of Mediterranean Sea (Ayaz et al., 2018). Furthermore, two isolates from Setiu (Terengganu) and 26 strains from Kuala Abai (Sabah) from Malaysian waters were formed a haplotype, H4; with the F_{ST} value of zero between

these two populations (Figure 5.14; Table 5.5). The estimated of F_{ST} indicate no genetic difference among the population. These suggests the existence of some type of mechanism for dispersion, together with the help of current to disperse before the benthic cells settled down and appear on sediment.

This study revealed genetic heterogeneity occurred where similar morphological characteristics but resulted in a total of 44 unique haplotypes among 355 isolates. Genetic variation among population might be increased during high gene flow. Some locations comprised of many different types of haplotypes from different clades in ITS2 phylogenetic tree. Location of Tok Bali from Kelantan, Malaysia comprised of six haplotypes (H2, H4, H6, H19, H33, and H37) from different clades in ITS2 phylogeny (clade A, B, E, F, and G) (Figure 5.12 and 5.14). It is hypothesized that haplotypes diversity formed due to the polymorphism occurred by exchange the single nucleotides resulting in SNPs (single-nucleotide polymorphisms) and thus lead to DNA sequence variation. The divergences among the Tok Bali' population revealed 0– 6 % and 0–16.9 % in LSU and ITS2 dataset, respectively. Based on the ITS2 region of *N. navis-varingica* (n=19) from Tok Bali, Kelantan, a total of 152 nucleotides (approximately 43.55 %) were different in the population (Appendix H). Clearly, more than one SNPs were found among the isolates and mutation steps were shown in the median-joining network (Figure 5.13). By looking into the morphology characteristics among this population, there are some minor morphological differences especially for H33 and H37, cells were longer and wider compared to others and the ranged of fibulae per 10 µm were small (Table 5.2; Figure 5.2–5.4, and 5.7–5.9). Furthermore, the estimated of F_{ST} suggests high genetic difference among the population, with the value of 0.78947 (Table 5.5). Hence, SNPs occurred in this population.

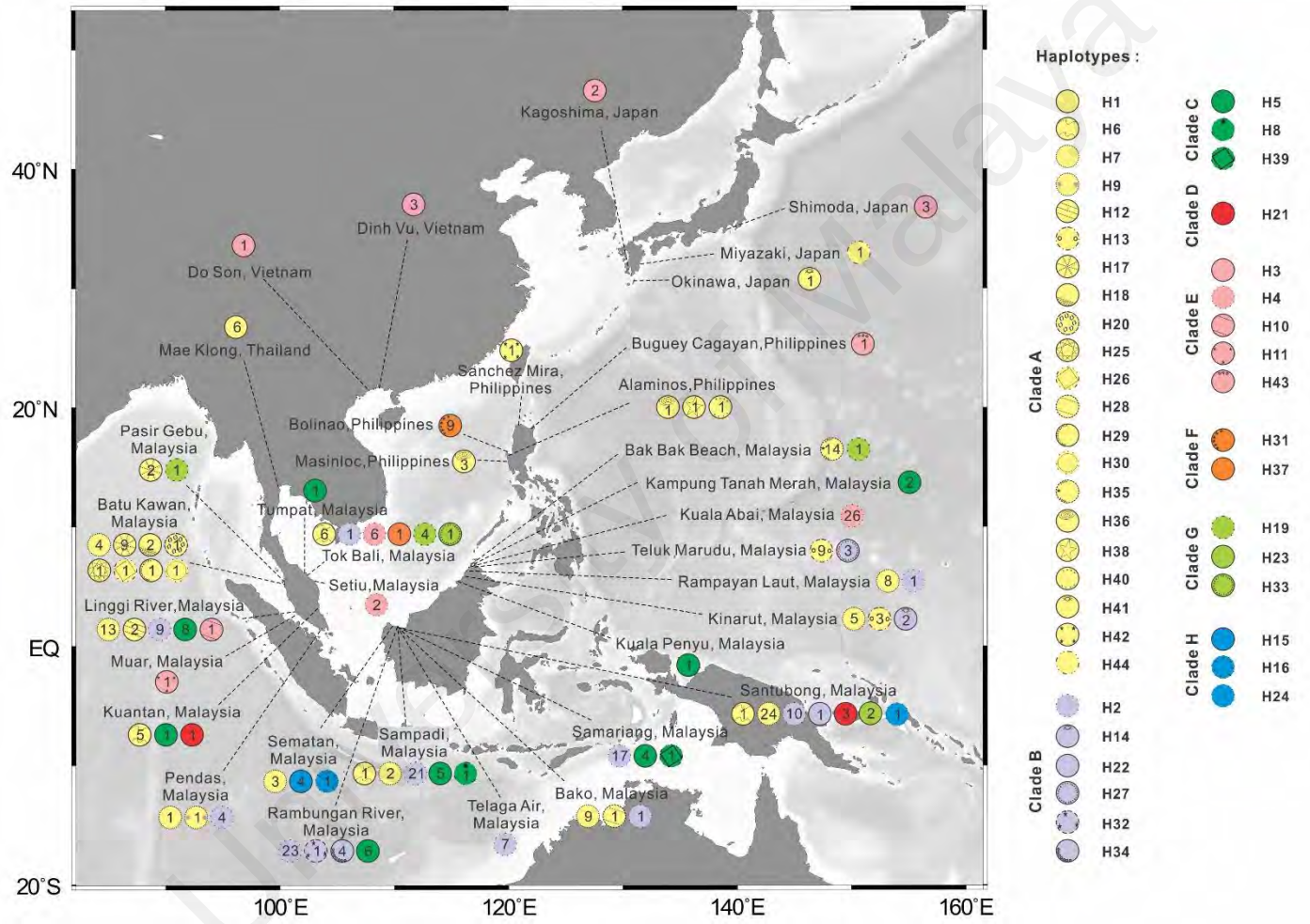

Figure 5.14: The geographical distribution of *N. navis-varingica* in the Western Pacific region, with the 44 uniques haplotypes. Lines point to the geographical location of strains isolated. The color of each haplotype represent the isolates from each clade; the number inside the haplotype circle represents the number of isolate for each haplotype in the location.

Strains from Bolinao (Philippines) and Tok Bali (Malaysia) formed two distinct haplotypes in clade F of ITS2 phylogeny (Figure 5.12). The intraspecific divergences in this clade shown a small degree of genetic variation; no divergence in LSU rDNA dataset and ranged from 0 to 2.2 % in ITS2 rDNA dataset (Table 5.3 and Table 5.4). In contrast, the estimated F_{ST} values among this two locations revealed high genetic differences, with the estimated value of 0.51540. Hence, it is possible that genetic drift might occur between these two populations. A total of eleven different nucleotide composition (loss of five nucleotides in a different position and replacement of other nucleotides for another 6 positions) found among the isolates from Tok Bali (n = 1) and Bolinao (n = 9) (Appendix H). Genetic drift could occur in a small population due to the process of migration; the changes of different nucleotide lead to genetic variation. In terms of the morphology characteristics of *N. navis-varingica* in clade F, some minor differences found among these two populations: length of isolate in Tok Bali (172.73–184.87 μm) was longer than isolates found in Bolinao (109.08–147.02 μm); number of fibulae per 10 μm of isolates in Tok Bali ranged from 7–10 but ranged from 8–12 for isolates in Bolinao; and the number of striae per 10 μm in the isolates of Tok Bali and Bolinao, ranged from 19–22 and 22–26, respectively (Table 5.2). Therefore, genetic variation can cause by genetic drift for these two populations in this study.

Interestingly, there was a consistency in the genetic relationship with respect to the geographic areas. *N. navis-varingica* from Vietnam and Japan formed a distinct haplotype H3 (F_{ST}, 0.41–1.00) suggesting possible genetic structuring between the water bodies of the northwestern Pacific and the South China Sea (SCS). We assumed that ocean current circulations (e.g. SCS currents and Kuroshiro current) play a role in this allopatric differentiation of *N. navis-varingica*. Several studies had reported there is a water exchange for northern SCS (NSCS) circulation (a) between the SCS and the Kuroshio, where the Luzon Strait then executes a tight, anticyclonic turn and exits the

SCS near Taiwan; and (b) between the SCS and the East China Sea (ECS) through the Taiwan Strait (Pohlmann, 1987; Li et al., 1992; Chao et al., 1996; Chu et al., 1999; Chen et al., 2012). It is postulated that H3 was separated due to the currents occurs in the regions and lead to allopatric speciation.

Additionally, haplotype H1, another distinct population appeared only at the mangrove area that closed to the Mae Klong river mouth, Thailand (F_{ST}= 0.47468–1.00; ITS2 rDNA genetic distance= 0.5–12.0 %). The separation of H1 of *N. navis-varingica* may suggest that speciation was controlled by the geographic boundary and seabed topology of the Gulf of Thailand. The upper part of the Gulf of Thailand has an inverted U-shape and shallower compared to the lower part of the Gulf of Thailand. Moreover, the boundary of the Gulf of Thailand was split from SCS by two underwater ridges; from the coastal city of Kota Bharu on the east coast of Peninsula Malaysia (average depth of 50 m) to Cape Camou in southern Vietnam (sill depth of 67 m). Furthermore, there is a shallow sill that acts as a hydraulic controller of current flow in the lower Gulf of Thailand (Emery & Niino, 1963; Pauly & Chuenpagdee, 2003). This shallow sill could, therefore, become a mechanism to limit water exchange between the Gulf of Thailand and SCS and the seabed topology lead to allopatric differentiation of *N. navis-varingica* for H1 in this study.

In this study, homogenous haplotypes: H2 (94 isolates), H7 (69 isolates), and H5 (28 isolates), found in the Malacca Strait (MS) and South China Sea (SCS) along the east coast and west coast of Peninsula Malaysia and coastal waters of Borneo (Figure 5.14). We hypothesized that the dispersal of *N. navis-varingica* isolates could be due to the post-glacial rise of the sea level from the melting of land ice and reduced sea level after the glacial period. The SCS and MS were separated by a geographic barrier known as the Malaysia Peninsula and connected by a narrow Tebrau Straits, thus, there was a

limited mixing between the two bodies of water. During the last glacial maximum (LGM) (2,588,000 to 11,700 years ago), the sea level falls and the size of SCS was reduced; land bridges and connecting river system were formed (Voris, 2000; Sathiamurthy & Voris, 2006). There was a continuously rising sea level in SCS when the LGM reached its terminal phase. During the late of Pleistocene, there was an accelerated rising of sea level due to a major melting event in the polar regions; lead to a number of Pleistocene Paleo River System submerged under the sea (14.6 to 14.3 thousand years ago) (Hanebuth et al., 2000; Voris, 2000; Sathiamurthy & Voris, 2006). Thus, the dispersal of homogeneous haplotypes found in two different bodies of water and restrictor of gene flow could be due to the sea level changes during the late Pleistocene and Holocene. Therefore, populations of common haplotypes of *N. navis-varingica* possibly expanded during the rising of seawater.

Batu Kawan (H7, H17, H18, H20, H25, H26, H29, and H30) comprised the highest frequencies on unique haplotypes where only one haplotype belonged to the homogenous group while most of the unique haplotype only found in this location (Figure 5.14). The F_{ST} values among these haplotypes (within populations) were high; up to 0.77368 but only nine nucleotide differences in locus can be found among this population (Table 5.5; Appendix H). We estimated the base calling error from sequencing platform caused the rare haplotypes formed. There was no difference in terms of frustule morphometric measurements of *N. navis-varingica* isolates from Batu Kawan and in the intraspecific divergences of this population ranged from 0 to 3.3 % in ITS2 dataset (Table 5.2). Thus, sequencing error could lead to the formation of rare haplotypes.

The F_{ST} value of location Mae Klong River, Dinh Vu, Kuala Abai, Telaga Air, Masinloc, Bolinao, and Shimoda resulted as zero and only one haplotype found within the population (Table 5.5; Figure 5.14). The rate of interbreeding among the population

can be speculated based on the estimated F_{ST} value (Wright, 1921, 1951, 1965). Inbreeding leads to an increasing frequency of homozygous genotypes and a decrease of heterozygous genotypes (Falconer & Mackay, 1996). Therefore, the high frequency of interbreeding happened when there is no genetic differences among the population. In contrast, Alaminos from the Philippines had the highest reading of F_{ST} value, F_{ST} =1.00 and no sharing of haplotype were found but three different haplotypes within the population were observed, inbreeding do not occur in this location (Figure 5.14).

To what extent the genetic structure of *N. navis-varingica* affecting DA production, where DA and its isomers were detected in some *N. navis-varingica* from different locations and some isolates were confirmed unable to produce DA. In this study, all isolates from Bolinao are DA positive but all isolates found from Alaminos are non-toxic (Y. Kotaki et al., per. comm.). Additionally, *N. navis-varingica* from Pendas and Muar, some isolates from Linggi River and Tok Bali were DA positive (Tan et al., 2016; chapter 4). However, more strains from different geographical areas need to be analyzed to get a more complete picture of its population and DA production.

5.6 Conclusion

This study revealed a considerably wide species distribution in the Malaysian waters and our data provide important first insights into the population structure of *N. navis-varingica* in the Western Pacific region. The analysed LSU rDNA revealed homogeneity among the population (0 to 0.9%). The ITS2 phylogenetic inferences identified eight distinct clades, with high sequence heterogeneity ranging from 0.5 to 19.7%; analysis of haplotype diversity recovered 44 haplotypes. The dispersal of distinct population and homogenous populations can be explained by the Last Glacial Maximum during late Pleistocene and Holocene. SNPs, migration and monsoon period also affect the population structures and lead to high gene flow of *N. navis-varingica* in the Western Pacific region. The species inventory gathered from this study has contributed essential information: taxonomic information and geographical distribution of this species for better monitoring and mitigation of HABs by relevant authorities in the country.

CHAPTER 6: CONCLUSION

Malaysia is one of the countries produce seafood and exporters to other countries but so far there is no any involvement on approval or monitoring from any authority. In Malaysia, PSP remains the most severe shellfish intoxication due to algal toxins. Till now, three species was confirmed to cause poisoning and fatalities in the country, the species are *Pyrodinium bahamense* in Sabah, *Alexandrium tamiyavanichii* in Sebatu, Malacca, and *A. minutum* in Tumpat, Kelantan (Lim et al. 2004, 2012c). However, ASP-related studies in the country are still poorly known and most of the studies undertaken in Malaysia was mainly focus on phytoplankton *Pseudo-nitzschia* species from the west coasts of the Peninsula, Sabah and Sarawak (e.g. Lim et al. 2010, 2012a, 2012b, 2013, 2014, 2016, 2018; Teng et al., 2013, 2014, 2015, 2016).

In this study, a total of 548 strains of *Pseudo-nitzschia* and *N. navis-varingica* were collected from coastal waters and mangrove waters in Malaysia. The species richness of *Pseudo-nitzschia* and *N. navis-varingica* in Malaysian waters was high and identification become more challenging especially for species complex groupings in *Pseudo-nitzschia* species. A pair of primer targeting *Pseudo-nitzschia* COI gene was designed and successfully amplified *Pseudo-nitzschia*. Three molecular markers were used for phylogeny and species delineation in *Pseudo-nitzschia* species: *cox*1, ITS2 and LSU (D1-D3 region). For phylogentic study of *Pseudo-nitzschia*, the challenging taxonomic status was resolved with supports from morphological and molecular data. This study confirmed that ITS2 revealed the most resolved tree, followed by *cox*1 and LSU; but the status of *P. cuspidata* and *P. pseudodelicatissima* remains unresolved and requires examination of material from the type localities.

For *N. navis-varingica*, this study revealed a considerably high species distribution in the Malaysian mangrove swamps. DA and its geometrical isomers, IA and IB, were detected in *N. navis-varingica* isolated. The cellular toxin content of *N. navis-varingica* ranged between 0.37 and 11.06 pg/cell. In the batch culture experiment, the toxin composition changed during cell growth. Generally, Malaysian *N. navis-varingica* belongs to the toxin profile types DA, DA-IB, DA-IA-IB, and DA-IA type. Furthermore, DA was detected in the mangrove-related fisheries products (cockles), even though DA content of our samples were much lower than the regulatory limit (20 mg/kg). In this study, the ITS2 rDNA was applied, for the first time, in *Nitzschia* phylogeny. The LSU and ITS2 region of *N. navis-varingica* were successfully amplified using selected primers and sequences were obtained. This study showed strong gene flow among *N. navis-varingica* populations in the Western Pacific region (Φ_{ST}=0.48095). However, the Malaysian populations were unlikely to undergo speciation through geographical isolation.

The occurrence of the toxigenic *N. navis-varingica* in the mangrove waters of Malaysia possessed a possible risk of ASP in the country. *N. navis-varingica* could be the source of DA contamination in bivalve shellfish. The low level of DA composition that detected in the cockles samples might due to the *N. navis-varingica* itself contained more geometrical isomers than the potent DA. Furthermore, the rate of cell growth for *N. navis-varingica* was likely one of the factors that affect less DA contamination in shellfish. The output of this study could serve as a baseline data for country monitoring. The risk of ASP in the seafood products should be assessed continuously by monitoring the toxic plankton and the level of DA in shellfish mollusks. Systematic monitoring and management program of HABs and ASP should be established to safeguard the public health and ensure seafood safety.

REFERENCES

Adams, N. G., Trainer, V. L., Rocap, G., Herwig, R. P., & Hauser, L. (2009). Genetic population structure of *Pseudo-nitzschia pungens* (Bacillariophyceae) from the pacific northwest and the north sea. *Journal of Phycology*, *45*, 1037–1045.

Álvarez, G., Uribe, E., Quijano-Scheggia, S., López-Rivera, A., Marino, C., & Blanco, J. (2009). Domoic acid production by *Pseudo-nitzschia australis* and *Pseudo-nitzschia calliantha* isolated from North Chile. *Harmful Algae*, *8*, 938–945.

Amato, A., Kooistra, W. H. C. F., Ghiron, J. H. L., Mann, D. G., Pröschold, T., & Montresor, M. (2007). Reproductive isolation among sympatric cryptic species in marine diatoms. *Protist*, *158*, 193–207.

Amato, A., Lüdelking, A., & Kooistra, W. H. C. F. (2010). Intracellular domoic acid productionin *Pseudo-nitzschia multistriata* isolated from the Gulf of Naples (Tyrrhenian Sea, Italy). *Toxicon*, *55*, 157–161.

Amato, A., & Montresor, M. (2008). Morphology, phylogeny, and sexual cycle of *Pseudo-nitzschia mannii* sp. nov. (Bacillariophyceae): a pseudo-cryptic species within the *P. pseudodelicatissima* complex. *Phycologia*, *47*, 487–497.

An, S. M., Noh, J. H., Choi, D. H., Lee, J. H. & Yang, E. C. (2016). Repeat region absent in mitochondrial genome of tube-dwelling diatom *Berkeleya fennica* (Naviculales, Bacillariophyceae). *Mitochondrial DNA*, *27*, 2137–2138.

Anderson, C. R., Brzezinski, M. A., Washburn, L., & Kudela, R. (2006). Circulation and environmental conditions during a toxigenic *Pseudo-nitzschia australis* bloom in the Santa Barbara Channel, California. *Marine Ecology Progress Series*, *327*, 119–133.

Ankenbrand, M., Keller, A., Wolf, M., Schultz, J. & Förster, F. (2015). ITS2 database V: Twice as much. *Molecular Biology and Evolution*, *32*, 3030–3032.

Armbrust, E. V., Berges, J. A., Bowler, C., Green, B. R., Martinez, D., Putnam, ... Rokhsar, D. S. (2004). The genome of the diatom *Thalassiosira pseudonana*: ecology, evolution, and metabolism. *Science*, *306*(5693), 79–86.

Ashworth, M. P., Nakov, T. & Theriot, E. C. (2013). Revisiting Ross and Sims (1971): towards a molecular phylogeny of the Biddulphiaceae and Eupodiscaceae (Bacillariophyceae). *Journal of Phycology*, *49*, 1207–1222.

Ayaz, F., Devell, E. E., & Sahin, M. (2018). First report of *Nitzschia navis-varingica* in the Mediterranean Sea and growth stimulatory effects of Nitzschia navis-varingica, Chrysochromulina alifera and Heterocapsa pygmaea on different mammalian cell types. *Molecular Biology Reports*, *45*(4), 571–579.

Bajarias, F. F. A., Kotaki, Y., Relox, J. J. R., Romero, M. L. J., Furio, E. F., Lundholm, N., … Kodama, M. (2006). Screening of diatoms producing domoic acid and its derivatives in the Philippines. *Coastal Marine Science*, *30*, 121–129.

Bandelt, H.J., Forster, P., Röhl, A. (1999). Median-joining networks for inferring intraspecific phylogenies. *Molecular Biology and Evolution*, *16*, 37–48.

Bargu, S., Koray, T., & Lundholm, N. (2002). First report of *Pseudo-nitzschia calliantha* Lundholm, Moestrup & Hasle 2003, a new potentially toxic species from Turkish coasts. *Journal of Fisheries & Aquatic Sciences, 19*(3-4), 479–483.

Bargu, S., Silver, M. W., Ohman, M. D., Benitez-Nelson, C. R., & Garrison, D. L. (2012). Mystery behind hitchcock's birds. *Nature Geoscience*, *5*, 2–3.

Bates, S. S. (1998). Ecophysiology and metabolism of ASP toxin production. In: Anderson, D.M., Cembella, A.D., Hallegraeff, G.M. (Eds.), Physiological Ecology of Harmful Algal Blooms. Springer-Verlag, Heidelberg, pp. 405–426.

Bates, S. S., Bird, C. J., De Freitas, A. S. W., Foxall, R., Gilgan, M., Hanic, L. A., … Wright, J. L. C. (1989). Pennate diatom *Nitzschia pungens* as primary source of domoic acid, a toxin in shellfish from eastern Prince Edward Island, Canada. *Canadian Journal of Fisheries and Aquatic Sciences*, *46*, 1203–1215.

Bates, S. S., de Freitas, A. S. W., Milley, J. E., Pocklington, R., Quilliam, M. A., Smith, J. C., & Worms, J. (1991). Controls on domoic acid production by the diatom *Nitzschia pungens* f. *multiseries* in culture: nutrients and irradiance. *Canadian Journal of Fisheries and Aquatic Sciences*, *48*, 1136–1144.

Bates, S. S., Hiltz, M. F., & Léger, C. (1999). Domoic acid toxicity of large new cells of Pseudo-nitzschia multiseries resulting from sexual reproduction. In: Martin, J. L., & Haya, K. (Eds.). *Proceedings of Sixth Canadian Workshop on Harmful Marine Algae, Canadian Technical Report of Fisheries and Aquatic Sciences*, *2261*, pp. 21–26.

Baugh, K. A., Bush, J. M., Bill, B. D., Lefebvre, K. A., & Trainer, V. L. (2006). Estimates of specific toxicity in several *Pseudo-nitzschia* species from the Washington coast, based on culture and field studies. *African Journal of Marine Science*, *28*(2), 403–407.

Behnke, A., Friedl, T., Chepurnov, V. A. & Mann, D. G. (2004). Reproductive compatibility and rDNA sequence analyses in *Sellaphora pupula* species complex (Bacillariophyta). *Journal of Phycology*, *40*, 193–208.

Bouchouicha Smida, D., Lundholm, N., Kooistra, W. H. C. F., Sahraoui, I., Ruggiero, M. V., Kotaki, Y., … Hlaili, A. S. (2014). Morphology and molecular phylogeny of *Nitzschia bizertensis* sp. nov. – a new domoic acid-producer. *Harmful Algae*, *32*, 49–63.

Boyden, C. R., & Russell, P. J. C. (1972). The distribution and habitat range of a brackish water cockle *Cardium* (*Cerastoderma*) in the British Isles. *Journal of Animal Ecology*, *41*(3), 719–734.

Buchheim, M. A., Keller, A., Koetschan, C., Förster, F., Merget, Benjamin, & Wolf, M. (2011). Internal transcribed spacer 2 (nu ITS2 rRNA) sequence-structure phylogenetics: towards an automated reconstruction of the green algal tree of life. *Plos One*, *6*(2), e16931.

Buchheim, M. A., Sutherland, D. M., Buchheim, J. A., & Wolf, M. (2013). The blood alga: phylogeny of *Haematococcus* (Chlorophyceae) inferred from ribosomal RNA gene sequence data. *European Journal of Phycology*, *48*(3), 318–329.

Buchheim, M. A., Sutherland, D. M., Schleicher, T., Förster, F., & Wolf, M. (2012). Phylogeny of Oedogoniales, Chaetophorales and Chaetopeltidales (Chlorophyceae): inferences from sequence-structure analysis of ITS2. *Annals of Botany*, *109*, 109–116.

Buck, K.R., Uttal-Cooke, L., Pilskaln, C. H., Roelke, D.L., Villac, … Chavez, F. P. (1992). Autecology of the diatom *Pseudonitzschia australis* Frenguelli, a domoic acid producer, from Monterey Bay, California. *Marine Ecology Progress Series*, *84*, 293–302.

Cao, M., Yuan, X. L. & Bi, G. (2016). Complete sequence and analysis of plastid genomes of *Pseudo-nitzschia multiseries* (Bacillariophyta). *Mitochondrial DNA*, *27*, 2897–2898.

Carballeira, R., Trobajo, R., Leira, M., Benito, X., Sato, S., & Mann, D. G. (2017). A combined morphological and molecular approach to Nitzschia varelae sp. nov., with discussion of symmetry in Bacillariaceae. *European Journal of Phycology*, *52*(3), 1–18.

Casteleyn, G., Chepurnov, V. A., Leliaert, F., Mann, D. G., Bates, S. S., Lundholm, N., Rhodes, L., Sabbe, K., Vyverman, W. (2008). *Pseudo-nitzschia pungens*

(Bacillariophyceae): A cosmopolitan diatom species? *Harmful Algae*, *7*, 241–257.

Casteleyn, G., Evans, K. M., Backeljau, T., D'hondt, S., Chepurnov, V. A., Sabbe, K., & Vyverman, W. (2009). Lack of population genetic structuring in the marine planktonic diatom Pseudo-nitzschia pungens (Bacillariophyceae) in a heterogeneous area in the Southern Bight of the North Sea. *Marine Biology*, *156*, 1149–1158.

Casteleyn, G., Leliaert, F., Backeljau, T., Debeer, A. E., Kotaki, Y., … Vyverman, W. (2010). Limits to gene flow in a cosmopolitan marine planktonic diatom. *Proceedings of the National Academy of Sciences*, *107*, 12952–12957.

Cefarelli, A. O., Ferrario, M. E., Almandoz, G. O., Atencio, A. G., Akselman, R. & Vernet, M. (2010). Diversity of the diatom genus *Fragilariopsis* in the Argentine Sea and Antarctic waters: morphology, distribution and abundance. *Polar Biology*, *33*, 1463–1484.

Cerino, F., Orsini, L., Sarno, D., Dell' Aversano, C., Tartaglione, L., & Zingone, A. (2005). The alternation of different morphotypes in the seasonal cycle of the toxic diatom *Pseudo-nitzschia galaxiae*. *Harmful Algae*, *4*, 33–48.

Chao, S. Y., Shaw, P. T., & Wu, S. Y. (1996). Deep water ventilation in the South China Sea. *Deep-Sea Research I*, *43*(4), 445–466.

Chen, C., Lai, Z., Beardsley, R. C., Xu, Q., Lin, H., & Viet, N. T. (2012). Current separation and upwelling over the southeast shelf of Vietnam in the South China Sea. *Journal of Geophysical Research*, *117*(C3), 1–16.

Chen, S., Yao, H., Han, J., Liu, C., Song, J., Shi, L., … Leon, C. (2010).Validation of the ITS2 region as a novel DNA barcode for identifying medical plant species. *Plos One*, *5*(1), e8613.

Cho, E. S., Kotaki, Y., & Park, J. G. (2001). The comparison between toxic *Pseudo-nitzschia multiseries* (Hasle) Hasle and non-toxic *P. pungens* (Grunow) Hasle isolated from Jinhae Bay, Korea. *Algae*, *16*(3), 275–285.

Chu, P. C., Edmons, N. L., & Fan, C.W. (1999). Dynamical mechanisms for the South China Sea seasonal circulation and thermohaline variabilities. *Journal of Physical Oceanography*, *29*, 2971–2989.

Churro, C. I., Carreira, C. C., Rodrigues, F. J., Craveiro, S. C., Calado, A. J., Casteleyn, G. & Lundholm, N. (2009). Diversity and abundance of potentially toxic

Pseudo-nitzschia Peragallo in Aveiro coastal lagoon, Portugal and description of a new variety, *P. pungens* var. *aveirensis* var. nov. *Diatom Research*, *24*, 35–62.

Costa, P. R., Rodrigues, S. M., Botelho, M. J. M., & Sampayo, M. A. (2003). A potential vector of domoic acid: the swimming crab *Polybius henslowii* Lench (Decapoda-brachyura). *Toxicon*, *42*, 135–141.

Costa, P. R., Rosa, R., Duarte-Silva, A., Brotas, V., & Sampayo, M. A. (2005). Accumulation, transformation and tissue distribution of domoic acid, the amnesic shellfish poisoning toxin, in the common cuttlefish, *Sepia officinalis*. *Aquatic Toxicology*, *74*, 82–91.

Coleman, A. W., & Vacquier, V. D. (2002). Exploring the phylogenetic utility of ITS sequences for animals: a test case for abalone (*Haliotis*). *Journal of Molecular Evolution*, *54*, 246–257.

Coleman, A. W. (2003). ITS2 is a double-edged tool for eukaryote evolutionary comparisons. *Trends in Genetics*, *19*(7), 370–375.

Coleman, A. W. (2007). Pan-eukaryote ITS2 homologies revealed by RNA secondary structure. *Nucleic Acids Research*, *35*(10), 3322–3329.

Coleman, A. W. (2009). Is there a molecular key to the level of "biological species" in eukaryotes? A DNA guide. *Molecular Phylogenetics and Evolution*, *50*, 197–203.

Cusack, C. K., Bates, S. S., Quilliam, M., A., Patching, J. W., & Raine, R. (2002). Confirmation of domoic acid production by *Pseudo-nitzschia australis* (Bacillariophyceae) isolated from Irish waters. *Journal of Phycology*, *38*, 1106–1112.

Cusack, C., Raine, R., & Patching, J. W. (2004). Occurrence of species from the genus *Pseudo-nitzschia* Peragallo in Irish waters. Biology and Environment: Proceedings of the Royal Irish Academy, *104B*(1), 55–74.

Cleve, P. T., & Grunow, A. (1880). Beiträge zur Kenntnis der arktischen Diatomeen. *Kongliga Svenska Vetenskaps Akademiens Handlingar*, *Stockholm*,*17*(2), 1–121.

D'Alelio, D., Amato, A., Kooistra, W. H. C. F., Procaccini, G., Casotti, R. & Montresor, M. (2009). Internal transcribed spacer polymorphism in *Pseudo-nitzschia multistriata* (Bacillariophyceae) in the Gulf of Naples: recent divergence or intraspecific hybridization? *Protist*, *160*, 9–20.

Dao, V. H., Lim, P. T., Pham, X. K., Takata, Y., Teng, S. T., Omura, T., Fukuyo, Y., Kodama, M. (2014). Diatom *Pseudo-nitzschia* cf. *caciantha* (Bacillariophyceae), the most likely source of domoic acid contamination in the thorny oyster *Spondylus versicolor* Schreibers 1793 in Nha Phu Bay, Khanh Hoe Province, Vietnam. *Asian Fisheries Society*, *27*, 16–29.

Dao, V. H., Phan, V. B., Teng, S. T., Uchida, H., Leaw, C. P., Lim, P. T., Suzuki, T., Pham, K. X. (2015). *Pseudo-nitzschia fukuyoi* (Bacillariophyceae), a domoic acid-producing species from Nha Phu Bay, Khanh Hoa Province, Vietnam. *Fisheries Science*, *81*, 533–539.

Dao, V. H., Takata, Y., Omura, T., Sato, S., Fukuyo, Y., & Kodama, M.. (2009). Seasonal variation of domoic acid in a bivalve *Spondylus versicolor* in association with that in plankton samples in Nha Phu Bay, Khanh Hoa, Vietnam. *Fisheries Science*, *75*, 507–512.

Dao, V. H., Takata, Y., Sato, S., Fukuyo, Y., & Kodama, M. (2006). Domoic acid in a bivalve *Spondylus cruentus* in Nha Trang Bay, Khanh Hoa Province, Vietnam. *Coastal Marine Science*, *30*, 130–132.

Darriba, D., Taboada, G. L., Doallo, R., & Posada, D. (2012). jModelTest 2: more models, new heuristics and parallel computating. *Nature Methods*, *9*, 772.

Darty, K., Denise, A. & Ponty, Y. (2009). VARNA: interactive drawing and editing of the RNA secondary structure. *Bioinformatics*, *25*, 1974–1975.

Douglas, D.J., & Bates, S. S. (1992). Production of domoic acid, a neurotoxic amino acid, by an axenic culture of the marine diatom *Nitzschia pungens* f. *multiseries* Hasle. *Canadian Journal of Fisheries and Aquatic Sciences*, *49*, 85–90.

Drummond, A. J., Suchard, M. A., Xie, D. & Rambaut, A. (2012). Bayesian phylogenetics with BEAUti and BEAST 1.7. *Molecular Biology and Evolution*, *29*, 1969–1973.

Edgar, R. C. (2004a). MUSCLE: a multiple sequence alignment method with reduced time and space complexity. *BMC Bioinformatics*, *5*, 113.

Edgar, R. C. (2004b). MUSCLE: multiple sequence alignment with high accuracy and high throughput. *Nucleic Acids Research*, *32*, 1792–1797.

Emer, K. O., & Niino, H. (1963). Sediments of the Gulf of Thailand and adjacent continental shelf. *Geological Society of America Bulletin*, *74*, 541–554.

Ehara, M., Watanabe, K. I. & Ohama, T. (2000). Distribution of cognates of group II introns detected in mitochondrial *cox1* genes of a diatom and a haptophyte. *Gene*, *256*, 157–167.

Emery, K. O., & Niino, H. (1963). Sediments of the Gulf of Thailand and adjacent continental shelf. *Geological Society of America Bulletin*, *74*, 541–554.

Evans, K. M., Kühn, S. F., & Hayes, P. K. (2005). High levels of genetic diversity and low levels of genetic differentiation in North Sea *Pseudo-nitzschia pungens*. *Journal of Phycology*, *41*, 506–514.

Evans, K. M., Wortley, A. H., & Mann, D. G. (2007). An assessment of potential diatom "barcode" genes (*cox*1, *rbc*L, 18S and ITS rDNA) and their effectiveness in determining relationships in *Sellaphora* (Bacillariophyta). *Protist*, *158*, 349–364.

Excoffier, L., & Lischer, H.E.L. (2010). Arlequin suite ver 3.5: a new series of programs to perform population genetics analyses under Linux and Windows. *Molecular Ecology Resources*, *10*, 564–567.

Falconer, D. S., & Mackay, T. F. C. (1996). Introduction to quantitative genetics. Essex, England: Pearson Education Limited.

Fehling, J., Davidson, K., Bolch, C., & Tett, P. (2006). Seasonality of *Pseudo-nitzschia* spp. (Bacillariophyceae) in western Scottish waters. Marine Ecology Progress Series, 323, 91–105.

Fehling, J., Green, D. H., & Davidson, K. (2004). Domoic acid production by *pseudo-nitzschia seriata* (Bacillariophyceae) in Scottish waters. *Journal of Phycology, 40*, 622–630.

Fernandes, L. F., Hubbard, K. A., Richlen, M. L., Smith, J., Bates, S. S., Ehrman, J., … Anderson, D. M. (2014). Diversity and toxicity of the diatom *Pseudo-nitzschia* Peragallo in the Gulf of Maine, Northwestern Atlantic Ocean. *Deep-Sea Research II*, *103*, 139–162.

Fire, S.E., Wang, Z., Berman, M., Langlois, G. W., Morton, S. L., Sekula-Wood, E., & Benitez-Nelson, C.R. (2010). Trophic transfer of the harmful algal toxin domoic acid as a cause of death in a minke whale (*Balaenoptera acutorostrata*) stranding in Southern California. *Aquatic Mammals*, *36*, 342–350.

Fire, S. E., Wang, Z. H., Byrd, M., Whitehead, H. R., Paternoster, J., & Morton, S. L. (2011). Co-occurrence of multiple classes of harmful algal toxins in bottlenose dolphins (*Tursiops truncates*) stranding during an unusual mortality event in Texas, USA. *Harmful Algae*, *10*, 330–336.

Friedrich, J., Dandekar, T., Wolf, M., & Müller, T. (2005). ProfDist: a tool for the construction of large phylogenetic trees based on profile distances. *Bioinformatics*, *21*, 2108–2109.

Fritz, L., Quilliam, M. A., & Wright, J. L. C. (1992). An outbreak of domoic acid poisoning attributed to the pennate diatom *Pseudonitzschia Australis*. *Journal of Phycology*, *28*, 439–442.

Fryxell, G. A., Garza, S. A. & Roelke, D. L. (1991). Auxospore formation in an Antarctic clone of *Nitzschia subcurvata* Hasle. *Diatom Research*, 6, 235–245.

Furey, A., Lehane, M., Gillman, M., Fernandez-Puente, P., & James, K.J. (2001). Determination of domoic acid in shellfish by liquid chromatography with electrospray ionization and multiple tandem mass spectrometry. *Journal of Chromatography A*, *938*, 167–174.

Gao, T., Yao, H., Song, J., Liu, C., Zhu, Y., Ma, X., … Chen, S. (2010a). Identification of medical plants in the family Fabaceae using a potential DNA barcode ITS2. *Journal of Ethnopharmacology*, *130*, 116–121.

Gao, T., Yao, H., Song, J., Zhu, Y., Liu, C., & Chen, S. (2010b). Evaluating the feasibility of using candidate DNA barcodes in discriminating species of the large Asteraceae family. *BMC Evolutionary Biology*, *10*, 324.

García-Robledo, C., Erickson, D. L., Staines, C. L., Erwin, T. L., & Kress, W. J. (2013). Tropical plant-herbivore networks: reconstructing species interactions using DNA barcodes. *Plos One*, *8*(1), e52967.

Garrison, D. L., Conrad, S. M., Eilers, P. P., & Waldron, E. M. (1992). Confirmation of domoic acid production by *Pseudonitzschia australis* (Bacillariophyceae) cultures. *Journal of Phycology, 28*, 604–607.

Goldstein, T., Mazet, J. A. K., Zabka, T. S., Langlois, G., Colegrove, K. M., Silver, M., … Gulland, F. M. D. (2008). Novel symptomatology and changing epidemiology of domoic acid toxicosis in California sea lions (*Zalophus californianus*): an increasing risk to marine mammal health. *Proceedings of the Royal Society B*, *275*, 267–276.

Grattan, L. M., Boushey, C. J., Liang, Y., Lefebvre, K. A., Castellon, L. J., Roberts, K. A., … Morris, J. G. Jr. (2018). Repeated dietary exposure to low levels of domoic acid and problems with everyday memory: research to public health outreach. *Toxins*, *10*, 103.

Grunow, A. (1862). Dic österreichischen Diatomeen ncbst ciniger neuer Arten von anderen Lokalitäten und ciner kritischen Uebersicht der bisher bekannten Gattungen and Arten. Nitzschiae. *Verhandlungen der Zoologisch-Botanischen Gesellschaft in Wien*, 12, 545–588.

Gu, W., Song, J., Cao, Y, Sun, Q., Yao, H., Wu, Q Duan, J. (2013). Application of the ITS2 region for barcoding medicinal plants of Selaginellaceae in Pteridophyta. *Plos One*, *8*(6), e67818.

Gulland, F. M. D., Haulena, M., Fauquier, D., Langlois, G., Lander, M. E., Zabka, T., & Duerr, R. (2002). Domoic acid toxicity in Californian sea lions (*Zalophus californianus*): clinical signs, treatment and survival. *Veterinary Record*, *150*, 475–480.

Guillard R. R. L., & Ryther J. H. (1962). Studies of marine planktonic diatoms. I. *Cyclotella nana* Hustedt, and *Detonula confervacea* (Cleeve) Gran. *Canadian Journal of Microbiology*, *8*, 229–239.

Guiry, M.D.，& Guiry, G.M. (2018). *AlgaeBase*. World-wide electronic publication, National University of Ireland, Galway. Retrieved from http://www.algaebase.org/search/genus/detail/?genus_id=e8157b922a1395e00&sk=0 on 11 September 2018.

Gunnel, M. L., Horner-Devine, M. C., & Rocap, G. (1990). Bacterial community composition dffers with species and toxigenicity of the diatom *Pseudo-nitzschia*. *Aquatic Microbial Ecology*, *64*, 117–133.

Hamsher, S. E., Evans, K. M., Mann, D. G., Poulíčková, A. & Saunders, G. W. (2011). Barcoding diatoms: exploring alternatives to COI-5P. *Protist*, *162*, 405–422.

Hanebuth, T., Stattegger, K., & Grootes, P. M. (2000). Rapid flooding of the Sunda Shelf: A late-glacial sea-level record. *Science*, *288*, 1033–1035.

Hansen, L. R., Soylu, S. í., Kotaki, Y., Moestrup, Ø., & Lundholm, N. (2011). Toxin production and temperature-induced morphological variation of the diatom *Pseudo-nitzschia seriata* from the Arctic. *Harmful Algae*, *10*, 689–696.

Hasle, G. R. (1974). Validation of the names of some marine planktonic species of *Nitzschia* (Bacillariophyceae). *Taxon*, *23*, 425–428.

Hasle, G. R. (1993). Nomenclatural notes on marine planktonic diatoms. The family Bacillariaceae. *Nova Hedwigia, Beiheft,* 106, 315–321.

Hasle, G. R. (1994). *Pseudo-nitzschia* as a genus distinct from *Nitzschia* (Bacillariophycea). *Journal of Phycology*, *30*, 1036–1039.

Hasle, G. R. (2002). Are most of the domoic acid-producing species of the diatom genus *Pseudo-nitzschia cosmopolites*? *Harmful Algae*, *1*, 137–146.

Hasle, G., Lange, C. & Syvertsen, E. (1996). A review of *Pseudo-nitzschia*, with special reference to the Skagerrak, North Atlantic, and adjacent waters. *Helgoland Marine Research*, *50*, 131–175.

Hasle, G. R., & Lundholm, N. (2005). *Pseudo-nitzschia seriata* f. *obtuse* (Bacillariophyceae) raised in rank based on morphological, phylogenetic and distributional data. *Phycologia*, *44*(6), 608–619.

Hasle, G., & Syvertsen, E. E. (1997). Marine diatoms. In Tomas, C. R. (Ed.) *Identifying marine phytoplankton*. San Diego, Academic Press, 99. 5–385.

Hassel, K., Segreto, R., & Ekrem, T. (2013). Restricted variation in plant barcoding markers limits identification in closely related bryophyte species. *Molecular Ecology Resources*, *13*, 1047–1057.

Heath, T. A., Hedtke, S. M. & Hillis, D. M. (2008). Taxon sampling and the accuracy of phylogenetic analyses. *Journal of Systematic and Evolution*, *46*(3), 239–257.

Hedtke, S. M., Townsend, T. M. & Hillis, D. M. (2006). Resolution of phylogenetic conflict in large data sets by increased taxon sampling. *Systematic Biology*, *55*, 522–529.

Heinrichs, G., de Hoog, G. S., & Haase, G. (2012). Barcode identifiers as a practical tool for reliable species assignment of medically important black yeast species. *Journal of Clinical Microbiology*, *50*, 3023–3030.

Higgins, M. J., Sader, J. E., Mulvaney, P., & Wetherbee, R. (2003). Probing the surface of living diatoms with atomic force microscopy: the nanostructure and

nanomechanical properties of the mucilage layer. *Journal of Phycology*, *39*, 722–734.

Holland, P. T., Selwood, A. L., Mountfort, D. O., Wilkins, A. L., McNabb, P., Rhodes, L. L., … King, K. L. (2005). Isodomoic acid C, an unusual amnesic shellfish poisoning toxin from pseudo-nitzschia australis. *Chemical Research in Toxicology*, *18*, 814-816.

Honculada-Primavera, J. (2000). Mangroves of Sourtheast Asia. In: Rimavera, J.H., Garcia, L. M. B., Castaños, M. T., & Surtida, M. B. (Eds.), Mangrove-friendly Aquaculture: Proceeding of the Workshop on Mangrove-Friendly Aquaculature, SEAFDEC Aquaculture Department, 11–15 January 1999, Iloilo City, Philippines, pp. 1–12.

Hubbard, K. A, Rocap, G., & Armbrust, E. V. (2008). Inter- and intraspecific community structure within the diatom genus *Pseudo-nitzschia* (Bacillariophyceae). *Journal of Phycology*, *44*, 637–649.

Hubbard, K. A., Olson, C. E., & Armbrust, E. V. (2014). Molecular characterization of *Pseudo-nitzschia* community structure and species ecology in a hydrographically complex estuarine system (Puget Sound, Washington, USA). *Marine Ecology Progress Series*, *507*, 39–55.

Hunter, R. L., LaJeunesse, T. C., & Santos, S. R. (2007). Structure and evolution of the rDNA internal transcribed spacer (ITS) region 2 in the symbiotic Dinoflagellates (*Symbiodinium*, Sinophyta). *Journal of Phycology*, *43*, 120–128.

Huyen, N.T.M., Thuoc, C. V., Ogata, T., Sato, S., Takata, Y., Kodama, M., & Fukuyo, Y. (2006). Seasonal variation of paralytic and amnesic shellfish toxicities in bivalves and microalgae in Haiphong area, Vietnam. *Coastal Marine Science*, *30*, 111–115.

Jeong, H. J., Lim, A. S., Lee, K., Lee, M. J., Seong, K. A., Kang, N. S., … Kim, K. Y. (2017). Ichthyotoxic *Cochlodinium polykrikoides* red tides offshore in the South Sea, Korea in 2014: I. Temporal variations in three-dimensional distributions of red-tide organisms and environmental factors. *Algae*, *32*(2), 101–130.

Kaczmarska, I., Davidovich, N. A. & Ehrman, J. M. (2007). Sex cells and reproduction in the diatom *Nitzschia longissima* (Bacillariophyta): discovery of siliceous scales in gamete cell walls and novel elements of the perizonium. *Phycologia*, *46*, 726–737.

Kaczmarska, I., Reid, C., Martin, J..L., & Moniz, M.B.J. (2008). Morphological, biological, and molecular characteristics of the diatom *Pseudo-nitzschia delicatissima* from the Canadian Maritimes. *Botany*, *86*, 763–772.

Keller, A., Förster, F., Müller, T., Dandekar, T., Schultz, J., & Wolf, M. (2010). Including RNA secondary structures improves accuracy and robustness in reconstruction of phylogenetic trees. *Biology Direct*, *5*(4), 1–12.

Keller, A., Schleicher, T., Schultz, J., Müller, T., Dandekar, T., & Wolf, M. (2009). 5.8S-28S rRNA interaction and HMM-based ITS2 annotation. *Gene*, *430*, 50–57.

Kelly, L. J., Hollingsworth, P. M., Coppins, B. J., Ellis, C. J., Harrold, P., Tosh, J., & Yahr, R. (2011). DNA barcoding of lichenized fungi demonstrates high identification success in a floristic context. *New Phytologist*, *191*, 288–300.

Kim, J. H., Park, B. S., Kim, J. H., Wang, P., & Han, M. S. (2015). Intraspecific diversity and distribution of the cosmopolitan species *Pseudo-nitzschia pungens* (Bacillariophyceae): morphology, genetics, and ecophysiology of the three clades. *Journal of Phycology*, *51*(1), 159–172.

Koetschan, C., Förster, F., Keller, A., Schleicher, T., Ruderisch, B., Schwarz, R., … Schultz, J. (2010). The ITS2 database III-sequences and structures for phylogeny. *Nucleic Acids Research*, *38*, D275–279.

Kolde, R. (2015). pheatmap: Pretty Heatmaps. R package version 1.0.8. https://CRAN.R-project.org/package=pheatmap.

Kotaki, Y., Furio, E. F., Bajarias, F. A., Satake, M., Lundholm, N., … Kodama, M. (2006). New stage of the study on domoic acid- producing diatoms–A finding of *Nitzschia navis-varingica* that produces domoic acid derivatives as major toxin components. *Coastal Marine Science, 30*(1), 116–120.

Kotaki, Y., Furio, E.F., Satake, M., Lundholm, N., Katayama, T., … Kodama, M. (2005). Production of isodomoic acids A and B as major toxin components of a pennate diatom *Nitzschia navis-varingica*. *Toxicon, 46*, 946–953.

Kotaki, Y., Koike, K., Sato, S., Ogata, T., Fukuyo, Y., & Kodama, M. (1999). Confirmation of domoic acid production of *Pseudo-nitzschia multiseries* isolated from Ofunato Bay, Japan. *Toxicon*, *37*, 677–682.

Kotaki, Y., Koike, K., Yoshida, M., Thuoc, C.V., Huyen, N. T.M., … Kodama, M. (2000). Domoic acid production in *Nitzschia* sp. (Bacillariophyceae) isolated from a shrimp- culture pond in Do Son, Vietnam. *Journal of Phycology, 36*, 1057–1060.

Kotaki, Y., Lundholm, N., Katayama, T., Furio, E. F., Romero, M. L., … Fukuyo, Y. (2008). ASP toxins of pennate diatoms and bacterial effects on the variation in toxin composition. In: Moestrup, Ø. (Ed.), Harmful algae, *The Proceedings of 12th International Conference on Harmful Algae*. IOC of UNESCO, Copenhagen, Denmark, pp. 300–302.

Kotaki, Y., Lundholm, N., Onodera, H., Kobayashi, K., Bajarias, F. A., … Kodama, M. (2004). Wide distribution of *Nitzschia navis-varingica*, a new domoic acid-producing benthic diatom found in Vietnam. *Fisheries Science, 70*, 28–32.

Kottè-Mapoko, E. F., Ngo-Massou, V. M., Essomè-Koum, L. G., Emane, J. M., Moussian, L. N., Tchoffo, R., & Din, N. (2017). Molluscs' composition and distribtion in mangroves of the cameroon central coast. *International Journal of Research Studies in Biosciences*, *5*(5), 4–13.

Kuzmina, M. L., Johnson, K. L., Barron, H. R., & Hebert, P. D. N. (2012). Identification of the vascular plants of Churchill, Manitoba, using a DNA barcode library. *BMC Ecology*, *12*, 25.

La Barre, S., Bates, S.S., & Quilliam, M. A. (2014). Domoic acid. In S. L., Barre & J.-M., Kornprobst (Eds.), Outstanding Marine molecules (pp. 189–216). Wiley-VCH Verlag GimbH & Co. KGaA.

Lange-Bertalot, H. (1978). Zur systematic, taxonomic and Ökologic des abwasserspezifisch wichtigen Formenkreiscs um "*Nitzschia thermalis*". *Nova Hedwigia*, *30*, 635–652.

Larsen, J., & Nguyen, N. L. (2004). Potentially toxic microalgae of Vietnamese waters. *Botanica*, *140*, 1–212.

Lefebvre, K. A., Bargu, S., Kieckhefer, T., & Silver, M. W. (2002). From sanddabs to blue whales: the pervasiveness of domoic acid. *Toxicon*, *40*, 971–977.

Lefebvre, K. A., Powell, C. L., Busman, M., Doucette, G. J., Moeller, P. D. R., … Tjeerdema, R. S. (1999). Detection of domoic acid in Northern anchovies and California sea lions associated with an unusual mortality event. *Natural Toxins*, *7*, 85–92.

Lefebvre, K.A., Quakenbush, L., Frame, E., Burek Huntington, K., Sheffield, G., Stimmelmayr, R., … Gill, V. (2016). Prevalence of algal toxins in Alaskan marine mammals foraging in a changing arctic and subarctic environment. *Harmful Algae*, *55*, 13–24.

Lelong, A., Hégaret, H., Soudant, P., & Bates, S.S. (2012). *Pseudo-nitzschia* (Bacillariophyceae) species, domoic acid and amnesic shellfish poisoning: revisiting previous paradigms. *Phycologia*, *51*, 168–216.

Li, R., Zeng, Q., Ji, Z., & Gun, D. (1992). Numerical simulation for a northeastward flowing current from area off the Eastern Hainan Island to Tsugaru/Soya Strait. *La mer*, *30*, 229–238.

Li, Y., Huang, C. X., Xu, G. S., Lundholm, N., Teng, S. T., Wu, H. Y., & Tan, X. J. (2017). *Pseudo-nitzschia simulans* sp. nov. (Bacillariophyceae), the first domoic acid producer from Chinese waters. *Harmful Algae*, *67*, 119–130.

Li, Y., Zhou, X., Feng, G., Hu, H., Niu, L., Hebert, P. D. N., & Huang, D. (2010). COI and ITS2 sequences delimit species, reveal crytic taxa and host specificity of fig-associated *Sycophila* (Hymenoptera, Eurytomidae). *Molecular Ecology Resources*, *10*, 31–40.

Librado, P., & Rozas, J. (2009). DnaSP v5: a software for comprehensive analysis of DNA polymorphism data. *Bioinformatics*, *25*(11), 1451–1452.

Lim, H.C., Suriyanti, S.N.P., Hartina Mohamed-Ali, Kotaki, Y., Leaw, C.P., & Lim, P.T. (2010). Toxicity of diatom *Pseudo-nitzschia* (Bacillariophyceae) analyzed using high performance liquid chromatography (HPLC). *Journal of Science and Technology in the Tropics*, *6*, S116–S119.

Lim, H. C., Leaw, C. P., Su, S. N. P., Teng, S. T., Usup, G., Noor, N. M., … Lim, P. T. (2012a). Morphology and molecular characterization of *Pseudo-nitzschia* (Bacillariophyceae) from Malaysian Borneo, including the new species *Pseudo-nitzschia circumpora* sp. nov. *Journal of Phycology*, *48*, 1232–1247.

Lim, P. T., Leaw, C. P., & Usup, G. (2004). First incidence of paralytic shellfish poisoning on the East Coast of Peninsular Malaysia. In *Marine Science Into the New Millennium: New Perspectives and Challenges* (Phang, S. M.; Chong, V. C.; Ho, S. C.; Mokntar, N. & Ooi, L.S.; eds.). UMMRec, Kuala Lumpur. Pp 661–667.

Lim, H.C., Lim, P.T., Su, S. P., Teng, S. T., & Leaw, C. P. (2012b). Genetic diversity of Pseudo-nitzschia brasiliana (Bacillariophyceae) from Malaysia. *Journal of Applied Phycology*, *24*, 1465–1475.

Lim, H.C., Lim, P.T., Teng, S.T., Bates, S.S., & Leaw, C.P. (2014). Genetic structure of *Pseudo-nitzschia pungens* (Bacillariophyceae) populations: implications of a global diversification of the diatom. *Harmful Algae*, *37*, 142–152.

Lim, H. C., Tan, S. N., Teng, S. T., Lundholm, N., Orive, E., David, H., … Leaw, C. P. (2018). Phylogeny and species delineation in the marine diatom *Pseudo-nitzschia* (Bacillariophyta) using *cox*1, LSU, and ITS2 rRNA gens: a perspective in character evolution. *Journal of Phycology*, *54*, 234–248.

Lim, H. C., Teng, S. T., Leaw, C. P. & Lim, P. T. (2013). Three novel species in the *Pseudo-nitzschia pseudodelicatissima* complex: *P. batesiana* sp. nov., *P. lundholmiae* sp. nov., and *P. fukuyoi* sp. nov. (Bacillariophyceae) from the Strait of Malacca, Malaysia. *Journal of Phycology*, *49*, 902–916.

Lim, H. C., Teng, S. T., Lim, P. T., Wolf, M., & Leaw, C. P. (2016). 18S rDNA phylogeny of *Pseudo-nitzschia* (Bacillariophyceae) inferrend from sequence-structure information. *Phycologia*, *55*(2), 134–146.

Lim, P. T., Usup, G., & Leaw, C, P. (2012c). Harmful algal blooms in Malaysian waters. *Sains Malaysiana*, *41*(12), 1509–1515.

Lu, S. H., Li, Y., Lundholm, N., Ma, Y. Y., & Ho, K. C. (2012). Diversity, taxonomy and biogeographical distribution of the genus *Pseudo-nitzschia* (Bacillariophyceae) in Guandong coastal waters, South China Sea. *Nova Hedwigia*, *95*(1–2), 123–152.

Lundholm, N. (Ed). (2017). Bacillariophyceae, in IOC-UNESCO Taxonomic Reference List of Harmful Micro Algae. Available online at http://www.marinespecies.org/hab. (Accessed on 2017-12-11).

Lundholm, N., Bates, S. S., Baugh, K. A., Bill, B. D., Connel, L. B., Léger, C., & Trainner, V. L. (2012). Crytic and pseudo-crytic diversity in diatoms–with descriptions of *Pseudo-nitzschia hasleana* sp. nov. and *P. fryxelliana* sp. nov. *Journal of Phycology*, *48*, 436–454.

Lundholm, N., Clarke, A. & Ellegaard, M. (2010). A 100-year record of changing *Pseudo-nitzschia* species in a sill-fjord in Denmark related to nitrogen loading and temperature. *Harmful Algae*, *9*, 449–457.

Lundholm, N., Daugbuerg, N. & Moestrup, Ø. (2002a). Phylogeny of the Bacillariaceae with emphasis on the genus *Pseudo-nitzschia* (Bacillariophyceae) based on partial LSU rDNA. *European Journal of Phycology*, *37*, 115–134.

Lundholm, N. & Hasle, G. R. (2010). *Fragilariopsis* (Bacillariophyceae) of the Northern Hemisphere - morphology, taxonomy, phylogeny and distribution, with a description of *F. pacifica* sp. nov. *Phycologia*, *49*, 438–460.

Lundholm, N., Hasle, G. R., Fryxell, G. A. & Hargraves, P. E. (2002b). Morphology, phylogeny and taxonomy of species within the *Pseudo-nitzschia americana* complex (Bacillariophyceae) with descriptions of two new species, *Pseudo-nitzschia brasiliana* and *Pseudo-nitzschia linea*. *Phycologia*, *41*, 480–497.

Lundholm, N., & Moestrup, Ø. (2000). Morphology of the marine diatom *Nitzschia navis-varingica*, sp. nov. (Bacillariophyceae), another producer of the neurotoxin domoic acid. *Journal of Phycology*, *36*, 1162–1174.

Lundholm, N. & Moestrup, Ø. (2002). The marine diatom *Pseudo-nitzschia galaxiae* sp. nov. (Bacillariophyceae): morphology and phylogenetic relationships. *Phycologia*, 41, 594–605.

Lundholm, N., Moestrup, Ø., Hasle, G. R. & Hoef-Emden, K. (2003). A study of the *Pseudo-nitzschia pseudodelicatissima/cuspidata* complex (Bacillariophyceae): What is *P. pseudodelicatissima*?. *Journal of Phycology*, *39*, 797–813.

Lundholm, N., Moestrup, Ø., Kotaki, Y., Hoef-Emden, K., Scholin, C. & Miller, P. (2006). Inter- and intraspecific variation of the *Pseudo-nitzschia delicatissima* complex (Bacillariophyceae) illustrated by rRNA probes, morphological data and phylogenetic analyses. *Journal of Phycology*, *42*, 464–481.

Lundholm, N., Skov, J., Pocklington, R., & Moestrup, Ø. (1994). Domoic acid, the toxic amino acid responsible for amnesic shellfish poisoning, now in *Pseudonitzschia seriata* (Bacillariophyceae) in Europe. *Phycologia, 33*, 475–478.

Lundholm, N., Skov, J., Pocklington, R., & Moestrup, Ø. (1997). Studies on the marine planktonic diatom *Pseudo-nitzschia*. 2. Autecology of *P. pseudodelicatissima* based on isolates from Danish coastal waters. *Phycologia, 36*, 381–388.

Liu, R. Y. (Liu, J. Y.) (Ed.) (2008). Checklist of biota of Chinese seas. Beijing: Science Press, Academia Sinica. pp. 1–1267.

Maddison, W. P. & Maddison, D. R. (2017). Mesquite: a modular system for evolutionary analysis. Version 3.2. http://mesquiteproject.org.

Manguin, E. (1957). Premier inventaire des diatomées de la Terre Adélie Antarctique. Espèces nouvelles. *Revue Algologique, Nouvelle Série*, *3*, 111–134.

Mann, D. G. (1986). Nitzschia subgenus Nitzschia. Notes for a monograph of the Bacillariaceae, 2nd ed. In Ricard, M. (Ed.). Proceedings of the 8th International Diatom Symposium. Koeltz Scientific Books, Königstein, pp. 215–226.

Maríc, D., Ljubešić, Z., Godrijan, J., Viličić, D., Ujević, I., & Precali, R. (2011). Blooms of the potentially toxic diatom *Pseudo-nitzschia calliantha* Lundholm, Moestrup & Hasle in coastal waters of the northern Adriatic Sea (Croatia). *Estuarine*, *Coastal and Shelf Science*, *92*(3), 323–331.

Martin, J. L., Haya, K., Burridge, L. E., & Wildish, D. J. (1990). *Nitzschia pseudodelicatissima*: a source of domoic acid in the Bay of Fundy, eastern Canada. *Marine Ecology Progress Series, 67*, 177–182.

Maso, M., & Garcés, E. (2006). Harmful microalgae blooms (HAB); problematic and conditions that induce them. *Marine Pollution Bulletin*, *53*, 620–630.

Mathews, D. H. (2014). Using the RNAStructure software package to predict conserved RNA structures. *Current Protocols in Bioinformatics*, *46*, 12.4.1–12.4.22.

McCabe, R. M., Hickey, B. M., Kudela, R. M., Lefebvre, K. A., Adams, N. G., Bill, B. D., … Trainer, V. L. (2016). An unprecedented coastwide toxic algal bloom linked to anomalous ocean conditions. *Geophysical Research Letters*, *43*, 10,366–10,376.

Miller, P. E., & Scholin, C.A. (1996). Identification of cultured *Pseudo-nitzschia* (Bacillariophyceae) using species-specific LSU rRNA-targeted fluorescent probes. *Journal of Phycology*, *32*, 646–645.

Miller, P. E., & Scholin, C.A. (1998). Identification and enumeration of cultured and wild *Pseudo-nitzschia* (Bacillariophyceae) using species-specific LSU rRNA-targeted fluorescent probes and filter-based whole cell hybridization. *Journal of Phycology*, *34*, 371–382.

Moniz, M. B. J., & Kaczmarska, I. (2009). Barcoding diatoms: Is there a good marker? *Molecular Ecology Resource*, *9*, 65–74.

Moschandreou, K. K., Papaefthimiou, D., Katikou, P., Kalopesa, E., Panou, A., & Nikolaidis, G. (2010). Morphology, phylogeny and toxin analysis of *Pseudo-nitzschia pseudodelicatissima* (Bacillariophyceae) isolated from the Thermaikos Gulf, Greece. *Phycologia*, *49*(3), 260–273.

Munday, R., Holland, P. T., McNabb, P., Selwood, A. I., & Rhodes, L. L. (2008). Comparative toxicity to mice of domoic acid and isodomoic acids A, B and C. *Toxicon*, *52*, 954–956.

Navarro, J. N. (1982). Marine diatoms associated with mangrove proproot in the Indian River Florida, U.S.A. Vadus: J. Cramer Publishing.pg 1–151.

Orive, E., Laza-Martinez, A., Seoane, S., Alonso, A., Andrade, R. & Miguel, R. (2010). Diversity of *Pseudo-nitzschia* in the Southeastern Bay of Biscay. *Diatom* Research, *25*, 125–145.

Orive, E., Pérez-Aicua, L., & David, H. (2013). The genus Pseudo-nitzschia (Bacillariophyceae) in a temperate estuary with description of two new species: *Pseudo-nitzschia plurisecta* sp. nov. and *Pseudo-nitzschia abrensis* sp. nov. *Journal of Phycology*, *49*, 1192–1206.

Orlova, T. Y., Stonik, I. V., Aizdaicher, N. A., Bates, S. S., Leger, C., & Fehling, J. (2008). Toxicity, morphology and distribution of *Pseudo-nitzschia calliantha*, *P. multistriata* and *P. multiseries* (Bacillariophyta) from the northwestern Sea of Japan. *Botanica Marina*, *51*, 297–306.

Orsini, L., Sarno, D., Procaccini, G., Poletti, R., Dahlmann, J., & Montresor, M. (2002). Toxic *Pseudo-nitzschia multistriata* (Bacillariophyceae) from the Gulf of Naples: morphology, toxin analysis and phylogenetic relationships with other *Pseudo-nitzschia* species. *European Journal of Phycology*, *37*, 247–257.

Outdot-Le Secq, M. P. & Green, B. R. (2011). Complex repeat structures and novel features in the mitochondrial genomes of the diatoms *Phaeodactylum tricornutum* and *Thalassiosira pseudonana*. *Gene*, *476*, 20–26.

Owczarzy, R., Tataurov, A. V., Wu, Y., Manthey, J. A., Mcquisten, K. A., Almabrazi, H. G., … Peek, A. S. (2008). IDT SciTools: a suite for analysis and design of nucleic acid oligomers. *Nucleic Acids Research*, *36*, W163–169.

Pan, Y., Parsons, M. L., Busman, M., Moeller, P. D. R., Dortch, Q., Powell, C. L., & Doucette, G. J. (2001). *Pseudo-nitzschia* sp. cf. *pseudodelicatissima*–a confirmed producer of domoic acid from the northern Gulf of Mexico. *Marine Ecology Progress Series, 220*, 83–92.

Pang, X., Luo, H., & Sun, C. (2012). Assessing the potential of candidate DNA barcodes for identifying non-flowering seed plants. *Plant Biology*, *14*, 839–844.

Park, J. G., Kim, E. K., & Lim, W. A. (2009). Potentially toxic Pseudo-nitzschia species in Tongyeong coastal waters, Korea. *Journal of the Korean Society of Oceanography*, *14*(3), 163–170.

Parsons, M. L., Scholin, C. A., Miller, P. E., Doucette, G. J., Powell, C. L., Fryxell, G. A., Dortch, Q., & Soniat, T. M. (1999). *Pseudo-nitzschia* species (Bacillariophyceae) in Louisiana coastal waters; molecular probe field trials, genetic variability, and domoic acid analyses. *Journal of Phycology*, *35*, 1368–1378.

Pauly, D., & Chuenpagdee, R. (2003). Development of fisheries in the Gulf of Thailand large marine ecosystem: analysis of an unplanned experiment. In G. hempeland & K. Sherman (Eds.), *Large marine ecosystems of the world 12: change and sustainability* (pp. 337–354). Amsterdam: Elsevier Science.

Patterson, C. (1988). Homology in classical and molecular biology. *Molecular Biology and Evolution*, *5*, 603–625.

Peragallo, H., & Peragallo, M. (1990). Diatomées marines des France, 2. Grez-sur-Loing. pp. 492.

Percopo, I., Ruggiero, M. V., Balzano, S., Gourvil, P., Lundholm, N., Siano, R., … Sarno, D. (2016). *Pseudo-nitzschia arctic asp*. Nov., a new cold-water cryptic *Pseudo-nitzschia* species within the *P. pseudodelicatissima* complex. *Journal of Phycology*, *52*, 184–199.

Perl, T.M., Bedard, L., Kosatsky, T., Hockin, J.C., Tood, E.C.D., & Remis, R.S. (1990). An outbreak of toxic encephalopathy caused by eating mussels contaminated with domoic acid. *New England Journal of Medicine*, *322*, 1775–1780.

Pham, M. N., Tan, H. T. W., Mitrovic, S., & Yeo, H. H. T. (2011). A checklist of the algae f Singapore. Singapore: Raffles museum of biodiversity research, National University of Singapore, pp. 1–100.

Pocklington, R., Milley, J. E., Bates, S. S., Bird, C. J., de Freitas, A. S. W., & Quilliam, M. A. (1990). Trace determination of domoic acid in seawater and phytoplankton by high-performance liquid chromatography of the fluorenylmethoxycarbonyl (FMOC) derivative. *International Journal of Environmental Analytical Chemistry*, *38*, 351–368.

Pohlmann, T. (1987). A three dimensional circulation model of the South China Sea. In J. J. Nihoul & B. m. Jamart (Eds.), *Three-Dimensional Models of Marine and Estuarine Dynamics* (pp. 245–268). New York: Elsevier.

Posada, D. (2008). jModelTest: phylogenetic model averaging. *Molecular Biology and Evolution*, *25*, 1253–1256.

Priisholm, K., Moestrup, Ø. & Lundholm, N. (2002). Taxonomic notes on the marine diatom genus *Pseudo-nitzschia* in the Andaman Sea near the Island of Phuket, Thailand, with a description of *Pseudo-nitzschia micropora* sp. nov. *Diatom Research*. *17*(1),153–175.

Pulido, O. M. (2008). Domoic acid toxicologic pathology: a review. *Marine Drugs*, 6, 180–219.

Quijano-Scheggia, S. I., Garcés, E., Lundholm, N., Moestrup, Ø., Andree, K., & Camp, J. (2009). Morphology, physiology, molecular phylogeny and sexual compatibility of the cryptic *Pseudo-nitzschia delicatissima* complex (Bacillariophyta), including the description of *P. arenysensis* sp. nov. *Phycologia*, *48*, 492–509.

R Core Team. (2014). R: A Language and Environment for Statistical Computing. R Foundation for Statistical Computing, Vienna, Austria. Available at https://www.r-project.org/.

Rambaut, A., Drummond, A. J., Xie, D., Baele, G., & Suchard, M. A. (2018). Posterior summarization in bayesian phylogenetics using Tracer 1.7. *Systematic Biology*, *67*(5), 901–904.

Ravin, N. V., Galachyants, Y. P., Mardanov, A. V., Beletsky, A. V., Petrova, D. P., Sherbakova, T. A., ... & Grachev, M. A. (2010). Complete sequence of the mitochondrial genome of a diatom alga *Synedra acus* and comparative analysis of diatom mitochondiral genomes. *Current Genetics*, *56*, 215–223.

Rhodes, L., White, D., Syhre, M., & Atkinson, M. (1996). Pseudo-nitzschia species isolated from New Zealand coastal waters: domoic acid production in vitro and links with shellfish toxicity. In: Yasumoto, T., Oshima, Y., & Fukuyo, Y. (Eds.) Harmful and Toxic Algal Blooms, Intergovernmental Oceanographic Commission UNESCO, Paris, pp. 155–158.

Rhodes, L. L., Scholin, C., & Garthwaite, I. (1998). *Pseudo-nitzschia* in New Zealand and the role of DNA probes and immunoassays in refining marine biotoxin monitoring programmes. *Natural Toxins*, *6*, 105–111.

Rimet, F., Kermarrec, L., Bouchez, A., Hoffmann, L., Ector, L., & Medlin, L. K. (2011). Molecular phylogeny of the family Bacillariaceae based on 18S rDNA sequences: focus on freshwater *Nitzschia* of the section Lanceolatae. *Diatom Research*, *26*(3), 273–291.

Roderic, D. M. (2001). NEXUS Data Editor for Windows: a program to edit NEXUS format data files. Version 0.5.0. Retrieved from https://www.ctu.edu.vn/~dvxe/Bioinformatic/Software/Rod%20Page/nde.html.

Romero, M. L. J., Lirdwitayaprasit, T., Kotaki, Y., Lundholm, N., Relox, R. J., Jr., Furio, E. F., … Fukuyo, Y. (2008). Isolation of ASP toxin-producing *Nitzschia* from Thailand. *Marine Research in Indonesia*, *33*, 225–228.

Romero, M. L. J., Kotaki, Y., Lundholm, N., Thoha, H., Ogawa, H., Relox, J. R., … Fukuyo, Y. (2011). Unique amnesic shellfish toxin composition found in the South East Asian diatom *Nitzschia navis-varingica*. *Harmful Algae*, *10*, 456–462.

Romero, M. L. J., Kotaki, Y., Relox, J. R., Lundholm, N., Takata, Y., Kodama, M., & Fukuyo, Y. (2012). Two new ASP toxin production types in strains of *Nitzschia navis-varingica* from the Philippines. *Coastal Marine Science*, *35*, 67–69.

Ronquist, F. & Huelsenbeck, J. P. (2003). MrBayes version 3.0: Bayesian phylogenetic inference under mixed models. *Bioinformatics*, *19*, 1572–1574.

Ronquist, F., Teslenko, M., van der Mark, P., Ayres, D. L., Darling, A., Höhna, S., … Huelsenbeck, J. P. (2012). MrBayes 3.2: efficient Bayesian phylogenetic inference and model choice across a large model space. *Systematic Biology*, *61*, 539–542.

Rönnbäck, P. (1999). The ecological basis for economic value of seafood production supported by mangrove ecosystems. *Ecological Economy*, *29*, 235–252.

Round, F. E., Crawford, R. M., & Mann, D. G. (1990). *The diatoms: Biology and Morphology of the Genera*. United State of America, New York: Cambridge University Press.

Rovira, L., Trobajo, R., Sato, S., Ibáñez & Mann, D. G. (2015). Genetic and physiological diversity in the diatom *Nitzschia inconspicua*. *The Journal of Eukaryotic Microbiology*, *62*, 815–832.

Sahraoui, I., Bates, S.S., Bouchouicha, D., Mabrouk, H.H., & Hlaili, A.S. (2011). Toxicity of Pseudo-nitzschia populations from Bizerte Lagoon, Tunisia, southwest Mediterranean, and first report of domoic acid production by *P. brasiliana*. *Diatom Research*, *26*(3), 293–303.

Sarno, D., & Dahlmann, J. (2000). Production of domoic acid in another species of *Pseudo-nitzschia*: *P. multistriata* in the Gulf of Naples (Mediterranean Sea). *Harmful Algae News*, *21*, 5.

Sathiamurthy, E., & Voris, H. K. (2006). Maps of Holocene sea level transgression and submerged lakes on the Sunda Shelf. *The Natural History Journal of Chulalongkorn University*, *Supplement 2*, 1–44.

Sawant, P. M., Holland, P. T., Mountfort, D. O., & Kerr, D. S. (2008). *In vivo* seizure induction and pharmacological preconditioning by domoic acid and isodomoic acids A, B and C. *Neuropharmacology*, *55*, 1412–1418.

Sawant, P. M., Tyndall, J. D. A., Holland, P. T., Peake, B. M., Mountfort, D. O., & Kerr, D. S. (2010). *In vivo* seizure induction and affinity studies of domoic acid and isodomoic acids D, E and F. *Neuropharmacology*, *59*, 129–138.

Sawant, P. M., Weare, B. A., Holland, P. T., Selwood, A. I., King, K. L., Mikulski, C. M., … Kerr, D. S. (2007). Isodomoic acids A and C exhibit low KA receptor affinity and reduced in vitro potency relative to domoic acid in region CA1 of rat hippocampus. *Toxicon*, *50*, 627–638.

Schliep, K. (2011). Phangorn: phylogenetic analysis in R. *Bioinformatics*, *27*, 592–593.

Scholin, C. A., Gulland, F., Doucette, G. J., Benson, S., Busman, M., … Van Dolah, F. M. (2000). Mortality of sea lions along the central California coast linked to a toxic diatom bloom. *Nature, 403*, 80–84.

Scholin, C. A., Herzog, M., Sogin, M., & Anderson, D. M. (1994). Identification of group- and strain-specific genetic markers for globally distributed *Alexandrium* (Dinophyceae). II. Sequence analysis of a fragment of the LSU rRNA gene. *Journal of Phycology*, *30*, 999–1011.

Scholin, C. A., Marin, R., Miller, E. P., Doucette, G. J., Powell, C. L., Haydock, P., Howard, J., & Ray, J. (1999). DNA probes and a receptor-binding assay for detection of *Pseudo-nitzschia* (Bacillariophyceae) species and domoic acid activity in cultured and natural samples. *Journal of Phycology*, *35*, 1356–1367.

Schultz, J., Müller, T., Achtziger, M., Seibel, P. N., Dandekar, T. & Wolf, M. (2006). The internal transcribed spacer 2 database - a web server for (not only) low level phylogenetic analyses. *Nucleic Acids Research*, *34*, W704–707.

Schwacke, L. H., Twiner, M. J., Guise, S. D., Balmer, B. C., Wells, R. S., Townsend, F. I., … Rowles, T. K. (2010). Eosinophilia and biotoxin exposure in bottlenose dolphins (*Tursiops truncates*) from a coastal area impacted by repeated mortality events. *Environmental Research*, 110, 548–555.

Seibel, P., Müller, T., Dandekar, T., Schultz, J., & Wolf, M. (2006). 4SALE–A tool for synchronous RNA sequence and secondary structure alignment and editing. *BMC Bioinformatics*, *7*, 498.

Seibel, P., Müller, T., Dandekar, T., & Wolf, M. (2008). Synchronous visual analysis and editing of RNA sequence and secondary structure alignments using 4SALE. *BMC Research Notes*, *1*, 91.

Selig, C., Wolf, M., Müller, T., Dandekar, T. & Schultz, J. (2008). The ITS2 Database II: homology modelling RNA structure for molecular systematics. *Nucleic Acids Research*, *36*, D377–380.

Sierra Beltran, A., Palafox-Uribe, M., Grajales-Montiel, J., Cruz-Villacorta, C., & Ochoa, J.L. (1997). Sea bird mortality at Cabo San Lucas, Mexico: evidence that toxic diatom blooms are spreading. *Toxicon, 35*, 447–453.

Silvagni, P. A., Lowenstine, L. J., Spaker, T., Lipscomb, T. P., & Gulland, F. M. D. (2005). Pathology of domoic acid toxicity in California sea lions. *Veterinary Pathology*, *42*, 184–191.

Siquiros Beltrones, D. A., & López Fuerte, F. O. (2003). Epiphytic diatoms associated with red mangrove (*Rhizophora mangle*) prop roots in Bahía Magdalena, Baja California Sur, Mexico. *Revista de Biologia Tropical*, *54*(2), 287–297.

Smith, W. (1853). *A synopsis of the Bristish Diatomaceae with remarks on their structure, function and distribution; and instruction for collecting and presenting specimens*. Vol. 1. London: John Van Voorst, pp. 89.

Sorhannus, U., Ortiz, J. D., Wolf, M., & Fox, M. G. (2010). Microevolution and speciation in *Thalassiosira weissflogii* (Bacillariophyta). *Protist*, *161*, 237–249.

Stehr, C. M., Connell, L., Baugh, K. A., Bill, B. D., Adams, N. G. & Trainer, V. L. (2002). Morphological, toxicological, and genetic differences among *Pseudo-*

nitzschia (Bacillariophyceae) species in inland embayments and outer coastal waters of Washington State, USA. *Journal of Phycology*, *38*, 55–65.

Subba Rao, D. V., Quiliam, M. A., & Pocklington, R. (1988). Domoic acid- a neurotoxic amino acid produced by the marine diatom *Nitzschia pungens* in culture. *Canadian Journal of Fisheries and Aquatic Sciences*, *45*, 2076–2079.

Sugie, K., & Yoshimura, T. (2013). Effects of pCO_2 and iron on the elemental composition and cell geometry of the marine diatom *Pseudo-nitzschia pseudodelicatissima* (Bacillariophyceae). *Journal of Phycology*, *49*, 475–488.

Suriyanti, S. N. P., & Usup, G. (2015). First report of the toxigenic *Nitzschia navis-varingica* (Bacillariophyceae) isolated from Tebrau Straits, Johor, Malaysia. *Toxicon*, *108*, 257–263.

Swofford, D. L. (2001). PAUP* Phylogenetic Analysis Using Parsimony (*and other methods) Version 4.04beta. Sinauer Associates, Sunderland, Massachusetts.

Takata, Y., Sato, S., Dao, V. H., Montojo, U. M., Lirdwitayaprasit, T., Kamolsiripichaiporn, S., … Kodama, M. (2009). Occurrence of domoic acid in tropical bivalves. *Fisheries Sciences*, *75*, 473–480.

Takemoto, T., & Daigo, K. (1958). Constituents of *Chondria armata*. *Chemical and Pharmaceutical Bulletin*, *6*, 578–580.

Tamura, K., Peterson, D., Peterson, N., Stecher, G., Nei, M., & Kumar, S. (2011). MEGA5: molecular evolutionary genetics analysis using maximum likelihood, evolutionary distance, and maximum parsimony methods. *Molecular Biology and Evolution*, *28*, 2731–2739.

Taroncher-Oldenburg, G., Kulis, D. M., & Anderson, D. M. (1997). Toxin variability during the cell cycle of the dinoflagellate *Alexandrium fundyense*. *Limnology Oceanography*, *42*, 1178–1188.

Tan, S. N., Lim, H. C., Teng, S. T., Lim, P. T. & Leaw, C. P. (2015). *Pseudo-nitzschia* species (Bacillariophyceae) identification and delineation using mitochondrial *cox1* gene sequences as compared to LSU rDNA. *Fisheries Science*, *81*, 831–838.

Tan, S. N., Teng, S. T., Lim, H. C., Kotaki, Y., Bates, S. S., Leaw, C. P., & Lim, P. T. (2016). Diatom *Nitzschia navis-varingica* (Bacillariophyceae) and its domoic

acid production from the mangrove environments of Malaysia. *Harmful Algae*, *60*, 139–149.

Taylor J. C., Harding W. R. & Archibald C. G. M. (2006). An illustrated guide to some common diatom species from South Africa. Report to the water research commission by DH environmental consulting.

Teitelbaum, J. S., Zatorre, R. J., Carpenter, S., Gendron, D., Evans, A. C., Gjedde, A., & Cashman, N. R. (1990). Neurologic sequelae of domoic acid intoxication due to the ingestion of contaminate mussels. *The New England Journal of Medicine*, *322*(25), 1781–1787.

Teng, S. T., Leaw, C. P., Lim, H. C. & Lim, P. T. (2013). The genus *Pseudo-nitzschia* (Bacillariophyceae) in Malaysia, including new records and a key to species inferred from morphology-based phylogeny. *Botanica Marina*, *56*, 375–398.

Teng, S. T., Lim, H. C., Lim, P. T., Dao, V. H., Bates, S. S. & Leaw, C. P. (2014). *Pseudo-nitzschia kodamae* sp. nov. (Bacillariophyceae), a toxigenic species from the Strait of Malacca, Malaysia. *Harmful Algae*, *34*, 17–28.

Teng, S. T., Lim, P. T., Lim, H. C., Rivera-Villarelle, M., Quijano-Scheggia, S., Takata, Y., … Leaw, C. P. (2015). A non-toxigenic but morphologically and phylogenetically distinct new species of *Pseudo-nitzschia*, *P. sabit* sp. nov. (Bacillariophyceae). *Journal of Phycology*, *51*, 706–725.

Teng, S. T., Tan, S. N., Lim, H. C., Dao, V. H., Bates, S. S. & Leaw, C. P. (2016). High diversity of *Pseudo-nitzschia* along the northern coast of Sarawak (Malaysian Borneo), with descriptions of *P. bipertita* sp. nov. and *P. limii* sp. nov. (Bacillariophyceae). *Journal of Phycology*, *52*, 973–989.

Thessen, A. E., Bowers, H. A., & Stoecker, D. K. (2009). Intra- and interspecies differences in growth and toxicity of *Pseudo-nitzschia* while using different nitrogen sources. *Harmful Algae*, *8*, 792–810.

Thoha, H., Kotaki, Y., Panggabean, L., Lundholm, N., Ogawa, H., Lim, P. T., … Fukuyo, Y. (2012). Screening of diatoms that produce ASP toxins in Southernmost Asian waters. *Coastal Marine Science*, *35*, 34–38.

Thompson, J. D., Gibson, T. J., Plewniak, F., Jeanmougin, F., & Higgins, D. G. (1997). The ClustalX windows interface: Flexible strategies for multiple sequence alignment aided by quality analysis tools. *Nucleic Acids Research*, *25*, 4876–4882.

Todd, E. C. D. (1993). Domoic acid and amnesic shellfish poisoning- a review. *Journal of Food Protection*, *56*(1), 69–83.

Trainer, V. L., Adams, N. G., Bill, B. D., Stehr, C. M., & Wekell, J. C. (2000). Domoic acid production near California coastal upwelling zones, June 1998. *Limnology and Oceanography*, *45*(8), 1818–1833.

Trainer, V. L., Bates, S. S., Lundholm, N., Thessen, A. E., Cochlan, W. P., Adams, N. G., & Trick, C. G. (2012). *Pseudo-nitzschia* physiological ecology, phylogeny, toxicity, monitoring and impacts on ecosystem health. *Harmful Algae*, *14*, 271–300.

Trick, C. G., Bill, B. D., Cochlan, W. P., Wells, M. L., Trainer, V. L., & Pickell, L. D. (2010). Iron enrichment stimulates toxic diatom production in high-nitrate, low-chlorophyll areas. *Proceedings of the National Academy of Sciences of the United States of America*, *107*(13), 5887–5892.

Trimborn, S., Lundholm, N., Thoms, Rost, B. (2008). Inorganic carbon acquisition in potentially toxic and non-toxic diatoms: the effect of pH-induced changes in seawater carbonate chemistry. *Physiologia Plantarum*, *133*, 92–105.

Trobajo, R., Clavero, E., Chepurnov, V. A., Clavero, E., & Cox, E. J. (2006). Taxonomy, life cycle, and auxosporulation of *Nitzschia fonticola* (Bacillariophyta). *Journal of Phycology*, *42*, 1353–1372.

Trobajo, R., Clavero, E., Chepurnov, V. A., Sabbe, K., Ishihara, S., & Cox, E. J. (2009). Morphological, genetic, and mating diversity within the widespread bioindicator *Nitzschia palea* (Bacillariophyceae). *Phycologia*, *48*, 443–459.

Troboja, R., Mann, D. G., Clavero, E., Evans, K. M., Vanormelingen, P. & McGregor, R. C. (2010). The use of partial *cox1*, *rbcL* and LSU rDNA sequences for phylogenetics and species identification within the *Nitzschia palea* species complex (Bacillariophyceae). *European Journal of Phycology*, *45*, 413–425.

Villac, M. C., & Frycell, G. A. (1998). *Pseudo-nitzschia pungens* var. *cingulata* var. nov. (Bacillariophyceae) based on field and culture observations. *Phycologia*, *37*(4), 269–274.

Villac, M. C., Roelke, D. L., Chavez, F. P., Cifuentes, L. A., & Fryxell, G. A. (1993b). *Pseudonitzschia australis* Frenguelli and related species from the west coast of the U.S.A.: occurrence and domoic acid production. *Journal of Shellfish Research*, *12*(2), 457–465.

Voris, H. K. (2000). Maps of Pleistocene sea levels in Southeast Asia: shorelines, river systems and time durations. *Journal of Biogeography*, *27*, 1153–1167.

Vrieling, E. G., Koeman, R. P. T., Scholin, C. A., Scheerman, P., Peperzak, L., Veenhuis, M., & Gieskes, W. W. C. (1996). Identification of a domoic acid-producing *Pseudo-nitzschia* species (Bacillariophyceae) in the Dutch Wadden Sea with electron microscopy and molecular probes. *European Journal of Phycology*, *31*, 333–340.

Wadt, P. R., Mafra, L. L., Jr., dos Santos Tavares, C. P., Fernandes, L. F. & Proença, L. A. O. (2017). Growth, chain formation, and toxin production by southern Brazilian *Pseudo-nitzschia* isolates under laboratory conditions. *Environmental Monitoring and Assessment*, *189*, 621.

Wang, P., Liang, J. R., Lin, X., Chen, C. P., Huang, Y. Y., Gao, Y., & Gao, Y. H. (2012). Morphology, phylogeny and ITS-2 secondary structure of *Pseudo-nitzschia brasiliana* (Bacillariophyceae), including Chinese strains. *Phycologia*, *51*(1), 1–10.

Weir, B. S., & Cockerham, C. C. (1984). Estimating F-statistics for the analysis of population structure. Evolution, 38, 1358–1370.

Wekell, J. C., Gauglitz, E. J. Jr., Barnett, H. J., Hatfield, C. L., Simons, D., & Ayres, D. (1994). Occurrence of domoic acid in Washington state razor clams (Siliqua patula) during 1991-1993. Nature Toxins, 2, 197-205.

Wekell, J. C., Hurst, J., & Lefebvre, K. A. (2004). The origion of the regulatory limits for PSP and ASP toxins in shellfish. *Journal of Shellfish Research*, *23*, 927-930.

White, T., Bruns, T., Lee, S., Taylor, J., Innis, M., Gelfand, D., Shinsky, J., & White, T. (1990). Amplification and direct sequencing of fungal ribosomal RNA genes for phylogenetic. In: Innis, M. A., Gelfand, D. H., Sninsky, J. J., White, T. J. (Eds.), PCR Protocols: A Guide to Methods and Applications. Academic Press, New York, pp. 315–322.

Wiemers, M., Keller, A., & Wolf, M. (2009). ITS2 secondary structure improves phylogeny estimation in a radiation of blue butterflies of the subgenus *Agrodiaetus* (Lepidoptera: Lycaenidae: *Polyommatus*). *BMC Evolutionary Biology*, *9*, 300.

Wolf, M., Achtziger, M., Schultz, J., Dandekar, T. & Müller, T. (2005). Homology modeling revealed more than 20,000 rRNA internal transcribed spacer 2 (ITS2) secondary structures. *RNA*, *11*, 1616–1623.

Wolf, M., Koetschan, C., & Müller, T. (2014). ITS2, 18S, 16S or any other RNA–simply aligning sequences and their individual secondary structures simultaneously by an automatic approach. *Gene*, *546*, 145–149.

Wolf, M., Ruderisch, B., Dandekar, T., Schultz, J., & Müller, T. (2008). ProfDistS: (profile–) distance based phylogeny on sequence-structure alignments. *Bioinformatics*, *24*, 2401–2402.

Work, T. M., Barr, B., Beale, A. M., Fritz, L., Quilliam, M. A., & Wright, J. L. C. (1993). Epidemiology of domoic acid poisoning in brown pelicans (*Pelecanus Occidentalis*) and brandt's cormorants (*Phalacrorax penicillatus*) in California. *Journal of Zoo and Wildlife Medicine*, *24*(1), 54–62.

Wright, S. (1921). Systems of mating, I–V. *Genetics*, *6*, 111–178.

Wright, S. (1951). The genetical structure of populations. *Annals of Eugenics*, *15*, 323–354.

Wright, S. (1965). The interpretation of population structure by F-statistics with special regard to system of mating. *Evolution*, *19*, 395–420.

Yao, H., Song, J., Liu, C., Luo, K., Han, J., Li, Y… Chen, S. (2010). Use of ITS2 region as the universal DNA barcode for plants and animals. *Plos One*, *5*(10), e13102.

Yap-Dejeto, L. G., Omura, T., Cinco, G. F., Cobacha, M. M., & Fukuyo, Y. (2013). Species account of marine diatoms of the genus *Pseudo-nitzschia* in San Pedro Bay, Philippines. *Philippine Journal of Science*, *142*(1), 27–37.

Yap-Dejeto, L. G., Omura, T., Nagahama, Y., & Fukuyo, Y. (2010). Observations of eleven *Pseudo-nitzschia* species in Tokyo Bay, Japan. *La mer*, *48*, 1–16.

Zingone, A., & Enevoldsen, H. O. (2000). The diversity of harmful algal blooms: a challenge for science and management. *Ocean & Coastal Management*, *43*, 725–748.

Zwickl, D. J. & Hillis, D. M. (2002). Increased taxon sampling greatly reduces phylogenetic error. *Systematic Biology*, *51*, 588–598.

LIST OF PUBLICATIONS AND PAPERS PRESENTED

Publications:

1. **Tan, S. N**., Lim, H.C., Teng, S. T., Lim, P. T & Leaw, C. P. 2015. *Pseudo-nitzschia* species (Bacillariophyceae) identification and delineation using the mitochondrial *cox*1 gene sequences as compared to LSU rDNA. **Fisheries Sciences**, **81**, 831–838.

2. Teng, S.T., **Tan, S.N**., Lim, H.C., Dao, V.H., Bates, S.S. & Leaw, C.P. 2016. High diversity of Pseudo-nitzschia along the northern coast of Sarawak (Malaysian Borneo), with descriptions of *P. bipertita* sp. nov. and *P. limii* sp. nov. (Bacillariophyceae). **Journal of Phycology**, **52**, 973–983.

3. **Tan, S. N.,** Teng, S. T., Lim, H.C., Kotaki, Y., Bates, S.S., Leaw, C.P., & Lim, P. T. 2016. Diatom *Nitzschia navis-varingica* (Bacillariophyceae) and its domoic acid production from the mangrove environments of Malaysia. **Harmful Algae**, **60**, 139–149.

4. Lim, H.C., **Tan, S.N**., Teng, S.T., Lundholm, N., Orive, E., David, H., Quijano-Scgeggia, S., Leong, S.C.Y., Wolf, M., Bates, S.S., Lim, P.T. & Leaw, C.P. Phylogeny and species delineation in the marine diatom *Pseudo-nitzschia* (Bacillariophyta) using cox1, LSU, and ITS2 rRNA genes: a perspective in character evolution. **Journal of Phycology**, **54**, 234– 248.

5. **Tan, S. N.,** Leaw, C. P., Gu, H., Chen, C., Gao, Y., Kotaki, Y., Gao, C., Lim, H. C., Teng, S. T., & Lim, P. T. 2018. **In preparation**. Genetics diversity of *Nitzschia navis-varingica* (Bacillariophyceae) in Malaysian waters.

Papers presented at conferences/ seminars/symposiums:

Poster Presentation:

1. **Tan, S. N**., Lim, H.C., Teng, S. T., Lim, P. T & Leaw, C. P. 2014. Molecular characterization of the diatom, *Pseudo-nitzschia* (Bacillariophyceae) using the mitochondrial genetic marker, cytochrome oxidase I (COI). IOC/WESTPAC 9th International Scientific Symposium: A healthy ocean for prosperity in the western pacific: Scientific challenges and possible solutions. Nha Trang, Vietnam, 22 – 25 April 2014. Book of Abstract, p. 364.
2. **Tan, S.N**., Teng, S.T., Lim, H.C., Kotaki, Y., Bates, S.S., Leaw, C.P., & Lim, P.T. 2017. Distribution of the diatom *Nitzschia navis-varingica* (Bacillariophyceae), a domoic acid producer from Malaysian waters. The Third Xiamen Symposium on Marine Environmental Sciences. 9–11 January 2017.
3. **Tan, S.N**., Teng, S.T., Lim, H.C., Kotaki, Y., Bates, S.S., Leaw, C.P., & Lim, P.T. 2017. Distribution of the diatom *Nitzschia navis-varingica* (Bacillariophyceae), a domoic acid producer from Malaysian waters. IOES HICoE seminar 2017: Air-Ocean-Land Interactions, 12 September 2017.
4. **Tan, S**.**N**., Leaw, C.P., Kotaki, Y., Teng, S.T., & Lim. P.T. The first report of toxigenic benthic diatom, *Nitzschia navis-varingica* from mangrove areas along the Strait of Malacca. Research and Education Network on Coastal Ecosystems in Southeast Asia (CCore-RENSEA: 2016–2018). University of the Philippines Visayas, Iloilo City, Philippines, 27 February – 1 March 2018. Book of Abstract, p. 63.

Oral Presentation:

1. **Tan, S.N**., Teng, S.T., Lim, H.C., Kotaki, Y., Leaw, C.P., & Lim, P.T. 2016. Morphology and molecular characterization of the diatom *Nitzschia navis-varingica* (Bacillariophyceae), a potential causative organism of Amnesic Shellfish Poisoning (ASP) from Malaysian waters. BSGC, 15– 16 December 2016.
2. **Tan, S.N**., Teng, S.T., Lim, H.C., Kotaki, Y., Bates, S.S., Leaw, C.P., & Lim, P.T. 2017. Distribution of the toxic diatom, *Nitzschia navis-varingica* (Bacillariophyceae) from Malaysia and its domoic acid production. IOC/WESTPAC 10th International Scientific Symposium: Advanced ocean knowledge, fostering sustainable development from the Indo-Pacific to the globe. Qingdao, China, 17 – 20 April 2017. Book of Abstract, p. 107.